TESTING, EVALUATION AND OPTIMISATION OF THE PERFORMANCE OF A STAND-ALONE PHOTOVOLTAIC SYSTEM IN MALTA

A dissertation submitted in fulfilment of the
requirements for the Degree of
Master of Philosophy
at the
University of Malta

By: Charles E. Iskander Yousif
February 1995

Institute for Energy Technology
University of Malta
Msida - Malta

To My Family

FRONTISPIECE

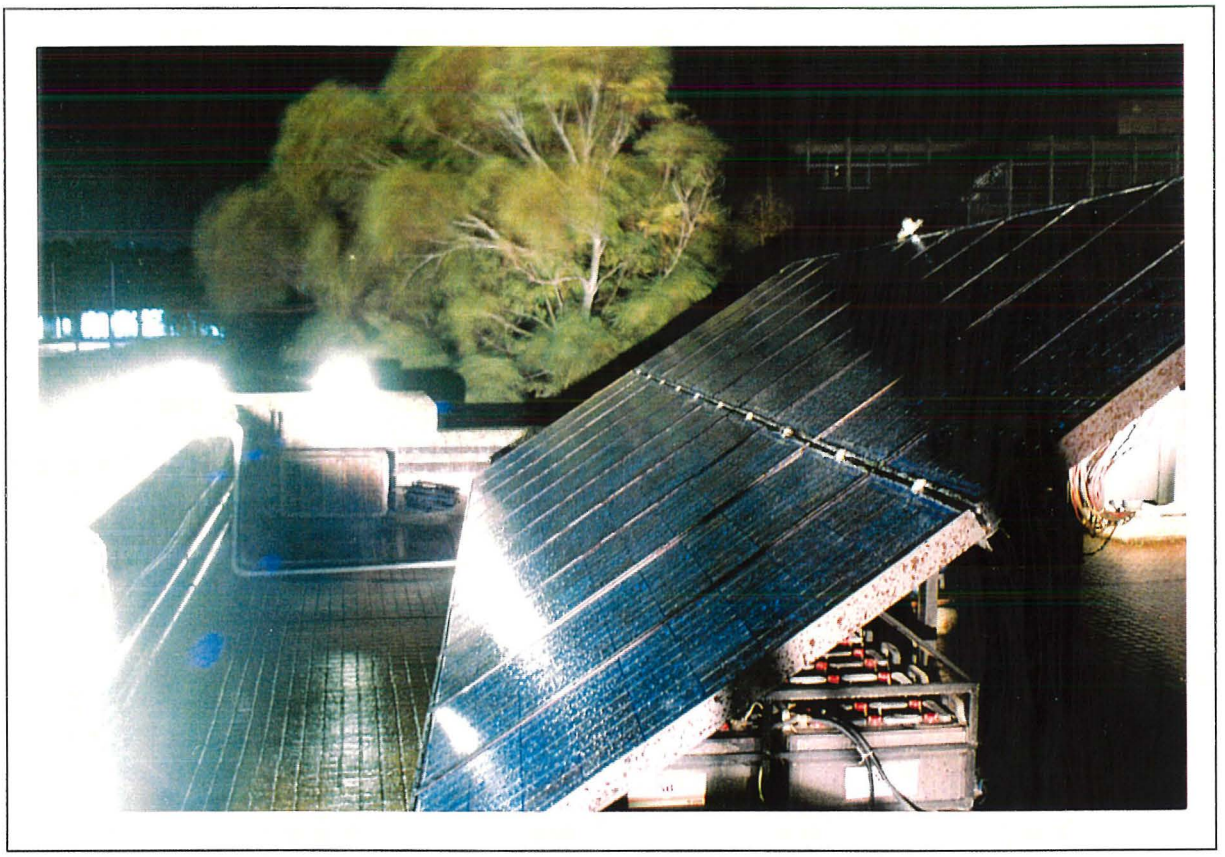

A photograph of the first 1.2 kWp stand-alone photovoltaic solar system with battery storage, set up in Malta and being studied in this project.

ACKNOWLEDGEMENTS

First and foremost, I would like to acknowledge the sincere dedication and undivided attention, advice and patience of my tutor Prof. Edward Scerri. My thanks are also extended to the Ministry of Education and Human Resources (Malta), the University of Malta, the Comboni Fathers - MCSJ - (Sudan), for offering me this opportunity and providing for all my needs, and to the Society of Christian Doctrine - M.U.S.E.U.M. - (Malta), for their assistance and good will.

My appreciation is also extended to the following Departments for their prompt support:

- Department of Chemistry: for providing their roof to set up the project, their premises to carry on my studies, and their expertise. Special thanks are due to Dr. Alfred Vella, Ms. Bernadette Mintoff, Ms. Lucienne Mercieca, Ms. Stephania Aquilina and Mr. Alfred Agius.
- Departments of Mechanical and Manufacturing Engineering: for allowing me to use their workshops and equipment to build up and maintain the system components. Thanks are due to all the members of the workshops especially to Mr. Jesmond Pace, Mr. Anthony Bezzina, Mr Noel Tonna and Mr. Michael Cumi, for their interest and assistance
- Department of Physics: for helping in the testing and maintenance of the electronic components. Special thanks are due to Mr. Anthony Buttigieg, Mr. Jesmond Debattista and Mr. Carmel Doublet.

I wish to thank Mr. Anthony Fenech and Mr. Kenneth Camilleri for their continuous support in matters dealing with computer hardware and software.

I would like to extend my sincere thanks and appreciation to Ms. Grace Micallef for her faithful support and unfailing care throughout my stay in Malta.

Last but not least, I thank my family for their patience and endurance. Their wonderful sacrifice and support for me, at the time when they needed me most, will always be cherished and remembered.

CONTENTS

SUBJECT	PAGE NO.
FRONTISPIECE	i
ACKNOWLEDGEMENTS	ii
SUMMARY	vii
PREFACE	ix
CHAPTER ONE: Design and Installation	
• [1.1] Sizing of the PV System	1
• [1.2] Choice of the PV Modules	11
• [1.3] Design of the PV Supporting Structure	13
• [1.4] Choice of the Storage Batteries	13
• [1.5] Choice of the Battery Control Unit (BCU)	16
• [1.6] Design of the Wiring Connections	16
• [1.7] Load Control and Management	18
• [1.8] Design of the Monitoring System	20
• [1.9] Design of the Case for the Integrators	28
• [1.10] Installation of the PV System	29
• [1.11] Precautions Taken During Installation	31
CHAPTER TWO: Operation and Maintenance	
• [2.1] Experience Gained at the Beginning of Operation	33
• [2.2] Maintenance of the PV Array	34

- [2.3] Operation and Maintenance of the Batteries 39
- [2.4] Operation and Maintenance of the BCU 41
- [2.5] Operation of the Load Control Units 44
- [2.6] Operation of the Lights 44
- [2.7] Operation and Maintenance of the Monitoring Equipment 45
- [2.8] Maintenance Schedules 46

CHAPTER THREE: Data Analysis and Presentation of Results

- [3.1] Systematic Checking of the Collected Data 49
- [3.2] General Analysis of the Collected Data 50
- [3.3] Presentation of Graphic Results 60
- [3.4] Hourly PV Array Efficiency Variations 65
- [3.5] Effect of Wind Speed on the Temperature of the Modules 77
- [3.6] Effect of Washing the Modules on Efficiency 77
- [3.7] Linear Regression Results 81
- [3.8] Results of the Battery Monitoring 81

CHAPTER FOUR: Cost Evaluation and Sensitivity Analysis

- [4.1] Life Cycle Costing (LCC) 88
- [4.2] Sensitivity Analysis 92
- [4.3] Variable Assumptions Used in the LCC Technique 95

CHAPTER FIVE: Conclusions and Recommendations

- [5.1] Conclusion of Operating Experience 97
- [5.2] Conclusions of Operational Results 98
- [5.3] Recommendations 99

APPENDIX A: Solar Radiation: Its Nature and Measurement

- [A.1] Total Radiation at the Top of the Atmosphere 101
- [A.2] Total Radiation at Sea-level 102
- [A.3] Phenomena which Cause Seasonal Variation in Solar Radiation 103
- [A.4] Factors which Cause Daily Variations in Solar Radiation 107
- [A.5] The Spectral Distribution of Solar Radiation at the Top of the Atmosphere 111
- [A.6] The Spectral Distribution of Solar Radiation at Sea-level 111
- [A.7] Factors which Affect the Spectral Distribution of Solar Radiation 113
- [A.8] Review of Solar Radiation Measuring Instruments 116
- [A.9] Measurement of Total Solar Radiation 117

APPENDIX B: Photovoltaic Cells and Balance of System Components

- [B.1] Properties of Mono-crystalline Silicon Cells 124
- [B.2] The Open-circuit Voltage and the Short-circuit Current 131
- [B.3] Maximum Output Power 133
- [B.4] Limitations to Cell Performance and Efficiency 134
- [B.5] Power Losses in PV Cells 137
- [B.6] Semi-crystalline Silicon Cells 139
- [B.7] Amorphous Silicon Cells 140
- [B.8] Gallium Arsenide Cells 141
- [B.9] Cadmium Sulphide/Copper Sulphide (CdS/Cu_2S) Cells 142
- [B.10] Cadmium Sulphide/Copper Indium Diselenide (CdS/CIS) Cells 142
- [B.11] Cadmium Telluride (Cd Te) Cells 143
- [B.12] Improvements to Cell Efficiency 143
- [B.13] Construction of Solar Modules 144
- [B.14] The Array Supporting Structure 147
- [B.15] The Battery Bank 1472

- [B.16] The Battery Control Unit (BCU) 152
- [B.17] Power Distribution at Low Voltage 152

APPENDIX C 154

APPENDIX D 188

REFERENCES 209

SUMMARY

The technology of photovoltaics is constantly progressing and likewise its market. It is envisaged that by the turn of this century, photovoltaic (PV) power production will be cost effective for many applications. It is well known that Malta has an abundance of sunshine, however, measurement of solar radiation has long been abandoned. At the same time, there is lack of information on the possible outcome of the use of PV systems for electricity production.

In this work, the measurement of solar radiation has been re launched together with a study of the performance of a 1.2 kWp stand-alone photovoltaic (PV) system, with battery storage Sixteen months of data has been collected and analysed in accordance with the guidelines set by the Joint Research Centre - Ispra Establishment. For this period, the mean global horizontal radiation was found to be 4.7 kWh/m²/day and the mean global radiation on the plane of the modules (36° to the horizontal), was 5.24 kWh/m²/day.

In order to study a PV system properly, a full knowledge of the characteristics of solar radiation and solar cells become essential. These have been described in the appendices An overview of the instruments used for solar radiation measurements was also presented and a comparison was made between the different types of PV cells and silicon cells. A.conclusion has been reached to use silicon cell-based pyranometers (solarimeters) for measuring solar radiation in studies related to photovoltaic systems.

A description of the design of the stand-alone PV system was presented together with the precautions that are to be taken during installation. The monitoring system was described in detail and solutions were offered to the problems encountered during data collection.

The analysis of data yielded a wealth of information on the performance of the PV system in Malta. Load management was identified as a key factor to the optimum utilisation of such a system.

The mean annual output of the PV system was found to be 750 kWh/kWp/annum with an annual mean performance ratio of 0.38, that had a peak of more than 0.5 in December 1993. A linear function was determined that correlated the array yield (Y_a, in kWh/kWp/day) to the mean solar radiation incident on the array (G_i, in kWh/m²/day) as:

$$Y_a = 0.6030G_i \quad 0.004$$

From the results obtained, it could be inferred that the modules were slightly cooled in summer, by winds that had speeds higher than 2 m/s. The loss in PV array efficiency that could be attributed to the accumulation of dust over the modules was determined to be 2%.

By performing the life cycle cost analysis for a system life-time of 20 years, it was found that the cost of one unit of electricity is Lm 0.77/kWh. This was compared to the cost of production of electricity by a similar grid-connected PV system and it was found that the price could be lower by as much as 70%.

PREFACE

Malta (latitude 35° 50' N, longitude 14° 26' E) depends solely on the importation of fossil fuels to provide for the islands' needs for energy. Due to the expansion of the industrial sector and the increase in the quality of life of the Maltese society, the need for electricity is increasing at the rate of 8.7% per annum, which is more than three times the world average and it is predicted to continue increasing at this rate for the next twenty years [88].

Besides the well-known advantages of photovoltaic (PV) solar modules for electricity generation - non-polluting, silent, reliable, modular, having a stabilised operation during their long lifetime of more than twenty years, having no moving parts and requiring minimal and technologically simple maintenance - the use of such systems as a subsidiary source of electricity in Malta, could lower the national energy bill, reduce pollution, prolong the life of the existing power stations, and relieve the summer peak demand on the electric utilities. Certain applications are already well suited for direct coupling to PV modules such as water pumping and air-conditioning, whose use increase with higher solar radiation. Also, the international policies and commitments for the protection of the environment prompts the country to promote the use of renewable energy.

Encouraged by the fact that the amount of solar radiation incident in Malta is abundant, averaging to about 5 kWh/m^2 per day on a horizontal surface and that the total amount of flat roof area, that is suitable to place the PV modules is at least 10 000 000 m^2, an interest in tapping this energy becomes obvious.

This thesis describes the first research work being done in Malta, aiming at testing and optimising the performance of a photovoltaic system under the local weather. As a start, it was thought to design and install a stand-alone PV system with battery storage. Though a grid-connected system could have been more adaptable to Malta, however, such a system required changes in the national energy legislations which was not possible at the time.

Nevertheless, the application of PV stand-alone systems could be useful in Malta for street lighting, to provide energy to boats and for emergencies. It was realised that before applying such a relatively expensive technology on a large scale, a proper scientific evaluation of the performance of such systems and their cost had to be carried out based on the local conditions

Another important aim of this study is to restart the collection of solar radiation data to serve as a data base for future applications of solar technology.

This study is divided into five chapters:

The first chapter describes the design and installation of the PV system. A full description of the monitoring system is also given as well as the experience gained during installation In the second chapter, the operation of the system is described together with the maintenance carried out on the different balance of system components.

The analysis of the collected data and the presentation of results are described in Chapter Three, while a cost evaluation and a sensitivity analysis are presented in Chapter Four. Finally, Chapter Five describes the conclusions and recommendations of this study.

Four appendices have been included that describe the nature of solar radiation and methods of measurement, the characteristics of solar cells, the tables and programmes prepared during this study and the relevant information collected for the project, respectively.

CHAPTER ONE

DESIGN AND INSTALLATION

INTRODUCTION

A 1.2 kWp PV stand-alone system was designed and installed at the Institute for Energy Technology with the aim to test, evaluate and optimise the system's performance under the local climatic conditions. A portable weather station was also erected to provide the essential weather data for the site. Figure 1.1, shows a schematic layout of the PV system and figure 1.2, shows the parameters that were monitored and the mode of transfer and storage of data. The stored energy of this system was used to energise fluorescent lights during the night.

In this chapter, the sizing of the PV system, the designs of the PV array supporting structure, the battery compartment and the casing for the monitoring equipment are shown. Full details on the monitoring techniques and instruments are discussed, followed by a description of the installation phase. The precautions taken during installation are also described.

1.1 SIZING OF THE PV SYSTEM

The sizing of a stand-alone PV system implies the proper dimensioning of the PV array and the battery storage, to meet the load requirements under the local climatic conditions and the desired degree of reliability.

As the nominal 1.2 kWp PV array power was already known, due to a donation by the Amoco Company, it was necessary to size the battery and the load that would ensure the best utilisation of the generated energy. A simple sizing method was employed, since the available solar radiation data was limited to the mean monthly values of the global radiation on a

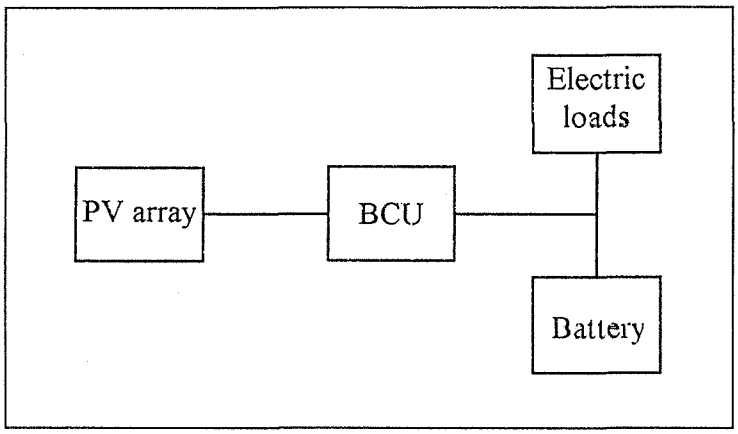

FIGURE 1.1: Schematic layout of the PV system

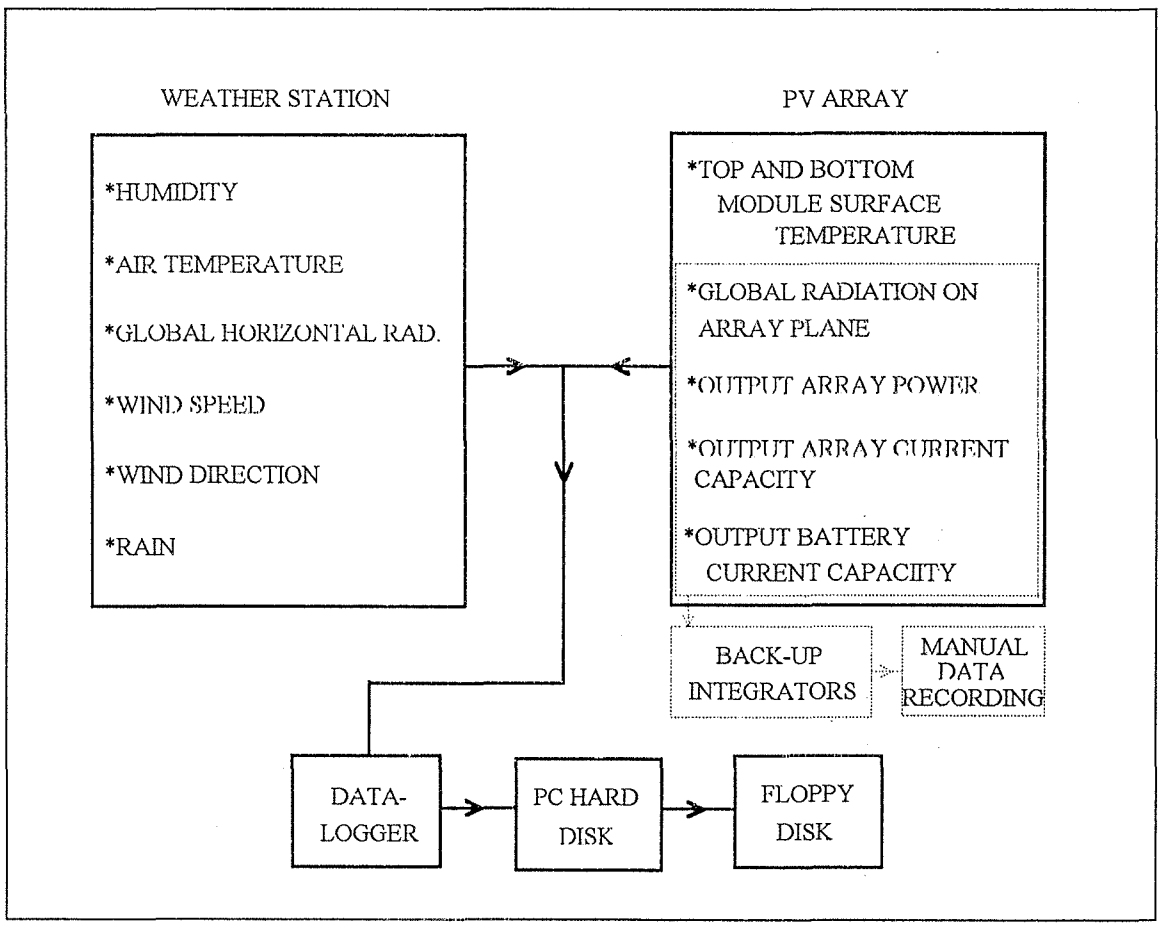

FIGURE 1.2: The weather data, being monitored by a data-logger. Data was transferred daily to the PC and then from the PC to the floppy disk every fortnight. The PV system parameters, were monitored by the data-logger as well as some back-up integrators.

horizontal surface and also because there were no simulation programmes available at the time.

The sizing of the system necessitates the following:

(a) The climate at the site, especially regarding solar radiation and ambient temperature;

(b) The load demand;

(c) The days of no-sunshine (days of autonomy) required for the battery storage.

The mean monthly global radiation incident on a horizontal plane for the period 1957 to 1972 is shown in figure 1.3, as measured by the Meteorological Office, using a Kipp pyranometer, placed at Qrendi (latitude 35° 50' N, longitude 14° 26' E and height of 135 m above mean sea level). The mean annual global radiation on a horizontal plane is found to be 5.097 kWh/m^2/day. As for temperature measurements at the same site, the mean and mean maximum monthly temperatures, for the period between 1947 and 1990, are given in table D.4, of appendix D.

The load demand was subject to a fixed nominal PV array power of 1.2 kWp. Hence, the amount of energy that can be generated had to be estimated using the available nominal power. This is similar to the case when there is a limited space to site the PV modules. Knowing that the generated electricity will not suffice the total demand, the interest of the designer would shift from deciding for the required number of modules to estimating the possible output power that can be produced by the installed PV peak Watts.

The output power will be utilised for lighting and for this purpose an autonomy of three days for the battery storage was assumed.

The sizing equation used here requires one solar radiation input value. Now, in order to decide which value to use, the following factors were considered:

1. The PV array was inclined at an angle of 36° to the horizontal. The data collected between July 1993 and October 1994, showed that the solar energy incident on this plane in winter was about 50% more on average, than the corresponding global radiation incident on a horizontal plane, while it was less by an average of 10%, in summer. Similar results were derived by interpolation from the graphs of the tilt factors presented in the PV Systems Design Manual [74].

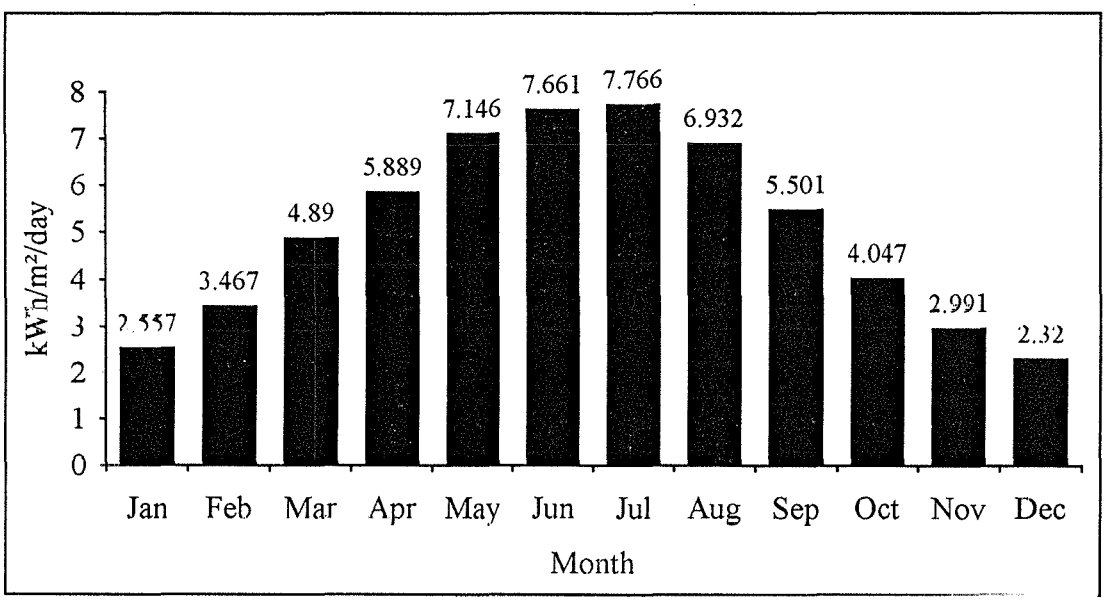

FIGURE 1.3: Mean monthly global radiation in Malta, incident on a horizontal plane for the period 1957 to 1972, as supplied by the Meteorological Office.

The tilt factor is defined as the ratio of the global radiation incident on the inclined plane to the global radiation incident on the same plane when it is placed horizontally, excluding the effect of the albedo of the place. The results are presented in table 1.1 and compared to the actual ratio calculated from the readings that were collected during the operation of the system. It was noted that in winter, the measured values were less than the calculated ones. It is to be noted that the measured data included the effect of albedo, that could vary between summer and winter. Also, clouding could have an effect on the results obtained.

Figure 1.4, shows the mean monthly global radiation incident on the horizontal and on the plane-of-array for the period from July 1993 to October 1994, calculated from measured data. The annual mean was 4.7 kWh/m²/day on a horizontal surface and 5.24 kWh/m²/day on the array plane.

2. The operating temperature of the PV modules is widely known to attain 50 °C during summer [6, 72], but it decreases in winter and this would have a positive effect on their power production capabilities. Figure 1.5, shows the average bottom surface module temperature, the mean monthly maximum temperature and the maximum monthly temperature of the module attained during the day when the solar radiation was above 80 W/m², for the period July 1993 to October 1994. Below this value, the output of the array was always less than 5% of the nominal 1.2 kWp. From the graphs, it can be seen that the mean maximum temperature of the surface of the module did not exceed 52 °C.

3. For Malta, a 3-day period of no sunshine is expected, so an autonomy of three days was considered as sufficient for PV lighting systems with a moderate degree of reliability.

4. The electric load would be decreased in winter due to lower solar intensity but in summer it can be increased again. This would allow the optimum utilisation of the generated electricity according to its seasonal availability.

The above results were determined during the operation of the system, long after a tentative sizing of the system was done. They are presented here, to show that the parameters used for the design equations were appropriate, namely, an average annual global horizontal radiation of 5 kWh/m²/day, a mean PV cell temperature of 50 °C and an autonomy of 3 days for the battery storage.

MONTH	30°	45°	36° BY INTER-POLATION	36° MEASURED
JAN.	1.64	1.75	1.7	Jan '94 1.51
FEB.	1.42	1.5	1.47	Feb '94 1.33
MAR.	1.23	1.24	1.23	Mar '94 1.19
APR.	1.07	1	1.04	Apr '94 1.03
MAY	0.98	0.88	0.94	May '94 0.95
JUN.	0.92	0.8	0.87	Jun '94 0.92
JUL.	0.94	0.82	0.89	Jul 93/94 0.94
AUG.	1.01	0.94	0.98	Aug 93/94 1.01
SEP.	1.17	1.13	1.15	Sep 93/94 1.18
OCT.	1.36	1.42	1.39	Oct 93/94 1.3
NOV.	1.54	1.68	1.62	Nov '93 1.52
DEC.	1.61	1.8	1.72	Dec '93 1.64

TABLE 1.1: The tilt factors as calculated from the graphs of ref. [74]. The last column shows the tilt factors calculated from actually measured values taken between July 1993 and October 1994. For the months of July to October, the values shown are the mean of the corresponding months in the year 1993 and 1994.

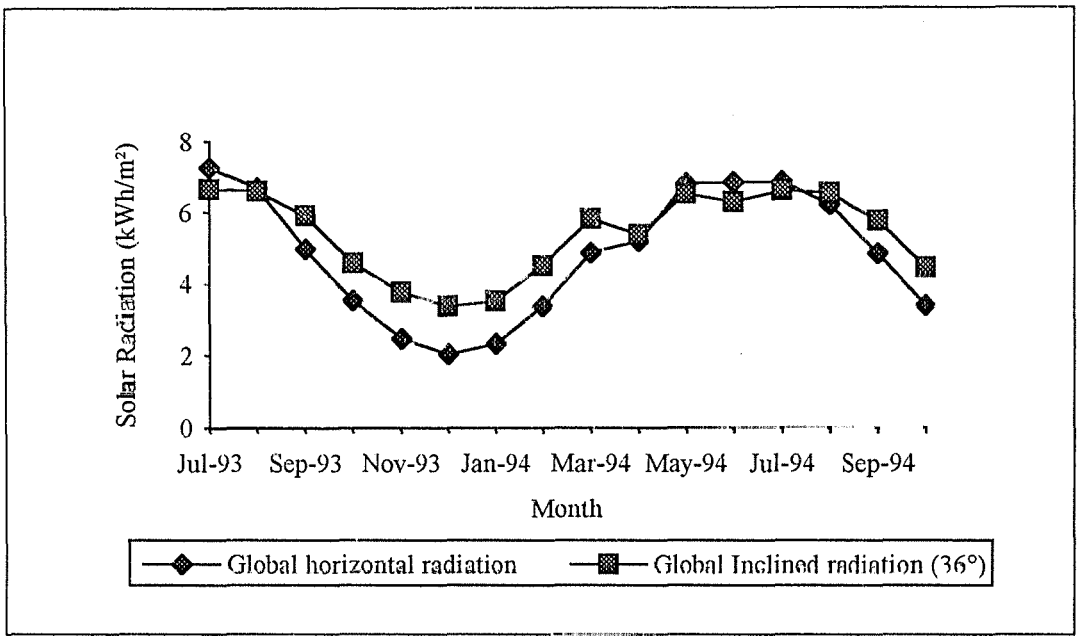

FIGURE 1.4: Measured mean monthly global solar radiation on a horizontal surface and on the plane of the PV array.

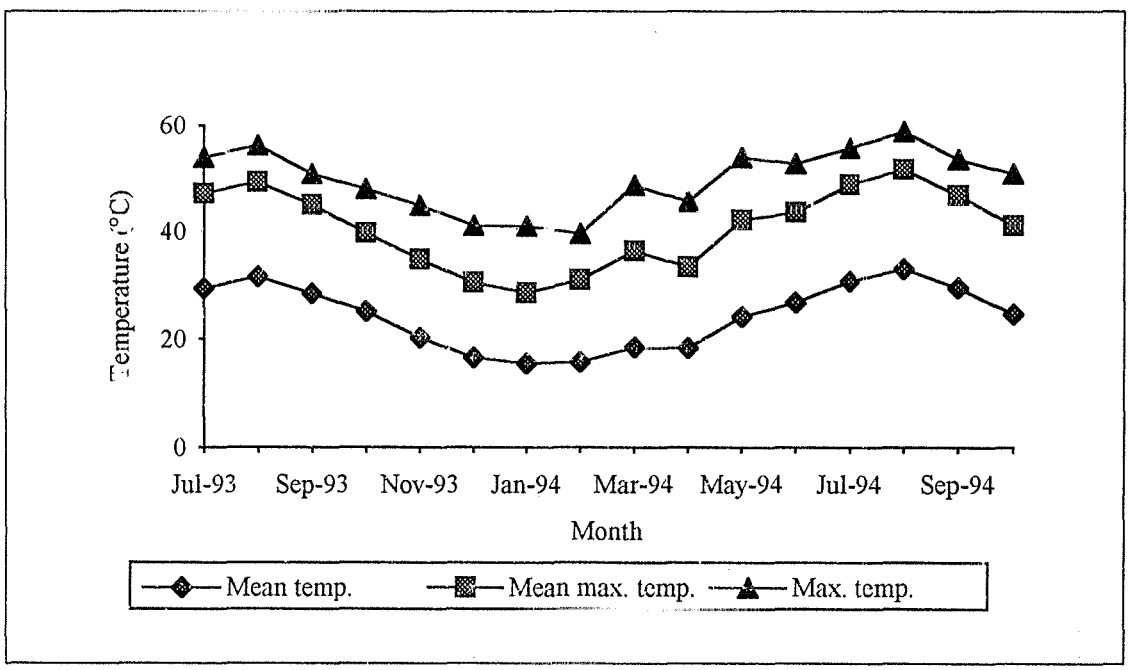

FIGURE 1.5: Mean monthly, mean maximum and maximum bottom surface temperatures of one PV module recorded during morning hours, for the period July 1993 to October 1994.

For silicon cells, the drop in efficiency is 0.4%/°C rise in temperature above the standard testing temperature of 25 °C. Therefore, the total drop in efficiency can be calculated from the following equation:

$$\text{Drop in efficiency} = 0.4(T_c - T_s) \quad \text{---------- (1.1)}$$

$$= 0.4(50 - 25)$$

$$= 10\%$$

where, T_c = cell temperature;

T_s = standard temperature.

This drop in efficiency will be taken as an oversizing factor of 0.1 in the following design equation [72]:

$$P_p\,(\text{STC}) = 1.1\,(W_l/\nu W_r) \text{ x } 1 \text{ kW/m}^2 \quad \text{---------- (1.2)}$$

where, P_p = reference array power at standard testing conditions (kWp);

W_l = useful output power (kWh per day);

ν = boss (gross) efficiency

= battery eff. x BCU eff. x matching eff. x conditioner eff.

= 0.8 x 0.95 x 0.95 x 0.9

= 0.65

W_r = global horizontal solar radiation (kWh/m^2 per day).

Hence, $W_l = 1.2 \text{ x } 5 \text{ x } 0.65/1.1$

= 3.54 kWh per day.

The array matching efficiency caters for the loss in power due to the different output voltages of the solar modules.

The battery size can now be determined from the following equation [39]:

$$E_b = W_l/V_b \text{ x } D/\text{DOD} \quad \text{---------- (1.3)}$$

where, E_b = battery rating (Ah);

W_l = input power (Wh per day);

V_b = battery voltage (V);

D = number of storage days (days of autonomy);

DOD = maximum depth of discharge.

Hence, E_b = 3540/12 x 3/0.45

≈ 2000 Ah

The electric load was comprised of 25 fluorescent lights, each rated at 0.9 A and operated for an average of 9 hours every night. For the months, November to February, only 18 lights would be switched on. The reason was that in winter, the average radiation on a horizontal plane drops to 2.6 kWh/m^2 and there would not be sufficient generated energy for all the lights.

Assuming that the temperature effect on the PV modules is reduced from 10% to 5% during winter, then the average output is calculated from equation (1.2) as 1.93 kWh/day, while the actual energy consumption of the lights would be:

E = n x p x t ---------- (1.4)

= 18 x 11 x 9

= 1.782 kWh/day

where, n = number of fluorescent lights;

p = power of one light (11 W);

t = number of operating hours per night.

Since, the consumption was less than the generated energy, then the load was expected to be fully satisfied. Also, the following had to be considered:

(a) As the batteries used for this project were not specifically designed for PV applications, a shallow depth of discharge was preferred to extend the battery life. Considering the actual consumption of the 25 fluorescent lights and using equation (1.3), the maximum DOD becomes:

DOD = 2475/12 x 3/2000

= 30%

This value was considered quite safe for these batteries.

(b) An allowance had to be provided for the seasonal charging of the batteries;

(c) The effective capacity of the batteries decreased in winter due to lower temperatures.

Table 1.2 shows the estimated mean monthly output and the load consumption, based on equations (1.2), (1.4) and figure 1.3. Whether these outputs would take place in reality

MONTH	ESTIMATED OUTPUT (kWh)	LOAD CONSUMPTION (kWh)
JANUARY	1.90*	1.78
FEBRUARY	2.57*	1.78
MARCH	3.47	2.47
APRIL	4.18	2.47
MAY	5.07	2.47
JUNE	5.43	2.47
JULY	5.51	2.47
AUGUST	4.92	2.47
SEPTEMBER	3.90	2.47
OCTOBER	2.87	2.47
NOVEMBER	2.12	1.78
DECEMBER	1.72*	1.78

* For these months the temperature effect on the efficiency was taken as a drop of 5% instead of 10%.

TABLE 1.2: The estimated mean monthly system output and the actual load requirements, calculated from equations (1.2) and (1.4), in kWh.

cannot be determined at this stage, because although solar radiation varies, the load was almost constant for extended periods of time. It might occur that on certain consecutive sunny days the batteries would get fully charged quickly, then the BCU would disconnect the PV array for the rest of the day and the actual generated power would be less than the estimated average.

From table 1.2, there seems to be a slight energy deficiency in December, but one has to keep in mind that the global radiation values on a horizontal plane of figure 1.3, were used in the calculation. Knowing that the radiation incident on the array during winter is greater than the corresponding global horizontal radiation, it could be safely assumed that the load would be satisfied. It was not possible to use the values of the radiation on the PV plane, presented in table 1.2, because they were not available at the time.

1.2 CHOICE OF THE PV MODULES

The choice of a module for a specific application requires a prior knowledge of the following information:

(a) Whether a battery control unit is used;

A discharged battery requires an initial high charging current. As it approaches its full capacity, the charging voltage should increase from about 13 V to 14.5V, while the current has to be lowered.

These requirements are satisfied by the I-V characteristic curves of PV modules, where the current decreases with increasing voltage between 13V to 15V. Hence, PV modules can be sized to charge batteries without the need for a battery control unit. In such cases, one has to ensure that the maximum current produced by the array is not so high as to cause gassing of the batteries when they are nearly fully charged. However, in doing so, it is inevitable that the current at the beginning of the day would also be low due to the weak solar intensity and this implies that the batteries would take a longer time to get fully charged. To increase the charging current, more modules have to be used.

However, the charging current would remain appreciably high even at noon-time, when the batteries have reached a high level of charge and here comes the need for a battery control unit, that will regulate the input current to the batteries for the rest of the day.

(b) Whether blocking diodes are in use;

The use of modules that have a high open-circuit voltage is desirable to compensate for the voltage losses caused by the presence of blocking diodes. Though germanium diodes cause a voltage drop of only 0.3 V, compared to 0.7 V for Schottky silicon diodes, nevertheless the latter types are commonly used because they can withstand higher reverse voltages.

(c) The ambient temperature of the site,

During the months when the mean temperature is above 20 °C, the temperature of a PV module could reach 50 °C at noon on a sunny day, which causes a drop in the open circuit voltage. To balance this effect, some extra cells in series are added to the module. Unfortunately, the voltage drops when it is mostly needed to remain high, i.e. at noon-time, when the batteries are approaching their full charge.

(d) The cost of the different types of modules;

The modules that are normally available in the local market are mono-crystalline, poly-crystalline and amorphous silicon modules. Amorphous silicon modules still suffer from low efficiency and degradation, though they are cheaper than the other two types. The cost of mono-crystalline modules is slightly greater than the semi-crystalline ones, but their efficiency is also higher. At the end, the choice seems to depend more on availability and the space required to place the PV array.

The PV array used in this project comprises of 20 Solarex MSX60 poly-crystalline silicon PV modules, each 60 Wp, that were donated by the Amoco Company. Each module can operate at 6 or 12 V.

Referring to appendix D, table D.5 gives the range of specifications for the PV modules used in this project. Detailed characteristics of each module are given in table D.6 and the main manufacturing stages, encapsulation and testing are described in table D.7, as supplied by the manufacturer. Typical I-V characteristic curves for the MSX60 modules and their mechanical characteristics are shown in figures D.2 and D.3.

1.3 DESIGN OF THE PV SUPPORTING STRUCTURE

Different types of materials can be used to build up the supporting frame such as aluminium, stainless steel and galvanised steel. Aluminium is light and does not rust but it is also more expensive than galvanised steel.

For the purpose of this demonstration project, a steel structure was designed. The frame was made into five identical pieces, that can be easily transported and fixed together by means of bolts and nuts. The design drawing of one piece is shown in figure C.1, of appendix C. Each piece can hold four modules, two on the top and two at the bottom, laid lengthwise and adjacent to one another.

Figure 1.6, shows a photograph of the structure with the PV modules fixed on it. The BCU is seen to the left, while the box containing the back-up monitoring integrators is placed to the right. The battery compartment was situated under the PV array.

The structure was inclined at an angle of 36° to the horizontal and was fixed on the roof of the Department of Chemistry at an elevation of 51.4 m above mean sea-level, facing the geographical South. Knowing the declination of the Sun for that time of the year from "The Star Almanac", which is published annually and finding the direction of the magnetic South, the true South could be easily determined to a fair degree of accuracy [77]. Other methods are available such as making use of the north pole star (Polaris) at night or observing the meridian transition of the Sun at noon

The lower edge of the structure was made 40 cm above the roof level, to reduce the warming up of the back of the modules by the heat radiating from the roof.

1.4 CHOICE OF THE STORAGE BATTERIES

Batteries that are specifically designed for PV systems are expensive. Hence, the choice was limited to normal starting-lighting-ignition (SLI) batteries or traction batteries. The latter have higher cycle life for deep discharges and are more reliable than SLI batteries. The common disadvantages of these batteries are:

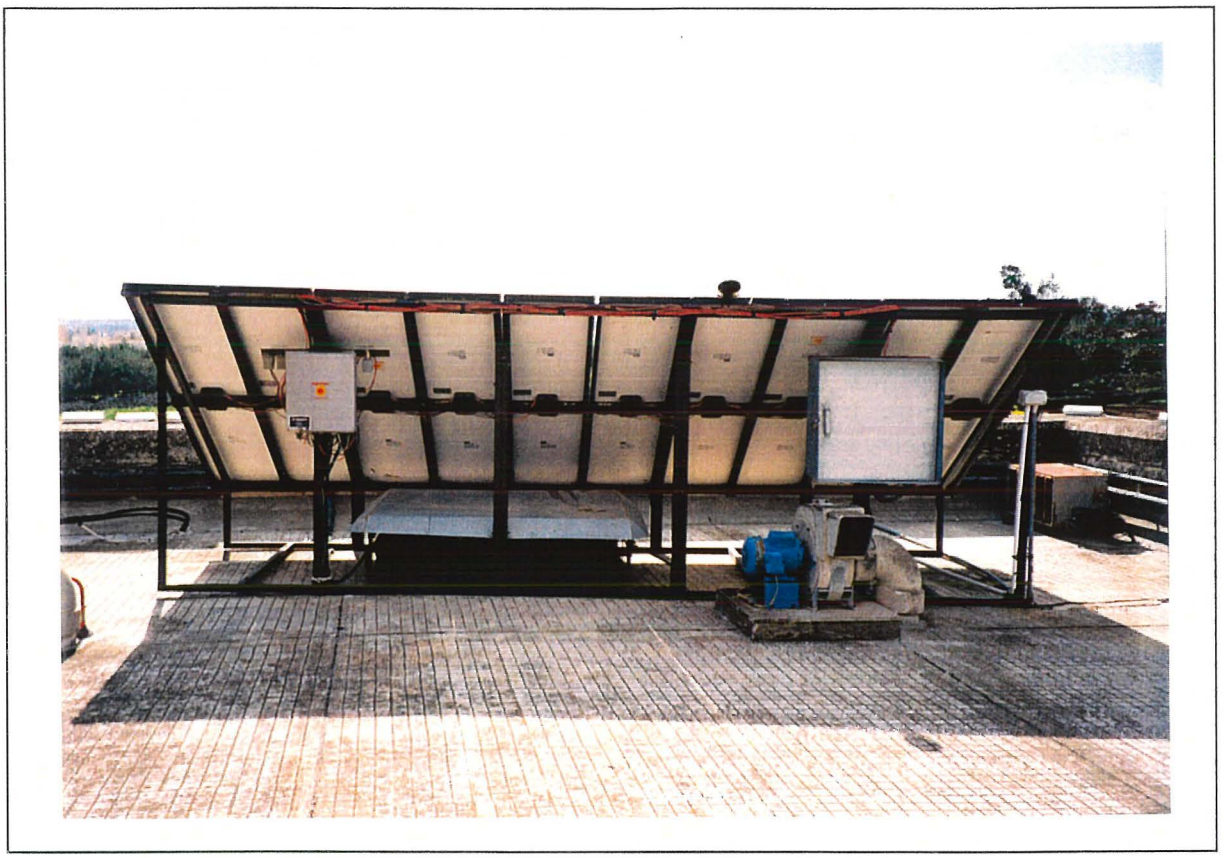

FIGURE 1.6: A photograph showing the PV system, comprising of the PV array, the battery storage underneath, the BCU to the left and the back-up integrators to the right.

(a) They require a control unit to limit the depth of discharge;

(b) Their self discharge increases with time;

(c) Acid fumes are given off while in use;

(d) High loss of distilled water from the vents;

(e) Regular inspection and maintenance are required.

When comparing these characteristics to the requirements of a good solar battery that were listed in section B.15 of appendix B, one realises that there is still a need for an improvement in the design of batteries, but having no option except to choose between the available types of batteries, the traction batteries were used and some safety precautions were implemented to protect them.

Firstly, a BCU was used to limit the input and output charge. Secondly, the batteries were placed under the PV array where the temperatures are equal to the air temperature, that does not normally exceed 33 °C in summer and 9 °C, in winter. Other advantages of placing the batteries under the array were the use of shorter cables which reduced power losses. Thirdly, regular maintenance was ensured: topping up the cells with distilled water, inspecting and cleaning the poles of the batteries and monitoring the voltage of the cells, the specific gravity and temperature of the acid. Fourthly, a boosting charge was given to the batteries, whenever changes in the cells' voltages or specific gravity were detected.

Batteries are found in different rated capacities, sizes and weights. The reasons for choosing one size of battery to another were to minimise the space needed for the accommodation of the batteries, to reduce maintenance work and to enable handling the batteries manually, without excessive effort or need of lifting cranes.

To satisfy the required design capacity of 2000 Ah, ten, 12 V batteries, type SB (locally assembled) were purchased. Each battery was made up of 6 cells in series with a rated capacity of 200 Ah. The terminals of each cell were bare to be able to check its voltage. No performance characteristics of these batteries were available.

The batteries were placed in an open structure and covered with a galvanised steel cover to protect the surface of the batteries from dew and rain. Moreover, the box was designed in

such a way that when the cover was opened there would be ample space to inspect, test and maintain the batteries. Bars were welded to the sides of the box to protect the batteries from vandalism. The material of the box and cover structure was mild steel, painted with a protective paint. Figure C.2, of appendix C, shows the design of the box and its cover, while figure 1.7 shows a photograph of the box with the batteries placed in it under the PV array.

1.5 CHOICE OF THE BATTERY CONTROL UNIT (BCU)

The choice of the BCU depends on the degree of reliability required, the availability and cost of the unit. In section B.16 of appendix B, the main types of charge controllers had been discussed. A BCU that uses transistors as switching units is more reliable than one which is controlled by relays. In more sophisticated systems, the use of a two-step regulator gives the chance for the operator to utilise the extra array energy to operate a secondary load in the morning.

In all cases, care must be taken not to exceed the maximum current that the BCU can handle and for larger systems, it would be better to divide the load into a number of smaller units, rather than to use one large BCU. By decentralising the power, the system would work even if part of it is out of order. Also, all the units would be working near their optimum load, which entails higher operating efficiency.

For this project, a Photowatt (France) PWR5421AS BCU with 4 separate mercury relays and blocking diodes, LED battery-state indicators, high voltage protection unit, low-voltage cut-off control and surge protection, was chosen. Each relay can handle a maximum of 20 A, which allowed a string of five Solarex MSX60 modules in parallel to be connected to it. The output relay was rated at 35 A.

Table D.8, of appendix D, gives the electric and mechanical characteristics of the BCU.

1.6 DESIGN OF THE WIRING CONNECTIONS

One of the factors that affect the overall efficiency of PV systems and which might pass

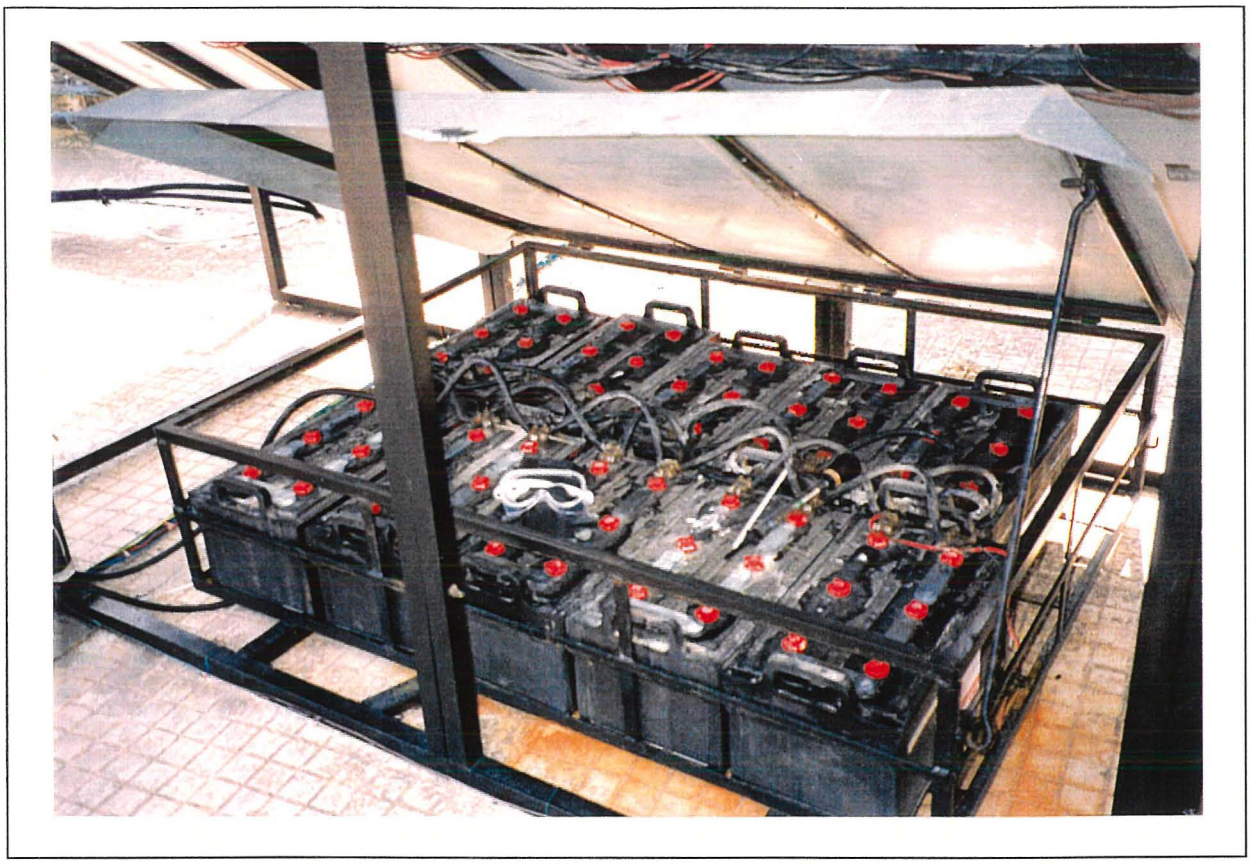

FIGURE 1.7: A photograph showing the battery storage placed under the PV array.

unnoticed is the improper design of wiring. Cables of insufficient size result in power losses and overheating which could cause fire.

To ensure minimum voltage drop along the cables, the proper sizes of the wires were determined for each route separately. Table 1.3, lists the sizes of the wires and their design specifications, based on a voltage drop of 0.5 V across the ends of the cables.

Following the same strategy of decentralisation used for the module connections, the fluorescent lights were divided into parallel groups each consisting of three lights in parallel. Other advantages of the use of parallel circuits were the use of smaller diameter wires, less need for special tools and fixtures and better control and management of the electric load.

Single PVC-insulated wires were used throughout, while special battery single cables connected the BCU to the batteries and the batteries to one another.

1.7 LOAD CONTROL AND MANAGEMENT

Power was delivered from the batteries through the BCU, via a 35 A fuse, to three light sensitive relays that were normally open, in the morning. At night, the relays closed and supplied the power to three timers, which energised the fluorescent lights. Each one of these relays and timers could carry a maximum current of 10 A.

The type of the light sensors was FINDER (Italy), type 10.11. The electronic circuitry was modified to make the sensors work on 12 V d.c. supply rather than 220 V a.c. supply. Technical data is given in table D.9, of appendix D.

The brand of the timers was SERAI (Italy). They had six functions including a delay in operation and a flashing mode, but for this project only one mode of operation was used, namely, the control of the number of hours that the lights operate from the moment the light sensors supply power to the timers. The technical data is found in table D.10, of appendix D.

Depending on the state of charge of the batteries and on the available radiation during an extended period of time, the load consumption was varied to make optimum use of the available energy. Naturally, it was much easier to manage the load during summer.

WIRING ROUTE	MAX. CURRENT (A)	MAX. CABLE LENGTH (m)	MIN. SIZE OF CABLE (mm^2)
MODULES - BCU	19	4	6 (SWG* 10)
BCU - BATTERIES	76	3	10 (SWG 8)
BCU - LIGHTS	2.7	10	4 (SWG 12)

*SWG = standard wire gauge.

TABLE 1.3: Calculated minimum cable sizes for the PV system and their design limits.

1.8 DESIGN OF THE MONITORING SYSTEM

Following the instructions set in the Guidelines for the Assessment of Photovoltaic Plants, Document A, that was prepared by the Joint Research Centre, Ispra Establishment [37], two independent monitoring systems were constructed. A Campbell 21X micrologger served as the backbone of the monitoring system, while three mechanical integrators made the back-up system. The back-up mechanical integrators were supplied by SUNPOWER (Germany) and they consisted of an insolation integrator, a two-channel current integrator and a power integrator.

The insolation integrator was used in conjunction with a MATRIX (U S A) silicon cell pyranometer to monitor the solar radiation incident on the array plane, in kWh/m^2. The two channels of the current integrator monitored the output current capacity from the PV array and from the batteries in Ah, while the power integrator read the output energy of the array in kWh.

The Campbell 21X micrologger is a portable battery-powered data-logger, that can be programmed by a special machine language, to sample data at regular intervals, together with the possibility of conditional logging, on-line computation and control of external circuits. There are 16 single-ended input channels that can be used as 8 differential analogue inputs, 4 switched excitation outputs, 4 pulse counters, 6 digital control ports and 2 programmable continuous analogue outputs. Detailed specifications are given in table D.11, of appendix D. Figure 1.8, shows a photograph of the data-logger and the weather station with the probes fixed to it. The PV system appears in the background.

Being the main monitoring equipment, the micrologger was programmed to monitor all the required data as follows:

(a) Humidity (%): measured using an MP100 ROTRONIC C-80 HYGROMER solid state humidity sensor, that changes its electrical characteristics with variations in humidity. These changes were detected, linearised and amplified by electronic circuitry within the probe and the resulting signal was fed to the data-logger, via a single-ended analogue input channel.

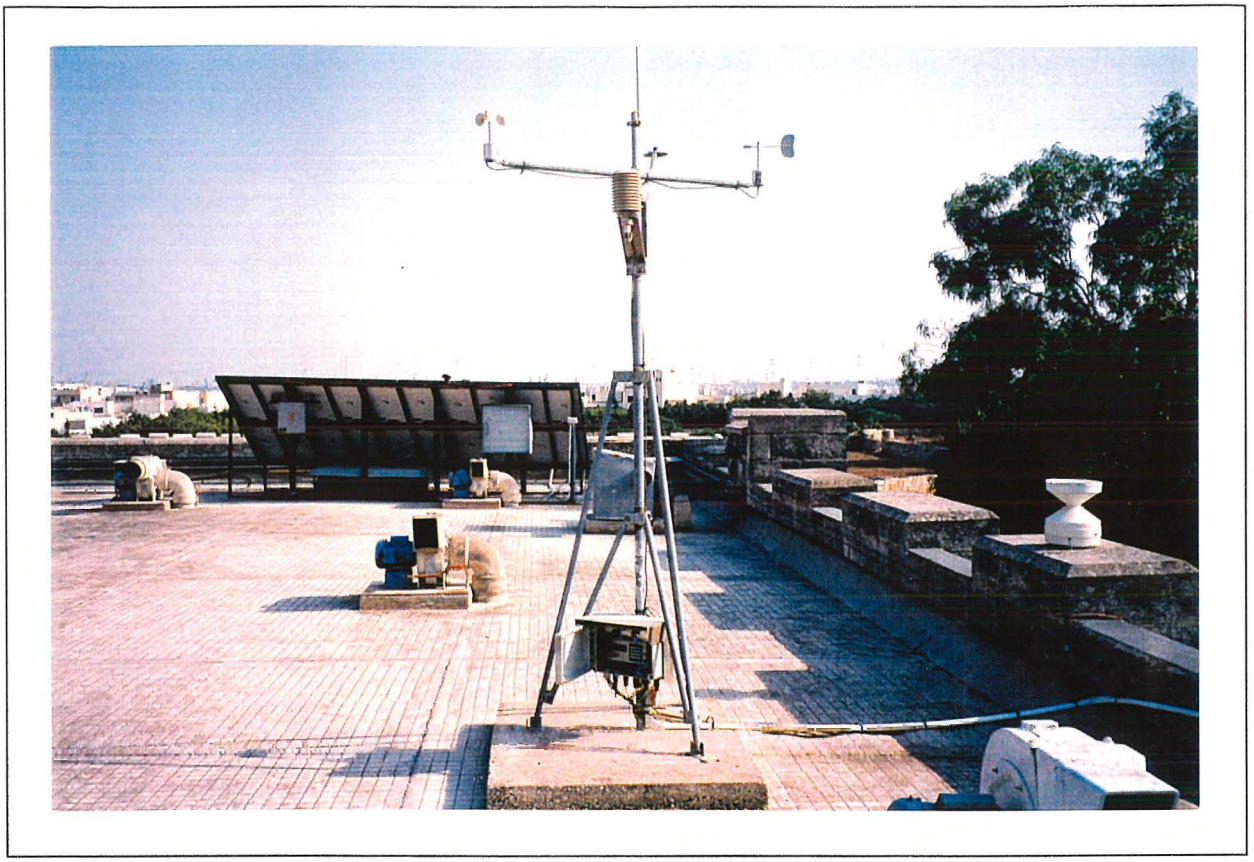

FIGURE 1.8: A photograph of the data-logger and some probes fixed on the weather station. The PV system is seen in the background.

(b) Ambient temperature (°C): measured with a resistance thermometer that is integrated in the same probe as the humidity sensor. The probe was put inside an unaspirated radiation shield, to measure the shade temperature and to protect the probe from direct contact with rain which could cause erroneous readings. The signal was fed to another single-ended analogue input channel in the micrologger

(c) Upper surface temperature of a PV module (°C): measured using an OMEGA self-adhesive copper-constantan thermocouple. The thermocouple was stuck to the upper surface of a PV module, to measure the temperature of one cell, selected at random. The output voltage was directly fed into an analogue differential channel. The micro-logger had an in-built function that can be programmed to convert the thermocouple voltage output to a temperature reading.

(d) Bottom surface temperature of a PV cell (°C): measured using another OMEGA thermocouple. The reason for measuring the upper and the lower surface temperatures was to see if there would be any difference between them. It was noted in the literature that some authors had measured the bottom surface temperature [67], while others measured the top surface temperature [73]. The output was fed into a separate differential analogue channel. Both thermocouples were referenced to the ambient temperature.

(e) Global horizontal radiation (W/m^2): measured using an LI200SZ LI-COR solar cell pyranometer that was calibrated by the manufacturers, against an Eppley precision spectral pyranometer, as stated on the calibration certificate. The LI-COR pyranometer is a compact, high-output, thermally stable silicon photocell that is sensitive to light between 400 and 1100 nm.

The output voltage was fed as a single-ended signal to one of the data-logger analogue inputs. The sensor was put at a height of 53.8 m above mean sea-level, at latitude 35° 54′ 13" and longitude 14° 29′ 05", and 13 m away from the PV array.

(f) Radiation at the plane of the PV array (36° to the horizontal, in W/m^2): measured using a MATRIX solarimeter, calibrated by the manufacturers against a thermopile radiometer. The sensor incorporates a silicon PV cell as a sensor, that has a response from 0.35 to 1.15 microns.

The pyranometer was bolted to a plate that was fixed to the upper end of a PV module, almost half-way on the array, at a height of 53 m above mean sea-level. The output voltage of the sensor was directly fed to a differential channel in the data-logger. This pyranometer was also linked in parallel to the back-up insolation integrator.

(g) Wind speed (m/s): measured using an A100R VECTOR switching anemometer, which contains a magnet that turns with the rotor spindle and produces a varying field. The variation in the field causes a mercury wetted reed switch to make and break contact once for every revolution of the rotor. The anemometer was connected to a pulse-counting channel of the data-logger.

(h) Wind direction (bearing from the North): measured using a W200P VECTOR potentiometer windvane. To measure the wind direction, a supply voltage was provided by the datalogger at fixed intervals, as set by the programme. A delay of few milli-seconds was allowed to give sufficient time for the reading to settle down and then it was sensed through a single-ended analogue input channel. The computer programme also determined the standard deviation of direction.

(i) Rainfall (mm): measured using an ARG100 tipping bucket raingauge. Rain was collected in a bucket that tips from one side to the other and forces a magnet to pass a reed switch, which makes contact for a few milliseconds. The raingauge was connected to a pulse-count input channel in the data-logger. Each tip of the bucket corresponded to 0.198 mm of rainfall.

(j) Output current from the PV array (A): The current generated by the array can reach 60 A, so it cannot be directly fed into the data-logger and not even to the back-up two-channel current integrator. To solve this problem, the wires were passed through a hall sensor that produced a lower current signal that was proportionally equal to 1/1000 of the current passing through it. This signal was fed into the integrator, which had a mechanical counter and a separate analogue output terminal. The counter served as the back-up monitoring system while the signal from the analogue terminals was fed to a differential channel in the data-logger. The output from these terminals could reach 10 V which corresponded to a current of 100 A passing through the hall sensor. Again, this signal was too high to be fed into the logger,

which did not tolerate higher than 5 V. So a voltage divider was incorporated to reduce the voltage by 50% and a multiplying factor was introduced in the programme of the data-logger to convert the reading back to the true value.

(k) Output current from the batteries (A): The wires that delivered power to the fluorescent lights, the integrators and the data-logger, were passed through a hall sensor, whose output was directly connected to a single-ended terminal in the two-channel current integrator. Similar to (j) above, the mechanical counter counts the number of Ampere-hours consumed, while the outputs from the analogue terminal and earth were fed into a differential channel in the data-logger. Here, no voltage divider was used because the current consumption of the lights and the monitoring equipment did not exceed 26 A, which corresponded to an analogue output of 2.6 V. This voltage was well below the 5 V input limit to the data-logger.

(l) Output power from the PV array (W): The signal was taken from the analogue terminals of the back-up power integrator and fed to an analogue differential channel in the data-logger. A voltage divider was used as in (j) above to reduce the voltage to a value less than 5 V.

The specifications of all the monitoring equipment are shown in tables D.12 - D.17, of appendix D. The signals from the integrators were connected to differential channels in the data-logger, to eliminate noise or distortion during data sampling.

Readings were taken automatically every five minutes for parameters (a) to (d), stored in an intermediate stage memory, averaged every fifteen minutes and the result was stored in the final memory. As for the other parameters, readings were taken every twenty seconds and averaged over a 15-minute interval, except for rainfall, which was summed up. The results were stored with the other previous parameters, in ASCII characters. Hourly and daily averages were then processed from the basic 15-minute interval data. Rainfall data was continuously summed up for the whole day.

Some logical conditional commands were added to purify the data from any parasitic results. For example, at night a small current was seen to leak through the blocking diodes back into the array. The result was that a negative reading was recorded for (j) and (l), above.

Lightning, light reflection from clouds or hanging dust and temperature effects made the

pyranometers record some radiation at night. Since the system was not sensitive to these small variations, it was decided to eliminate them, to assist in data analysis and to make a definite division between day and night. At night, the solar radiation and the array output must be zero. These refinements were gained from experience between February 1993 and June 1993.

Table C.1, of appendix C, shows the computer programme that was devised to carry out the monitoring jobs. It was divided into two main tables. The first, contained all the commands that were initialised every 5 minutes and the second gathered all those that occurred at 20 seconds intervals. These were followed by the processing commands such as averaging and totalling.

A 3A fuse and a voltage limiting integrated circuit no. 78T12CT (3 A) were incorporated and were placed together with the dividing resistors inside the micrologger weather proof compartment. The data-logger was connected to the serial port of a personal computer (PC) via an SC932 9-pin, an RS232-DCE interface, two RAD SRM asynchronous short range modems and two RAD SP surge protectors. Specifications of the interface modems are given in tables D.18 and D.19, of appendix D. Figure 1.9, shows a block diagram of the order of connections.

Data was transferred from the micro logger to the hard disk of the PC, with the aid of a special support software programme supplied by Campbell Scientific and called "TELCOM". Other software programmes included "TERM" that enabled the transfer of programmes, the monitoring of the input stations and the adjustment of the micro-logger clock, "SPLIT" which allowed the manipulation of data and the creation of new files that contain data of a specific criteria, "EDLOG" which aided in the programming of the data-logger and "SMCOM" which could be used to transfer data that was collected in the field by solid state storage modules to the PC.

The back-up integrators were grouped together in a galvanised steel box, fixed to the array. Voltage limiting integrated circuits no. 7812CSP (1 A), joined to aluminium heat sinks were incorporated to protect them.

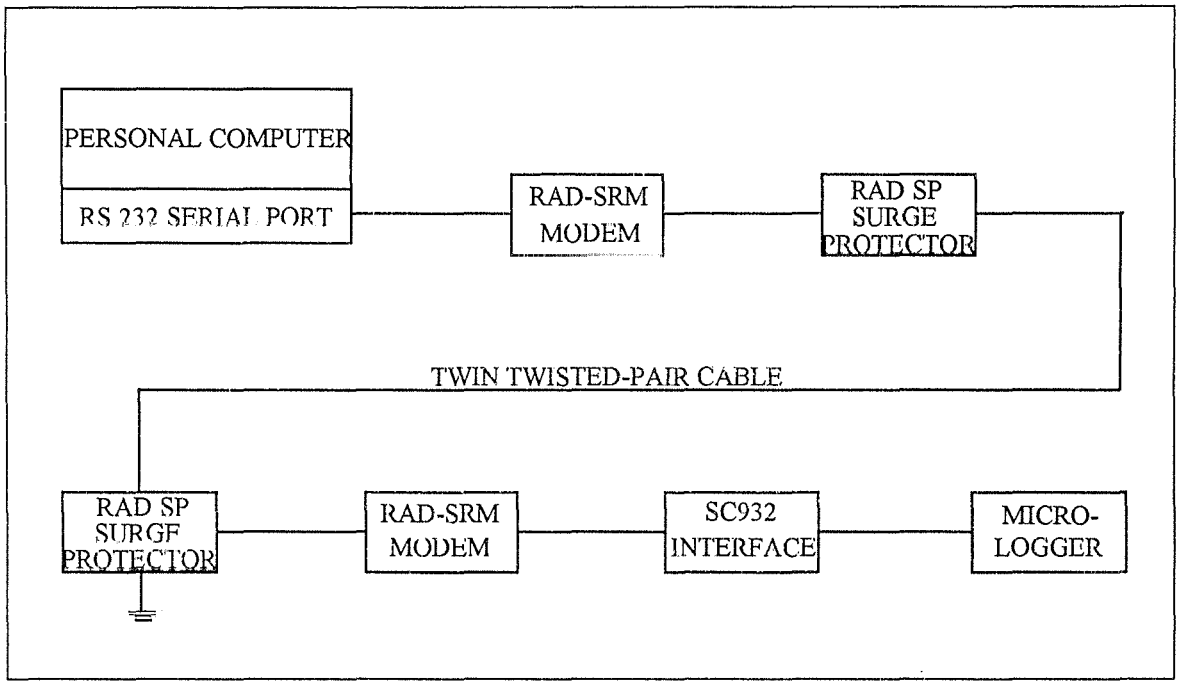

FIGURE 1.9: A block diagram showing the connections made between the data-logger and the personal computer.

WIRING OF THE INTEGRATORS

The voltage signal was directly fed from the MATRIX solarimeter into the signal terminals of the insolation integrator, while d.c. power from the batteries was supplied to the proper terminals.

As for the other two integrators, the input signal could not be directly fed into them, because they carried high currents. Hall sensors were used instead, that proportionally converted the current passing through them to a lower current suitable to be fed into the integrators. The hall sensors received their supply of + 15 V and - 15 V, from the dedicated terminals of each integrator

When current passed through the power cables, a proportional current was produced by the hall sensors which was 1/1000 of the main current. It was fed into the integrator via a single-ended wire of each channel.

CALIBRATION OF THE INTEGRATORS

(a) The insolation integrator:

This integrator was used with a MATRIX (U.S.A.) Mk 1-G solarimeter that had an output of 38.4478 mV at an irradiation of 1000 W/m^2, as provided in the certificate of calibration. The integrator had now to be calibrated accordingly.

The calibration was done as follows: A constant voltage power supply type: THANDAR TS1541S (U.K.), was connected to the signal terminals. The voltage was adjusted to read 38.45 mV. The integrator was energised by a 12 V d.c. source.

Then, the adjusting screw on the front of the integrator was rotated until the reading on the LCD screen of the integrator showed 1000 W/m^2. For double checking, the reading at the analogue output terminals of the integrator was found to be 10 V and at the pulse output terminals was 10 kHz.

(b) The power integrator:

This integrator had no adjusting screw, but a test was carried out to ensure its proper operation. For this integrator there were two inputs namely, the voltage and the current. After connecting a 12 V d.c. power supply to the integrator, a constant d.c. source of 12 V was fed into the voltage terminals, and a variable current source was used at the current input terminals. By varying the current between 0 and 100 mA, in steps of 10 mA, the readings that appeared on the LCD screen of the integrator were compared to the product of the corresponding input voltage and current. As they were found to agree, the integrator could be accepted as properly calibrated.

(c) The two-channel current integrator:

The integrator was connected to a 12 V d.c. supply and a calibration test was carried out for each channel separately as follows: A constant voltage source of 5V and 100 mA, that corresponds to a current of 100 A passing through the hall sensor was connected to sensor terminals. The adjusting screw on the front of the integrator was adjusted so that the analogue output reading was 10 V and the pulse output read 10 kHz.

These methods of calibration were not clearly defined in the user's manuals of the integrators, but were acquired after direct communication with the manufacturers.

The power integrator did not function properly when operated with the hall sensor, because one of the terminals was not referenced to the ground. It took almost six months of communication and tests to discover the cause of the malfunction. The reason that the terminal was not originally referenced to the ground, like the other integrators, was not known but it could be presumed to be an unintentional manufacturing error.

1.9 DESIGN OF THE CASE FOR THE INTEGRATORS

Using the available material and funds, a casing had to be designed that would protect the integrators from direct precipitation of dew, rain and solar radiation. The best material to be

used should be glass reinforced polyester similar to the one supplied to protect the micrologger and the BCU, but this material and the necessary moulding machines were not available. At the end galvanised steel sheets were used.

To shadow the casing and its contents from the sun, it was installed on the PV array and facing North To make sure that no rain water seeped in, the edges were extended by 10 cm, as shown in figure C.3, of appendix C. As for humidity, the integrators were individually properly sealed with a silicon sealant. Figure 1.10, shows a photograph of the installed box with the integrators fixed in place.

Three small 12 V bulbs were installed inside the compartment to provide light during the taking of readings at night. The power consumption of the lights and the integrators were accounted for as part of the total load, by passing all the wires through the hall sensor of the second channel of the current integrator, before connecting them to their terminals.

1.10 INSTALLATION OF THE PV SYSTEM

Five separate PV array structures, were taken up on the roof of the Department of Chemistry, at the University of Malta, (latitude 35° 54′ 13", longitude 14° 29′ 05") and at a height of 51 4 m, above mean sea level. They were joined together by means of stainless steel bolts and nuts, and on each structure four PV modules were fixed.

Next, the battery case was manufactured, covered with an anti-rust paint and put under the PV array. Then, the batteries were put in place. There was a delay in transporting this equipment up the stairs, which are the only accessible means to reach the roof, owing to its heavy weight.

The BCU was bolted to the PV array structure and put close to the batteries, about 1 metre above roof level and facing North. The casing for the integrators was also bolted to the array structure, but not near the BCU, because together with the BCU, they might hinder the free circulation of air under the modules which need to be cooled.

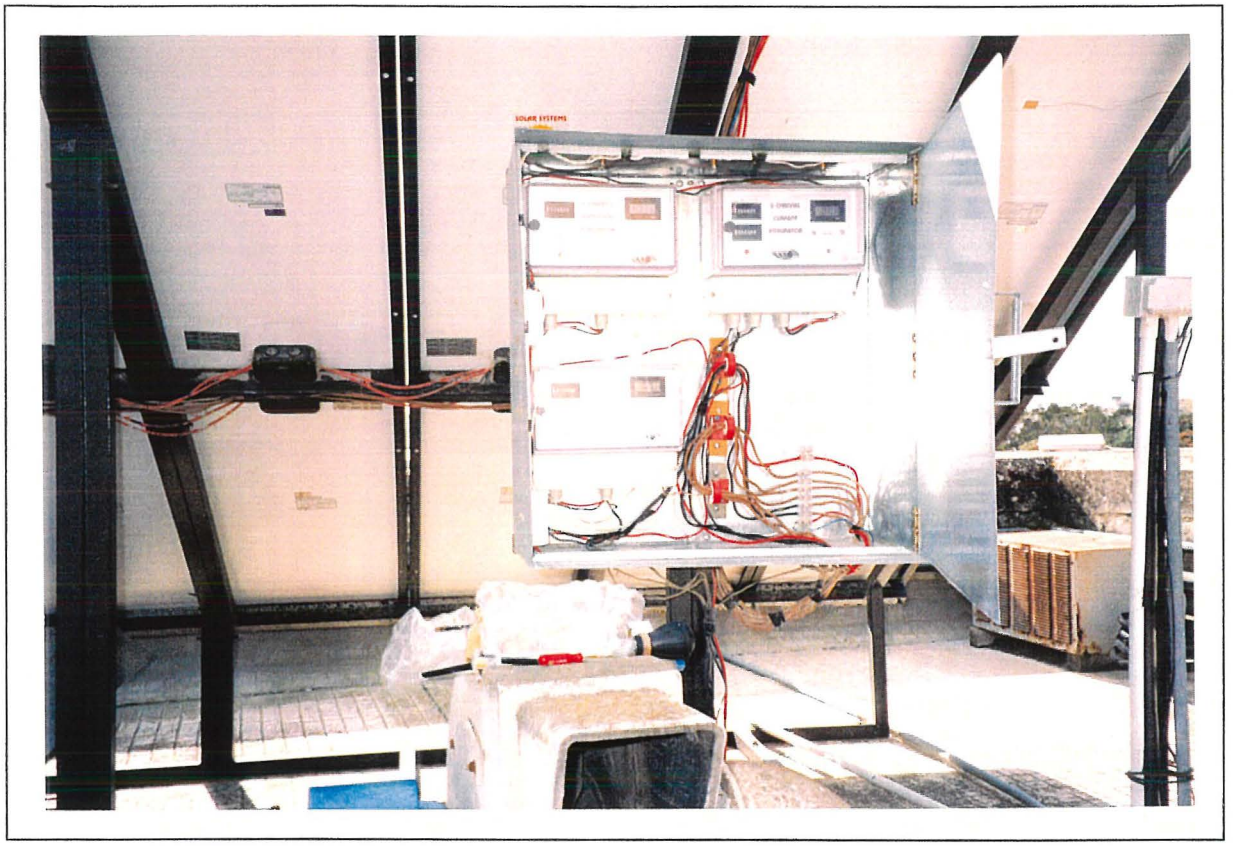

FIGURE 1.10: A photograph of the box with the integrators fixed in place.

Every five modules were connected in parallel and joined to a separate relay and blocking diode in the BCU, with single wires of size 6 mm^2 (SWG 10). Two thick cables were then connected between the BCU and the batteries, which were wired in parallel with each other. Sixteen, 4 mm^2 (SWG 12) single wires were then connected to the load terminals of the BCU, eight to the positive and eight to the negative terminals, to supply power to groups of three fluorescent lights connected in parallel. The last group had 4 fluorescent lights to make a total of 25 lights.

The array-BCU cables and the BCU-lights wires were first passed through the hall sensors of the integrators, to monitor the performance of the PV system, in this manner: First, the array-BCU wires were passed through the hall sensor of the first channel of the two-channel current integrator and then passed through the hall sensor of the power integrator. Second, the wires carrying the power to the fluorescent lights were passed from the BCU, through the hall sensor of the second channel of the current integrator, back to the light sensing relays and timers and then to the loads, while the wires that supply power to the monitoring equipment were passed through the last hall sensor and then directly to their respective terminals. Earthing of the data-logger and the BCU was carried out.

After programming the data-logger, the system was commissioned on 19th February 1993. During the next four months, experience was gained on the process of data collection and several problems were corrected as described in the next chapter.

The beginning of the official collection of data was on July 1st, 1993.

1.11 PRECAUTIONS TAKEN DURING INSTALLATION

Some precautions were implemented during installation to ensure the safety of the personnel and the proper operation of the system:

(a) works were carried out in late afternoons to avoid risk of electric shock or short-circuit;

(b) work was suspended during or immediately after a rainfall;

(c) there was a continuous checking of the polarity of all terminals to avoid wrong connections;

(d) proper levelling of the pyranometers;

(e) close inspection of the contractor's work;

(f) earthing of all electronic equipment.

The ordering of the equipment and installation of the PV system and the weather station took six months to be completed.

CHAPTER TWO

OPERATION AND MAINTENANCE

INTRODUCTION

In this chapter, the performance of the PV array and the balance of system components are presented, followed by a description of the maintenance procedures applied to ensure best results. At the end, a table of the necessary maintenance jobs is outlined.

2.1 EXPERIENCE GAINED AT THE BEGINNING OF OPERATION

In February 1993, the PV system started producing power while the monitoring system was being set up until the whole project was ready for operation at the beginning of July 1993. In the mean time, experience was gained and several problems were solved. Eighteen out of the twenty five fluorescent lights were in use during the first year of operation due to a delay in the supply of the required quantity.

As mentioned in section 1.8, the data that was monitored by the back-up integrators was also monitored by the data-logger. However, the multiplying factors that had to be included in the monitoring programme to convert the signals to their true values, had to be determined by:

(a) assuming approximate values;

(b) writing them in the programme;

(c) loading the data-logger with the programme;

(d) perceiving the total after 24 hours, and

(e) comparing the results to the integrated values registered by the corresponding integrators.

Better approximations were determined by multiplying the originally assumed values by the ratio of the two monitored readings. This was repeated until the two readings were very

similar. It was noted that the factor used in the micro-logger programme could not be greater than 5 digits. This might have limited the accuracy of the results but did not really affect it.

Table 2.1 and figure 2.1, show the comparison made between the readings taken with both the data-logger and the integrators. It is to be noted that the data-logger took instantaneous readings every 20 seconds and averaged them every 15 minutes, while the mechanical integrators continuously monitored and integrated the results instantaneously

A test was carried out on the two pyranometers used to demonstrate their proper calibration. They were placed horizontally side by side and connected to the data-logger. The results obtained showed that the difference between the two readings did not exceed 5% both on cloudy and sunny days.

The main problems that were remedied were:

(a) the occurrence of out of range data;

(b) bad collection of data, due to the poor quality of the floppy disks; and

(c) interference during data collection in the morning.

Out of range data occurred when the readings were too high for the data-logger to read at low resolution. Low resolution mode was chosen because it required less memory per character than high resolution. The solution to the problem was achieved by including a multiplier in the programme which converted the values to higher units, e.g. W/m^2 to kW/m^2.

As for data collection, new high quality diskettes were used and the retrieval of data from the data-logger was conducted at night, when most of the surrounding electric exhaust fans of the Chemistry laboratories were not in use.

2.2 MAINTENANCE OF THE PV ARRAY

During the past two years, while the array was exposed to the Sun, some discoloration of the cells was noticed, as shown in figure 2.2, but no physical deterioration or humidity penetration was noted in the modules. At the back of the modules, the outer white tedlar layer had slightly deformed, due to temperature variation. No corrosion had occurred at the

TABLE 2.1: Comparison between the monthly totals of the readings taken by the datalogger and the back-up integrators.

Δ = difference between two readings expressed as a percentage of the integrator's reading.

Inplane Radiation (kWh/m²)				Input Current to Batt (Ah)			
	Data-logger	Integrator	Δ %		Data-logger	Integrator	Δ %
Jul-93	203.5	202.34	0.573	Jul-93	7307.7	7328	-0.277
Aug-93	204.4	203.31	0.536	Aug-93	8311.4	8348	-0.438
Sep-93	177.5	176.39	0.629	Sep-93	7976.2	8002	-0.322
Oct-93	142.4	141.25	0.814	Oct-93	7582.7	7585	-0.030
Nov-93	113.16	112.1	0.946	Nov-93	5495.9	5474	0.400
Dec-93	104.87	103.25	1.569	Dec-93	6048.2	6004	0.736
Jan-94	108.91	108.12	0 731	Jan-94	6121.2	6092	0.479
Feb-94	126.57	125 65	0.732	Feb-94	5765.6	5715	0 885
Mar-94	180.58	179 18	0 781	Mar-94	9445	9449	0.042
Apr-94	161.22	159.74	0.927	Apr-94	8574	8572	0 023
May-94	202.12	200.23	0.944	May-94	10374	10406	-0.308
Jun-94	197.52	193.88	1.877	Jun-94	9764.3	9704	0.621
Jul-94	205.13	203.34	0.880	Jul-94	9692.8	9730	-0.382
Aug-94	202.9	201.43	0.730	Aug-94	9660.9	9720	-0.608
Sep-94	167.53	166.07	0.879	Sep-94	8156.7	8178	-0.260
Oct-94	143.85	142.21	1.153	Oct-94	7772.5	7753	0.252
Battery Output Current (Ah)				Array Output Energy (kWh)			
Jul-93	5458.5	5554	1.7195	Jul-93	101.529	101.71	-0.178
Aug-93	6125.3	6197	-1.157	Aug-93	116.561	116.43	0.11251
Sep-93	6552.2	6641	-1.3371	Sep-93	113.03	112.96	0.06197
Oct-93	6283.8	6368	-1.3222	Oct-93	106.89	106.77	0.11239
Nov-93	4363.3	4387	0.5402	Nov-93	78.352	78.27	0.10477
Dec-93	5087	5135	-0.9348	Dec-93	86.485	86.03	0.52889
Jan-94	5122.2	5125	-0.0546	Jan-94	86.933	86.9	0.03797
Feb-94	4483.7	4513	-0.6492	Feb-94	80.828	80.62	0.258
Mar-94	7455.7	7587	-1.7306	Mar-94	134.535	134.01	0.39176
Apr-94	6817.6	6905	-1.2657	Apr-94	121.06	120.82	0.19864
May-94	7682.6	7808	-1.606	May-94	146.272	145.97	0.20689
Jun-94	7719	7798	-1.0131	Jun-94	135.584	134.19	1.03883
Jul-94	7466	7624	-2.0724	Jul-94	134.213	134.17	0.03205
Aug-94	6417.8	6518	-1.5373	Aug-94	134.23	134.19	0.02981
Sep-94	4733.2	4777	-0.9169	Sep-94	114.886	114.87	0.01393
Oct-94	5596.9	5647	-0.8872	Oct-94	109.027	108.96	0.06149

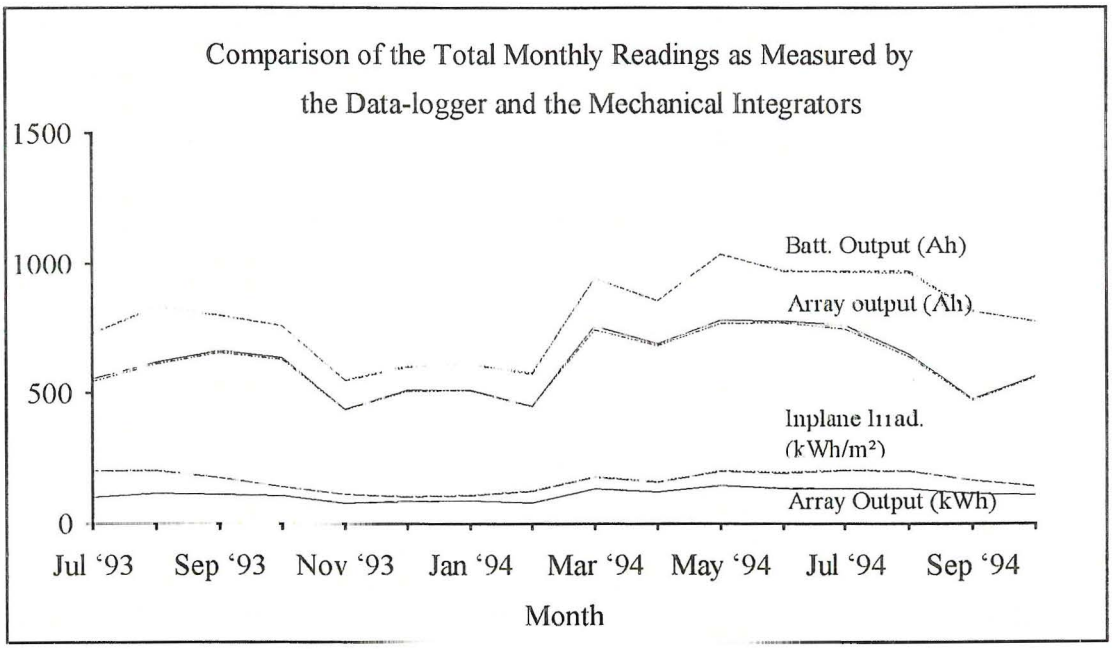

FIGURE 2.1: Graphical presentation of the comparison between the data-logger readings and the back-up mechanical integrators.

FIGURE 2.2: A photograph showing the browning of the PV modules.

terminals of the modules.

A tree on the western side of the array partially shadowed the modules after 4 p.m.(G.M.T.+1 hour). Though this would not cause damage to the cells due to the low solar intensity, the radiation data recorded on the array plane might be lower than expected. Also the array efficiency is expected to suffer heavily. The pyranometer used for this purpose could not be moved because it was necessary to determine the actual amount of energy incident on the array.

The modules were washed in summer, using water and a soft sponge, as detailed in table 2.2. Washing was always done in late afternoons, starting from the top modules and proceeding downwards. It took fifteen minutes to wash the array (11.117 m^2). The type of dirt that accumulated was typically fine dust broken by streaks of dried rivulets caused by dew during the night. Bird droppings were rarely detected on the surface

In summer, the array output was reduced at noon, due to high cell temperatures which exceeded 50 °C on some days. However, excluding this effect, the best total output current of the 20 modules was recorded in spring as 52.4 A, during the 15-minute interval between 12:15 and 12:30 p.m., on 6th April 1994. The insolation on the array was 1.064 kW/m^2 and the cell temperature was 26 °C. This value represented 88% of the estimated reference output at maximum power point and STC, given by the manufacturer (see table D.5, of appendix D).

The reasons that caused this drop could be inferred to the browning of the PV cells [75], which could amount to 9% [76], the imperfect matching between the batteries and the array that causes the I-V characteristics of the PV cells to deviate from the maximum power curve, the mismatch losses between the modules, the difference in the spectral distribution of the light source used to test the modules in the laboratory and the true solar light, where these modules actually perform and keeping in mind the fact that the internal temperature of the PV cells is actually 2 to 3 °C higher than the measured surface temperature of the module [83].

DATE	COMMENTS
18.04.93	Washed the array after a dusty day followed by droplets of rain (30 minutes). Browning of the PV modules was noted.
04.05.93	Washed the array. Accumulation of dust and formation of dew at night.
08.08.93	Washed the array and checked for corrosion of cells or terminals.
12.03.94	Washed the array and checked for corrosion and humidity penetration into cells.
22.04.94	Washed the array. In April aerosols in the air reach their peak concentration. This required more frequent washing
30.06.94	Washed the modules and checked terminals for corrosion.
29.08.94	Washed the modules.

TABLE 2.2: The log book for the PV array.

2.3 OPERATION AND MAINTENANCE OF THE BATTERIES

The batteries were supplied dry-charged and were topped with sulphuric acid in January 1993. A chemical test was carried out to check whether these batteries contained antimony additives. The presence of antimony improves the low-state charge characteristics of the battery. Some acid was taken from one cell and analysed using the principle of atomic absorption spectrometry. This method was used after failing to get an indication of the presence of antimony with the aid of cation testing due to interference caused by the presence of other substances.

Atomic absorption is an analytical method based on the absorption of ultraviolet or visible light by gaseous atoms. The sample was partly converted into atomic vapour by spraying the solution into a flame. A hollow-cathode lamp containing antimony was used as the light source. The atoms of antimony in the flame, absorb at precisely the wavelength emitted by the light source. The wavelength is extremely narrow, for both the emission line of the antimony light source and the absorption line of the antimony gas in the flame. For this reason, interference from the spectral lines of other elements is almost nil. The instrument used for this testing was VARTAN AA-1275 atomic absorption spectrometer. The results showed that antimony was present in the batteries.

In February 1993, the batteries were connected to the PV array via the BCU and were monitored once every month. The voltage and specific gravity of each cell were recorded at dusk and at the dawn of the next day. Also, the temperature of some pilot cells was sampled. As far as possible, monitoring was done after a series of sunny days to ensure that the batteries were charged.

The batteries were isolated for one hour, after which measurements commenced manually for the 60 cells, using a mercury-in-glass thermometer, a hydrometer that measured to an accuracy of five units in the third decimal place (e.g. 1.235) and a digital voltmeter that measured to an accuracy of two decimal places. An alcohol thermometer would have been preferred since it would not contaminate the acid in the batteries in case it accidentally breaks.

The order of the readings started with battery no. 1, the nearest to the BCU and proceeded to the adjacent battery no. 2 till battery no. 10. The monitoring of the cells of each battery started with cell no. 1, being the nearest to the positive pole and following in order till cell no. 6, being the nearest to the negative pole. The time required for monitoring was one hour. The temperature of the first cell of each battery was also taken.

Visual checks were made for any cracks on the surfaces or the sides of the batteries. Topping of the cells with di-ionised water and washing the surface with a neutralising solution of sodium hydrogen carbonate (100g dissolved in 1 litre of water) were carried out when necessary. The data-logger also recorded the overall voltage of the battery bank every day at midnight.

Though the battery poles were covered with Vaseline, corrosion was frequently detected (especially on the positive poles), after six months of operation Figure 2.3, shows the corrosion on one of the poles. The residue was chemically analysed and the following results were obtained:

Test for anions: Sulphate radical was detected and, to a lesser extent, carbonate and chloride radicals.

Test for cations: Copper and sodium ions were detected.

Clearly, the sulphate radical originated from the acid fumes given off from the vents during charging. The carbonate radical was a residue of the neutralising solution used to wash the surface of the batteries while the chloride radical was a result of the condensation of the salty air at night. As for the cations, copper originated from the pole clamps which were made of galvanised copper, while sodium was the other ion present in the salty air of the island.

An effective solution to the corrosion of the battery poles was found by replacing Vaseline with an anti-corrosive gel made of a mixture of products and produced by Holt Lloyd Ltd. (U.K.), with the brand name NO CRODE. Table D.21, of appendix D, gives the main constituents of this gel, as supplied by the manufacturer.

Though monitoring of the batteries was done with care, a short-circuit occurred once while disconnecting the batteries from the PV array. The effect was the breaking up of the top

tar layer that sealed one of the cells due to the excessive build-up of gases inside it. Also, one battery connector had slightly melted down. The surface was resealed and continuous monitoring of the cell showed no deterioration in its performance.

Such an incident draws the attention to the importance of applying all the safety measures to avoid harm to the operator. Safety goggles and rubber gloves should always be worn during the inspection and monitoring of the batteries. Figure 2.4, shows the affected cell immediately after the incident.

Boosting of the batteries was done once at the end of the winter season and once in summer, as shown in table 2.3. In winter, the batteries were boosted to avoid stratification of the acid and sulphation. In summer, the batteries were noticed to lose some charge as the load was increased. Though the availability of solar radiation increased, the operating PV cell temperatures were high near and at noon, so that the array did not produce enough power to balance the extra consumed energy. The load was eventually decreased in September 1994.

Boosting can be carried out by using a battery charger or by disconnecting the high voltage electronic alarm card of the BCU to make full use of the available solar energy, and simultaneously reducing the load consumption to a minimum, for several days.

2.4 OPERATION AND MAINTENANCE OF THE BCU

For most of the year the BCU had worked satisfactorily, though no specific tests were carried out on the mode of variation of its efficiency with load because it would require extra monitoring equipment.

In February 1994, one of the mercury relays stopped functioning and was immediately replaced. This was noted when the voltage of the PV string connected to that relay was found to be equal to the open circuit voltage of the modules (21 V), at noon-time. The heat sink fixed on the blocking diode was also noted to be cool and the total current output of the array at noon was lower than expected.

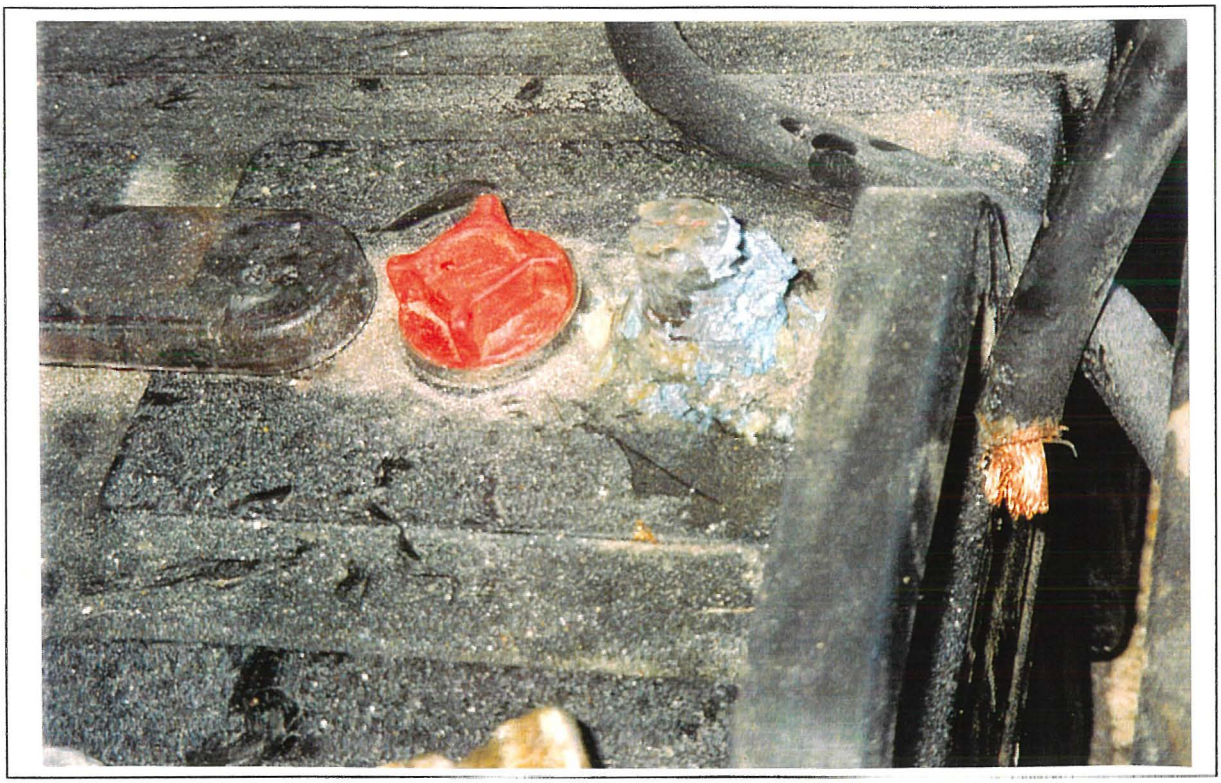

FIGURE 2.3: A photograph showing the corrosion on one of the battery poles.

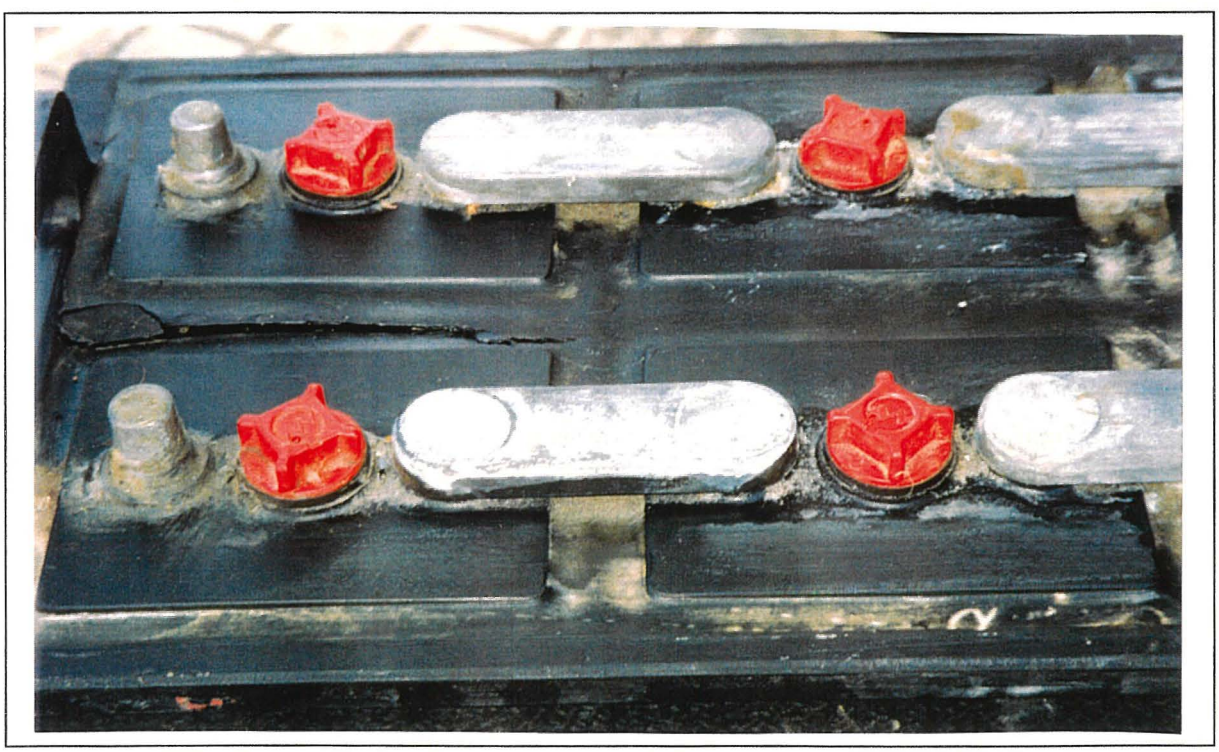

FIGURE 2.4: A photograph showing the condition of a cell after a short-circuit occurred.

TABLE 2.3: The log book for monitoring the batteries. Visual inspection for cracks and spilling of acid, testing the specific gravity, cell voltage and temperature were carried out.

18/19.06.93	Monitored batteries. One positive pole was corroded.
19/20.07.93	Monitored batteries. Three positive poles were corroded.
19/20.08.93	Monitored batteries. Three positive poles were corroded. Cleaned the whole surface with sodium hydrogen carbonate solution
22/23.09.93	Monitored batteries. Two positive poles were corroded.
20/21.10.93	Monitored batteries. They were low because the solar radiation became weaker, the hours of sunshine decreased and the night-time increased. Also, the weather was bad for one week. Timers were adjusted to make the lights work for 8 hours every night.
19/20.11.93	Checked batteries and monitored them. Two poles were corroded.
29/30.12.93	Monitored batteries.
07/08.01.94	Cleaned surface of batteries. Short-circuit accident which caused the breaking-up of the tar sealant at the top of one cell. The system was operating with nine batteries. One-hour delay to find assistance to remove battery from its box. The damaged cell was cell no. 6 of battery no. 2.
14.01.94	Re-connection of the battery. Two poles were corroded. Chemical analysis of residue was carried out.
26/27.01.94	Monitored the batteries. Some cells were weak. Added di-ionised water to all the cells after one year. Boosting of the batteries.
25/26.02.94	Monitored battery. Discovered that one of the relays of the BCU was not functioning.
23/24.03.94	Monitored the batteries.
04/05.05.94	Monitored the batteries. Two poles were corroded. Cleaned all the poles of the batteries and applied NO CRODE jelly instead. A slight crack was observed on the surface of one of the batteries. It was sealed with molten tar. Topped cells with di-ionised water.
25/26.05.94	Monitored the batteries.
30.06/01.07.94	Monitored batteries. The charge was low. Boosted the batteries.
27/28.07.94	Monitored batteries.
19/20.08.94	Monitored batteries. Some cells were weak. Reduced the load for some days and gave a boost charge to the batteries.
13/14.09.94	Monitored the batteries and added distilled water to them.
25/26.10.94	Monitored the batteries.

The modularity of the BCU helped to allow it to work partially. Also, the replacement time was reduced to a minimum. A stock of spare relays and diodes are recommended to be available on site.

2.5 OPERATION OF THE LOAD CONTROL UNITS

From the start, it escaped the installers to place the light sensing relays upside down, as recommended by the manufacturer. This caused two of them to fail during winter due to the infiltration of rain water into the unit, even though they were sealed all around with a silicon sealant. One integrated circuit had to be replaced in each sensor, after which they worked reliably well. Obviously, this time they were mounted properly.

The timers had worked reliably, though one of them was affected when the light sensing relay that supplied it with power mal-functioned. It was difficult to control the exact number of hours of operation, because the control knob was of a continuous variation type between two time limits and not in steps of say, one hour. The only way to set a definite number of hours of operation was by trial and error. A timer that could be varied in steps would have been preferred for our purpose.

2.6 OPERATION OF THE LIGHTS

The first eighteen lights had accumulated 4500 hours of operation, till the end of October 1994. So far only one light failed, in June 1994, after 3500 hours of operation and one choke in August 1994, after 4000 hours of operation. The remaining seven lights were installed at the beginning of March 1994 and had operated for 2175 hours till the end of October 1994, without failure.

Occasionally, some fluorescent lights would not switch on immediately. It was noticed that these lights had some condensed humidity captured in them. This implies that the humidity in the whole unit is very high which reduces the resistivity of the unit and causes an

electric leakage to the ground. Calcium chloride was introduced in some units to act as a drying agent, after which the units were sealed with silicon sealant. This improved the situation for few weeks after which the condensation was noted again. It was not possible to seal the whole unit perfectly. Also, sealing the unit is not advisable as there would be the need to re-open the cover to change the lights in the future Since these covers are subjected to UV radiation, they tended to change colour and to become more brittle.

A solution to the problem of starting was found by spraying a silicon compound on the whole surface of the choke of the fluorescent unit to isolate it from humidity. Also, the electric terminals were too weak to withstand any over-tightening and the unit was not fully weather proof.

2.7 OPERATION AND MAINTENANCE OF THE MONITORING EQUIPMENT

Besides the routine daily inspection of the proper operation of the data-logger and the data collection, using the support software programmes of TERM and TELCOM, visual checking was carried out on the pyranometers and the rain gauge. The dry-cell batteries that supply emergency power to the data-logger were changed every three months as recommended by the manufacturer. This was important, because even though the batteries were of the best quality, some expansion of the batteries could be detected after three months of placement in summer, however no leakage had occurred. An external lead-acid battery would be preferred.

The MATRIX pyranometer had a glass dome which had to be inspected for any humidity leakage and cleaned once a week, while the LI-COR pyranometer did not need so much cleaning.

Some incorrect readings were noticed and the humidity sensor recorded some values exceeding 100%, when dew condensed on it or during rain. Weather data was sampled for each month and compared to a similar weather station situated about 100 m away. The readings were very close and this assured us of the proper calibration of the humidity, air temperature, horizontal global radiation, wind speed, wind direction and rainfall sensors.

The integrators operated reliably and one of the advantages of placing them on the roof near the PV system, was that the operator had to go up every night to write down the integrated values and while doing so, the fluorescent lights were checked for proper operation as well as the other balance of system components. The 10-cm edge of the box containing the integrators was sufficient to keep away rain water from seeping in.

2.8 MAINTENANCE SCHEDULES

DAILY INSPECTION AND MAINTENANCE:

- Collection of data from data-logger to the hard disk of the PC using the TELCOM programme, at night
- Using a viewing programme such as XTREE GOLD to view the collected data and check for any discrepancies in the readings. Checking the battery voltage reading at midnight gave an indication of the general state of the battery charge. In particular, checking was done to ensure that the current and power produced by the array around noon was as expected. Lower values imply either the mal-functioning of the BCU or the full charge of the batteries.
- Manual recording of integrated values recorded by the back-up integrators and the visual checking of the proper operation of the fluorescent lights.

WEEKLY INSPECTION AND MAINTENANCE

- Cleaning of the dome of the MATRIX pyranometer at night
- Transferring the collected data from the hard disk of the PC to floppy disks and back-up copies, once every two weeks

MONTHLY INSPECTION AND MAINTENANCE

- Inspection of the surface of the PV modules and cleaning them if necessary.
- Monitoring the batteries and checking for loss of di-ionised water from the cells.
- Checking the rain gauge levelling and washing the filter

MAINTENANCE JOBS EVERY THREE MONTHS

- Checking the levelling of the LI-COR pyranometer.
- Replacing the emergency dry cell batteries of the data-logger and the drying agent packets.
- Considering the change of the load consumption according to the season.
- Washing the surface of the batteries with neutralising solution, if necessary.
- Checking for any shade on the PV array.
- Checking for corrosion for all terminals.

MAINTENANCE JOBS EVERY TWO YEARS

- Recalibration of all monitoring equipment such as pyranometer and anemometers.
- Evaluating the performance of the batteries.
- Checking for cracks in the cables.

Some miscellaneous inspection and maintenance jobs that were carried out during the testing period of the system, are given in table 2.4. These may help in the analysis of the collected data.

TABLE 2.4: Log book of some miscellaneous inspection and maintenance jobs carried out during the testing period.

04.05.93	Changed dry cell batteries of the micrologger.
10.08.93	Changed batteries of data-logger.
12.11.93	Replaced batteries of data-logger.
24.02.94	Replaced batteries of data-logger.
28.02.94	Found out that relay no. 4 of the BCU was not functioning, one timer was out of order and one light sensor was not functioning.
06.04.94	Light sensors did not operate because rain water had accumulated inside them
13.05.94	Changed position of the thermocouples that measured the PV cell temperature to measure the top and bottom temperatures of the same cell. Previously, they were not placed under each other.
25.05.94	Changed batteries of data-logger.
30.06.94	Changed one fluorescent light.
13.07.94	Forgot to connect the voltage sensing wire between the BCU and the batteries between 8 a.m. and 2 p.m. No energy had flowed to the batteries during this time.
13.08.94	Changed one choke of one of the fluorescent lights.
17.08.94	Changed batteries of data-logger.
14.09.94	Changed one choke of a fluorescent light unit.

CHAPTER THREE

DATA ANALYSIS AND PRESENTATION OF RESULTS

INTRODUCTION:

The first part of this chapter describes the procedure followed to check the data collected over sixteen months, starting from July 1994. Any discrepancies or missing data is presented in a report which would help in data analysis.

The second part deals with the analysis of data and presentation of some general summary results such as the number of hours of significant irradiance, PV array output and the monthly performance of the system. At this stage, the guidelines set by The Joint Research Centre - Ispra Establishment for the assessment of PV plants were employed [79].

The last part presents more detailed analysis, accompanied with any necessary explanations and comments.

3.1 SYSTEMATIC CHECKING OF THE COLLECTED DATA

The data collected over sixteen months of monitoring were subjected to detailed and systematic checks as follows:

(a) Each ASCII data file was arranged to contain data for fifteen or sixteen days. This was essential since the editing programme 'PERFECT EDITOR', which was used could not hold the data of a whole month. This programme was chosen because it was simple to use and it occupied a relatively small memory space in the computer hard disk, equivalent to that occupied by one month of collected data. By importing the data files into this programme, a preliminary visual check was carried out to ensure that there were no abnormal characters or corrupted sectors in the files.

The last file October 15-31, 1994, contained some corrupted data, which was caused by an electric surge that affected the personal computer and caused a disk error. However, the original uncorrupted data was successfully recovered from the micro-logger, using the TERM support software of the micro-logger. This incident draws attention to the necessity of creating back-up files and the importance of on-line data monitoring

(b) The number of data sets were counted using the 'SPLIT' software, which was supplied as part of the support software to the micro-logger. A set of data was produced by the micro-logger every fifteen minutes, one hour and twenty-four hours. This test revealed no missing sets.

(c) The SPLIT programme was again used to point out any abnormal data points. For each season, two parameter files were created, one for the morning hours and the other for night-time, which included threshold values for each data point. Any point that fell outside those limits blinked on the screen. It was visually checked, noted and an explanation had to be found for its diversion with the help of the log books, presented in Chapter Two and the other data points of the same set. Table 3.1, shows all the out-of-range data and the time at which they occurred.

(d) In case there was anomalous data, a decision had to be made whether to eliminate the whole set from subsequent analysis or whether it could be arranged without loosing all the set, depending on the original reason of deviation. A report was produced for all the changes that were made, as shown in table 3.2 and where necessary, new healthy files were constructed to be used for the presentation of results.

3.2 GENERAL ANALYSIS OF THE COLLECTED DATA

A chart is presented in table C.2, of appendix C, of all the hours of significant irradiance incident on the PV array (> 80 W/m^2) and significant array output power (> 5% of P_{nom}, i.e. > 60 W), each indicated with a star. From the chart, it can be seen that the array did not produce significant power for some hours during the days of July up to October 1993. This was

TABLE 3.1: A chart of all the out-of range data which was found during the checking of the data for the sixteen months of monitoring, starting from July 1993.

DATE	JULIAN DAY	TIME RANGE	COLUMN NO.	DATA NAME	VALUE RANGE
06/07/93	187	8:00	all	15-minute set	low/high values
28/09/93	271	19:15-20:45	4	Humidity	100.1-102.1
09/10/93	282	00:30-08:45	4	Humidity	100.1-102.1
16/10/93	289	5:15-07:15	4	Humidity	100.1-100.6
21/10/93	294	6:15 and 6:30	5	Air temperature	40.43 and 50 °C
21/10/93	294	6:15 and 6:30	6	Temp. of top module surface	39.71 and 44.2 °C
21/10/93	294	6:15 and 6:30	7	Temp. of bottom module surface	39.94 and 44.26 °C
21/10/93	294	6:15 and 6:30	8	Horiz. global rad.	0.192 and 0.344
21/10/93	294	6:15 and 6:30	16	Array power out.	23.19 and 11.99
31/10/93	304	2:15-2:45	4	Humidity	100.1-100.4
01/11/93	305	5:00-6:30	4	Humidity	100.2-100.8
28/12/93	362	18:15-22:30	4	Humidity	100.1-101.6
30/12/93	364	7:45-8:30	5	Air temperature	3.882-10.54
30/12/93	364	7:45-8:30	6	Temp of top module surface	13.74-28.16
30/12/93	364	7:45-8:30	7	Temp. of bottom module surface	15.65-30.24
30/12/93	364	7:45-8:30	8	Horiz. global rad.	0.274-0.841
18/01/94	18	18:45	4	Humidity	100.2
19/01/94	19	5:30-11:00	4	Humidity	100.1-102
19/10/94	19	18:15-18:45	4	Humidity	100.1-100.5
19/10/94	19	19:30-20:30	4	Humidity	100.2-101
27/01/94	27	8:00-9:45	14	Array current out	0
27/01/94	27	8:00-9:45	16	Array power out.	0
14-28/02/94	45-59	Around noon	14	Array current out	< 38 A
16/02/94	47	4:00-9:45	4	Humidity	100.1-102.4
16/02/94	47	21:30-23:45	4	Humidity	100.2-101.4
17/02/94	48	00:00-1:30	4	Humidity	100.2-101.5
24/04/94	114	5:00-7:00	4	Humidity	100.1-101.6
30/04/94	120	9:15-10.45	14	Array current out	0
30/04/94	120	9:15-10:45	16	Array power out.	0
15/05/94	135	2:30-7:00	4	Humidity	100.3-101.1
17/05/94	137	21:15-23:30	4	Humidity	100.1-100.4
18/05/94	138	4:00-6:30	4	Humidity	100.4-101.2
13/07/94	194	8:00-14:00	14	Array current out	0
13/07/94	194	8:00-14:00	16	Array power out.	0
17/08/94	229	4:15-7:00	4	Humidity	100.1-101.8

TABLE 3.2: A list of all the adjustments that were made to the errors found in the data files, in preparation for further analysis.

DATE	DISCUSSION OF ERROR AND FURTHER ACTION TAKEN
06/07/93	The 15-minute data set at 8:00 a.m. had very low values of air and module surface temperatures, and high values of irradiation. Moreover the hourly average at 8 a.m. was an exact copy of the 8 o'clock 15-minute interval data. Both sets were eliminated and the hourly average was adjusted to be the mean of the remaining three intervals, namely, 7:15, 7:30 and 7:45. The daily average was adjusted accordingly.
28/09/93	Humidity readings above 100% were caused by the condensation of water vapour on the probe. Since humidity does not directly affect the performance of the system, the readings were left unchanged. This explanation applies to all the cases where humidity was higher than 100%.
21/10/93	These sets were deleted from the file and the average hourly data points at 7 o'clock were adjusted to be the average of the remaining two 15-minute intervals, namely 6:45 and 7:00. Also, the average values for that day were adjusted using the 'SPLIT' and 'PERFECT EDITOR' software programmes.
30/12/93	The sets that contained errors were completely eliminated and the hourly average at 8:00 was re-calculated using the 15-minute data points of 7:00, 7:15 and 7:30. The hourly average at 9:00 was determined from the 15-minute intervals of 8:45 and 9:00. The daily average was also adjusted. The reason for such errors on that day could be due to lightning.
27/01/94	During this time, cleaning and monitoring of the batteries were being carried out. Hence, this is not a data error.
14-28/02/94	One of the relays of the BCU was not functioning. It was discovered when the batteries were monitored on 25.02.94 and was replaced. Hence, the data is acceptable.
30/04/94	The poles of the batteries were being cleaned and 'NO CRODE' anti-corrosion jelly was applied. Hence, the zero value is acceptable.
13/07/94	The previous night, the batteries were being monitored and one of the voltage sensing leads was not re-connected. This paralysed the BCU and no current passed from the PV array to the batteries. Hence, the data is acceptable. The wire was connected at 14:00 of the same day.

caused by the action of the BCU which shunted the array whenever the batteries reached their full capacity. For all the other hours when the array was not producing significant power in the morning, the common reason was that maintenance work was being carried out on the system, as indicated in tables 2.3 and 2.4.

Two energy balance sheets are presented in tables 3.3(a) and 3.3(b), for all the monitored months. Table 3.3(a) used the data that was collected by the automatic 21X micro-logger, while table 3.3(b) employed the data that was collected by the back-up mechanical integrators, (shown as shaded).

As seen from these tables, the data collected by the integrators differed from the corresponding micro-logger readings as was shown and discussed in section 2.1. Since the same sources of error apply to all the data points, they tended to cancel each other and did not affect the final results of efficiencies, performance yields and performance ratios.

The performance ratio (*PR*) was relatively low for the first three months because the fluorescent lights were not operated at full load. Since it was summer and the batteries were not optimally discharged during the previous night, they used to reach their full charge at noon, leaving the PV array idle for the rest of the day. The total quantity of unutilised solar radiation for each month is given in table 3.4. It shows that experience could improve the utilisation of solar radiation. This is clearly shown in the scatter diagrams of the array yields versus solar radiation incident on the array, of figures 3.1.1 to 3.1.16.

During February 1994, one of the BCU relays was out of order but it was not realised till towards the end of the month when the batteries were being monitored. As a consequence, the total energy supplied to the batteries and to the load decreased. At the same time the actual amount of solar energy falling on the system had increased from that of the previous month, thus the *PR* was adversely affected.

During late spring and summer 1994, the electric consumption was increased to upgrade the *PR*, but it turned out that towards the end of August the batteries were discharged to the extent that the load had to be reduced again, to allow them to get recharged. This has affected the *PR* of August and September 1994.

TABLE 5.3 (a) Monthly energy balances based on the data collected by the micro-logger

NOMINAL ARRAY POWER: 1.2 kWp | TOTAL ARRAY AREA: 11.11 m² | NOMINAL ARRAY EFFICIENCY: 0.108

		Jul-93	Aug-93	Sep-93	Oct-93	Nov-93	Dec-93	Jan-94	Feb-94	Mar-94	Apr-94	May-94	Jun-94	Jul-94	Aug-94	Sep-94	Oct-94
hrs	hours	744	744	720	744	720	744	744	672	744	720	744	720	744	744	720	744
MF		1	1	1	1	1	1	1	1	1	1	1		1	1	1	1
IG	kWh/m²	222.43	207.26	154.82	109.59	74.26	63.56	72.12	94.67	150.97	155.55	211.17	211.85	213.19	193.06	145.61	105.29
ESA	kWh	2262.3	2272.98	1973.05	1582.28	1257.47	1161.73	1214.24	1407.08	2007.62	1792.39	2246.97	2174.26	2280.99	2255.08	1923.46	1538.15
IGm	kWh/m²/day	7.18	6.69	5.16	3.54	2.48	2.05	2.33	3.38	4.87	5.19	6.81	7.06	6.88	6.23	4.85	3.40
IAm	kWh/m²/day	6.56	6.60	5.92	4.59	3.77	3.37	3.52	4.52	5.83	5.37	6.52	6.52	6.62	6.54	5.77	4.46
EA	[= EBCU+] kWh	101.525	116.55	113.03	106.82	78.35	86.2	87.16	80.83	134.53	121.06	146.27	134.27	134.23	134.22	118.77	105.09
JBCU+	Al:	7307.8	8310	7975	7578	5494	6028	6137	5768	9444	8575	10374	9669	9693	9661	8428	7496
JB -	Al:	5541.7	6130	6525	6313	4332	5116	5081	4505	7403	6901	7578	7732	7714	6450	4806	5565
UDCM	V	13.89	14.03	14.17	14.10	14.26	14.30	14.20	14.01	14.25	14.12	14.10	13.89	13.85	13.89	14.09	14.02
UDCN	V	12.45	12.44	12.43	12.54	12.51	12.26	12.1	12.25	12.2	12.02	12.28	12.6	12.33	12.37	12.47	12.15
EB -	kWh	68.99	76.26	81.11	79.17	54.19	62.72	61.48	55.19	90.32	82.95	93.06	97.42	91.41	79.79	59.93	67.61
Yr=IAm	kWh/day/kWp	6.64	6.6	5.92	4.59	3.77	3.37	3.52	4.52	5.83	5.37	6.52	6.52	6.62	6.54	5.77	4.46
Ya	kWh/day/kWp	2.73	3.13	3.14	2.87	2.18	2.32	2.34	2.41	3.62	3.36	3.93	3.75	3.61	3.61	3.30	2.83
Yf	kWh/day/kWp	1.85	2.05	2.25	2.13	1.51	1.69	1.65	1.64	2.43	2.30	2.50	2.7	2.46	2.14	1.66	1.82
Lc	kWh/day/kWp	3.91	3.47	2.78	1.72	1.59	1.05	1.18	2.11	2.21	2.01	2.59	2.79	3.01	2.93	2.47	1.64
Ls	kWh/day/kWp	0.87	1.08	0.89	0.74	0.67	0.63	0.69	0.76	1.19	1.06	1.43	1.02	1.15	1.46	1.63	1.01
PR		0.28	0.31	0.38	0.46	0.40	0.50	0.47	0.36	0.42	0.43	0.38	0.42	0.37	0.33	0.29	0.41
NAmean,t		0.04	0.05	0.06	0.07	0.06	0.07	0.07	0.06	0.07	0.07	0.07	0.06	0.06	0.06	0.06	0.07
Ntot,t		0.03	0.03	0.04	0.05	0.04	0.05	0.05	0.04	0.04	0.05	0.04	0.04	0.04	0.04	0.03	0.04
NBQ&NBCU,t		0.76	0.74	0.82	0.83	0.79	0.85	0.83	0.78	0.78	0.80	0.73	0.80	0.76	0.67	0.57	0.74
NBE&NBCU,t		0.68	0.65	0.72	0.74	0.69	0.73	0.71	0.68	0.67	0.69	0.64	0.73	0.68	0.59	0.50	0.64
Ya/Yr		0.41	0.47	0.53	0.63	0.58	0.69	0.67	0.53	0.62	0.63	0.60	0.57	0.55	0.55	0.57	0.63
Array losses		0.59	0.53	0.47	0.37	0.42	0.31	0.33	0.47	0.38	0.37	0.40	0.43	0.45	0.45	0.43	0.37

TABLE 3.3 (a): Monthly energy balances based on the data collected by the micro-logger

TABLE 5.3 (b): Monthly energy balances of the PV system based on data collected by the mechanical integrators

NOMINAL ARRAY POWER: 1.2 kWp | TOTAL ARRAY AREA: 11.117 m² | NOMINAL ARRAY EFFICIENCY: 0.108

		Jul-93	Aug-93	Sep-93	Oct-93	Nov-93	Dec-93	Jan-94	Feb-94	Mar-94	Apr-94	May-94	Jun-94	Jul-94	Aug-94	Sep-94	Oct-94
hrs	hours	744	744	720	744	720	744	744	672	744	720	744	720	744	744	720	744
MF		1	1	1	1	1	1	1	1			1	1	1	1	1	1
IG	kWh/m²	225.04	207.26	154.82	109.59	74.26	63.56	72.12	94.67	150.97	155.55	211.17	211.85	213.29	193.06	145.61	105.29
ES4	kWh	2249.41	2260.2	1960.93	1570.25	1246.22	1147.83	1201.97	1396.85	1999.94	1775.83	2225.96	2155.36	2260.53	2239.3	1846.2	1580.95
IGm	kWh/m²/day	7.26	6.69	5.16	3.54	2.48	2.05	2.33	3.38	4.87	5.19	6.81	7.06	6.88	6.23	4.85	3.40
IAm	kWh/m²/day	6.53	6.55	5.88	4.56	3.74	3.33	3.49	4.49	5.78	5.32	6.46	6.46	6.56	6.50	5.54	4.59
E4	[= EBCU+] kWh	101.71	116.43	112.96	106.77	78.27	86.03	86.9	80.62	134.01	120.32	145.97	134.19	134.17	134.19	114.87	108.96
JBCU+	Ah	7328	8348	8302	7585	5474	6004	6092	5715	9449	8572	10406	9705	9730	9720	8178	7753
JB-	Ah	5554	6057	6541	6368	6387	5135	5125	4513	7547	5905	7808	7795	7624	6518	4777	5647
UDCM	V	13.88	13.95	14.12	14.08	14.30	14.33	14.26	14.11	14.18	14.09	14.03	13.83	13.79	13.81	14.05	14.35
UDCN	V	12.45	12.44	12.43	12.54	12.51	12.26	12.1	12.25	12.2	12.02	12.28	12.6	12.33	12.37	12.47	12.15
EB -	kWh	69.15	77.09	82.55	79.35	54.88	62.96	62.01	55.28	92.56	83.00	95.88	98.25	94.00	80.53	59.57	68.61
Yr=IAm	kWh/day/kWp	6.53	6.56	5.88	4.56	3.74	3.33	3.49	4.49	5.78	5.32	6.46	6.46	6.56	6.50	5.54	4.59
Ya	kWh/day/kWp	2.73	3.13	3.14	2.87	2.17	2.31	2.34	2.40	3.60	3.36	3.92	3.73	3.61	3.61	3.19	2.93
Yf	kWh/day/kWp	1.86	2.07	2.29	2.15	1.52	1.69	1.67	1.65	2.49	2.31	2.58	2.73	2.53	2.17	1.65	1.84
Lc	kWh/day/kWp	3.80	3.43	2.74	1.69	1.57	1.02	1.15	2.09	3.18	1.96	2.54	2.73	2.95	2.89	2.35	1.66
Ls	kWh/day/kWp	0.88	1.06	0.84	0.72	0.65	0.62	0.67	0.75	1.21	1.05	1.35	1.00	1.08	1.44	1.54	1.08
PR		0.28	0.32	0.39	0.47	0.41	0.51	0.48	0.37	0.45	0.43	0.40	0.42	0.39	0.33	0.30	0.40
NAmean.t		0.05	0.05	0.06	0.07	0.06	0.07	0.07	0.06	0.07	0.07	0.07	0.06	0.06	0.06	0.06	0.07
Ntot.t		0.03	0.03	0.04	0.05	0.04	0.05	0.05	0.04	0.05	0.05	0.04	0.05	0.04	0.04	0.03	0.04
NBQ&NBCUt		0.76	0.74	0.83	0.84	0.80	0.86	0.84	0.79	0.83	0.81	0.75	0.80	0.78	0.67	0.58	0.73
NBE&NBCU,t		0.68	0.66	0.73	0.75	0.70	0.73	0.71	0.69	0.69	0.69	0.66	0.73	0.70	0.60	0.52	0.63
Ya/Yr		0.42	0.48	0.53	0.63	0.58	0.69	0.67	0.53	0.62	0.63	0.61	0.58	0.55	0.55	0.58	0.64
Array losses		0.58	0.52	0.47	0.37	0.42	0.31	0.33	0.47	0.38	0.37	0.39	0.42	0.45	0.45	0.42	0.36

Shaded numbers are data measured by the back-up mechanical integrators or calculated from measured data.

TABLE 3.3 (b): Monthly energy balances based on the data collected by the mechanical integrators.

The definitions of the abbreviations used in the tables are described below.

hrs = Number of hours per month, when monitoring of the data was functioning;

MF = Monitoring fraction, defined as the ratio of the monitored hours to the total number of hours of the month;

IG = Total global horizontal radiation for the month in kWh/m^2;

ESA = Total global radiation falling on the array, in kWh, calculated by multiplying the total radiation falling on the PV array per square metre by the array area;

IG_m = Mean global horizontal radiation in kWh/m^2 per day;

IA_m = Mean radiation falling on the PV array in kWh/m^2 per day;

EA = Total energy produced by the PV array, which is equal to the energy input to the BCU, assuming negligible power losses in the cables, in kWh;

$IBCU^+$ = Total input current capacity to the BCU, assumed equal to the total current capacity produced by the PV array, in Ah;

IB^- = Total output current capacity from the batteries, equal to the total Ah units consumed by the fluorescent lights and any transmitting losses between the battery and the lights;

$UDCM$ = D.C. line voltage in the morning, while power was being produced by the PV array, found by dividing EA by $IBCU^+$;

$UDCN$ = D.C. line voltage during the night, while power was being delivered to the lights. It is the mean daily battery voltage, which was recorded by the data-logger once at midnight, multiplied by a correcting factor of 1.135. Since, there was a voltage regulator and a fuse fixed between the batteries and the data-logger, the voltage read by the data-logger was lower than the true battery voltage. By measuring the actual battery voltage and comparing it to the data logger reading, a straight line correlation was established with a slope of 1.135;

EB^- = Energy delivered by the battery, which is the product of IB^- and $UDCN$ in kWh;

Y_r = Reference yield in kWh/kWp per day, defined as the ideal yield of the PV array at 100% efficiency, and is equal to IA_m/HA_{ref}, where HA_{ref} is the reference inplane irradiation equal to 1 kW/m^2;

Y_a = Array yield = $EA/(P_{nom}$ x n),

where, P_{nom} = Nominal power of the PV array at STC = 1.2 kWp,

and, n = Number of days in the month;

Y_f = Final useful system yield = $EB^-/(P_{nom}$ x n);

L_c = Capture losses = $Y_r - Y_a$;

L_s = System losses = $Y_a - Y_f$, mainly comprised of losses in the batteries and the BCU;

PR = Performance ratio = Y_f/Y_r, which indicates the extent to which the PV system is used;

$N_{a\,mean,t}$ = Mean monthly array efficiency = EA/ESA;

$N_{tot,t}$ = Overall PV plant efficiency = EB^-/ESA;

$NBQ\&NBCU_t$ = Combined coulomb efficiency of the battery and BCU = $JB^-/JBCU^+$;

$NBE\&NBCU_t$ = Energy efficiency of the battery and the BCU = EB^-/EA;

Array losses = $1 - Y_a/Y_r$.

TABLE 3.4: The total monthly solar energy incident on the PV array during which the PV array was not producing power.

MONTH	SOLAR ENERGY (kWh)
JULY 93	23.768
AUGUST 93	24.849
SEPTEMBER 93	21.564
OCTOBER 93	3.439
NOVEMBER 93	5.983
DECEMBER 93	0.156
JANUARY 94	2.693
FEBRUARY 94	0.111
MARCH 94	1.673
APRIL 94	1.403
MAY 94	0.509
JUNE 94	0.078
JULY 94	4.887
AUGUST 94	0.023
SEPTEMBER 94	0.02
OCTOBER 94	0

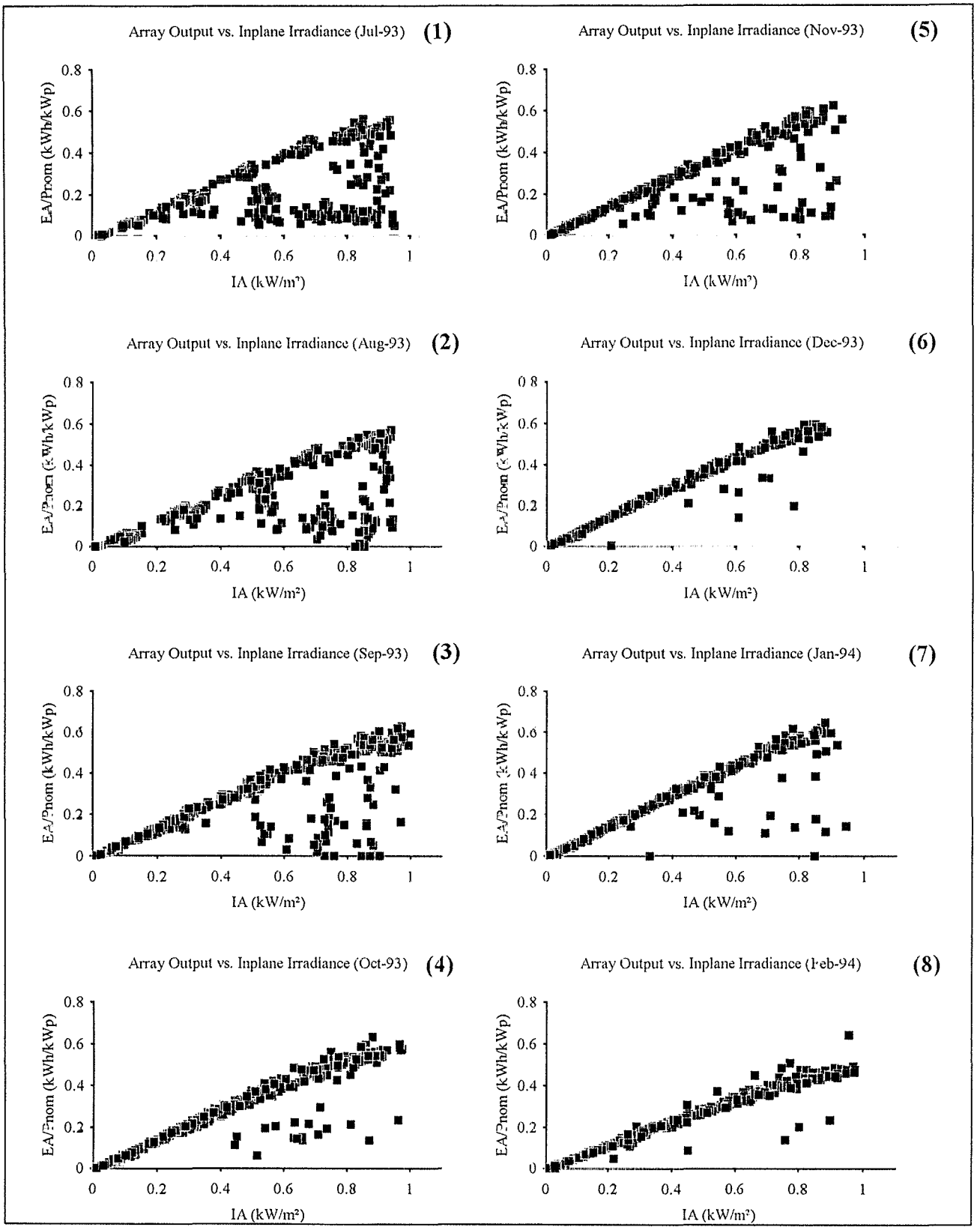

FIGURES 3.1.1 - 3.1.8: Scatter diagrams of hourly array yield vs. the corresponding radiation incident on the array plane, for the months of July 1993 to February 1994.

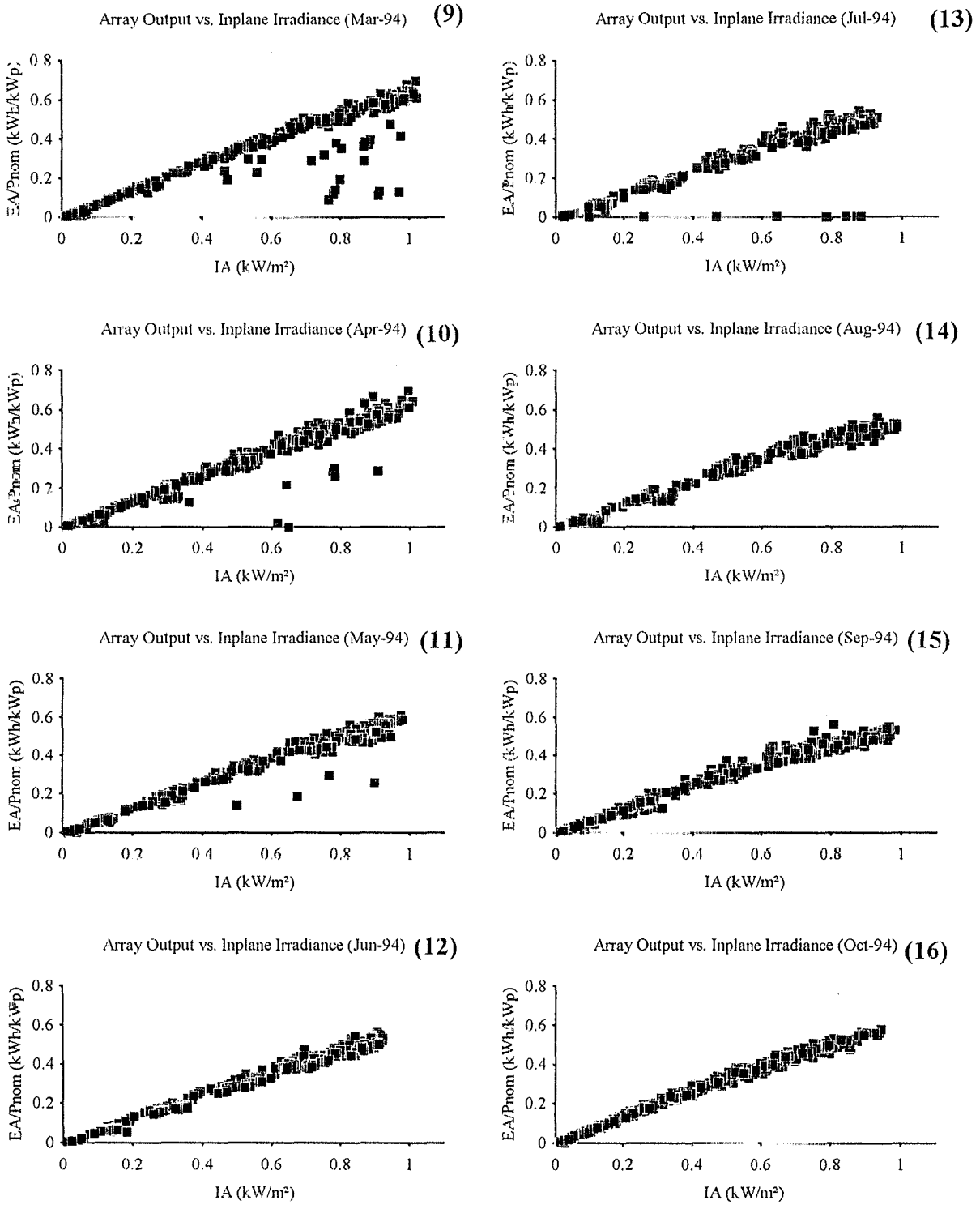

FIGURES 3.1.9 - 3.1.16: Scatter diagrams of hourly array yield vs. the corresponding radiation incident on the array plane, for the months of March to October 1994.

Simultaneously, it was realised that the energy efficiency of the battery and the BCU have degraded during these two months to reach 50%. The main reason for this drop was that the energy absorbed over the days by the batteries to restore them to their full charge did not appear in the final yield calculations, since it was not yet consumed.

The mean *PR* of this system over the sixteen months period was 0.38, as compared to the mean *PR* of 0.34 of professional stand-alone systems, monitored in the Thermie programme [80].

3.3 PRESENTATION OF GRAPHIC RESULTS

The frequency distribution of hourly radiation values incident on the array plane are presented in figures 3.2.1 to 3.2.16, for each month. During the months from April to September, it was noted that the hourly frequency distribution fluctuated considerably between the radiation ranges of 0.15 to 0.65 kW/m^2, while it smoothed down during the winter months.

New frequency distribution charts were constructed using the basic 15-minute interval radiation data, as shown for some months in figures 3.3.1 to 3.3.8. The fluctuations disappeared and this led to the conclusion that the use of hourly averages tended to give more statistical importance to higher radiation values. This phenomenon could be detrimental in the design of solar systems especially those that use concentrators because it could result in an undersized system.

This statistical behaviour appeared also on the frequency distribution of the PV array output energy, as shown for selected months in figures 3.4.1 to 3.4.8. This is expected since the array output power is almost directly proportional to solar radiation as expressed in figures 3.1.1 to 3.1.16. Here, the x-axis scales differ for each month because they were constructed to match the x-axis intervals of the corresponding months of figure 3.2, taking into consideration the linear regression functions that described the relationship between the array output and the solar radiation of figures 3.1.

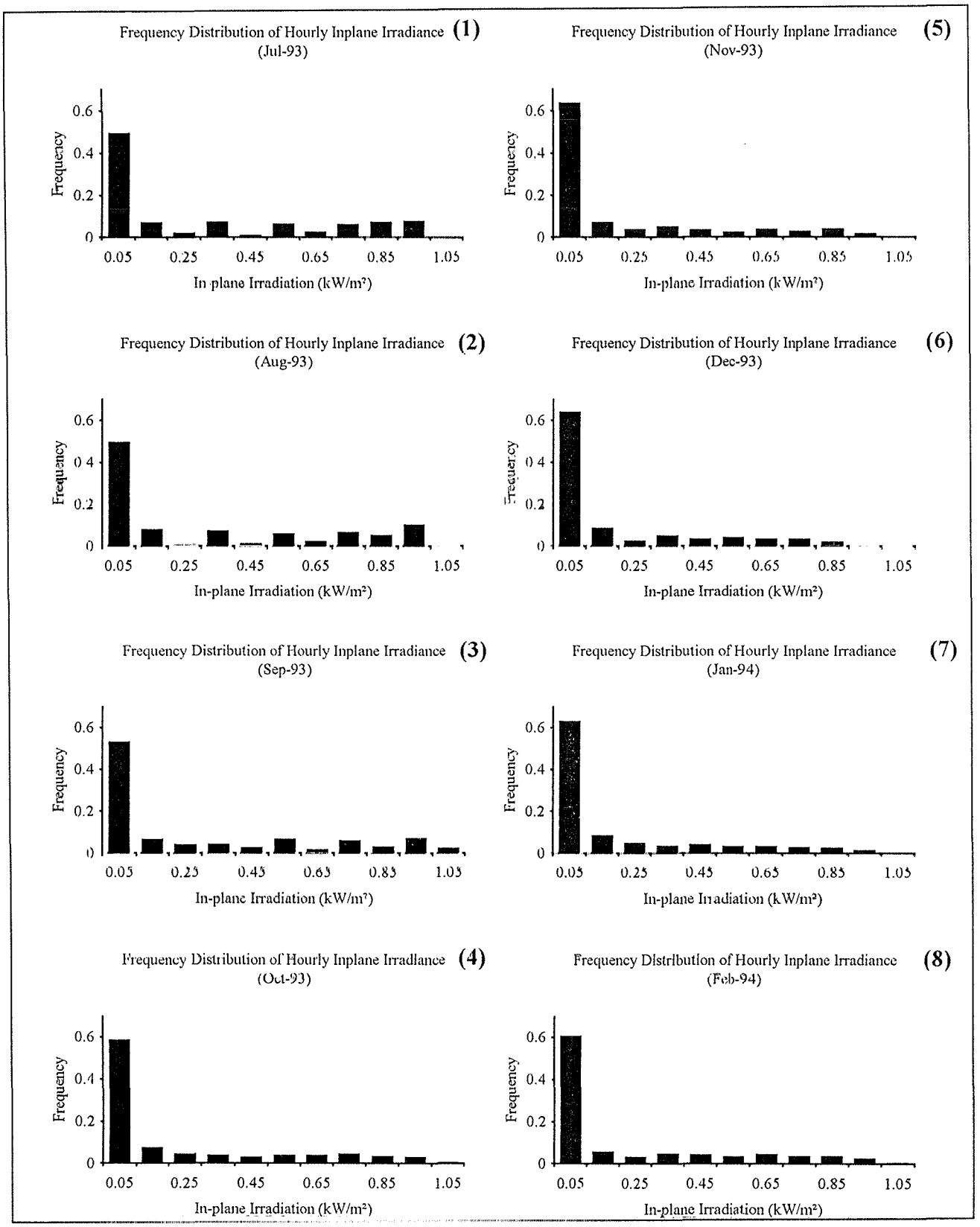

FIGURES 3.2.1 - 3.2.8: The frequency distribution of hourly radiation incident on the array plane, for the months July 1993 to February 1994.

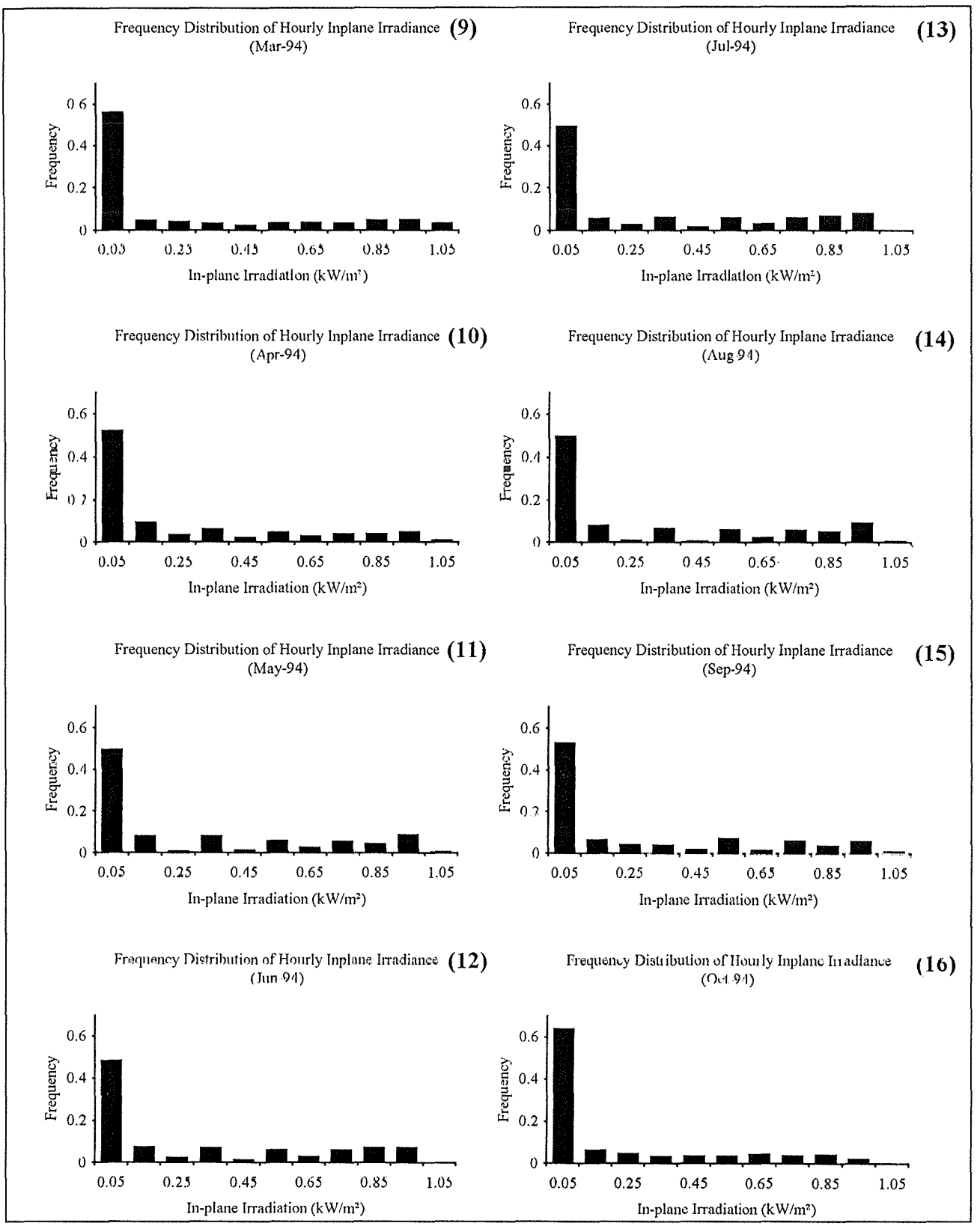

FIGURES 3.2.9 - 3.2.16: The frequency distribution of hourly solar radiation incident on the array plane, for the months of March to October 1994.

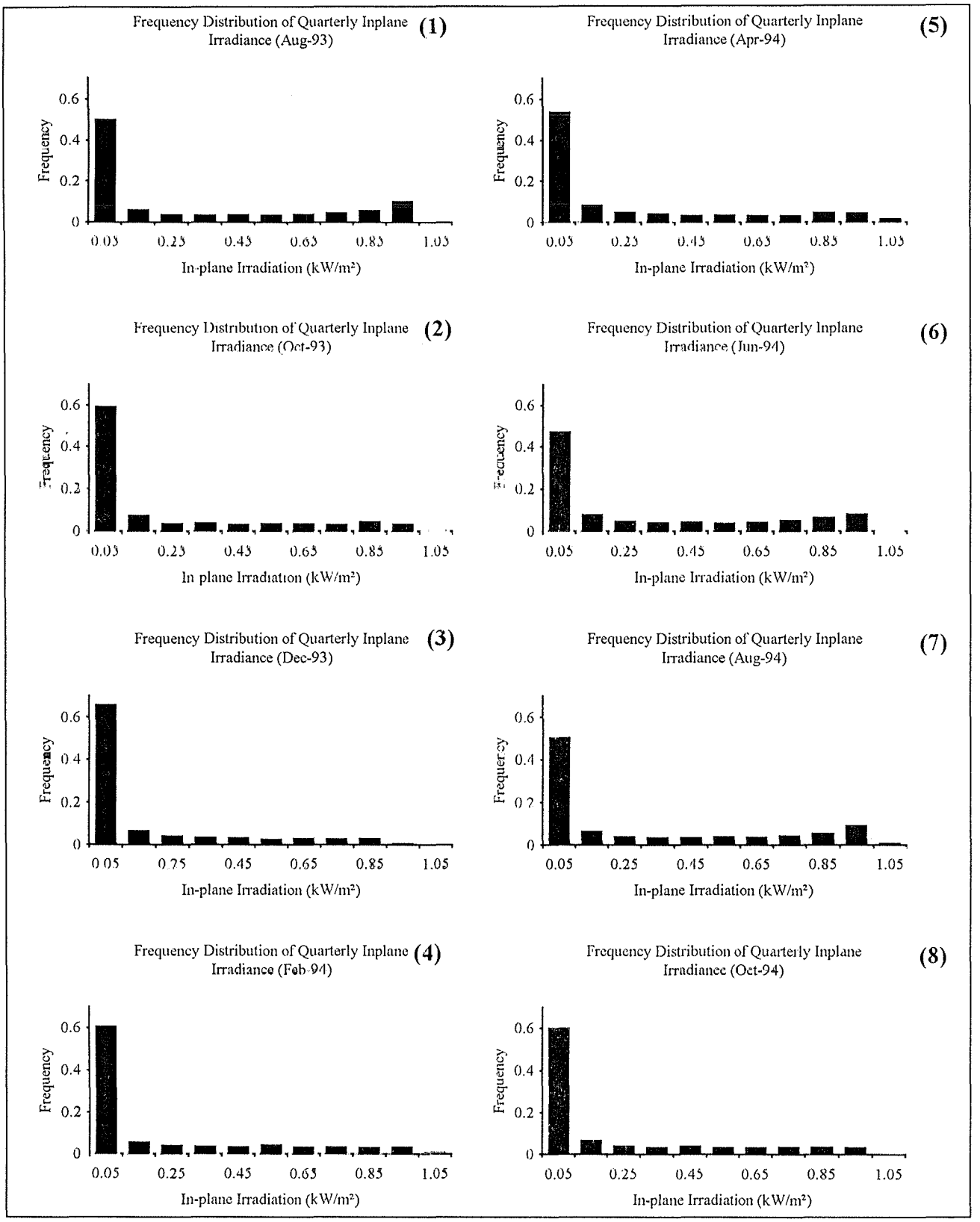

FIGURES 3.3.1 - 3.3.8: The frequency distribution of quarterly (15-minutes interval) solar radiation incident on the array plane for some selected months.

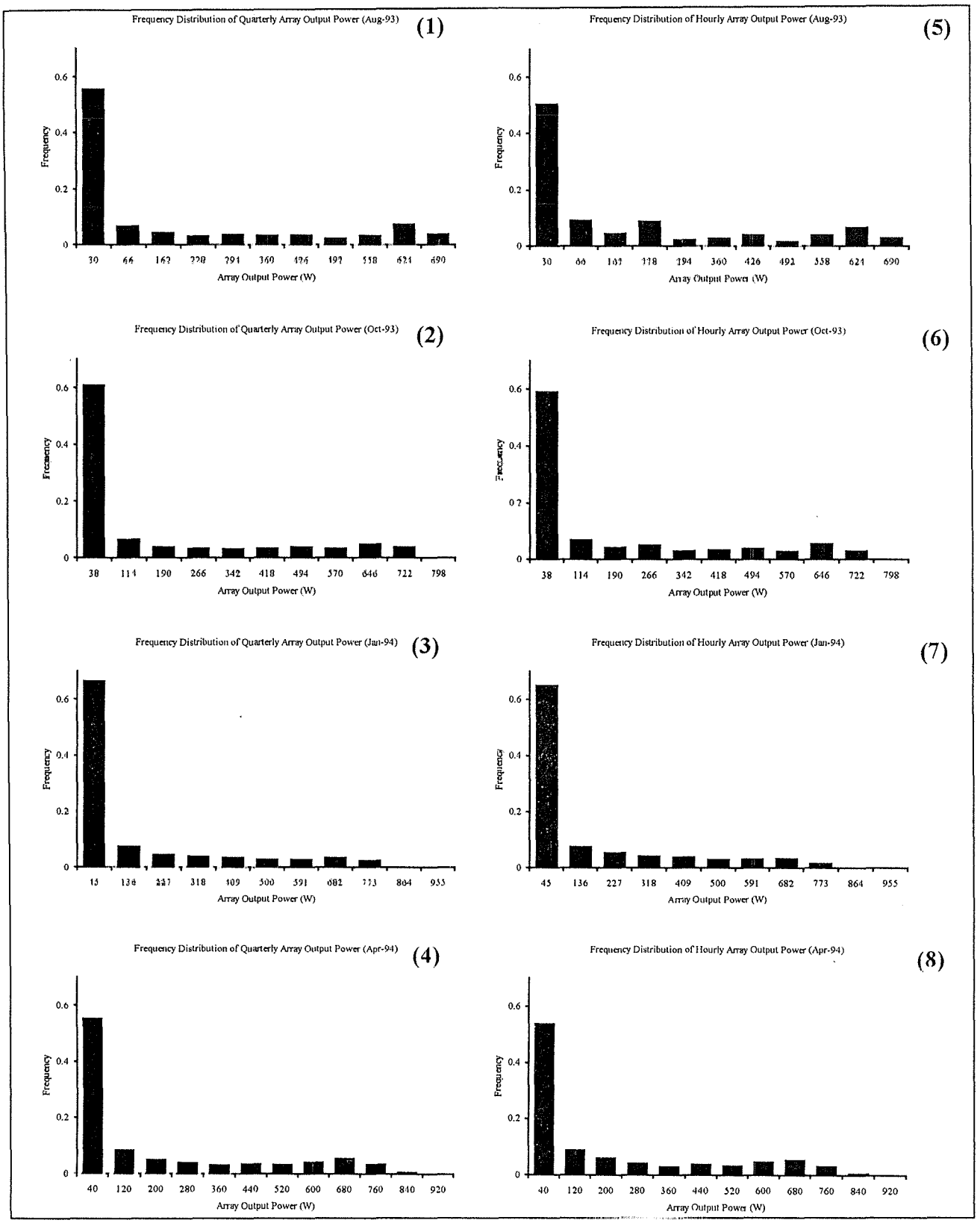

FIGURES 3.4.1 - 3.4.8: A comparison between the frequency distribution of quarterly (15-minute interval) and hourly array output of four representative months for the four seasons.

Another useful graphical presentation is shown in figures 3.5.1 to 3.5.16, for the daily array yields and capture losses. The first months showed a large proportion of losses but by time it decreased considerably due to improved utilisation of solar radiation. The stacked bar charts represent the reference yields, which are simply the sum of the array yields and capture losses. Since the reference yield is numerically equal to the mean daily solar radiation, it can be deduced that during the operation of the system the maximum number of consecutive days with low insolation (< 2.5 kWh/day) incident on the array, was three days and it occurred on 31st October and 1st November 1993, and in April 1994. Two consecutive sunless days occurred once a month during winter, while one sunless day occurred more frequently. It is also clear that the amount of solar radiation falling on the array immediately after bad weather contained several times more energy than that during cloudy days.

Figures 3.6.1 to 3.6.16, describe the hourly distribution of the useful electric consumption over the sixteen months of operation. Since the fluorescent lights were switched on at night at an almost constant consumption rate, the energy distribution was mainly concentrated in the region of 0.2 kW/kWp per hour. The lower energy levels represent the energy consumed by the monitoring equipment. As from March 1994, a new set of fluorescent lights were installed to bring the total number of lights to the designed twenty five lights. This increase in energy consumption caused a shift in the bar chart towards the 0.25 and 0.3 kW/kWp levels.

3.4 HOURLY PV ARRAY EFFICIENCY VARIATIONS

Figures 3.7.1 to 3.7.16 show the hourly variation of the efficiency of the modules vs. the solar radiation incident on the array. Clearly, the efficiency is not constant with radiation, but rises steeply for the first 50 to 100 W/m², levels off up to about 700 W/m² and then slightly drops for higher radiation.

However, a closer look on efficiency is shown in figure 3.8, for bright sunshine conditions in July 1994. The change in efficiency during early morning could be attributed to the fact that some energy was required to overcome the internal losses in the cells before they could

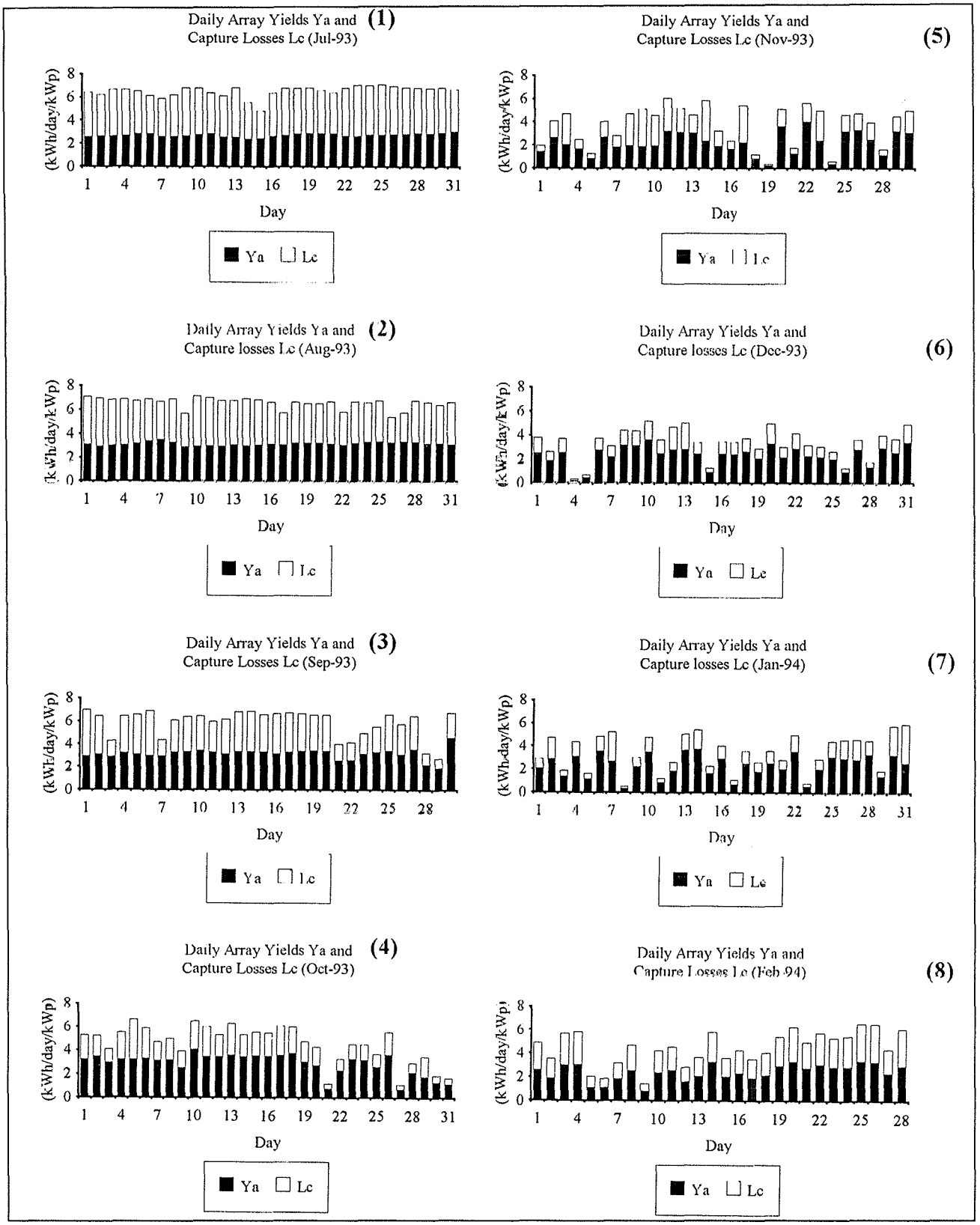

FIGURES 3.5.1 - 3.5.8: Stacked bar charts of the daily array yields and the array capture losses, for the months July 1993 to February 1994.

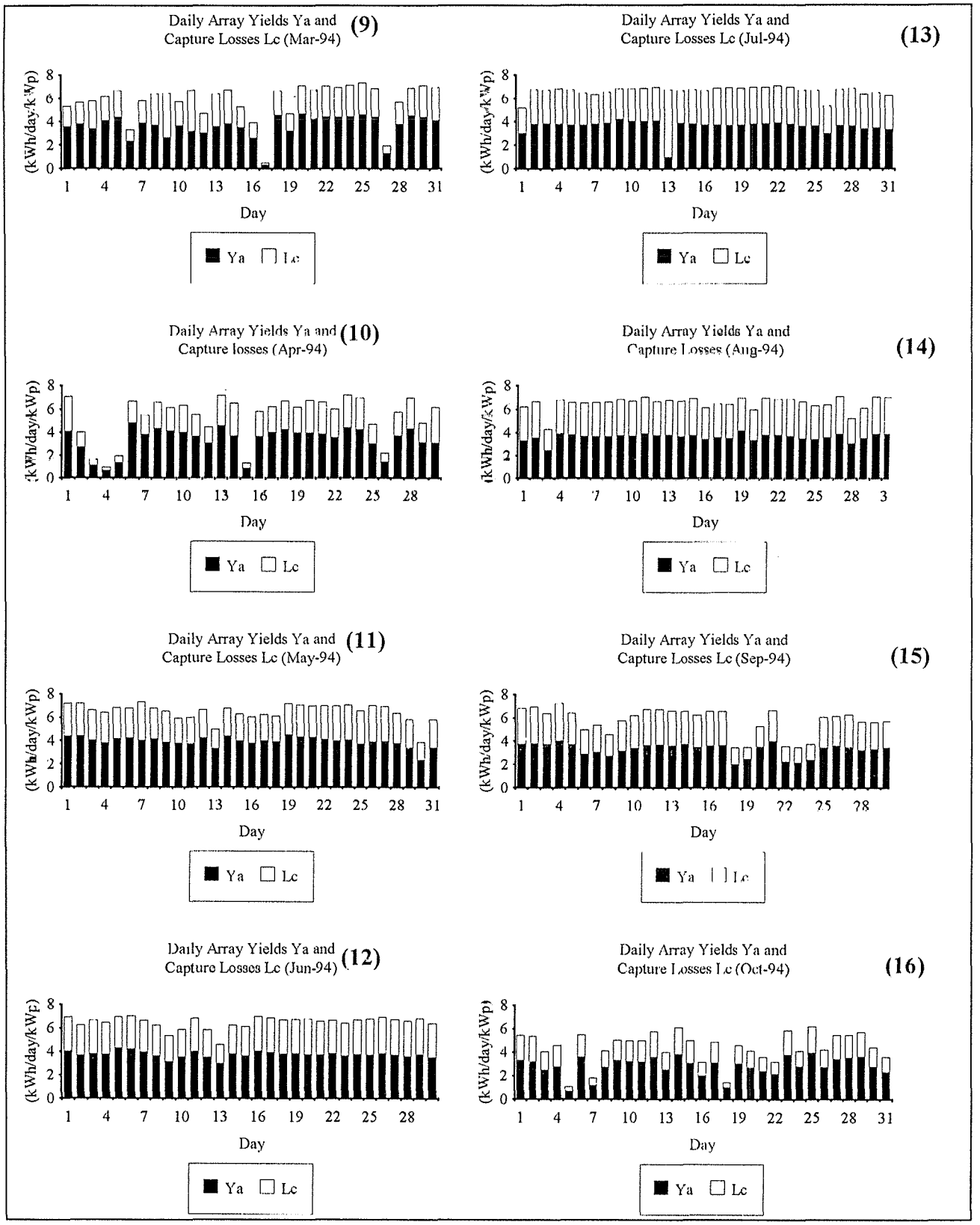

FIGURES 3.5.9 - 3.5.16: Stacked bar charts of the daily array yields and the array capture losses, for the months March to October 1994.

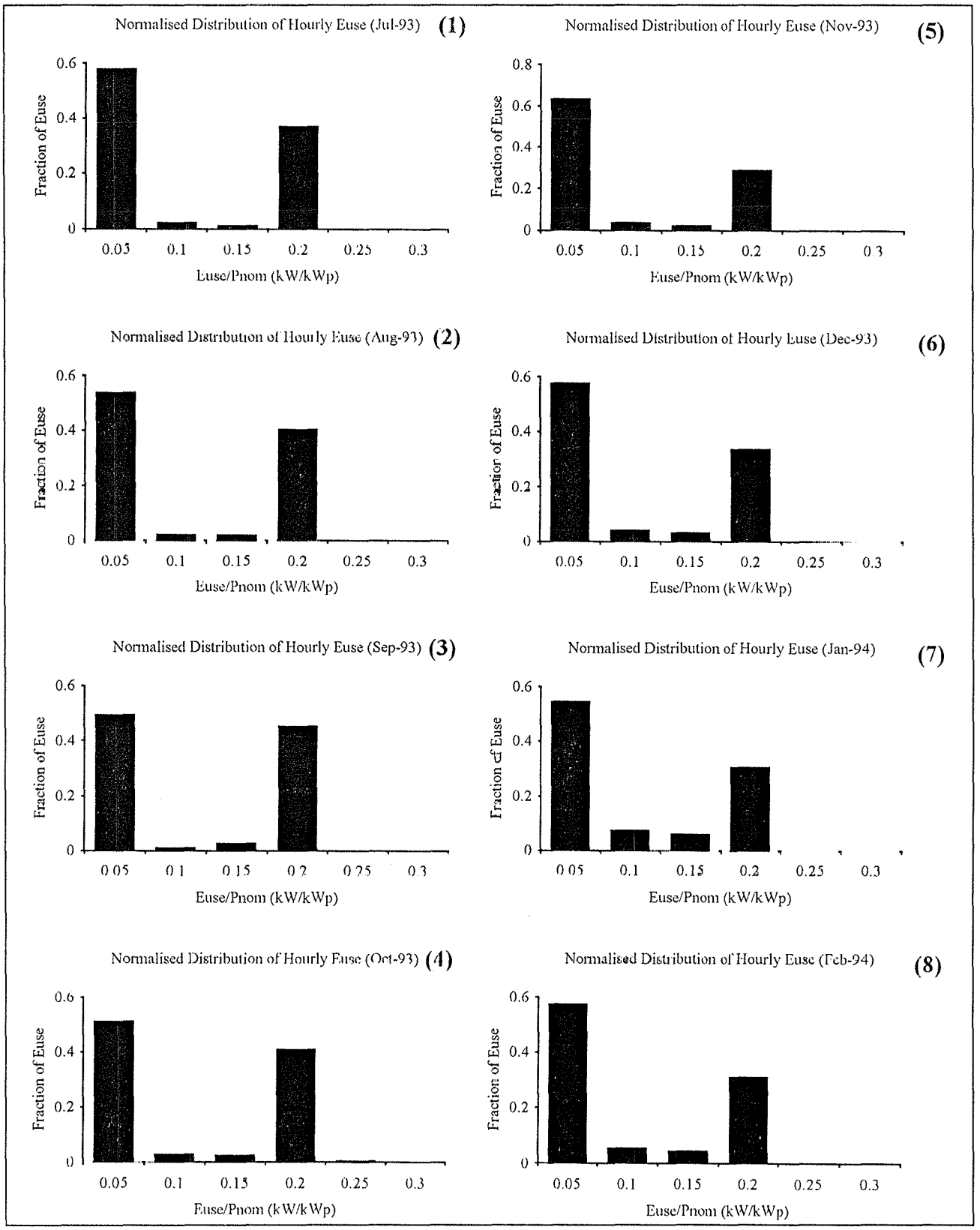

FIGURES 3.6.1 - 3.6.8: The normalised distribution of the hourly useful energy consumed by the electric load, for the months July 1993 to February 1994.

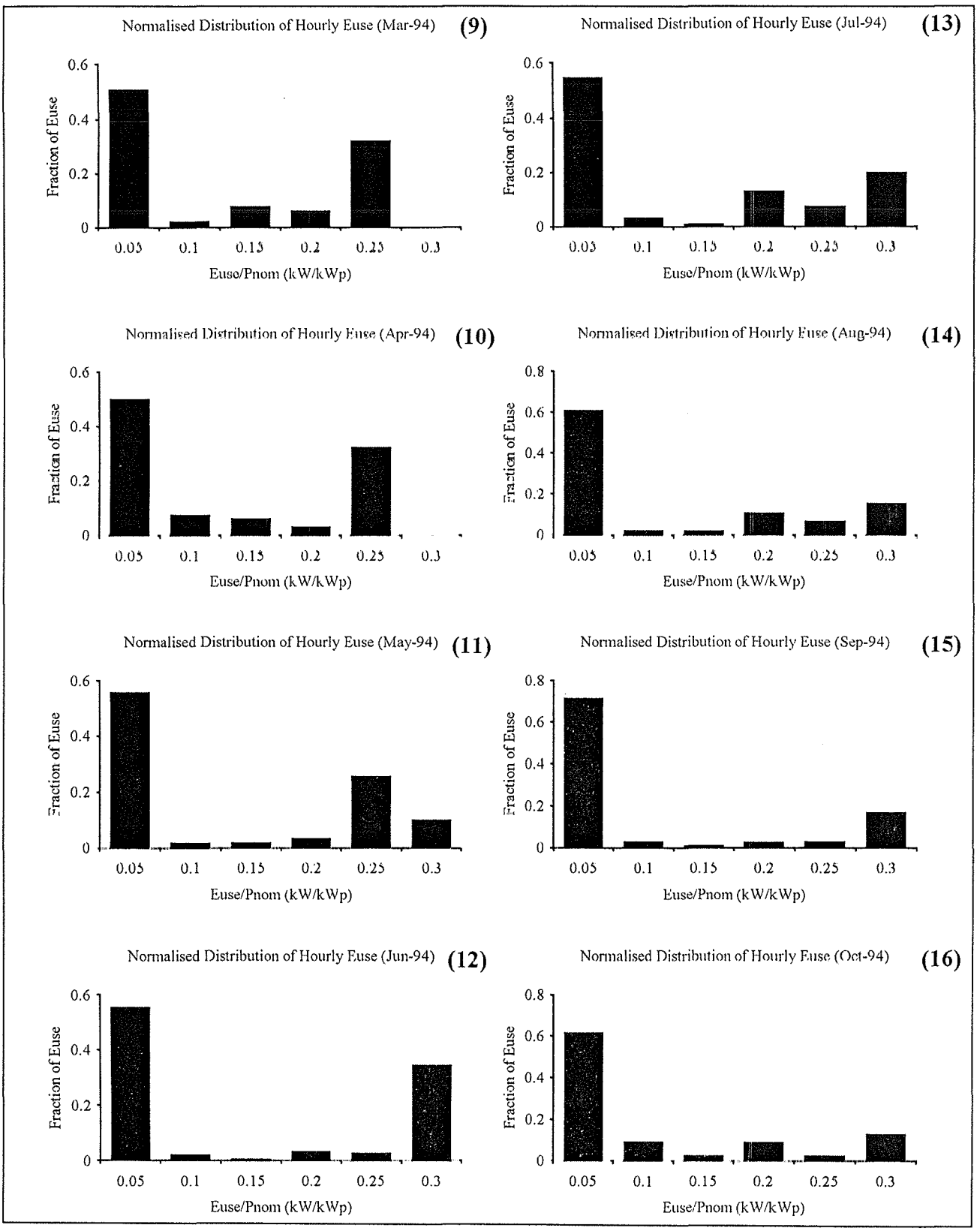

FIGURES 3.6.9 - 3.6.16: The normalised distribution of the hourly useful energy consumed by the electric load, for the months March to October 1994.

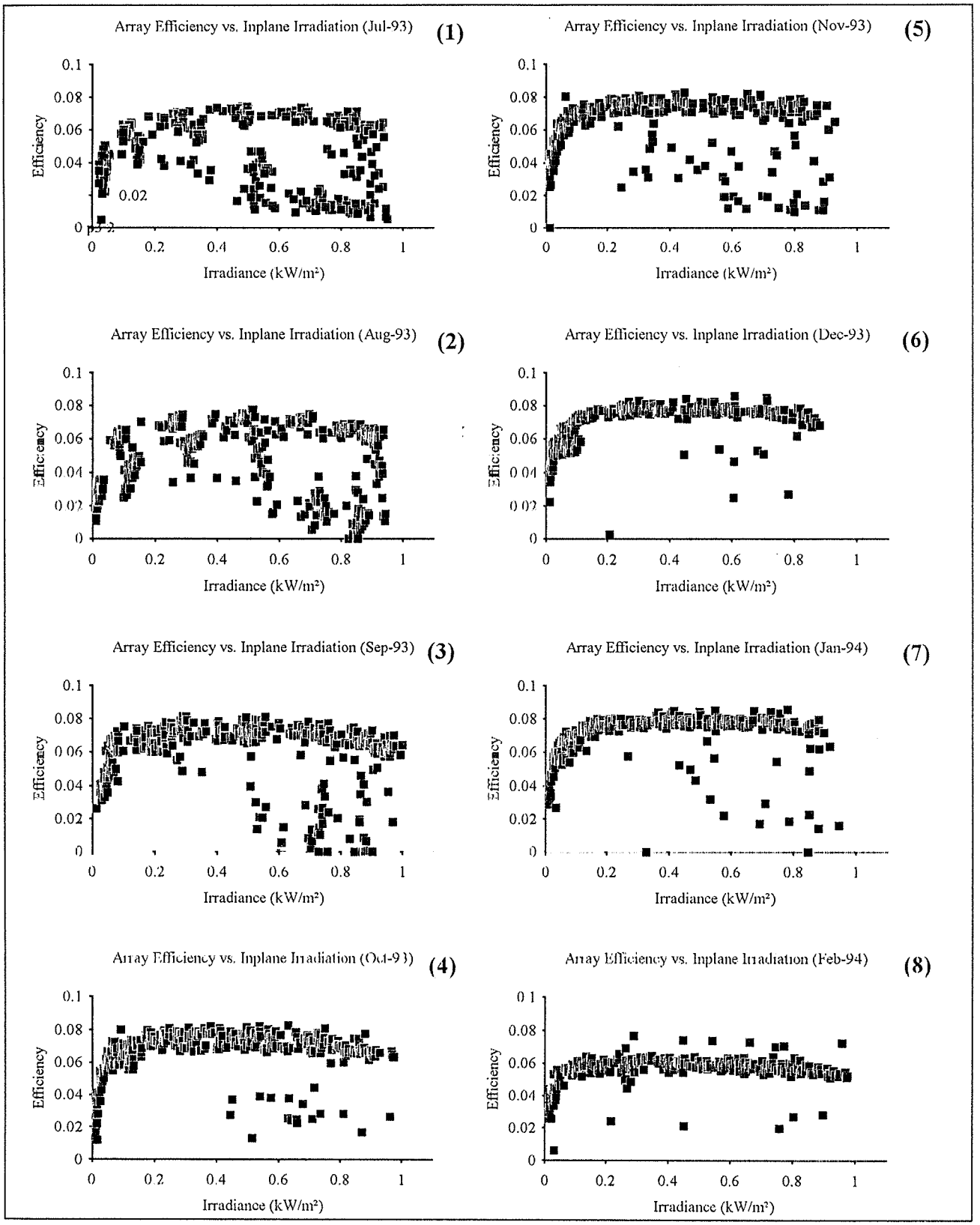

FIGURES 3.7.1 - 3.7.8: Hourly PV array efficiency vs. inplane irradiance, for the months July 1993 to February 1994.

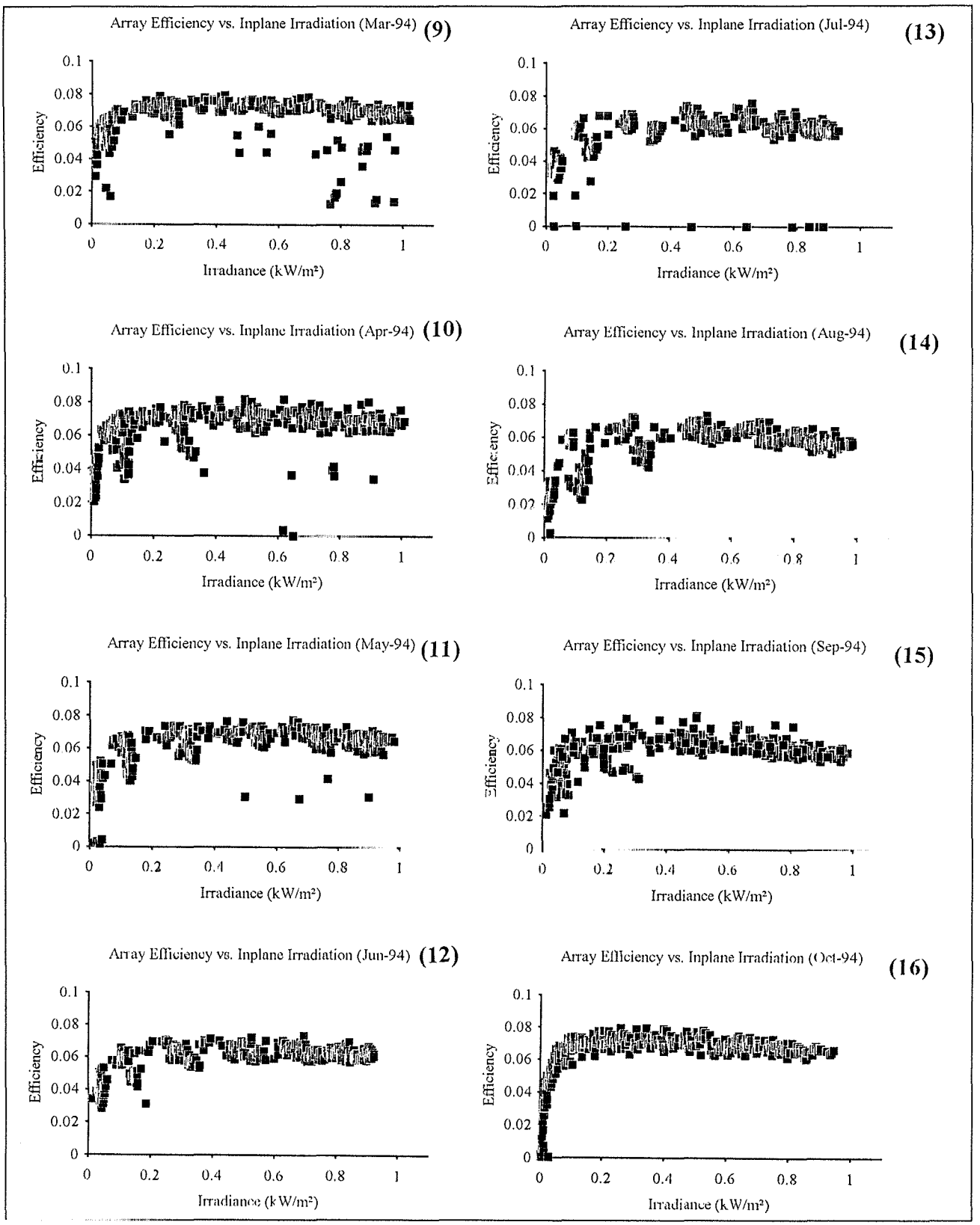

FIGURES 3.7.9 - 3.7.16: Hourly PV array efficiency vs. inplane irradiance for the months March 1994 to October 1994.

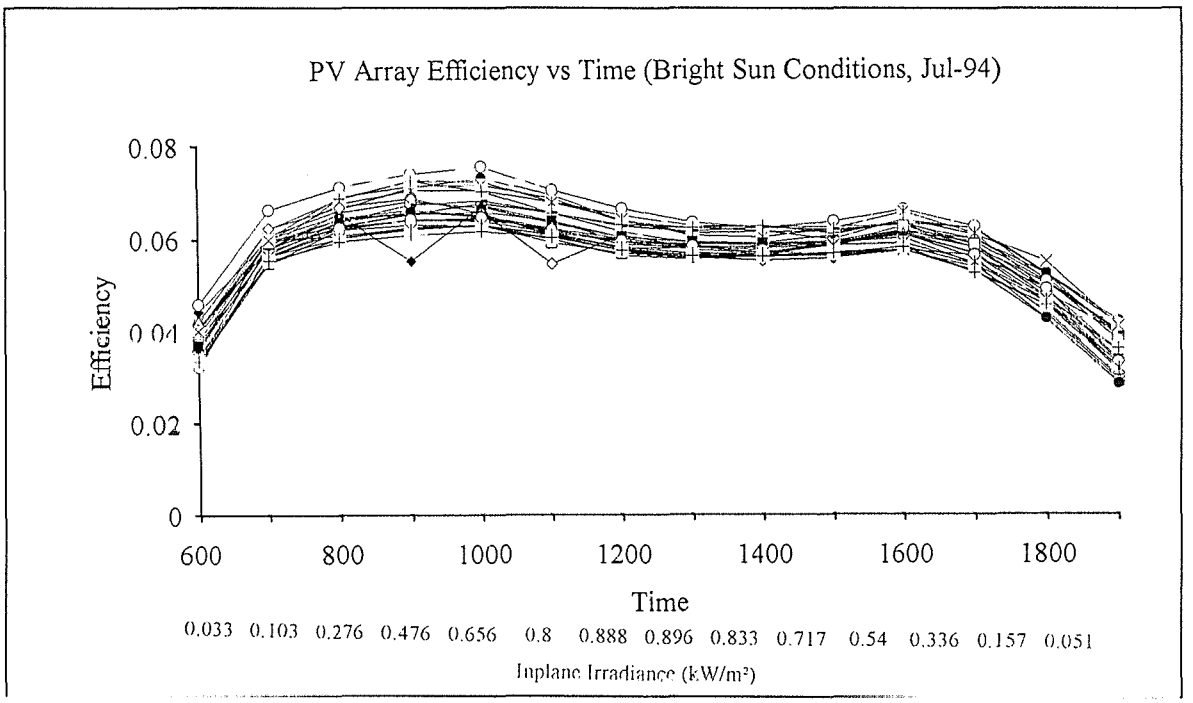

FIGURE 3.8: PV array efficiency vs. time and the corresponding solar radiation for bright sunshine conditions (July 1994).

generate useful power, while the steep decline in efficiency after mid afternoon was caused by the shadow cast on the modules by the tree, as explained earlier in Section 2.3.

The efficiency peaks twice daily with the higher one occurring in the morning at a radiation of about 650 W/m². For this value, the corresponding temperature difference between the modules and the ambient was read off from figure 3.9, as an average of 10 °C for July 1994. For higher temperatures, the efficiency started dropping up to a minimum value that was 9% lower than the maximum. This compared well with the established information that a maximum drop of 10% in module efficiency is expected due to heating of the PV cells.

The second lower peak of efficiency occurred in the afternoon at about 550 W/m² and an average temperature difference between the modules and the ambient of 7 °C. Even though the modules were cooler than during the morning peak, the efficiency did not exceed the morning value. This change in efficiency was brought up by a decrease in the array output power and a simultaneous increase in solar radiation in the afternoon.

From figure 3.10, it was seen that the solar radiation recorded during the afternoon was higher than that in the morning. The same behaviour was also observed by Katsoulis and Papachristopoulos in Greece [82].

Since the pyranometer used was made of a silicon cell, its response to the solar spectrum was expected to be close to that of the PV modules. Since there was more radiation recorded in the afternoon, it implies that this radiation could have been converted to electricity. Hence, the reason for the decrease in efficiency in the afternoon is not related to the spectral distribution of solar radiation but rather to a loss in the PV system itself

This was demonstrated in figure 3.11, where the proportionality between the output current and radiation was not the same during the morning and afternoon, which suggested that the array was operating further away from the maximum power curve in the afternoon, as shown in the I-V curve of figure 3.12, and this could be the direct effect of the increase of the resistance of the system caused by the accumulation of charge in the batteries during the morning. Though the array temperature was cooler in the afternoon as shown in figure 3.13, the increase in the array voltage is so small that it could not offset the drop in current and as a result the output power decreased.

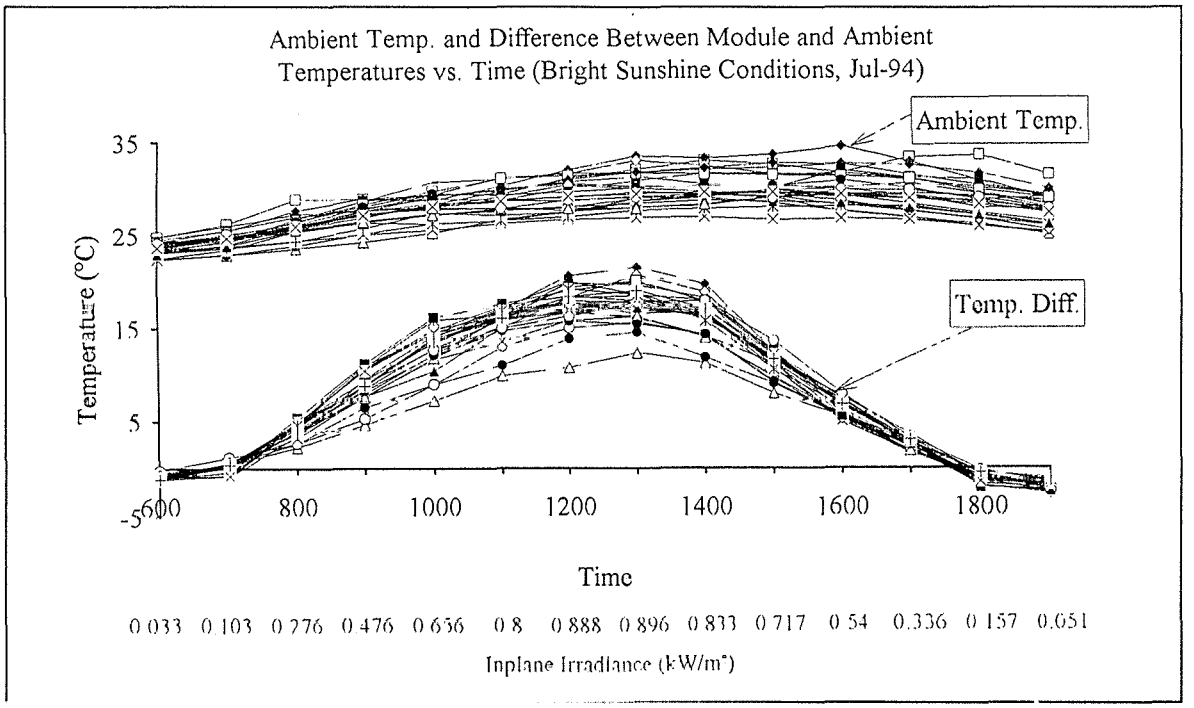

FIGURE 3.9: Ambient temperature and difference between module and ambient temperatures vs. time and the corresponding solar radiation for bright sunshine conditions, (July 1994).

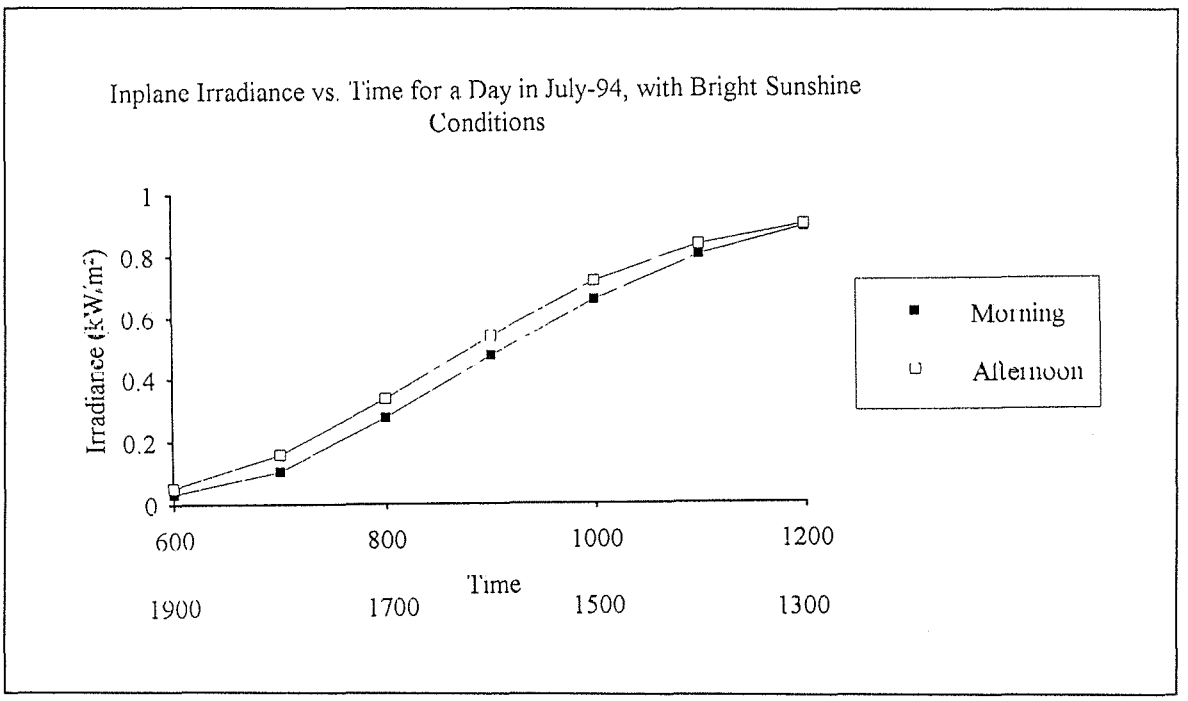

FIGURE 3.10: A graph of the inplane irradiance vs. time for 2nd July 1994, (bright sunshine conditions).

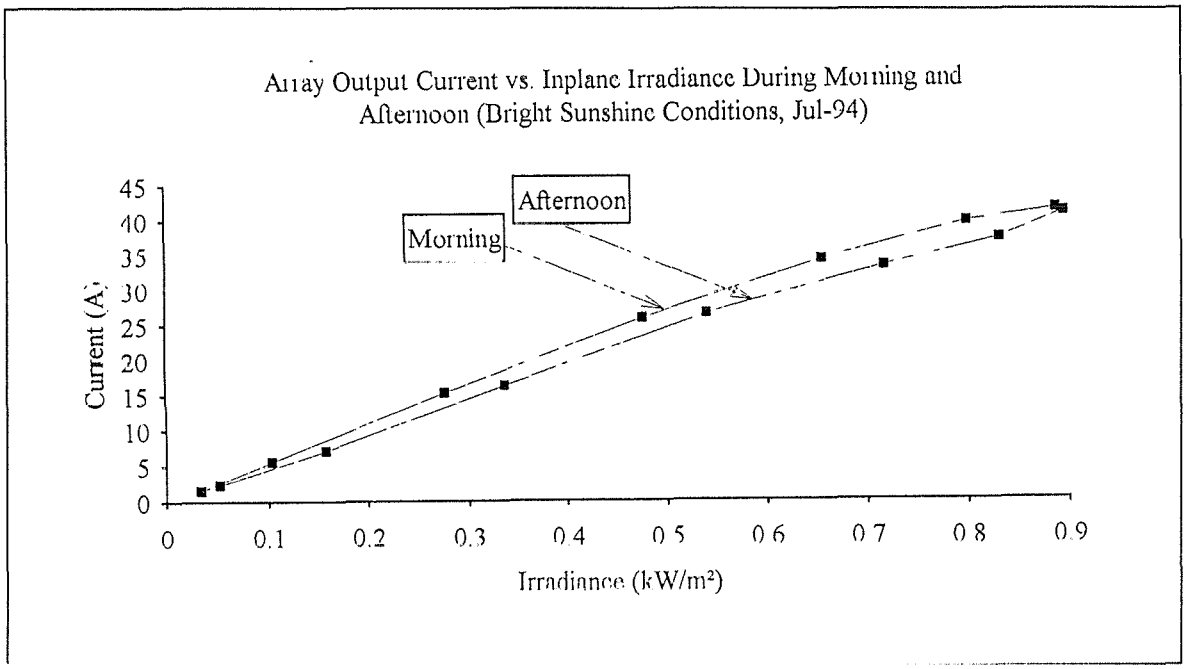

FIGURE 3.11: A graph of the array output current vs. the inplane irradiance for 2nd July 1994, (bright sunshine conditions).

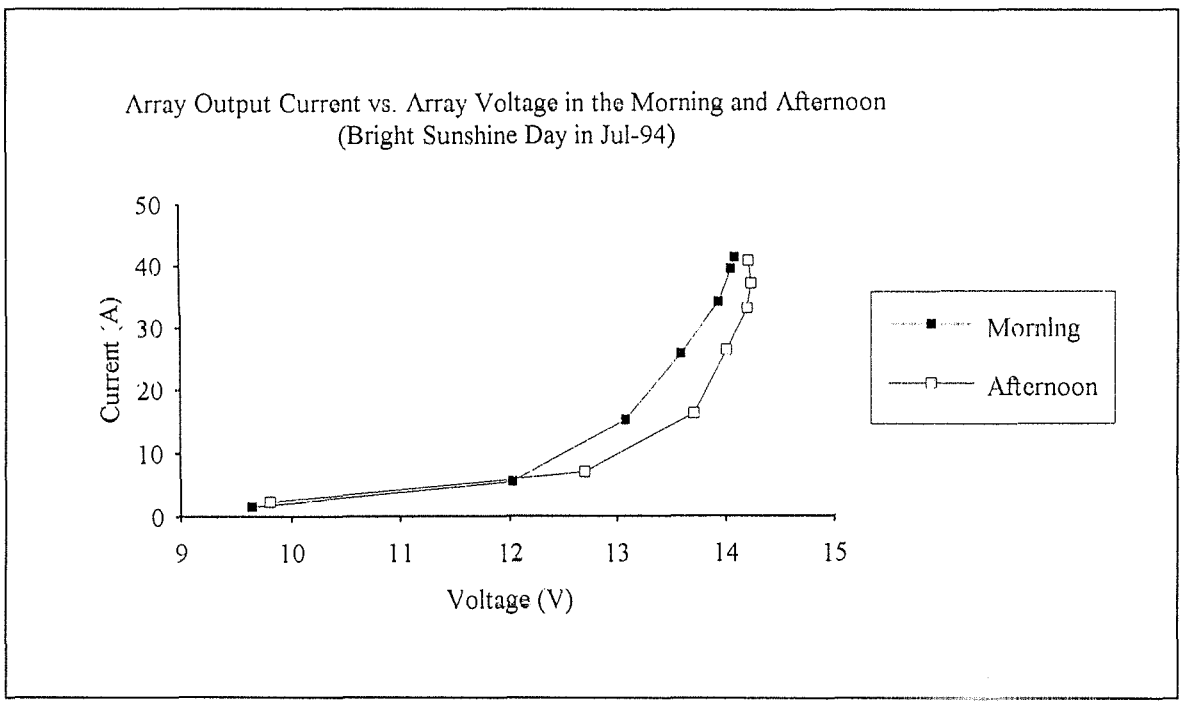

FIGURE 3.12: The current vs. voltage performance of the PV array for 2nd July 1994, (bright sunshine conditions).

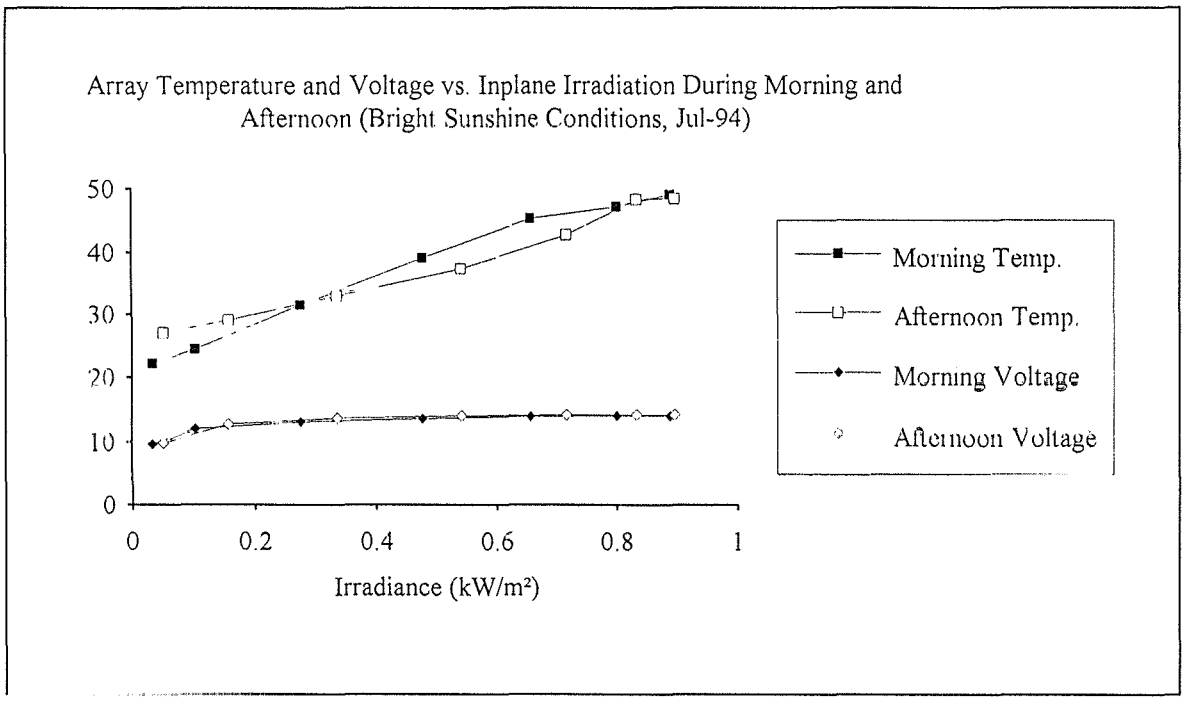

FIGURE 3.13: A graph of the array temperature and its effect on its voltage vs. Irradiation for 2nd July 1994, (bright sunshine conditions).

It has to be mentioned that the back-surface module temperature was measured for only one cell chosen at random. At the beginning, the top surface temperature of an adjacent cell was also monitored but as from April 1994, the top and bottom temperatures were measured for the same cell.

Figure 3.14, shows the recorded temperature for 5 days before and after changing the position of the thermocouples. It is seen that there was some deviation in temperature between different cells but when it was measured for the same cell, the top and bottom temperatures were almost identical. This concludes that both the top or the bottom surface temperature could be used as an indicator to the cell temperature, however it is reported by Hammond and Backus that the actual internal cell temperature is usually 2 to 3 °C higher than that on the surface [83]. Measuring the bottom temperature is preferred because shadowing of the top cell by the thermocouple would be avoided.

3.5 EFFECT OF WIND SPEED ON THE TEMPERATURE OF THE MODULES

Figures 3.15 to 3.17 show the effect of the wind speed on the temperature difference between the modules and the ambient at 11:00, 12:00 and 13:00 for bright sunshine days in July 1994. Clearly, the temperature difference between the modules and the air decreased for wind speeds that were higher than 2 m/s and they tended to level off for speeds greater than 3 m/s.

3.6 EFFECT OF WASHING THE MODULES ON EFFICIENCY

Figure 3.18 showed a slight increase of 2% in the efficiency of the modules after washing them on 30th August over 27th August 1994. The radiation incident on these two days, the array temperature and the electric consumption of the batteries during the previous night were almost identical, so that it was possible to conclude that the increase in efficiency was the result of washing the modules only.

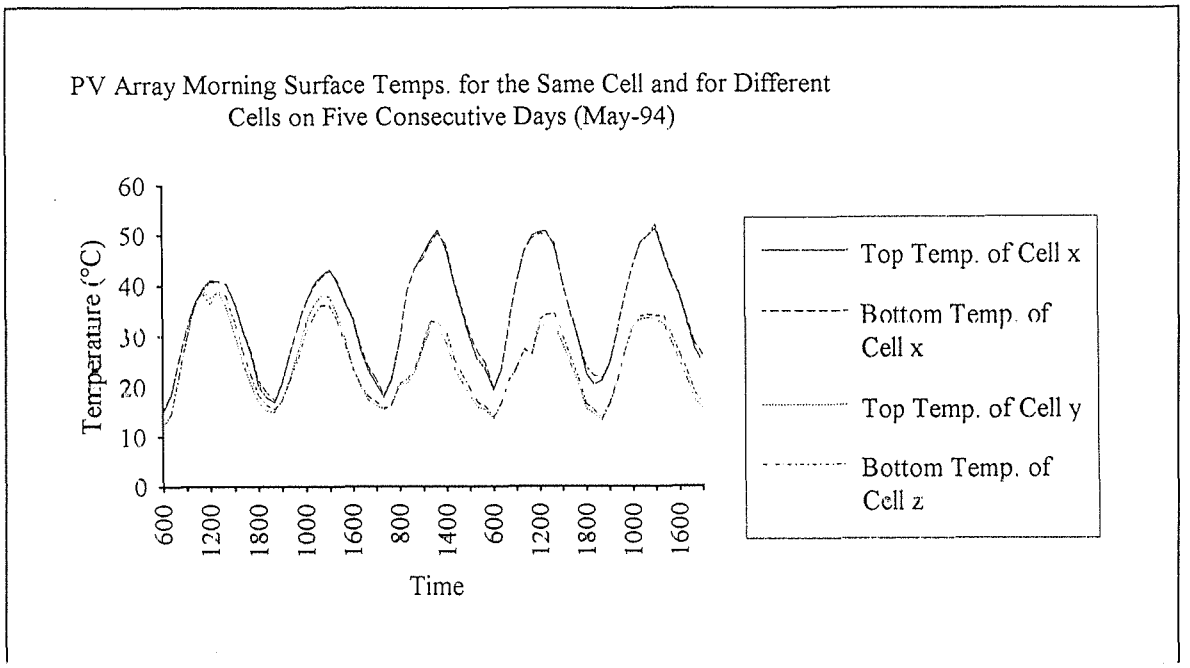

FIGURE 3.14: Top and bottom PV array temperatures for different cells (8th - 12th May 1994) and for the same cell (13th - 17th May 1994).

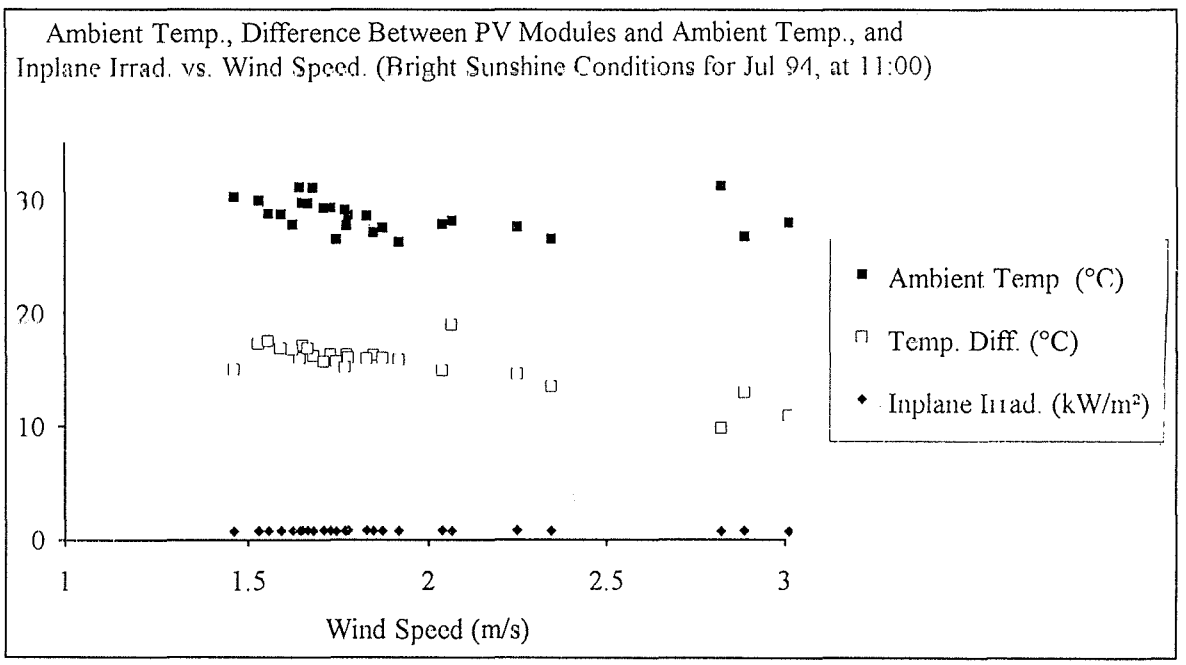

FIGURE 3.15: A graph of ambient temperature, difference between module and ambient temperature and inplane irradiance at 11:00 a.m. vs. wind speed for bright sunny days (Jul-94).

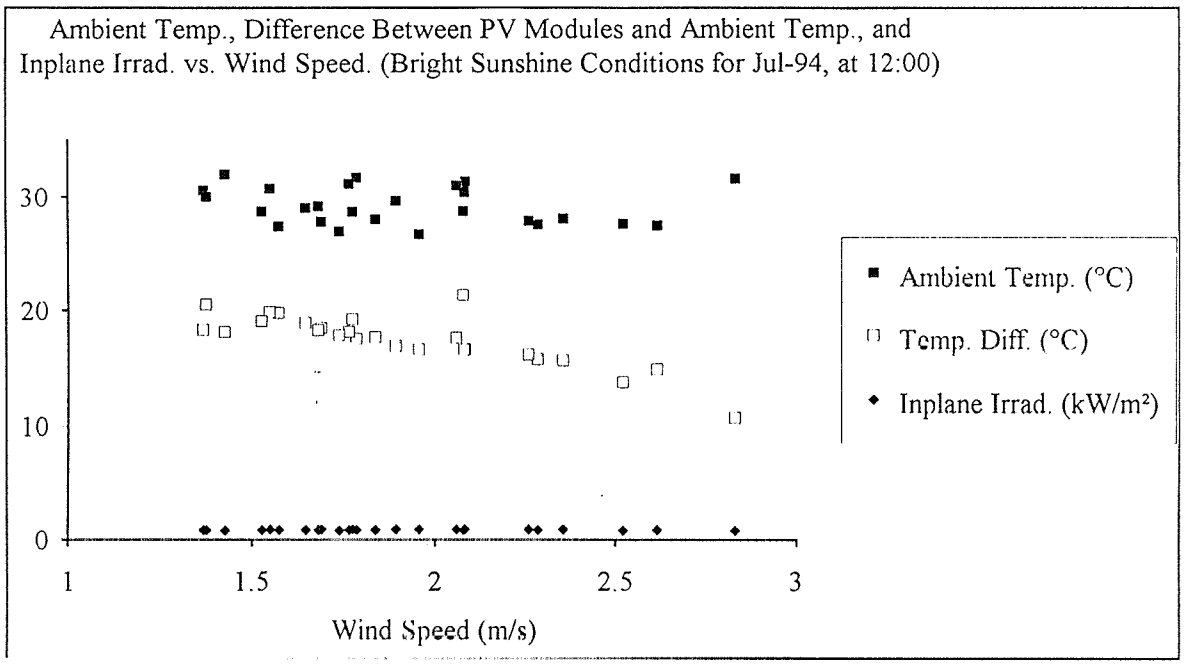

FIGURE 3.16: A graph of ambient temperature, difference between module and ambient temperature and inplane irradiance at 12 noon vs. wind speed, for bright sunny days (Jul-94).

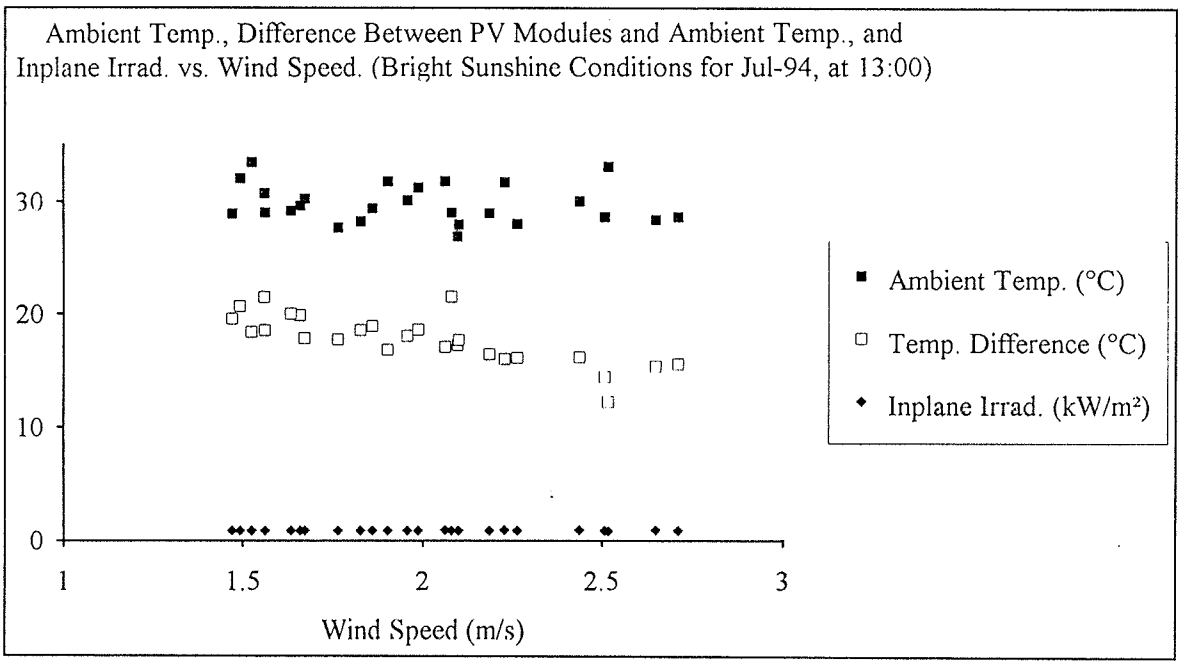

FIGURE 3.17: A graph of ambient temperature, difference between module and ambient temperature and inplane irradiance at 13:00 vs. wind speed for bright sunny days (July 1994).

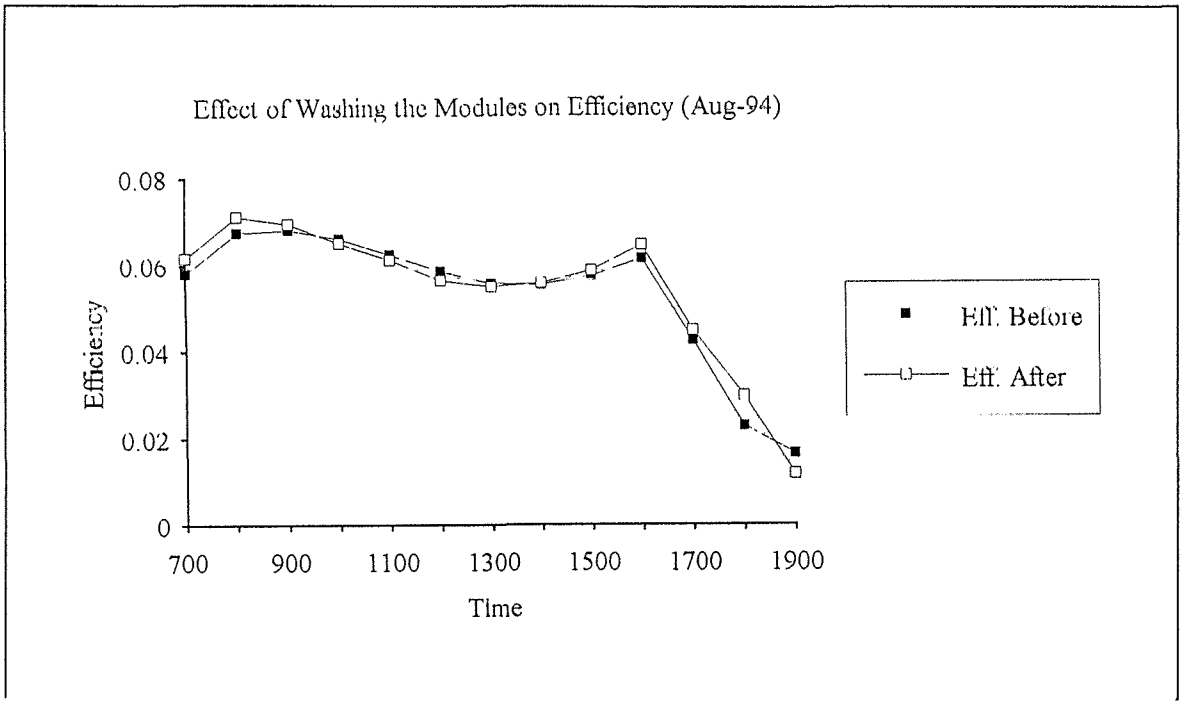

FIGURE 3.18: A graph of array efficiency before and after washing the modules vs. time.

3.7 LINEAR REGRESSION RESULTS

Figures 3.1.1 to 3.1.16, had showed the monthly array yield (kWh/kWp) vs. the inplane irradiance (kW/m²), which could be represented by linear functions, as shown in table 3.5.

In order to present a reasonably valid average relationship, only the months that had a correlation coefficient R of 0.98 or higher were considered and the mean annual regression line was calculated as:

$Y_a = 0.6030(x_i - 0.004,$

with R = 0.99, a standard gradient error of 0.0115 and a standard intercept error of 0.0036.

Figure 3.19 shows the regression lines of the months that had R > 0.98. It was clear that the array yield decreased for the summer season but started increasing again in October and reached a maximum in December.

3.8 RESULTS OF THE BATTERY MONITORING

The voltage and specific gravity measurements that were taken once a month, on two consecutive charge/discharge days, were normalised to a temperature of 25 °C, using the correction factors presented in table D.20 of Appendix D [39].

The voltage was plotted against the corresponding specific gravity for each of the sixty cells, as shown in figure 3.20. It was clear that the performance of the cells differed considerably from each other and no clear-cut conclusion could be reached regarding their ageing. Since every six cells were grouped in parallel in one battery, new sets of data were prepared for the total voltage and mean specific gravity of each battery and a similar graph was plotted, as shown in figure 3.21. It showed that the voltage remained fairly constant, while the specific gravity varied according to the depth of discharge.

Figure 3.22 shows the specific gravity for the different batteries plotted against the date of testing. It was noted that the difference between the peaks and bottoms tended to widen by

TABLE 3.5: Linear regression functions of the array yield (in kWh/kWp) and the inplane irradiance (in kW/m²).

Month	Linear Regression Function	Correl. Coeff. R	Slope std. error	Intercept std. error
Jul. 1993	$Y_a = 0.3467\ G_i + 0.0325$	0.652	0.019	0.0109
Aug. 1993	$Y_a = 0.4294\ G_i + 0.0222$	0.753	0.018	0.0106
Sep. 1993	$Y_a = 0.4683\ G_i + 0.0311$	0.767	0.021	0.0121
Oct. 1993	$Y_a = 0.6028\ G_i + 0.0094$	0.947	0.011	0.0055
Nov. 1993	$Y_a = 0.5203\ G_i + 0.0211$	0.833	0.020	0.0093
Dec. 1993	$Y_a = 0.6883\ G_i - 0.0007$	0.981	0.008	0.0034
Jan. 1994	$Y_a = 0.6329\ G_i + 0.0110$	0.917	0.016	0.0070
Feb. 1994	$Y_a = 0.5188\ G_i + 0.0052$	0.976	0.007	0.0034
Mar. 1994	$Y_a = 0.5992\ G_i + 0.0103$	0.944	0.011	0.0064
Apr. 1994	$Y_a = 0.6318\ G_i - 0.0025$	0.975	0.007	0.0038
May 1994	$Y_a = 0.6121\ G_i - 0.0042$	0.988	0.005	0.0025
Jun. 1994	$Y_a = 0.5849\ G_i - 0.0058$	0.995	0.003	0.0016
Jul. 1994	$Y_a = 0.5668\ G_i - 0.0037$	0.992	0.003	0.0020
Aug. 1994	$Y_a = 0.5556\ G_i - 0.0020$	0.991	0.004	0.0021
Sep. 1994	$Y_a = 0.5594\ G_i - 0.0064$	0.989	0.004	0.0026
Oct. 1994	$Y_a = 0.6248\ G_i - 0.0031$	0.996	0.003	0.0014

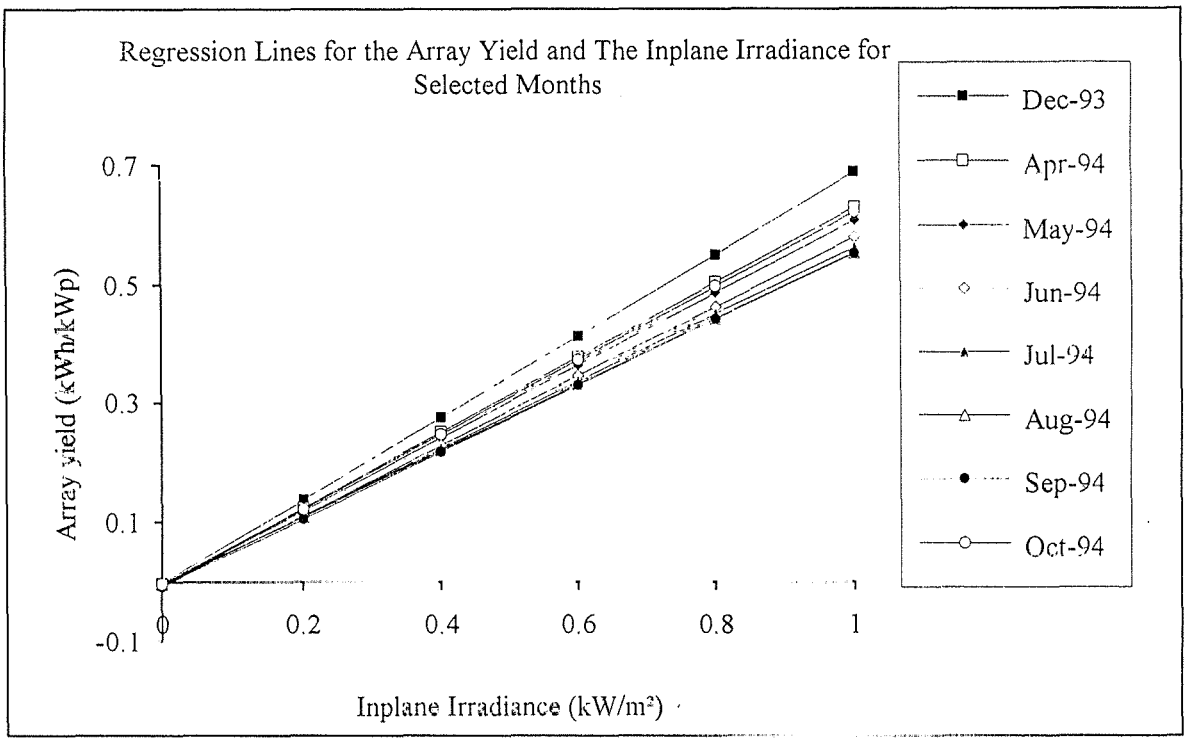

FIGURE 3.19: Linear regression lines of array yield vs. Inplane Irradiance.

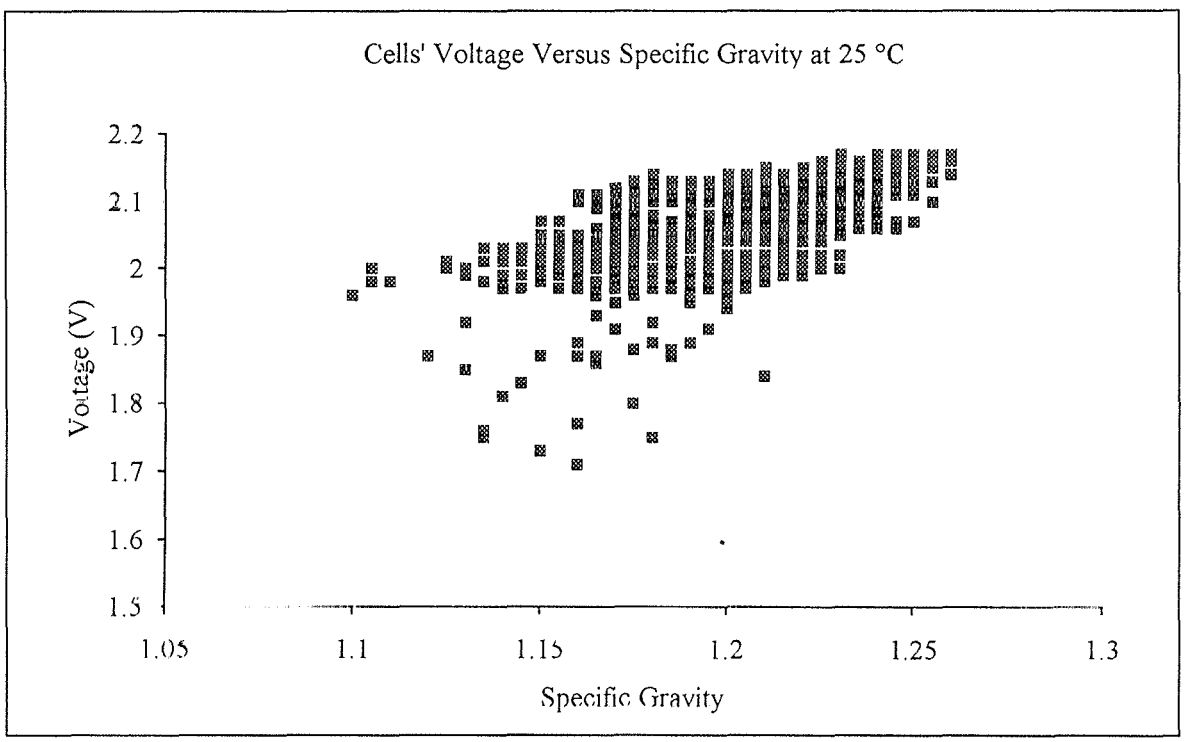

FIGURE 3.20: A scatter diagram of cell voltages vs. the corresponding specific gravity.

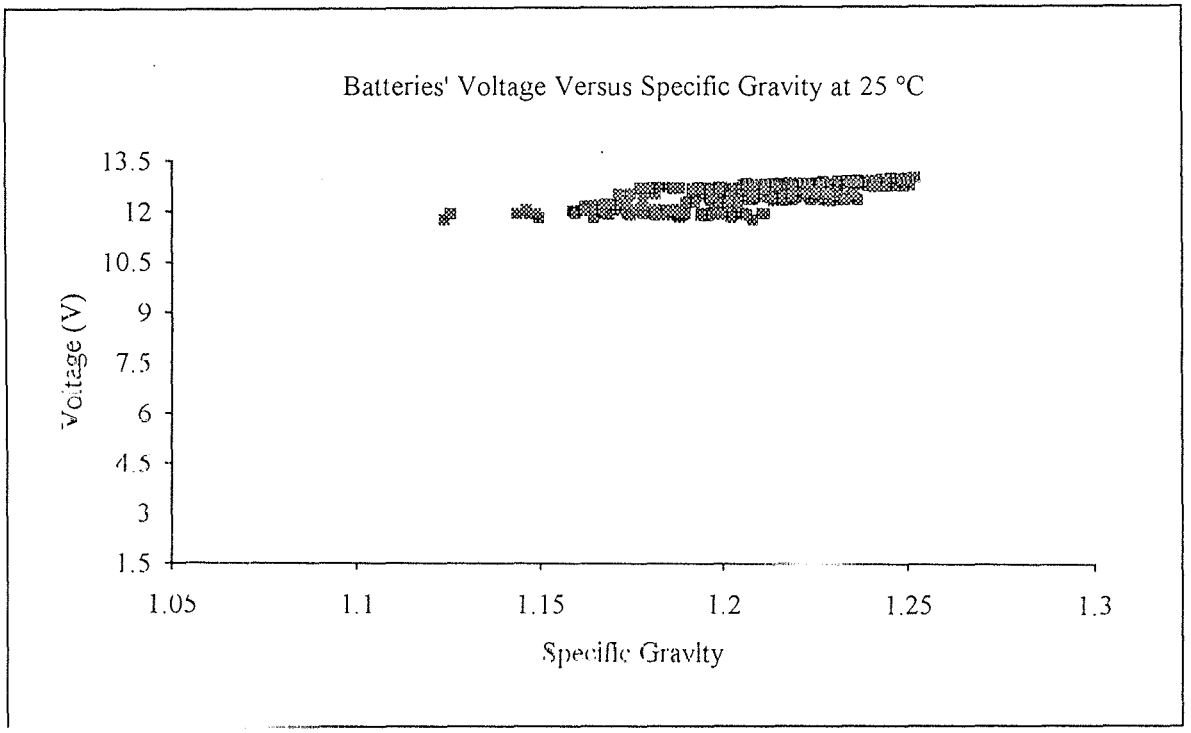

FIGURE 3.21: A scatter diagram of total battery voltage vs. specific gravity.

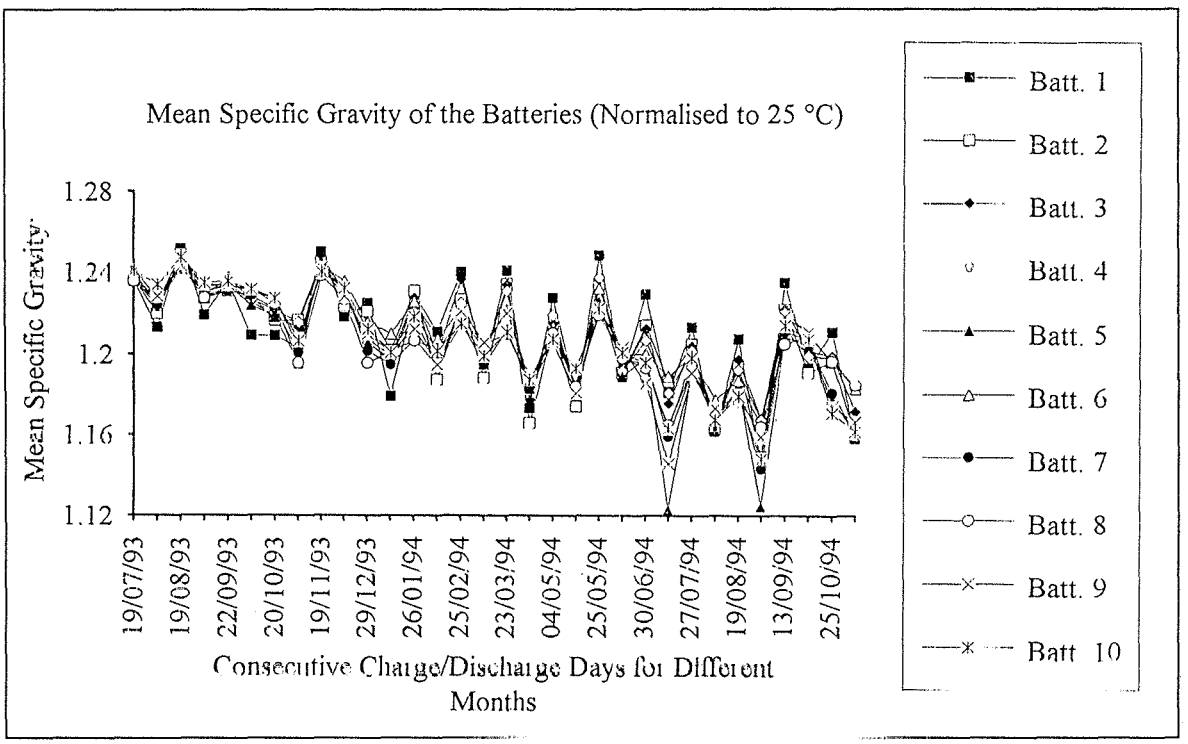

FIGURE 3.22: A graph of the average battery specific gravity vs. date of monitoring.

time, while the specific gravity tended to decrease. Battery no. 5, seemed to suffer most, since it was the battery from which current was passed to feed the monitoring equipment.

Figure 3.23 shows a topographical view of figure 3.22, which clearly displays that during the second year, the specific gravity of the batteries fell below 1.2 overnight, which corresponded to less than 70% state of charge [81] However, it could be shown from the data collected that the actual daily consumption never exceeded 20% of the nominal battery capacity and this indicated that the batteries had deteriorated after the first year, and consequently they were no longer able to withstand the original design autonomy of three days.

From these results, it was clear that for PV systems, individual monitoring of each cell in a battery was more important than its overall performance and that traction batteries were not suitable for solar applications.

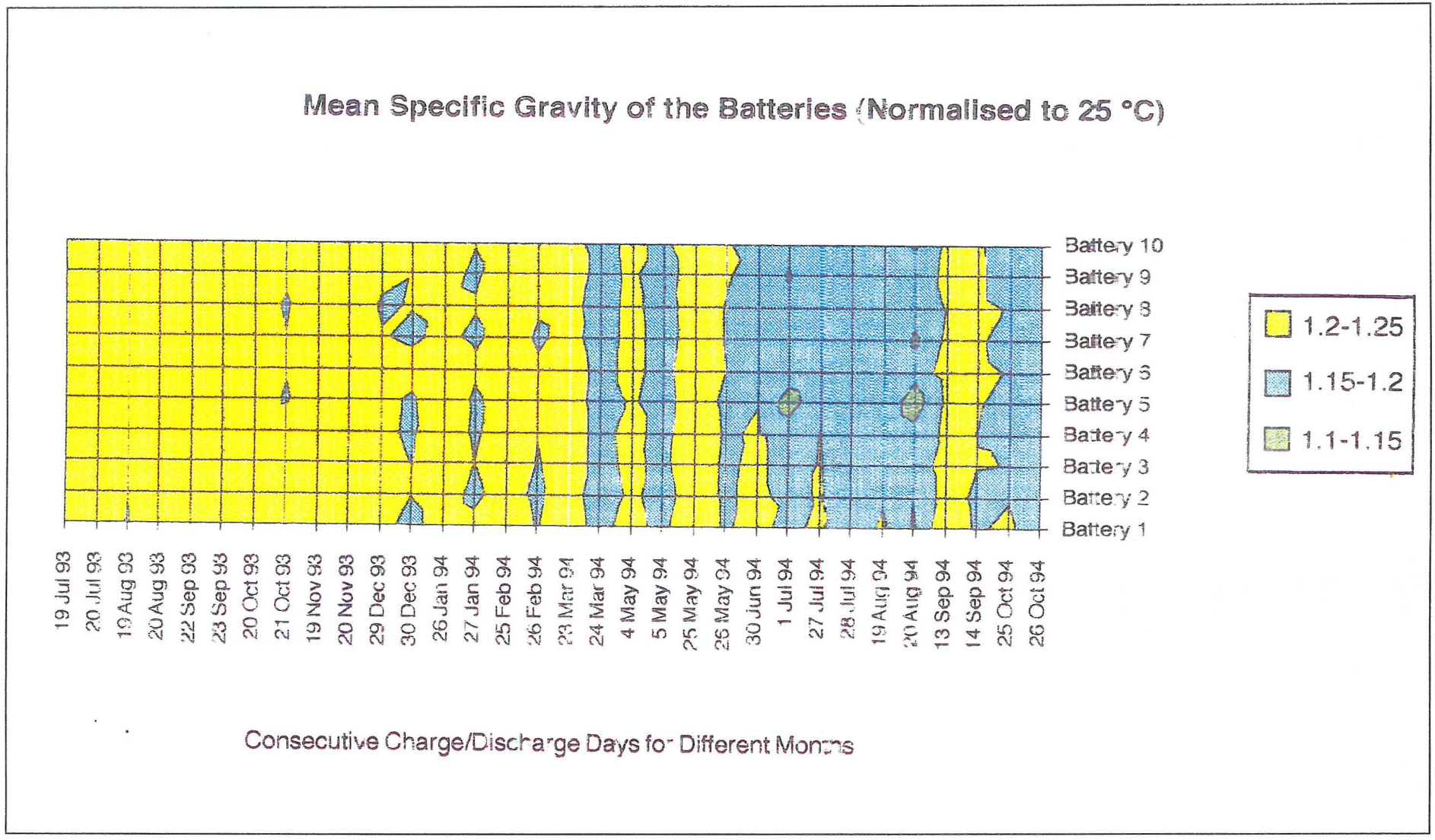

FIGURE 3.23: A topographical view of the mean specific gravity of the batteries on different consecutive charge/discharge days.

CHAPTER FOUR

COST EVALUATION AND SENSITIVITY ANALYSIS

INTRODUCTION

For any PV system, an evaluation of the life cycle cost (LCC), has to be made to quantify the true cost of electricity and to be able to compare between different PV systems and other alternatives of energy sources.

The LCC method takes into consideration the initial costs as well as all other future costs or cash benefits such as maintenance and fuel or the income gained from selling the extra electricity of a grid-connected system to a nearby consumer or to the grid, all discounted to their present value.

In the LCC technique, it is important to converge (discount) all future expenses and cash benefits to a common point in time, usually taken as the present time for convenience. Because of inflation, a unit of money paid now is worth less in the future but simultaneously if this unit was invested it would earn interest over the appointed period The difference between these two factors gives the net discount factor to be used in the LCC technique.

Another advantage of the LCC technique is that it allows the breaking down of costs and this could be useful in studying the effect of each source of expense/income and try to optimise it. Yet one has to keep in mind that this method does not take into account the non-quantifiable social benefits of PV applications such as the elimination of pollution, noise, health hazards, and dumping of residuals, as well as higher reliability.

In this chapter sensitivity analysis will also be used to investigate the impact of changing each of the parameters involved in the LCC, on the cost of energy. This enables the setting up of a table of priorities whereby one can work to reduce the unit cost of electricity.

4.1 LIFE CYCLE COSTING (LCC)

The LCC can be expressed by the equation [84]:

$$LCC = (C + M + R - S)/E \qquad \text{---------- (4.1)}$$

where, LCC = life cycle cost (Lm/kWh);

C – total initial capital;

M = total maintenance cost;

R = replacement cost anticipated for the whole life of the system;

S = salvage or scrap value at the end of system life, and;

E = energy produced (kWh/annum).

All the above values have to be converged to their present values by using the appropriate discount factors that are supplied in tables of standard textbooks [85] or by calculation using the equations given below [84]:

For a fixed amount of money to be paid in n years time, the present value interest factor is given by:

$$PVIF_{k,n} = 1/(1+k)^n; \qquad \text{---------- (4.2)}$$

where, $PVIF_{k,n}$ = present value interest factor of one unit of money at a discount rate k at year no n

For an annual recurrent expenditure, the present value interest factor annuity is given by:

$$PVIFA_{k,n} = \sum_{t=1}^{n} \frac{1}{(1+k)^t}; = \frac{1 \quad 1/(1+k)^n}{k}. \qquad \text{---------- (4.3)}$$

The life cycle costing for the PV system of this project is presented in table 4.1. In order to choose a suitable value for the discount rate, it is necessary to know the highest rate of return - known as the nominal discount rate - on the money invested, had it not been spent on the project. Also, the inflation rate during the initial year, known as year no. zero, has to be defined. The net discount rate is then found using the equation:

$$(1 + r) = (1 + m)/(1 + I), \qquad \text{---------- (4.4)}$$

where, m = nominal discount rate

LIFE CYCLE COST (LCC) ANALYSIS

ECONOMIC PARAMETERS:

1. Life-time = 20 years

2. Net discount rate = 4.2%

STAND-ALONE PV SYSTEM

Column No.	1	2	3	4	5
Item	Year	Cost (Lm)	PVIF	PVIFA	P V. (Lm)
					(2x3 or 2x4)
1. Capital and Installation					
PV Modules	0	2400	1		2400
Structure	0	200	1		200
Batteries and Cables	0	970	1		970
Battery Control Unit	0	1110	1		1110
Labour	0	300	1		300
Wires	0	20	1		20
TOTAL					**5000**
2. Operation & Maintenance	1...20	12		13.3528	160.233
3. Repair and replacement					
Battery Bank	1...3	950	0.8839		839.693
	4...6	950	0.7813		742.194
	7..9	950	0.6905		656.016
	10...12	950	0.6104		579.844
	13...15	950	0.5395		512.516
	16...18	950	0.4768		453.007
Battery Control Unit	11...20	1110	0.6627		735.607
4. Salvage value					
20% of total initial cost	20	1000	0.4392		439.183
Total LCC (Items 1+2+3-4)					**9239.926**
Annuity = Present Value/PVIFA		9239.926		13.3528	691.985
Cost/kWh = Annuity/E, E = 900 kWh					**0.769**

Table 4.1: Life Cycle Costing for the stand-alone PV system of this project.

r= net (real) discount rate;

i = inflation rate.

For Malta, the maximum interest charged by the commercial banks is 8.5% and this can be considered equal to m, while the inflation rate was 4.14% for 1993, as published by the Central Bank of Malta [86]. By substituting these values in the above equation we get r = 4.2%.

As for the life-time of the PV system components, they were assumed as follows [72].

PV modules and supporting structure – 20 years,

Battery control unit and electronics = 10 years;

Traction lead-acid batteries = 3 years.

Since the electric grid covers most of the Maltese Islands, the chances of using a stand-alone system are limited to certain applications such as street lighting and for boats. On the other hand, grid-connected PV systems could be installed to relieve the country's dependence on fossil fuels, to provide the means to shave off summer peak loads and to reduce pollution. Hence, it would be interesting here to evaluate their LCC, as presented in table 4.2.

The costs of the balance of system (BOS) components used in the LCC analysis were the true purchasing values in Malta inclusive of taxes and delivery. Since most of the components are sold by agents of mother companies abroad and owing to the fact that such systems are not yet popular, the prices are relatively higher than in other countries. However the new 1995 prices of a complete grid-connected system are already lower than the prices quoted in table 4.2 by Lm 800, as found out from recent tenders, and this brings the LCC of PV grid-connected electricity down to Lm 0.24/kWh, i.e. almost 70% less than a stand-alone PV system.

While the cost of batteries could increase in the future, the cost of the PV modules and the electronic equipment shall probably decrease. Hence, for this analysis it was assumed that the changes in costs shall balance each other and consequently the prices were considered the same for the whole 20 years period. Nevertheless, the sensitivity analysis described in the next section took the changes in prices into consideration and gave a clear idea of the expected effect on the unit price of electricity.

LIFE CYCLE COST (LCC) ANALYSIS

GRID-CONNECTED PV SYSTEM

Column No.	1	2	3	4	5
Item	Year	Cost (Lm)	PVIF	PVIFA	P.V. (Lm)
					(2x3 or 2/4)
1. Capital and Installation					
PV Modules	0	2400	1		2400
Structure	0	200	1		200
DC/AC Inverter	0	1110	1		1110
Labour	0	300	1		300
Wires	0	20	1		20
TOTAL					**4030**
3. Repair and replacement					
Inverter	11...20	1110	0.6627		735.607
4. Salvage value					
20% of total initial cost	11...20	806	0.4392		353.982
Total LCC (Items 1+2+3 4)					**4411.625**
Annuity = Present Value/PVIF		4411.625		13.3528	330.390
Cost/kWh = Annuity/E, E = 1125 kWh					**0.294**

Table 4.2: Life cycle costing for a grid-connected PV system having the same peak PV power as the stand-alone system.

The annual energy produced by the 1.2 kWp stand-alone PV system was calculated as 900 kWh/annum using the actual output that was presented in table 3.3. As for the estimated output energy of a similar grid-connected system, the overall balance of system components efficiency would be higher by about 30% due to the elimination of batteries and the possibility to operate the PV modules continuously at their maximum power point. Hence, the output energy would be about 1125 kWh/annum.

It is common practice to assume the salvage value to be 20% of the total initial cost [87]. A similar result could also be reached by assuming that at the end of the life of the system only one-half of the PV modules are fit for further use. By discounting their present cost over this period a slightly higher salvage value is obtained

The maintenance cost for a stand-alone system was assumed to be Lm 1 per month and this covers the cost of topping up the batteries with distilled water, and the periodic cleaning of their poles and surface. As discussed before and from figure 5.18, there is no dire need to wash the modules in summer and hence, no cost was attributed to this service.

4.2 SENSITIVITY ANALYSIS

Sensitivity analysis entails the changing of one parameter that affects the LCC, while keeping the others constant, and repeating the LCC technique to find the new price of one unit of electricity. A spider diagram can then be constructed and analysed accordingly. Here, the main parameters involved are the costs of the PV modules, the batteries, the battery control unit or inverter and the total initial capital. Also the discount rate, the lifetime and the output energy shall be varied. Table 4.3 shows the results obtained.

In figures 4.1 and 4.2, spider diagrams have been constructed for the stand-alone and grid-connected systems, whereby each parameter is varied by up to 50%. It can be seen that the most critical factor that affects the life cycle cost is the output energy from the system. This can be increased by optimising the BOS efficiency of the system.

Table 4.3: Sensitivity analysis results for the stand-alone (S.A.) and grid-connected (G.C.) PV systems.

SENSITIVITY ANALYSIS RESULTS

PV MODULES

Variation %	50%	25%	0	25%	50%
Total cost of modules	1200	1800	2400	3000	3600
Cost S.A. (Lm/kWh)	0.678	0.723	0.769	0.815	0.86
Cost G.C. (Lm/kWh)	0.221	0.257	0.294	0.33	0.366

BATTERIES

Variation %	-50%	-25%	0	25%	50%
Total Cost of batteries	475	712.5	950	1187.5	1425
Cost S.A. (Lm/kWh)	0.575	0.672	0.769	0.865	0.962
Cost G.C. (Lm/kWh)	-	-	-	-	-

BCU/INVERTER

Variation %	-50%	-25%	0	25%	50%
Cost of BCU/Inverter	555	832.5	1110	1387.5	1665
Cost S.A. (Lm/kWh)	0.697	0.733	0.769	0.805	0.841
Cost G.C. (Lm/kWh)	0.235	0.264	0.294	0.323	0.352

LIFE-TIME

Variation %	-50%	-25%	0	25%	50%
Life-time	10	15	20	25	30
Cost S.A. (Lm/kWh)	0.922	0.877	0.769	0.77	0.741
Cost G.C. (Lm/kWh)	0.386	0.352	0.294	0.288	0.264

DISCOUNT FACTOR

Variation %	-50%	-25%	0	25%	50%
Discount Factor	0.021	0.0315	0.042	0.0525	0.063
Cost S.A. (Lm/kWh)	0.689	0.728	0.769	0.811	0.853
Cost G.C. (Lm/kWh)	0.241	0.268	0.294	0.32	0.349

ENERGY OUTPUT

Variation %	-50%	-25%	0	25%	50%
Energy Output of S.A.	450	675	900	1125	1350
Cost S.A. (Lm/kWh)	1.537	1.025	0.769	0.615	0.512
Energy Output of G.C.	562.5	843.75	1125	1406.25	1687.5
Cost G.C. (Lm/kWh)	0.587	0.391	0.294	0.235	0.196

INITIAL CAPITAL

Variation %	-50%	-25%	0	25%	50%
Capital of S.A. System	2500	3750	5000	6250	7500
Cost S.A. (Lm/kWh)	0.578	0.673	0.769	0.863	0.958
Capital of G.C. System	2015	3022.5	4030	5037.5	6045
Cost G.C. (Lm/kWh)	0.172	0.233	0.294	0.355	0.416

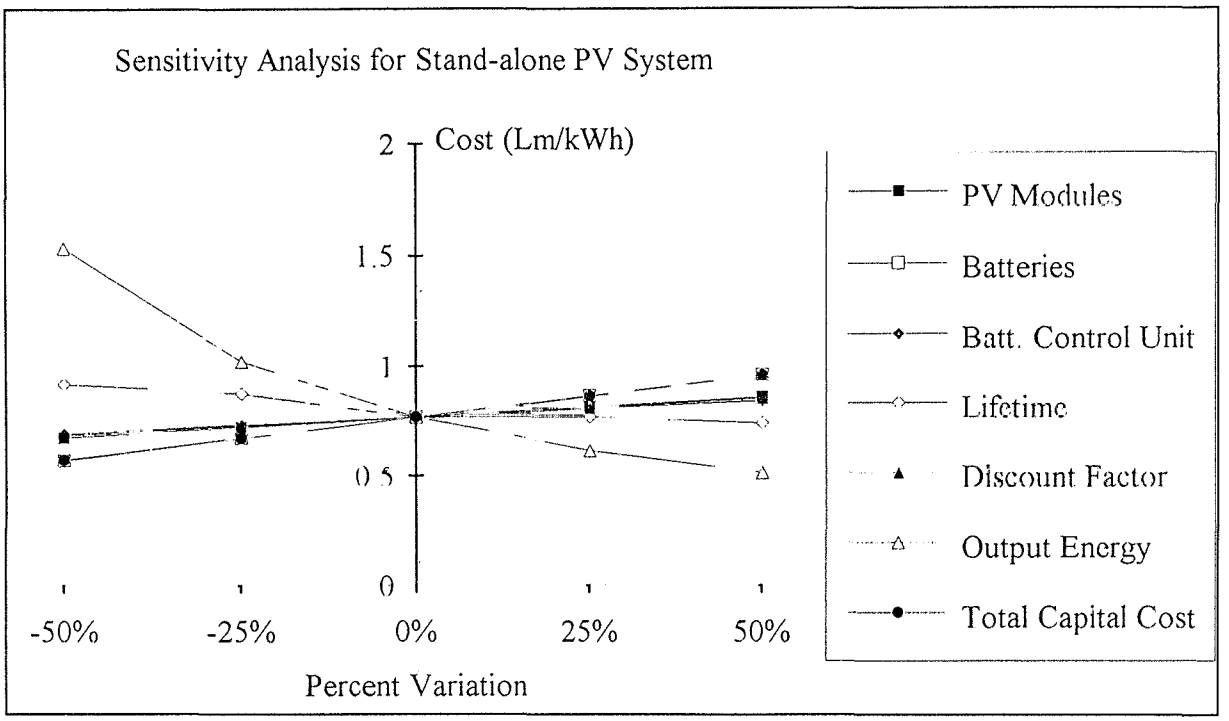

Figure 4.1: Spider diagram for the cost variation of the 1.2 kWp stand-alone PV system.

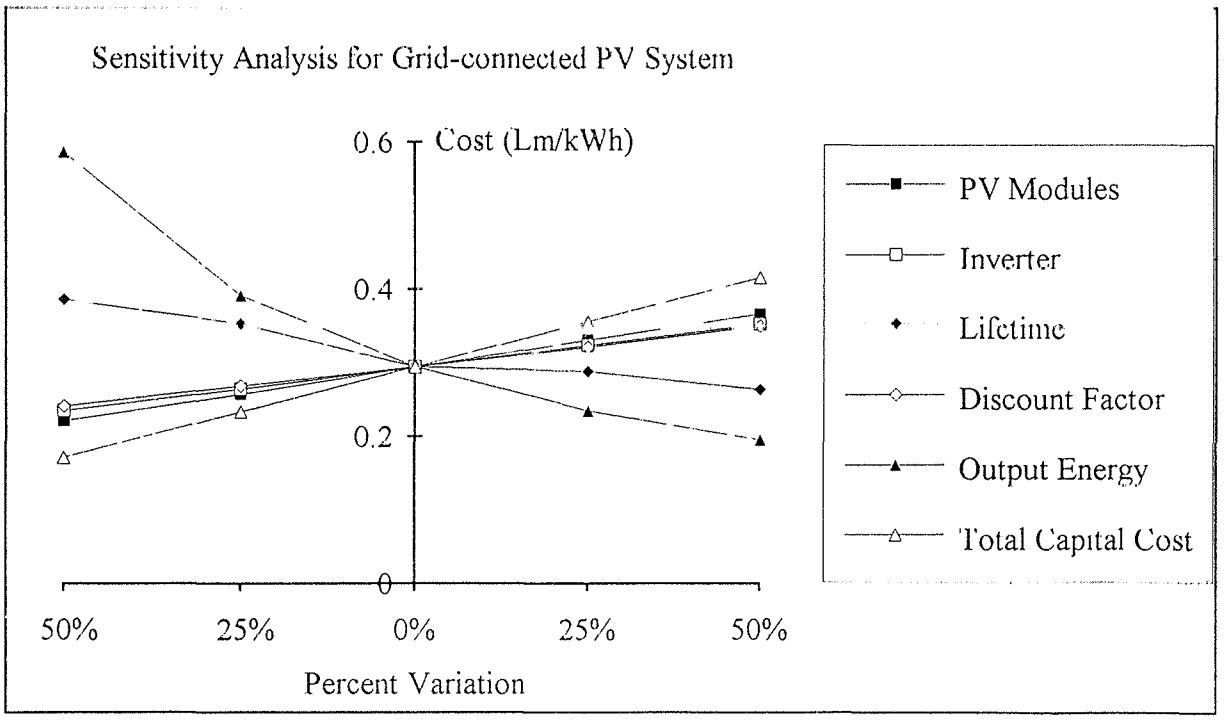

Figure 4.2: Spider diagram for the cost variation of the 1.2 kWp grid-connected PV system.

From figure 4.1 and 4.2, it is obvious that when the PV system covers 20 years, the cost/life-time ratio is optimum. Lower life-times increases the life cycle cost while longer life-times have a negligible effect on the cost and this justifies the use of a 20 year LCC analysis.

The life cycle percentage cost of the BOS components of a stand-alone and grid-connected system are presented in the pie charts of figures 4.3 and 4.4. It is clear that for a stand-alone system, the batteries have a major effect on the cost while for the grid-connected system, the modules take the largest percentage of the cost. For the former, it might be more economical to use solar batteries, while for the latter case, it might be wise to consider the use of thin-film photovoltaic cells.

4.3 VARIABLE ASSUMPTIONS USED IN THE LCC TECHNIQUE

In this LCC technique, no revenues were considered, rather it was assumed that the demand just balances the electricity produced for both systems under consideration. Also, it was assumed that the capital was fully paid during installation. In case that only part of the capital is paid, the remaining amount can be divided into annual payments and discounted accordingly but this would lead to a higher cost for electricity.

The net discount rate of 4.2% that was used to calculate the present value interest rates is the true rate for the year 1993. The use of higher discount rates would result in giving more importance to the initial cost over the future costs, while lower discount rates increases the weight of future costs in the analysis.

As discussed in Section 3.8, the traction lead-acid batteries have started deteriorating and this lead to the estimation of a 3-year life-time for such batteries, which was used in the LCC analysis. However, it is now possible to find batteries for solar applications at moderate prices such as Delco 1000, which could live for 6 years.

Finally, the cost of the inverter was assumed to be equal to the cost of the battery control unit, in order to have a closer feeling of the effect of the removal of the batteries on the unit cost of electricity. However, the market prices of such inverters in Malta are lower by about 20% than the assumed value.

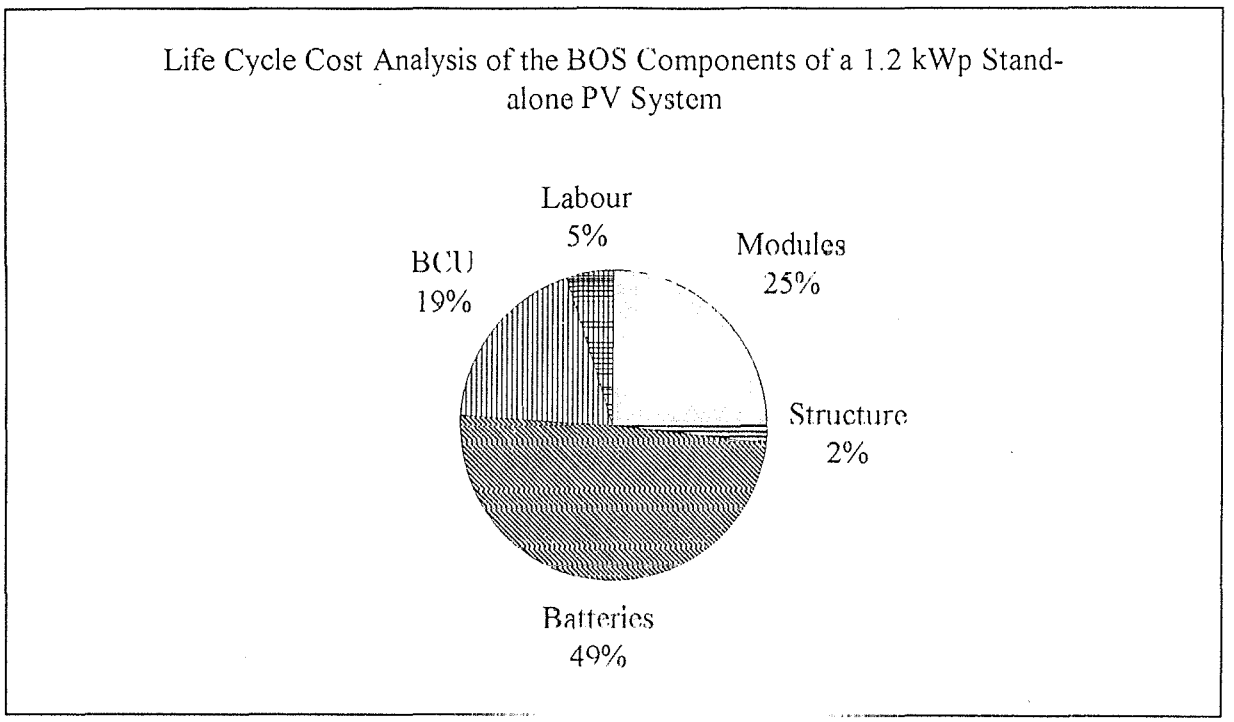

Figure 4.3: A pie chart of the percentage life cycle costs of the balance of system components of a stand-alone PV system.

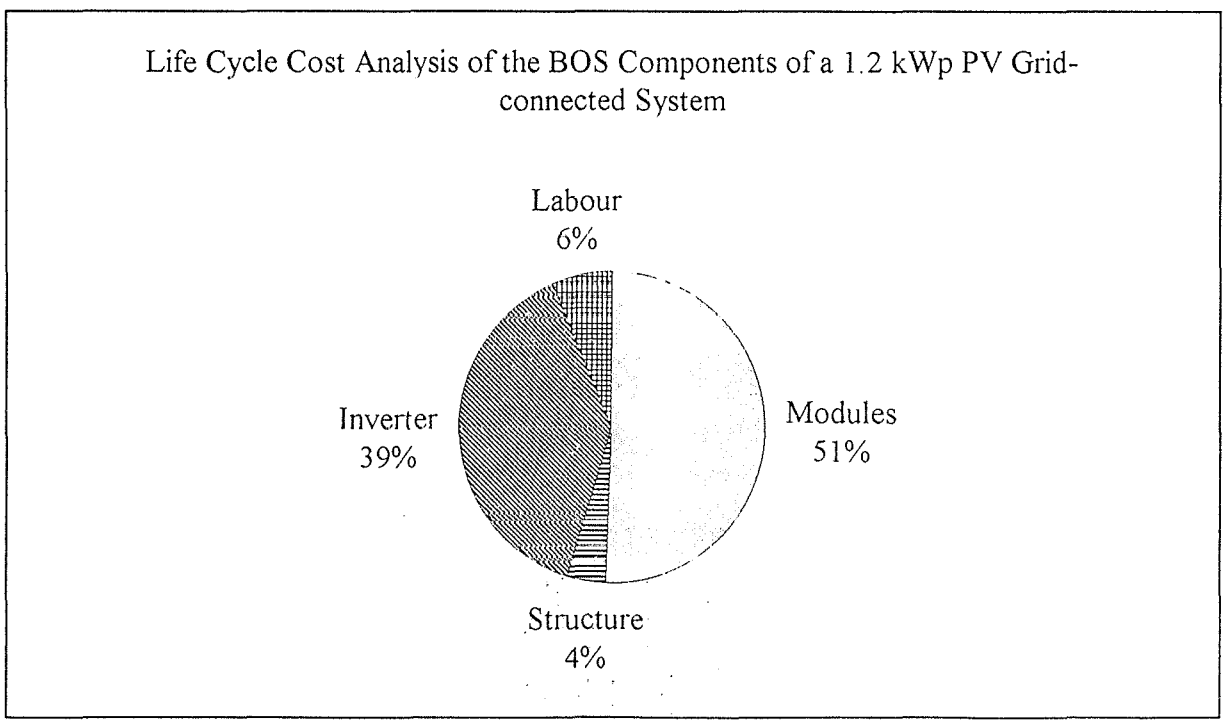

Figure 4.4: A pie chart of the percentage life cycle costs of the balance of system components of a grid-connected PV system.

CHAPTER FIVE

CONCLUSIONS AND RECOMMENDATIONS

INTRODUCTION

In this chapter, a summary of the main results are given and final conclusions are drawn together with the recommendations suggested for further work in this field.

The principal aims of this study were to set up, test and optimise the performance of a PV solar system under the weather conditions of Malta and to start collecting solar radiation data for the purpose of forming a data base. The stored energy was used for lighting with the intention of creating awareness among the University students of the capabilities and benefits of the use of solar electricity.

In the first place, a stand-alone PV system was chosen for testing because it did not require any special permits for its installation. Also, it was envisaged that similar systems would be used to provide night lighting on the University Campus and hence, it was necessary to test their performance before hand

5.1 CONCLUSION OF OPERATING EXPERIENCE

Besides the hands-on experience gained at the time of setting up of the PV system and the monitoring equipment [61], and that described in Section 1.11, more lessons were learned during operation, being summarised as follows:

(a) Electronic equipment are sensitive to humidity and have to be well protected.

(b) Daily checking of the collected data could reveal any corrupted sectors or help to discover any malfunctions of the monitoring equipment, thus saving time and ensuring the continuity of proper data collection.

(c) Careful and systematic inspection of the batteries helps to discover cracks, corrosion and loss of distilled water, which would otherwise reduce their life-time.

(d) Considering the seasonal availability of solar radiation, a close follow-up and management of the electric load could be a key factor towards the optimisation of the PV array yield.

5.2 CONCLUSIONS OF OPERATIONAL RESULTS

It is realised that there is more need for the use of simulation programmes such as PV F-CHART, PV FORM and TRNSYS, to get information on the possible performance of the system under study before carrying a final design.

One of the essential requirements for the use of professional simulation programmes is the availability of solar radiation data. This has already been started in this project and it should continue and expand according to the specific requirements.

From the data collected over the sixteen months, it is concluded that the annual mean radiation is 4.7 kWh/m²/day on a horizontal plane and 5.24 kWh/m²/day for a plane inclined at 36° to the horizontal, which is equal to the latitude of Malta. The minimum mean monthly global solar radiation incident on this plane in December was found to be 3.37 kWh/m²/day, which is about 1.65 times the corresponding global horizontal radiation. However, more data need to be collected in order to be able to present a typical solar radiation year for Malta.

The average annual performance ratio of the PV system was 0.38, peaking at 0.5 in December. This result was compared favourably with other professional stand-alone systems that were monitored in the Thermie programme [80].

The analysis of the array yield in kWh/kWp and the corresponding inplane irradiance measured in kW/m², yielded linear functions for each month of the year. The percentage difference in the array yield between the best performance linear function of December 1993 and the worst performance function of July 1994, amounted to 20% per kWp.

The annual average yield in kWh/kWp/day correlated to the inclined radiation in kW/m²/day as follows:

$Y_a = 0.6030G_i - 0.004$

The total electricity output was found to be 750 kWh/kWp/annum for a stand-alone system, and it was estimated that it would increase to at least 950 kWh/kWp/annum for a grid-connected system.

Wind speeds above 2 m/s had a cooling effect on the PV modules during July 1994, which is considered as one of the hottest months during the year.

Considering the weather of Malta, it was found that the amount of dust that accumulated on the surface of the PV modules during summer, reduced the photovoltaic conversion efficiency by 2%.

The performance of the batteries was not fully satisfactory since they were not specifically designed for solar applications. During the operation of the system, the electric supply to the fluorescent lights was occasionally cut-off by the action of the BCU low-charge controller. Considering the actual number of consecutive cloudy days, an autonomy of five days would be more sensible than the previously estimated three-day period.

The life cycle cost of one unit of electricity produced by a stand-alone PV system was calculated to be Lm 0.77, while that produced by a grid connected system was Lm 0.3. However, it has to be mentioned that this is the pessimistic result and different means of reducing these costs have been suggested in the previous chapter

5.3 RECOMMENDATIONS

In order to get more accurate results on the performance of this system, testing has to continue for a minimum of two years as recommended by the Joint Research Centre, Ispra Establishment [37].

It is suggested that the systematic checking and presentation of data that was adopted in this study, could be implemented for the next stage. From experience, it is always beneficial and easier to analyse the data of one month as soon as it is available. Also, a more detailed monitoring technique has to be adopted to get a better insight about the ageing process of the batteries.

Considering the fact that the electric utility covers most of the Maltese islands, it is suggested to test the performance of a grid-connected PV system. New challenges are expected to appear for such a project mostly concentrated on the optimisation of the performance of the PV modules, the interfacing of the generated energy with the grid and the determination of the PV system size that would produce the minimum life cycle cost of energy, taking into account the initial capital required and the revenue estimated from selling the extra energy to the utility.

It is also suggested that the monitoring of global horizontal solar radiation be continued and expanded to include the diffuse radiation component and the radiation incident on different tilt angles. Radiation monitoring stations are to be situated at different representative sites such as residential areas, industrial sites and country fields.

In the future, the use of a standard programming language has to be used for the data-loggers to ensure the easy transfer of know-how from one user to the other.

The use of 10-minute intervals in the collection of data is advisable according to the recommendations by the Joint Research Centre. It would rather be more reliable and environmentally friendly to power the data-logger from a lead acid battery that is recharged by a small PV module, rather than using dry cell batteries.

The use of properly double-walled insulated wires is recommended for extended use of a PV system to avoid cable cracks that might develop from exposure to the Sun.

Recalibration of all radiation and measuring instruments has to be carried out every two years or as recommended by the manufacturer.

APPENDIX A

SOLAR RADIATION: ITS NATURE AND MEASUREMENT

INTRODUCTION:

As solar radiation is the only source of energy to any photovoltaic (PV) plant, studying of its nature and measurement of its potential are two necessary actions that are to be taken before carrying out an estimation of the possible useful output energy of a PV array. In so doing, a solar radiation history of the site can also be established for statistical purposes and to be as a data-base for sizing future PV projects.

To study solar radiation, it has to be viewed from two points:

1. The total radiation;
2. The spectral distribution of radiation.

Measuring the total radiation will show the availability of solar energy at the site at that moment or during the period of measurement, while knowing its spectral distribution will help to investigate the performance of solar cells whose response change with variations in the solar spectrum.

For each of the above two cases, analysis has to be carried out at:

(a) The top of the atmosphere;

(b) The ground level.

A.1 TOTAL RADIATION AT THE TOP OF THE ATMOSPHERE

Previously, the total radiation incident normally on a surface at a distance equal to the average orbital radius of the Earth, and known as the solar constant or air mass zero (AM0) radiation, was measured as 1353 W/m^2 [5, 6]. As this value is widely adopted, it was used in this study.

A.2 TOTAL RADIATION AT SEA-LEVEL

At sea-level, the maximum global radiation reaching a horizontal surface at solar noon, at equinox, rarely exceeds 1000 W/m² [6, 7, 12]. Occasionally and only for short periods, can the solar radiation be higher, due to reflection from surrounding clouds [5, 21], as shown in figure A.1.

Obviously, at high altitudes, the maximum global radiation at one time during the year, is expected to be higher than 1000 W/m², due to lower atmospheric pressure, turbidity and air mass, while at places near and at the poles, it is zero for many months and does not exceed 100 W/m² for the rest of the year, due to lower solar elevations and higher latitudes. Also, besides the effect of altitude, solar radiation reaching a point on the Earth varies more prominently with the daily and seasonal variations in the climatic conditions [18].

The phenomena that cause seasonal variation in the reception of solar radiation are:

(a) The position of the Earth in its orbit round the Sun;

(b) The latitude of the site.

While the factors that cause daily variations fall in two categories, those that affect the total solar radiation and those that attenuate selected parts of the solar spectrum.

The factors that cause daily variations in the total amount of radiation received are:

(a) the time of the day;

(b) reflection from clouds and the ground;

(c) absorption and scattering by dust particles, solid impurities and pollen grains;

(d) shading due to the topography of the site.

The factors that affect the solar spectrum are:

(a) selective absorption by the ozone layer and other atmospheric gases such as oxygen, carbon dioxide, nitrogen oxides and water vapour;

(b) scattering and absorption by cloud masses;

(c) molecular (Rayleigh) scattering;

(d) scattering by aerosols (Mie scattering).

A.3 PHENOMENA WHICH CAUSE SEASONAL VARIATION IN SOLAR RADIATION

(A) THE POSITION OF THE EARTH IN ITS ORBIT ROUND THE SUN

The movement of the Earth round the Sun generates an elliptical orbit, with the Sun centred at one of the foci of the ellipse. The mean orbital radius, which is called one astronomical unit (1 AU) is 1.496×10^8 km, and this occurs on April 4th and October 5th. Only on those two days is the actual extra-terrestrial solar radiation equals to 1353 W/m², the minimum being 1309 W/m², occurring on July 4th and known as the aphelion, while the maximum is 1399 W/m², occurring on January 3rd and known as the perihelion.

Figure A.2, shows the starting dates of each season, as well as the maximum, minimum and mean distances of the Earth from the Sun and their corresponding dates.

(B) THE LATITUDE OF THE SITE

The Earth has two distinct movements, namely, its rotation round the Sun once a year and its spinning once a day, around its own axis, which makes an angle of 23° 27′ with the vertical, and known as the ecliptic of the Earth. The former causes variations in the solar altitude or elevation (γ), at different times and latitudes, while the latter defines the azimuth (φ). Together, they contribute to the change in the air mass ratio, and hence, to the variation in solar radiation.

The following equation gives the solar elevation at any time of the year [1]:

$$\sin\gamma = (\cos\phi \times \cos\delta \times \cos\omega) + (\sin\phi \times \sin\delta), \qquad \text{----------(A 1)}$$

where, γ = sun's elevation,

ϕ = local latitude;

δ = sun's declination angle;

ω = hour angle.

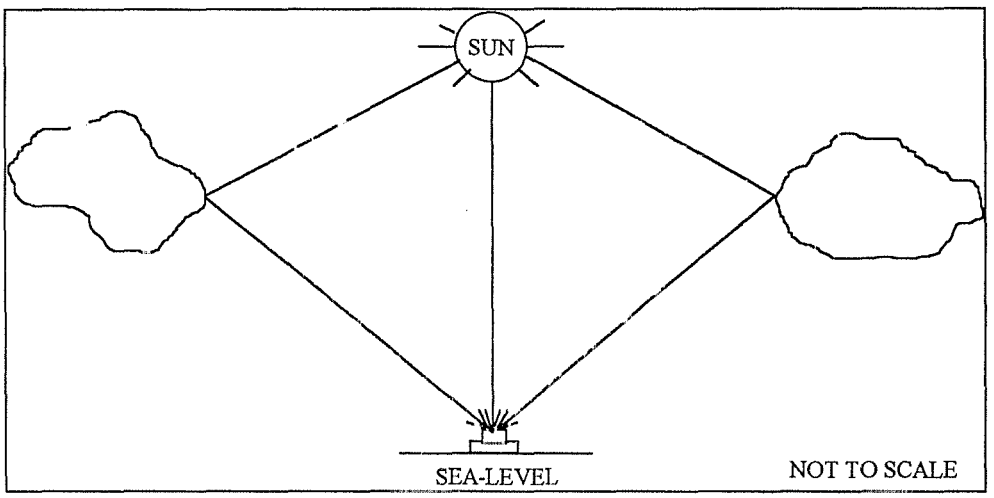

FIGURE A.1: Possible climatic setting that may cause the global solar radiation incident on a point at sea-level to be greater than 1000 W/m^2.

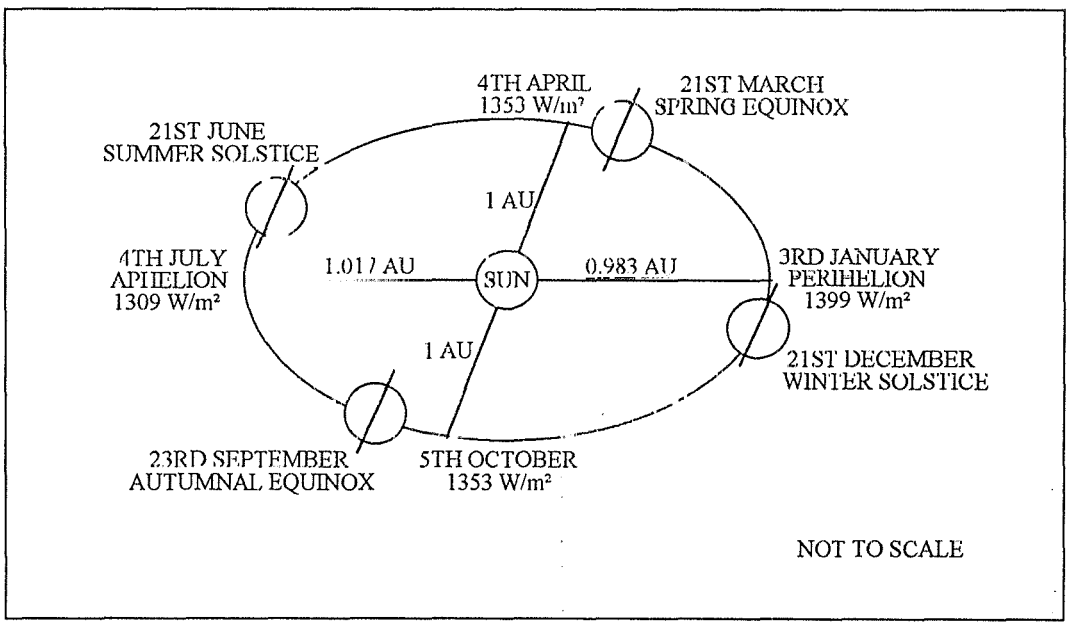

FIGURE A.2: The Earth in its orbit round the Sun.

The sun's declination angle, δ, is available from special tables found in standard textbooks [5], but an approximate value, with a maximum margin of error of ±2°, can be calculated using the equation:

$$\delta = 23.45 \times \sin[\frac{360}{365} \times (K + 284)]; \qquad \text{----------(A.2)}$$

where, K – number of the day in the year, being 1 on January 1st.

The hour angle is found from the equation:

$$\omega = \frac{360}{24} \times (t - 12); \qquad \text{----------(A.3)}$$

where, t = true local time, (true solar time), being 24 at midnight;

= local standard time - $c_1 + c_2 + c_3$;

c_1 = 1, for summer time, in countries which add 1 hour;

= 0, for winter time;

$+ c_2$ = longitude correction;

$= \frac{4}{60} \times (\lambda_s - \lambda_g)$ hours;

where, λ = local longitude;

λ_s = standard time meridian;

c_3 = equation of time, found from table D.3, of appendix D [59]. It caters for the variation in the speed of the Earth and ranges from $\frac{+16.3}{60}$ to $\frac{-14.2}{60}$ hours.

At midday, the equation of the Sun's elevation reduces to:

$$\gamma = 90 - \phi + \delta, \qquad \varphi - 0 \qquad \text{----------(A.4)}$$

and at the equinoctial noon, δ = ± 23° 27′, being positive for the northern hemisphere and negative for the southern hemisphere.

As for the azimuth, it is calculated from the equation [1]:

$$\sin \varphi = \cos \delta \times \frac{\sin \omega}{\cos \gamma}. \qquad \text{----------(A.5)}$$

Figure A.3, gives the solar elevation and the equation of time for the different days during the year [59]. It is known as the Analemma and can be used where accuracy is not essential.

Due to its tilted axis of rotation, the Earth would appear to wobble about the plane of its annual orbit, when viewed from the Sun. So referring to figure A.4, a point A at the Equator

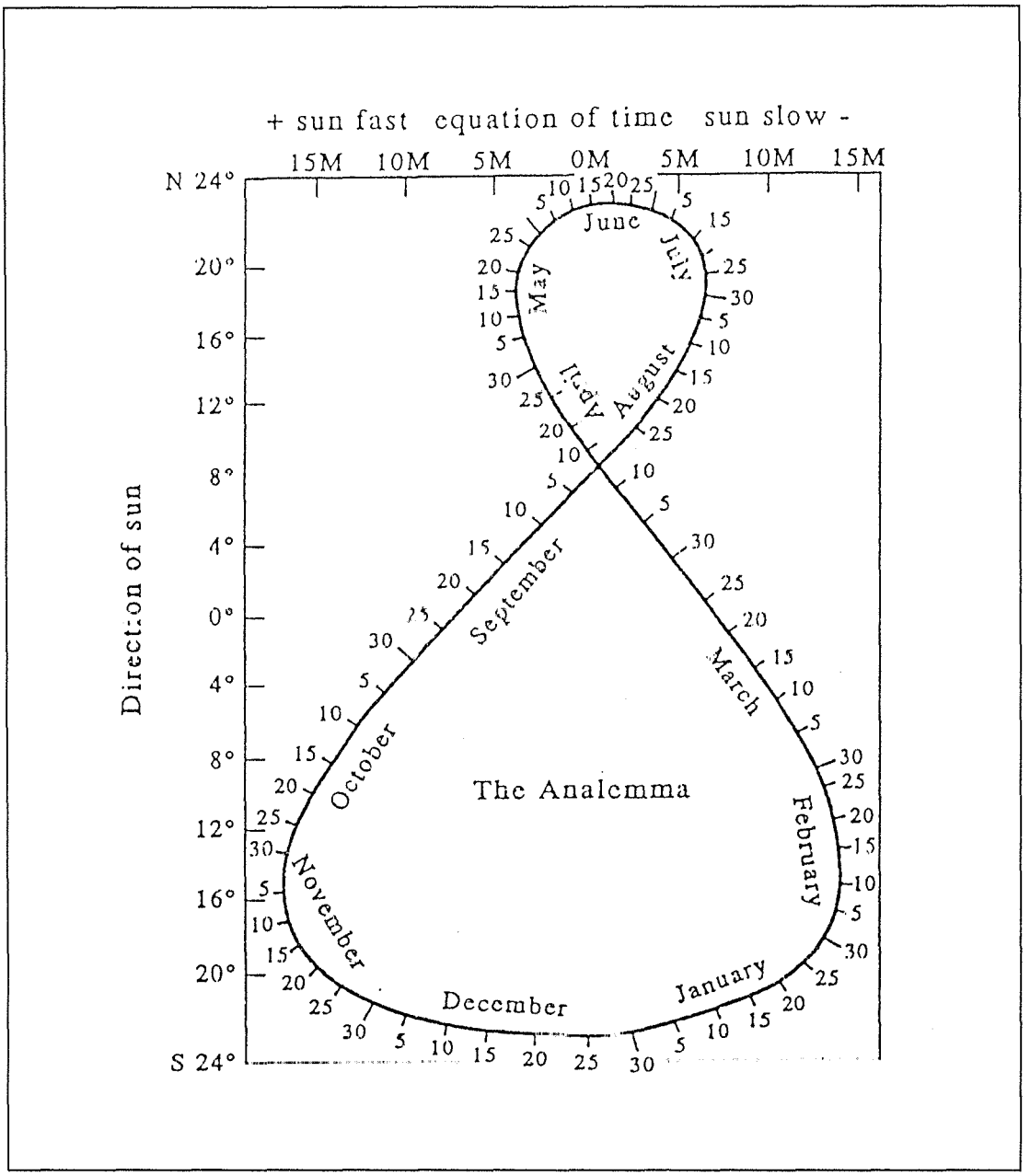

FIGURE A.3: The Analemma: gives the equation of time and the sun's declination throughout the year.

and a point B at a higher latitude would be at different distances from the Sun, simultaneously. In figure A.4(a) and A.4(c), the Sun is directly overhead at point A, while in figure A.4(b) and A.4(d), it reaches its minimum altitude of 66° 33′.

Considering point B and assuming its latitude to be 40° N, the maximum solar altitude occurs on June 21st and is 73° 27′, shown in figure A.4(b) and the minimum altitude occurs on December 21st and is 26° 33′, as in figure A.4(d).

Figure A.5, shows the apparent motion of the Sun as seen by an observer at the Equator and at a latitude of 40° N [19]. The points A and B now appear as horizontal circles.

These variations together with the formation of clouds near the Equator in summer, cause the mean solar radiation at A to remain relatively constant throughout the year [8]. Maximum solar radiation occurs in deserts and at around 40° latitude, known as the Sun Belt, but not near the Equator. However, the variation between the mean winter and summer radiation values increases as one moves nearer to the poles and this is shown in figure A.6.

To conclude, the latitude of a place, leads to different air mass ratios and different amounts of sunshine hours, which in turn, affect the amount of solar radiation reaching there.

A.4 FACTORS WHICH CAUSE DAILY VARIATIONS IN SOLAR RADIATION

(A) THE TIME OF THE DAY

From sunrise to solar noon, the air mass ratio decreases and inversely repeats itself from noon to sunset. Hence, excluding all other factors, the radiation decreases with increasing air mass ratio, both daily and seasonally. Also, the length of the day changes and affects the total amount of radiation.

(B) REFLECTION BY CLOUDS AND THE EARTH

Unlike absorption, reflection of solar rays is independent of the spectral distribution of

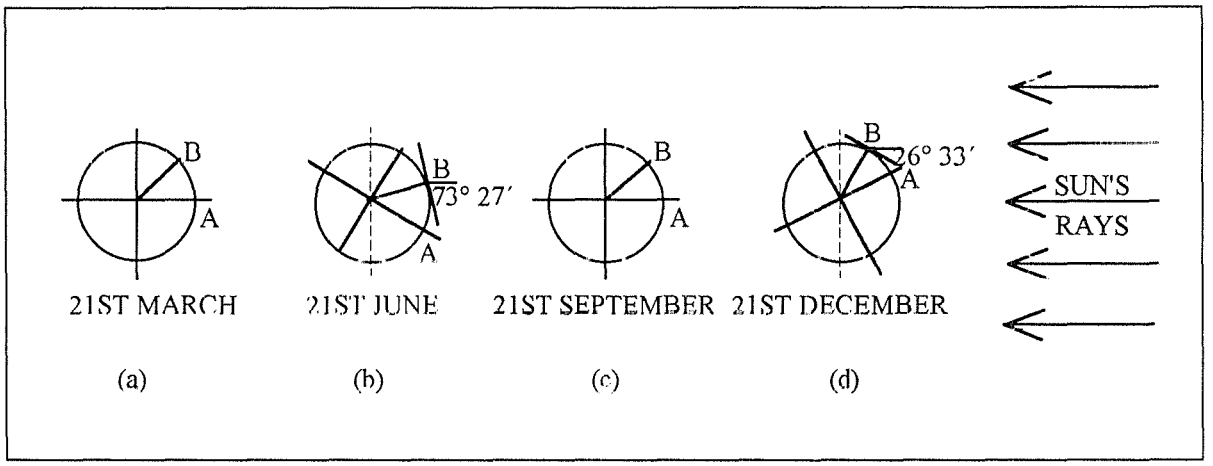

FIGURE A.4: The position of the Earth at the beginning of the four seasons, as viewed from the Sun

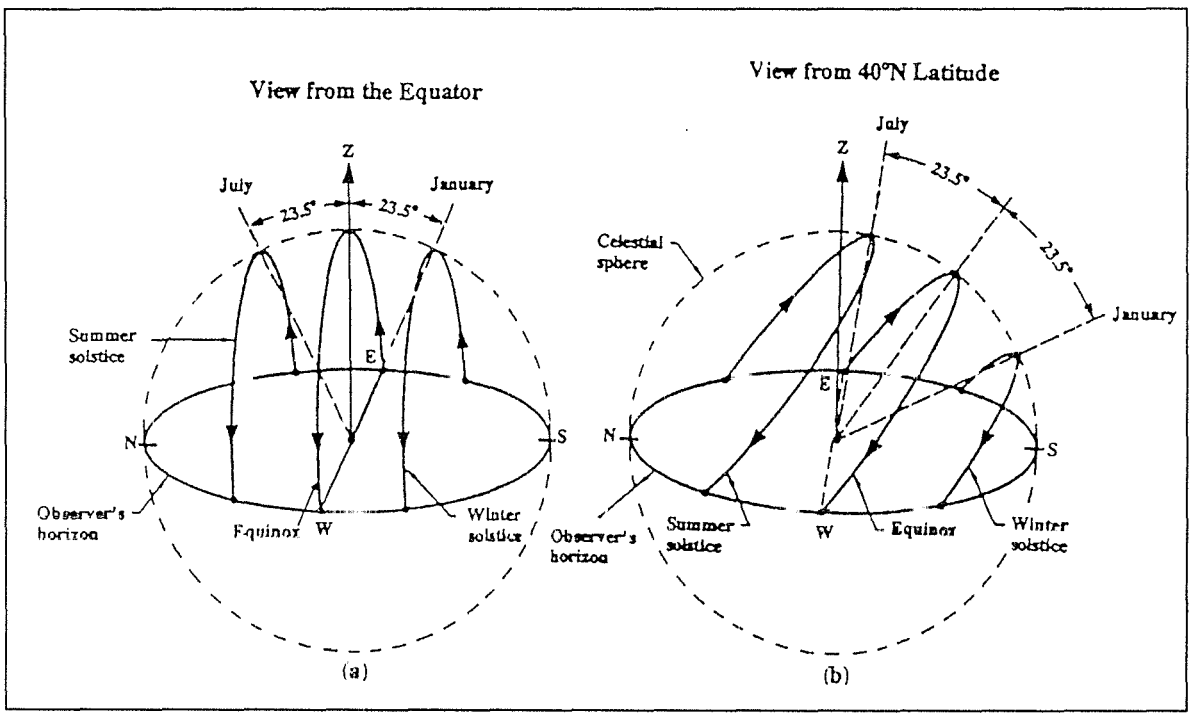

FIGURE A.5: The Sun's path across the sky as seen by an observer at (a) the Equator and (b) at latitude 40° N [9].

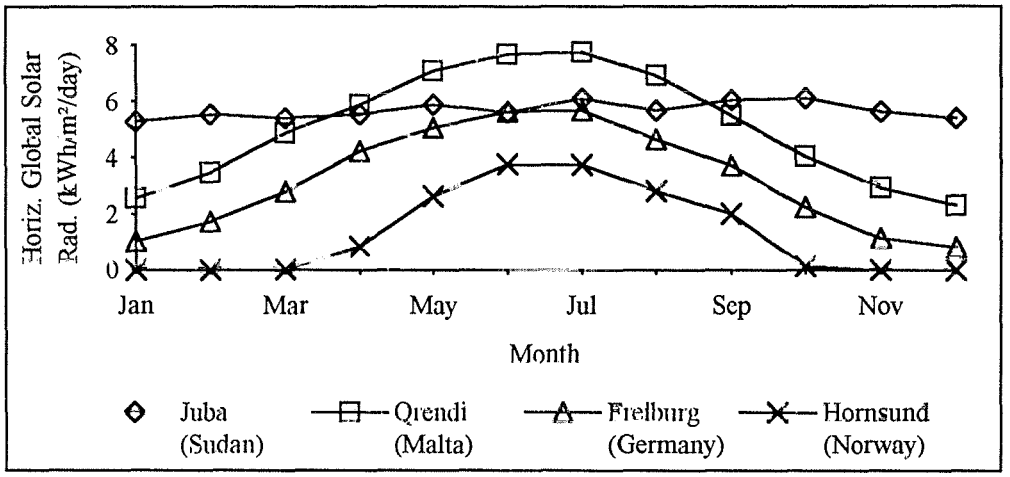

FIGURE A.6: Measured mean monthly global horizontal solar radiation at four different latitudes [7, 48]. Values are converted from langley (cal/cm^2) to kWh/m^2/day by multiplication by 0.01163.

solar radiation [4], but it rather depends on the thickness of the clouds and the nature of the ground below.

Reflection due to cloud masses could reach up to 90% of the total solar radiation and could remain so, for several hours. However, the amount of reflection is dependent on the sun's elevation and zenith angle, as well.

As for ground reflection, the highest naturally reflecting surface is the one covered with fresh snow, where the reflection could reach up to 90%, while the minimum reflection occurs from bare stone and is about 15%.

In conclusion, the total reflection from clouds and ground is site dependent and varies continuously It is known as the albedo of the place. On average, the albedo of the Earth is 32%, with the solar constant taken as 1353 W/m^2 [1].

(C) ABSORPTION AND SCATTERING BY DUST PARTICLES, SOLID IMPURITIES AND POLLEN GRAINS

Dust particles, solid impurities and pollen grains attenuate all the wavelengths of solar radiation. This is due to their large sizes when compared to the attenuated wavelengths [19]. Scattering and absorption by these particles become more significant in polluted cities and during sand storms.

(D) THE TOPOGRAPHY OF THE SITE

In some cases, obstacles may shade a place for a few minutes or for many hours. They range from a pole or tree to a tall building or mountain Carefil consideration of this factor is to be ensured before choosing the site for the solar modules, particularly the possibility of the emergence of new objects that were not existing at the time of construction.

A.5 THE SPECTRAL DISTRIBUTION OF SOLAR RADIATION AT THE TOP OF THE ATMOSPHERE

Solar radiation is a mixture of electromagnetic radiation of different wavelengths and percentage compositions. It is divided into three parts [4]:

1. The ultra-violet region ($\lambda < 0.4$ μm) 9%
2. The visible light region (0.4 μm $\leq \lambda \leq 0.7$ μm) 45%
3. The infra-red region ($\lambda > 0.7$ μm) 46%

A.6 THE SPECTRAL DISTRIBUTION OF SOLAR RADIATION AT SEA-LEVEL

The solar spectrum at sea-level differs from the extra-terrestrial distribution in three aspects [6]:

1. The spectral range of wavelengths;
2. The energy content of each wavelength band;
3. The percentage share of each range in the total radiation.

The atmosphere totally absorbs some wavelengths and partially attenuates or scatters the others, leading to lower energy content and different percentage share of the wavelengths in the remaining transmitted radiation, at sea-level.

These variations are also strongly dependent on the air mass ratio. Table D.1 of Appendix D, gives an idea of the effect of change in the air mass ratio, on the percentage constituency of the solar spectrum in the ultra-violet, visible light and infra-red regions [5].

The reference air mass ratio used in photovoltaic studies is AM1.5. Hence, in many publications, the solar spectrum is plotted for that value. Figure A.7, shows a graph of the solar spectrum at AM0 and AM1.5 for the wavelength range, 0.115 μm $< \lambda < 4$ μm. This range includes the region where solar cells respond [1], which is between 0.3 μm and 1.5 μm.

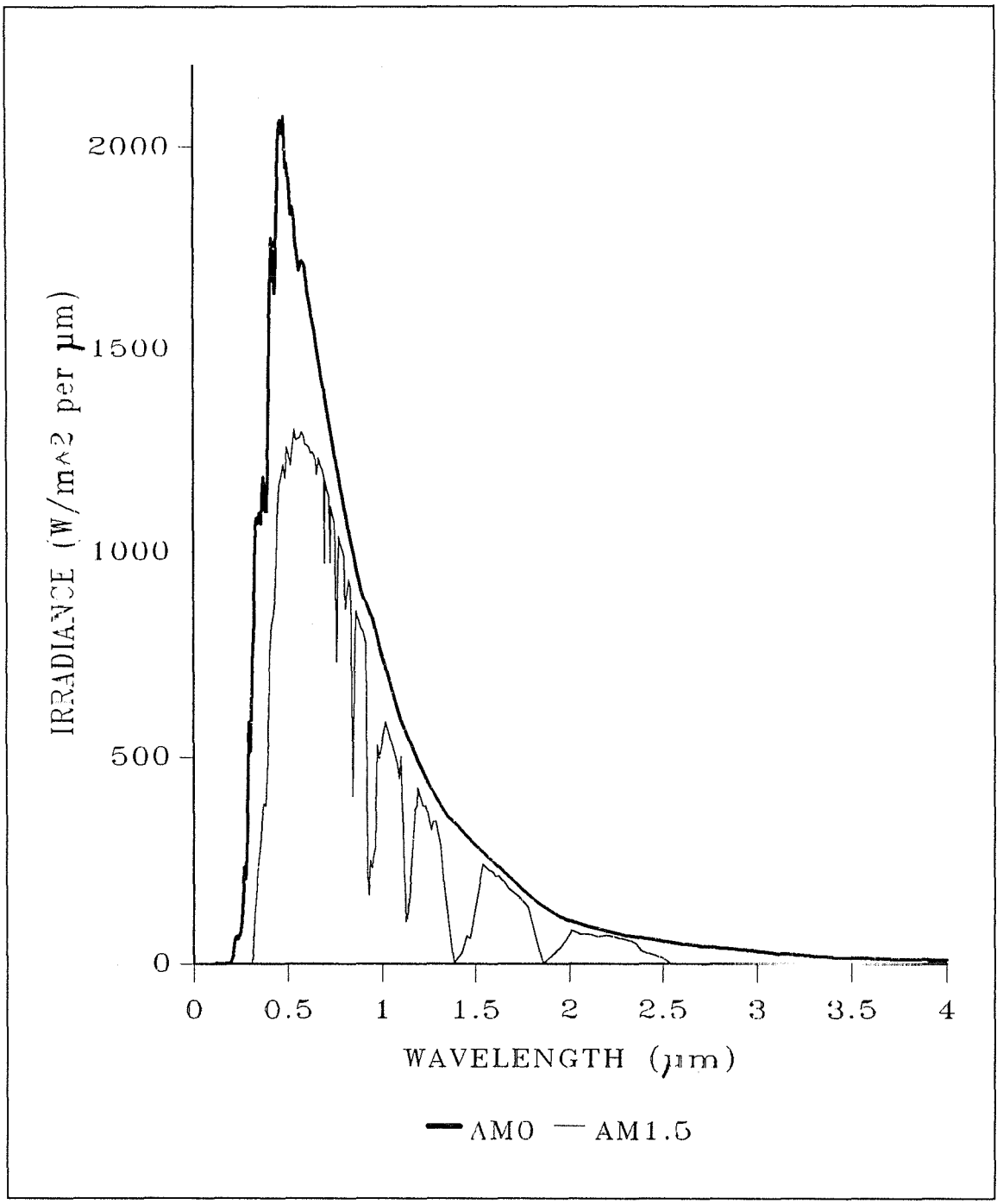

FIGURE A.7: Spectral distribution of global horizontal solar radiation at AM0 and AM1.5, plotted from given tabulated data [5, 6].

A.7 FACTORS WHICH AFFECT THE SPECTRAL DISTRIBUTION OF SOLAR RADIATION

(A) SELECTIVE ABSORPTION BY THE OZONE LAYER AND OTHER ATMOSPHERIC GASES

As the Sun's rays travel through the atmosphere, the ultra-violet region suffers great attenuation by the ozone layer, oxygen, nitrogen oxides, gas atoms and ions, which absorb all radiation having a wavelength less than 0.3 μm, and partially reduce the intensity of those wavelengths between 0.3 μm and 0.4 μm. Clouds and aerosols affect the visible light region by absorption, diffusion and reflection, while water vapour and carbon dioxide are responsible of absorbing up to 20% of the radiation in the wavelength region of 0.7 μm < λ < 12 μm and up to 100% for higher wavelengths of the infra-red region [4, 19].

(B) SCATTERING AND ABSORPTION BY CLOUD MASSES

Clouds have a strong scattering effect on the solar spectrum. The prediction of the amount of scattering and absorption of solar radiation is difficult, because the presence of clouds is highly variable in quantity and type.

Table D.2, of appendix D, gives an idea about the percentage transmission of solar radiation through different types of clouds as registered in Pavlovsk, near Leningrad [1]. It is noted that the transmission decreases with the increase in the zenith angle. Obviously, thin cirrus clouds offer the least attenuation, while the thunderous altocumulus clouds can absorb up to 90% of the solar radiation.

Scattering of solar rays by clouds results in diffused light, that is rich in long-wave radiation, as different from diffused radiation on a clear day. This is manifested by the grey colour of the sky on a cloudy day and a blue colour on a clear day [17, 18].

Figure A.8(a), shows the low intensity of diffuse radiation, on a clear day, most of which lies in the short-wave region, while figure A.8(b), shows a higher intensity of diffuse radiation on a cloudy day, with a considerable amount lying in the long-wave region [2].

(C) MOLECULAR (RAYLEIGH) SCATTERING

Rayleigh scattering is the attenuation of solar radiation by atmospheric molecules whose average radii are much smaller than the attenuated wavelength. The characteristic phenomenon of Rayleigh scattering is that, approximately, the scattered portion of light is equal to the reflected part for that wavelength [18], though it could be less [35, 36] Rayleigh scattering affects all wavelengths of the solar spectrum, but it is more effective at short wavelengths [6].

(D) SCATTERING BY AEROSOLS (MIE SCATTERING)

Aerosols are particles whose average radii are usually equal to or greater than the attenuated wavelength. The part of radiation absorbed by aerosols and transmitted as long waves to the Earth is greater than the part being reflected to the sky. The absorption is independent of the wavelength but it varies with the zenith angle [35]. In cases when the particle's size is smaller than the attenuated wavelength, the scattering behaviour will be a function of the wavelength similar to Rayleigh scattering [18].

Aerosols cause turbidity in the atmosphere and it becomes more significant in humid areas or in places where the concentration of aerosols is high. Variations in their concentration, size and chemical composition cause changes in the amount of scattering of solar radiation particularly in the visible and infra-red regions.

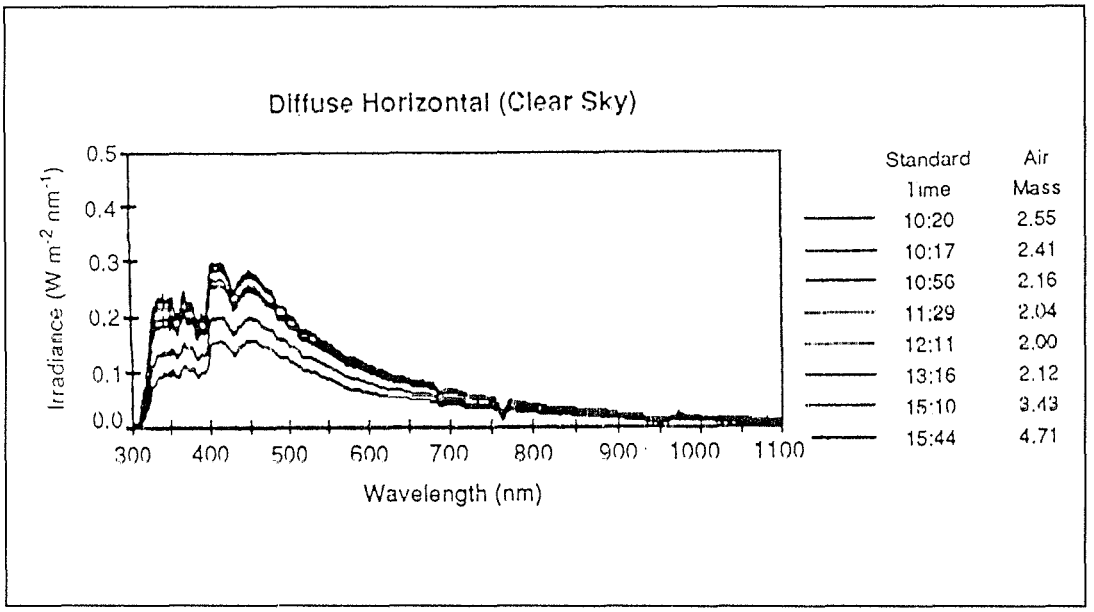

(a)

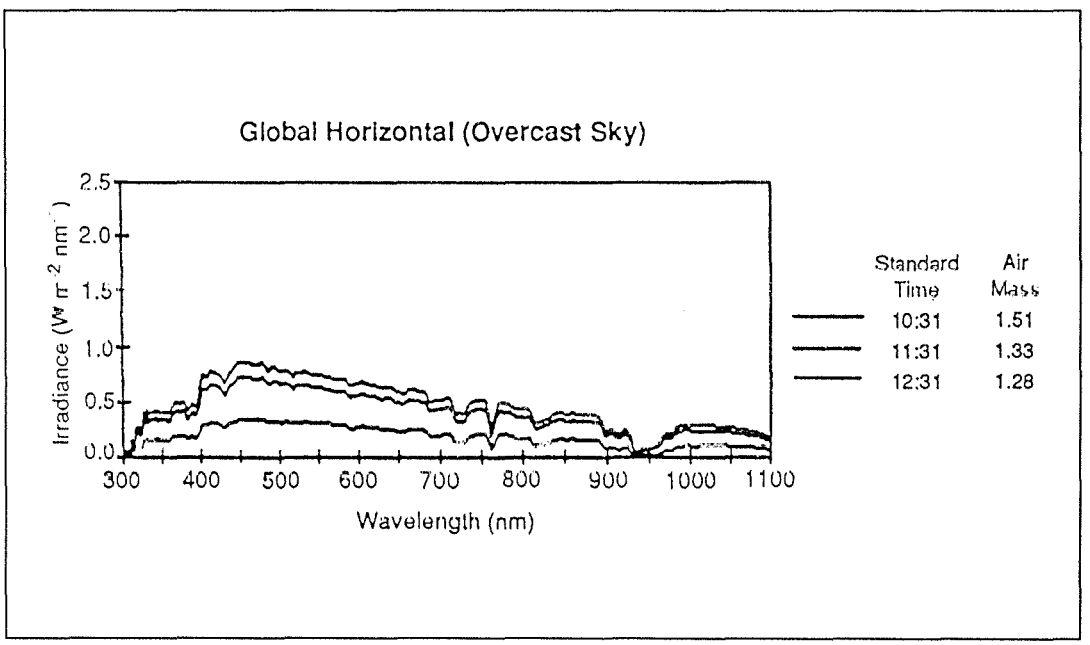

(b)

FIGURE A.8: Diffuse radiation, (a) on clear days and (b), on cloudy days, measured between wavelengths $0.3 < \lambda < 1.1$ μm, for different air mass ratios [2].

A.8 REVIEW OF SOLAR RADIATION MEASURING INSTRUMENTS

Solar radiation incident on the surface of the Earth can be divided into two main components, namely, the direct and diffuse radiation. The direct radiation is that part of the total global solar radiation, which comes directly from the Sun's disc without suffering attenuation on its way, while the diffuse radiation is that part that reaches the Earth after being scattered or absorbed and re-emitted as long-wave radiation.

A third part can sometimes be of significance, and is termed the reflected radiation, which can reach a place by reflection from surfaces or objects. It becomes more significant in cases where there are shiny surfaces such as snow or objects such as glass and when the receiving surface is tilted rather than being horizontal.

Before measuring the amount of solar radiation, it is necessary to decide which component of radiation would be useful for that project. For example, solar systems that use concentrating lenses, require information on the direct radiation, while flat-plate non-concentrating systems, require a knowledge of the total global radiation incident on them. Sometimes, only a selected part of the solar spectrum is measured. Hence, by knowing the purpose, a choice of the appropriate instrument is facilitated.

The reference instrument that measures the direct radiation and serves as a standard instrument for calibrating other instruments is called the standard pyrheliometer. It requires an accurate two-axes sun tracking mechanism and professional experience.

A more commonly used instrument is the pyranometer that measures the global solar radiation. If a shading ring or a shadowband is added to the pyranometer, it would be possible to measure the diffuse radiation. Pyranometers can also measure the reflected radiation, by mounting them in an inverted position.

A new instrument called the rotating shadowband radiometer measures the global and diffuse radiation simultaneously, using a silicon cell pyranometer. The direct radiation can then be calculated by subtracting the diffuse from the global radiation values and dividing the result by the cosine of the solar zenith angle [2, 13]. Such pyranometers are already available in the market [38].

Optical filters can be added to pyrheliometers and pyranometers to enable them to measure the energy content of small wavelength bands of the solar spectrum. In such cases the instrument is termed a spectro-radiometer.

The atmospheric Optical Calibration System (AOCS) is another specialised new instrument that measures the solar intensity at different wave bands in a short time, to avoid errors, during sampling, that are caused by the short-term fluctuation of solar radiation [14].

In the last few decades, satellite observations are being used to measure solar radiation on the Earth's surface. It is to be noted that satellite readings are instantaneous observations taken for a large area, typically 5 km square, depending on the latitude [15], while terrestrial observations using pyranometers and pyrheliometers give integrated values at the point of measurement.

The best way to know how much solar energy reaches a place is to measure it there and then. This is not always possible and in such cases, an estimation of the amount of solar radiation can be made using statistical data of a nearby meteorological station, or of a place having a similar climate, or by calculating it using existing correlation that require easily accessible data such as the number of sunshine hours and cloud cover. However, sometimes the local conditions could affect the micro-climate of the site to such an extent, that projections from near-by meteorological stations, become unrealistic.

Advances in instrumentation, accuracy and reliability are continuously progressing. No doubt, more and more use is being made of automatic and programmed monitoring systems.

A.9 MEASUREMENT OF TOTAL SOLAR RADIATION

Flat-plate non concentrating solar modules produce energy by making use of the total (direct, diffuse and reflected) radiation of the Sun, though they cannot exploit the whole range of the spectrum. Hence, there is a need to consider the instruments used for monitoring this radiation, namely, the pyranometers, in more detail.

There are two main types of pyranometers that work on different principles and have different characteristics. A study of their properties should reveal which of them would be more suitable for this study. The first type is known as the thermopile pyranometer and the second is called the silicon cell-based pyranometer or solarimeter.

(A) THE THERMOPILE PYRANOMETER

This pyranometer is essentially made up of alternate black and white painted surface, arranged in concentric circles or star-shaped designs and connected to a series of thermo-couples. When a thermopile is exposed to sunlight, the black surfaces absorb more energy than the white ones and heat up to a higher degree. As a result, a temperature gradient is set up, which is detected by the thermocouples and transformed into an electric voltage.

Provided that the black and white paints have uniform sensitivity to all wavelengths of the incident rays, the generated voltage can be considered as independent of the wavelength. This is not always true, as the white pigments used until few years ago, had different reflectivity to the infra-red and ultra-violet regions [24]. New types of paints made of barium sulphide have been used lately, that ensure perfectly uniform reflecting properties of the surface, to the whole solar spectrum.

Due to the heat capacity of the different parts of the pyranometer, thermopiles are slow to respond to quick changes in solar radiation and the layer of paint adds up to this effect. In a flash test, it has been shown that for a Kipp and Zonen pyranometer, there was a time lag of 20.8 seconds before the instrument responded fully to the incident radiation and 28.4 seconds were required for it to come back to its zero value [19]

Thirty years later, no significant improvement has been achieved to the response time. A recent brochure of a new pyranometer called SOLRAD, manufactured by Kipp and Zonen, quotes a response time of 18 seconds for the pyranometer to reach 95% of the incident radiation [28]. As a result, drifts occur to the readings and the errors become more

pronounced when instantaneous readings are taken during partly cloudy weather [25]. It is reported, however, that if readings are integrated over a reasonable time, such errors tend to cancel each other, though it might not always be true [29].

Figure A.9, shows experimental results made by Suehrcke [25], to compare between the drift effects of a thermopile and a silicon cell pyranometer, during rapid changes in solar radiation. This effect can be corrected by using a software program suggested by the same author, but this will add to the already high cost of thermopile pyranometers, that is caused by the careful manufacturing techniques used and the facilities and skill required for their calibration.

Another factor that affects the accuracy of the readings is the improper cosine response of the thermopile for high incident angles between the Sun's rays and the perpendicular to the sensor's surface [32, 33, 59] Ideally, the output of the sensor should decrease as the cosine of the angle of incidence of the Sun, or in other words, of the complementary angle of the solar altitude [19, 22].

The results presented by Nast [23], on testing different types of pyranometers, showed that no sensor behaves exactly as another and that some of them exhibit some dependence on the azimuth and the tilt angle of the pyranometer.

(B) SILICON CELL-BASED PYRANOMETERS

This pyranometer is essentially made up of a silicon cell, usually of the mono-crystalline type with a resistor connected in parallel to produce a voltage rather than a current. Since, the current produced is proportional to the incident solar radiation, at constant temperature, then the output voltage will behave similarly. A thermistor is incorporated to compensate for the deviation of the reading caused by the rise in the cell's temperature during operation.

The doped silicon material of the cell has a band-gap of 1.1 eV. Incident light that has an equal or greater amount of energy than the band-gap is able to excite an electron and produce a current. The extra energy is dissipated as heat and will not be detected by the cell [30]. This

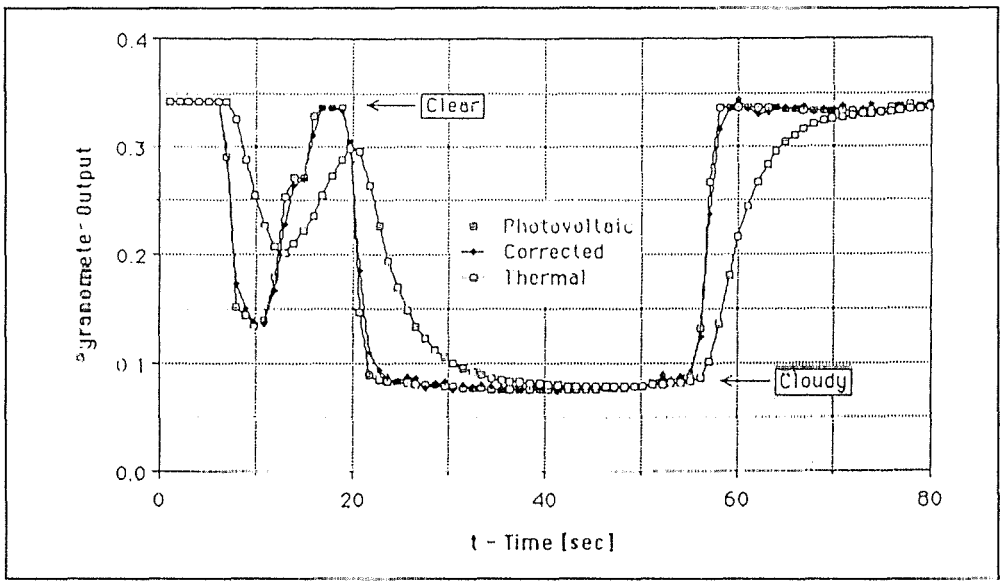

FIGURE A 9: Response of thermopile and silicon cell pyranometers to rapid radiation changes [25].

explains why a solar cell is said to be spectrally dependent and as a result, it cannot measure the total energy in the solar spectrum. This would not have been a limitation had the solar spectrum been invariable. On the contrary, it varies all the time due to changes in the air mass ratio and the weather [26].

Figure A.10, shows the response of a silicon cell to the solar spectrum at AM1. The maximum response of the cell is at a wavelength of 0.83 μm. This does not match the maximum available energy of the solar spectrum, at a wavelength of 0.535 μm, at AM1.5 [20]. This difference diminishes during cloudy days, as the solar spectrum shifts towards the long-wave region, as seen in figure A.8(b). Hence, if the solar cell is used as a pyranometer, it will give more realistic results during cloudy weather [22].

Another limitation to the use of silicon cell-based pyranometers is the cosine effect. It has already been mentioned that all types of pyranometers have this problem, but for silicon cell solarimeters the effect is more striking. It has been shown that these sensors obey the cosine law for angles of incidence up to 20° [31], i.e. for solar elevations of 70° to 90°.

As reported, the azimuth does not affect the response of the solarimeter much, and it can be ignored [20].

Regarding the relationship between the response of a silicon cell-based pyranometer and a thermopile one, experiments showed no definite ratio between them [19].

An advantage of silicon solarimeters over thermopiles is their fast response time of about 10 μs, so they can closely follow the variation in solar radiation, as shown in figure A.9.

Also, as their prices are much lower than the costs of thermopile pyranometers, silicon cell solarimeters are more often used in small and medium-sized PV projects, that usually have limited budgets. However, it is worth noticing that the prices of the new types of thermopiles, such as SOLRAD pyranometer of Kipp and Zonen, is comparable to that of solarimeters [28].

Other advantages of silicon cell pyranometers is their long life time and their low impedance. The latter results in high output signals, that give better accuracy in measurement and makes it possible to connect the pyranometers directly to a data-acquisition system.

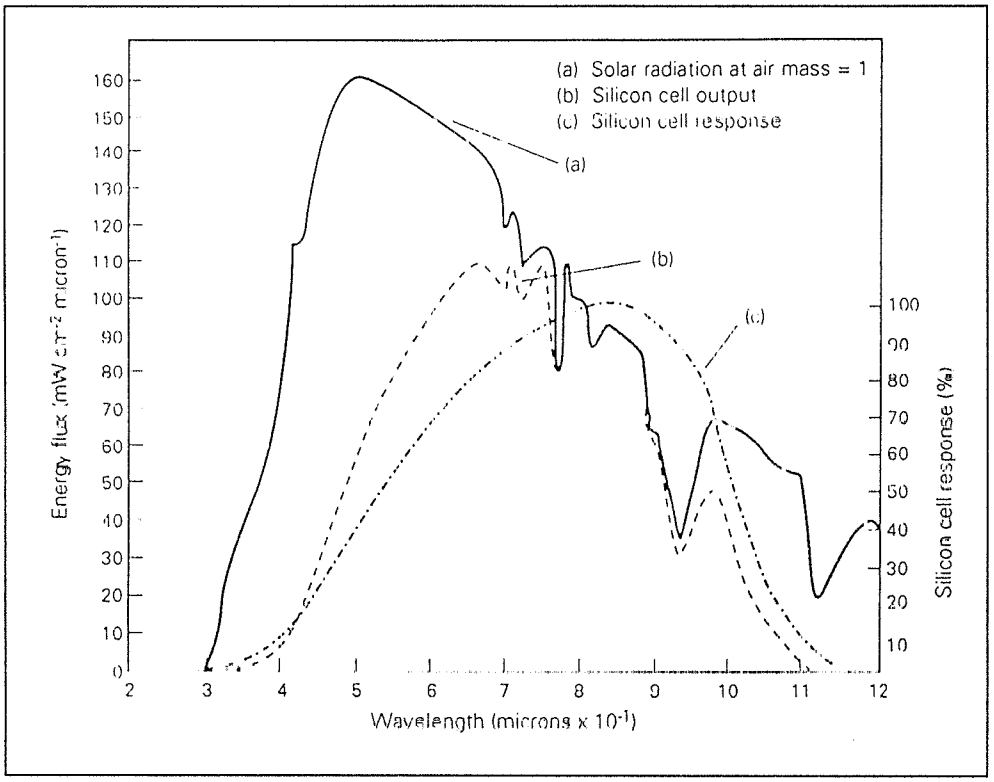

FIGURE A.10: A plot of (a) the spectral distribution of direct solar radiation for air mass 1, (b) silicon cell output and (c) silicon cell spectral response [20].

The development of silicon cell-based pyranometers is continuously progressing. Michalsky et al, have showed that the readings produced by such pyranometers can be corrected, after which they would differ by only 1% from the corresponding thermopile readings, for the case of horizontal global radiation [26].

The use of silicon cell based pyranometers for the monitoring of solar radiation is more acceptable for use in PV systems, because both the pyranometer and the PV cells match in their optical and spectral responses to sunlight. As for solar thermal applications, thermopile pyranometers are more suitable because thermal systems benefit from the whole solar spectrum.

Based on the above analysis, silicon cell-based pyranometers are chosen to monitor solar radiation on a horizontal surface and on the plane of the solar modules, of this project.

This decision agrees with the guidelines set by the Joint Research Centre - Ispra Establishment, for the monitoring of PV systems [37].

APPENDIX B

PHOTOVOLTAIC CELLS AND BALANCE OF SYSTEM COMPONENTS

INTRODUCTION:-

The properties of solar cells are reviewed, to help to understand their characteristics and to explain why their performance vary with changes in the intensity and spectral distribution of solar radiation as well as temperature. First, mono-crystalline, poly-crystalline and amorphous silicon cells shall be considered, then the other main types of PV cells shall be briefly described and compared to them.

Another important part to be considered, is the technique used to build up solar modules, capable of delivering the required voltage and current at an efficiency close to that of the individual cells comprising them.

Finally, attention will also be given to the balance of system (BOS) components of a PV plant. As the prices of PV modules decrease and their efficiency increase, the performance and cost of the BOS components become more critical and have to be equally upgraded.

B.1 PROPERTIES OF MONO-CRYSTALLINE SILICON CELLS

Solar cells are doped semi-conductors, that can absorb light energy and generate their own current, driven by an in built electric field [4]

The doping of the intrinsic silicon material is divided into two stages. First, the whole silicon wafer is produced as a p-type boron-doped wafer, then phosphorus is diffused into it to produce an upper n-type layer.

The doped cell does not possess a net charge, or in other words, it is not ionised. Rather, the presence of dopants gives rise to charges that do not take part in the covalent bonds of the atoms. This implies that the forces that keep these charges linked to their atoms are relatively weak and can be easily overcome by an external source of energy. This is manifested by the shifting of the Fermi level, from the centre of the forbidden gap to a new position, that is nearer to the conduction band, for n type materials and nearer to the valence band, for p-type materials. Figure B.1, shows the effect of doping on the Fermi level for an n-type and a p-type substance [5].

Since the p-type and the n-type layers are present simultaneously in a solar cell, electrons and holes *drift* through the junction, from one layer to the other, driven by the existing imbalance of charges on either side [16]. As a result, there will be a build-up of opposite charges that creates an electric field there. Figure B.2, shows the condition of the cell after drifting has occurred [38]. As these particles move from one region where they are a majority to another where they are a minority, they are termed *majority carriers*.

The built-in voltage can be shown on a diagram as a difference in potential between the n-type and the p-type layers. At the junction, there is only one Fermi level and the only way to satisfy this condition is to shift the relative positions of the bands, as shown in figure B.3 [38].

Now, at room temperature, some electrons in both types of doped layers, will absorb enough energy to make their journey to the conduction band. Considering the n-type layer, the probability of thermal excitation of electrons is high, because the Fermi level is very near to the conduction band, but due to the presence of the electric field at the junction, electrons that are excited in the n-type side cannot *diffuse* to the p-type side. The only way of diffusion of electrons is from the p-type to the n-type side, but since there are few free electrons there, the current produced remains very small.

Similarly, the holes diffuse from the n-type to the p-type region. This type of diffusion is known as the diffusion of *minority carriers*, because the electron-hole pairs migrate from a region where they are a minority to another where they are a majority. It is to be noted that the majority carriers mentioned before, do not take part, because they are held in place by the electric field and that the minority carriers originate from the bulk of the material.

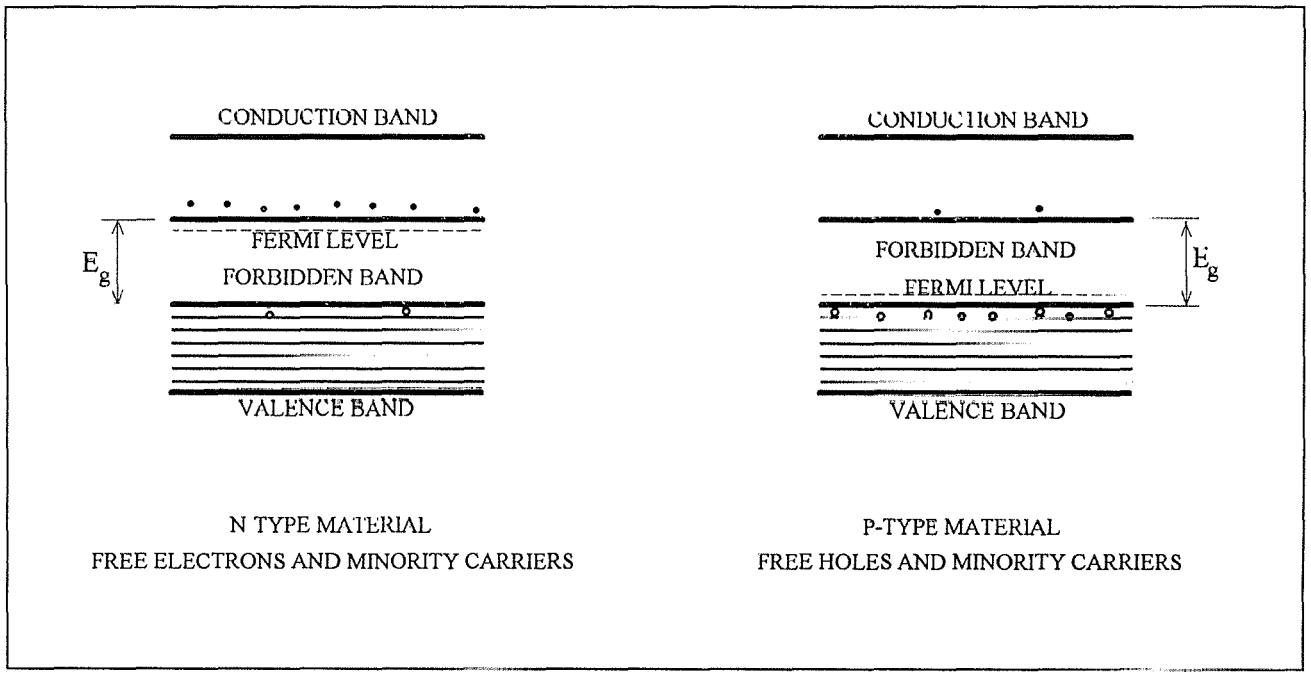

FIGURE B.1: Effect of doping on the position of the Fermi level and on the distribution of charges, in n-type and p-type materials [5].

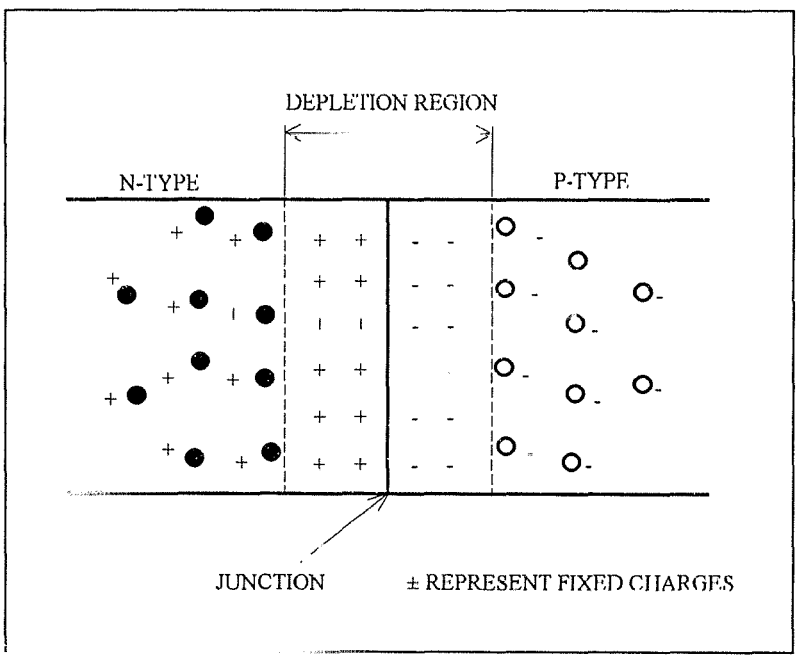

FIGURE B.2: The creation of a potential at the junction of a semiconductor, due to the drifting of the majority carriers [38].

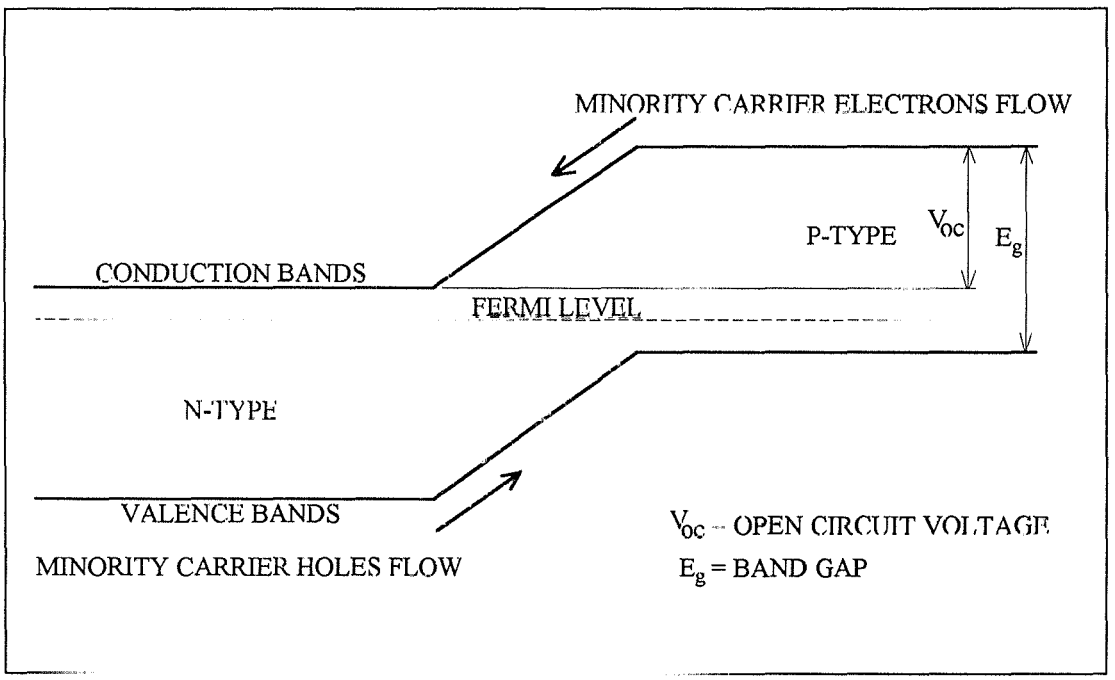

FIGURE B.3: A schematic diagram showing the energy levels at the p-n junction on open circuit (no illumination) [38].

The *drift* of the majority carriers cannot exceed the *diffusion* of the minority carriers, otherwise the potential at the junction would rise to counter-balance this effect. Hence, in the dark, the generation current of the minority carriers, also known as the saturation, dark, leakage or diffusion current I_0, equals the recombination current of the majority carriers [4, 38, 39] It could be written as a function of the band gap and temperature as follows [?, 6].

$$I_0 = cT^{\alpha} e^{-F/kT} \quad \text{----------(B.1)}$$

where, c = constant that depends on the band-gap;

T = absolute temperature;

α = coefficient ranging between 1 and 4;

E = band gap energy;

k = Boltzmann's constant.

As the cell's temperature rises, the rate of diffusion of the minority carriers increases and causes the short-circuit current I_{SC}, and the open-circuit voltage V_{OC}, to increase. Simultaneously, the rise in temperature reduces the band gap and causes the saturation dark current I_0 to increase, which reduces V_{OC} considerably. The net result is that both V_{OC} and the cell's efficiency decrease and this explains why solar cells are less efficient at higher temperatures.

If the cell is fitted with metallic contacts on either side of the junction and an external potential difference is applied, in such a way as to oppose the external natural flow of electrons from the n-type to the p-type material, the field in the depletion region at the junction increases and lowers the majority carrier current flow, but the minority carrier current remains equal to I_0, because it is only affected by temperature and light. Hence, the external current remains equal to the higher of the two currents, namely to the minority carrier current, which is quite small. By behaving in such a manner, the PV cell acts as a diode

If the polarity of the battery is now reversed, the field at the junction decreases and causes the recombination current of the majority carriers I_r, to increase exponentially with the applied voltage as follows [27]:

$$I_r = I_0 e^{qV/kT}, \quad \text{---------- (B.2)}$$

where, q = electronic charge;

V = voltage across the junction;

k = Boltzmann's constant;

T = absolute temperature.

The generation current I_g of the minority carriers remains equal to the saturation current I_0, at constant temperature. Hence, the net current seen externally will be the difference between I_r and I_g.

$$I = I_0 e^{qV/kT} - I_0$$

$$= I_0(e^{qV/kT} - 1) \qquad \text{---------- (B.3)}$$

This equation is called the Shockley or the ideal-diode equation and is represented graphically on curve (1), of figure B.4. [4].

When the cell is subjected to solar radiation, extra electrons are freed in the p-type layer and extra holes in the n-type layer. This creates a light-induced current I_L, that flows across the junction in the same direction as the generation current of the minority carriers I_g, but much more intensive in value. This current causes a reduction in the potential difference across the junction and an increase in the recombination current of the majority carriers I_r, which balances the photon-generated current I_L. Hence, the net external current is zero and the voltage is equal to the open circuit voltage.

If the external circuit is a resistance, then the net external flow of current will be equal to the difference between I_r and $(I_g + I_L)$ [6]:

$$I = I_0(e^{qV/kT} - 1) - I_L$$

This result is shown in figure B.4, curves (2 - 6), for different illumination intensities [6]. The fourth quadrant is the area where power can be extracted from the cell. It is noted that curves (2 - 6) are very similar to curve (1), except that they are shifted down by a current equal to I_L.

For an illuminated cell, it is more convenient to consider the net current I as positive, since it is produced and not consumed by the cell. Then, the above equation can be written as follows [4]:

$$I = I_L - I_0(e^{qV/kT} - 1) \qquad \text{---------- (B.4)}$$

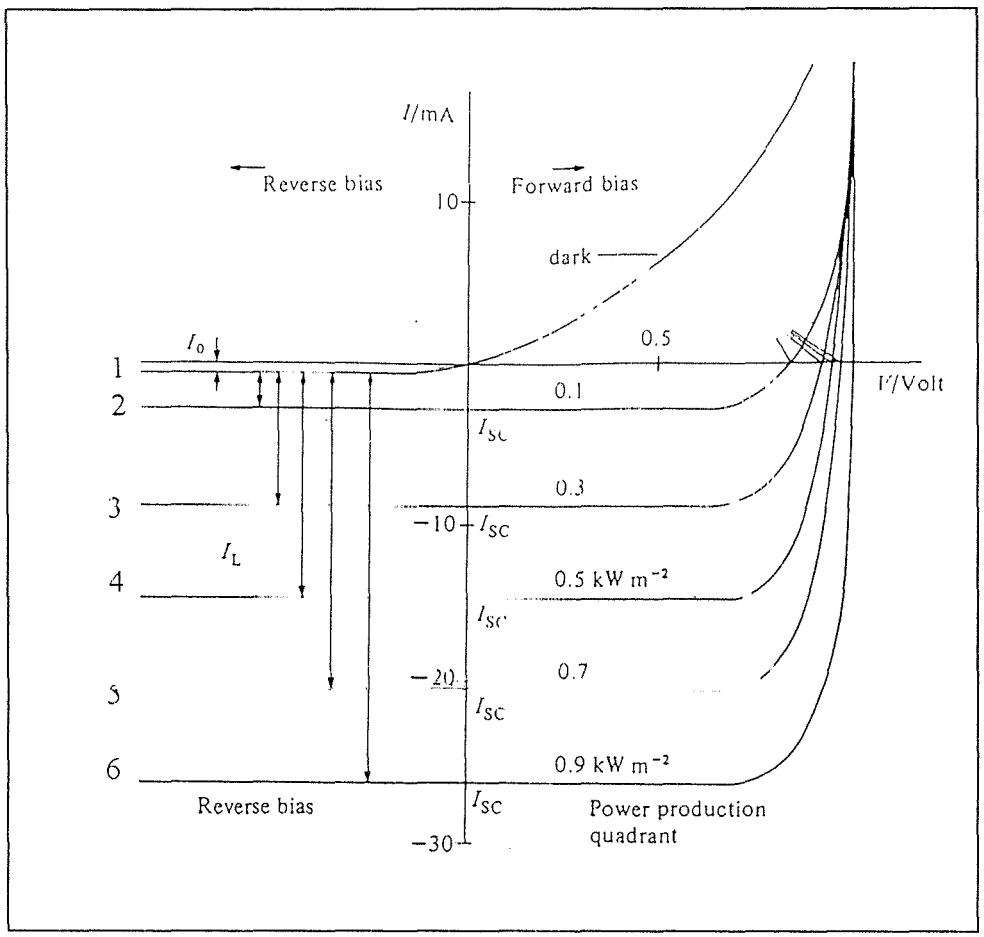

FIGURE B.4: P-N junction I-V characteristics, drawn in the convention used for rectifying diodes under varying intensities of solar radiation [4]

In figure B.5, the power-generating quadrant of the current-voltage characteristic of a solar cell is shown. This diagram resembles the fourth quadrant of figure B.4, but with the current I taken as positive.

The total equivalent circuit of a solar cell is shown in figure B.6 [4]. The series resistance (R_s), represents the resistance of the contacts and the shunt resistance (R_{sh}), represents defects across and at the edges of the cell, where there is an abrupt change in the constituents of the material or the presence of foreign atoms. As a result, equation B.4 is modified to include these effects as follows [58]:

$$I = I_L - I_0\left(e^{q(V+IR_s)/BkT} - 1\right) - \frac{V + IR_s}{R_{sh}}.$$

where, B = diode ideality factor, that varies between 1 and 5.

Since $R_{sh} >> R_s$, the equation reduces to

$$I = I_L - I_0\left(e^{q(V+IR_s)/BkT} - 1\right) - \frac{V}{R_{sh}}. \qquad \text{----------(B.5)}$$

The value of the shunt resistance of a cell at a certain temperature, is approximately equal to the tangent of the dark current-voltage (I-V) curve at the origin and when the cell is illuminated, it is equal to the tangent of the curve at the short-circuit current [58].

The series resistance of a cell can be calculated if one knows two similar points at different intensities on the I-V curve. For example, in figure B.5, one can choose the maximum power point on curve 1 and 2. The series resistance is the difference in voltage between these points (V_1 - V_2), divided by the difference in currents, (I_1 - I_2) [58].

The peak power line shown in figure B.5, is the locus of all the maximum power points at different solar intensities. It is dealt with in section B.3.

B.2 THE OPEN-CIRCUIT VOLTAGE AND THE SHORT-CIRCUIT CURRENT

If the voltage V across the cell is zero, then the current I is termed the short circuit current, I_{SC}. Substituting V = 0, in equation B.4, we get,

$I = I_{SC} = I_L$ ---------- (B.6)

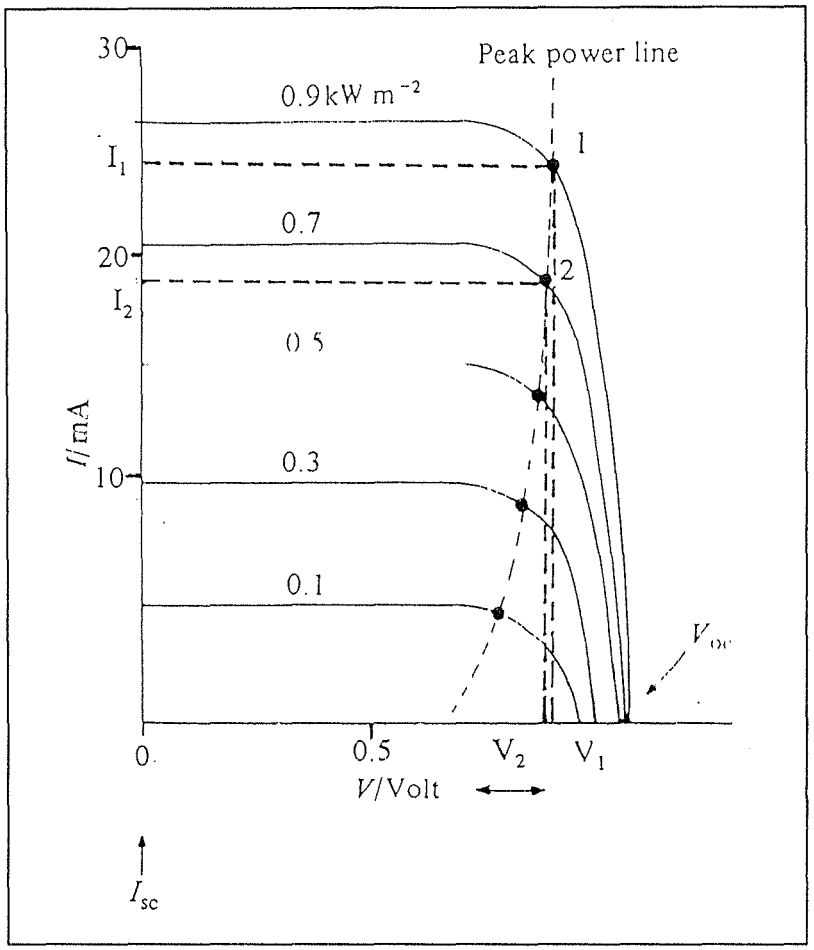

FIGURE B.5: The power generating quadrant of the I-V curve with the current I, conventionally taken as positive.

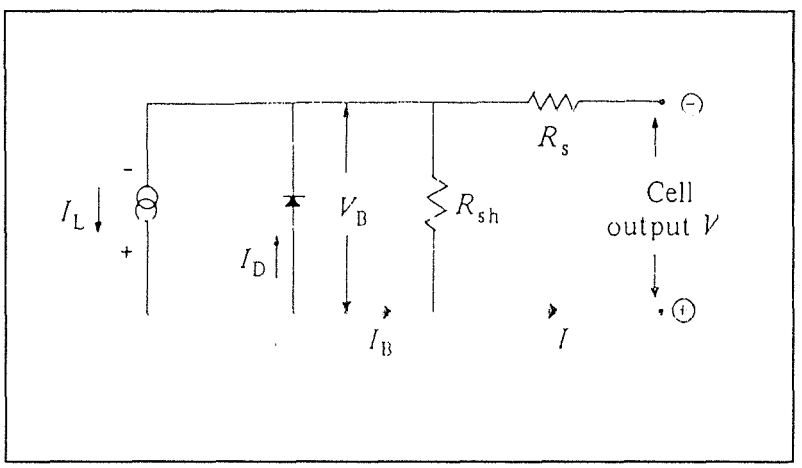

FIGURE B.6: Equivalent circuit of a solar cell [4].

When the current is zero, the voltage is known as the open-circuit voltage, V_{OC}. Re-arranging equation B.4, yields:-

$V_{OC} = (kT/q) \ln (I_L/I_0 + 1)$ ----------(B.7)

At first sight, it might appear from equation B.6, that I_{SC} is independent of temperature, however, it increases slightly as shown in figure B 7 [27], because at higher temperatures the band gap decreases, as discussed in section B.1. The current is also proportional to the cell's surface area [6, 7, 39], and varies directly with the photon-generated current, which in turn is proportional to the intensity of solar radiation.

Looking at equation B.7, one might be misled to deduce that V_{OC} varies directly with temperature. This is not true, because I_0 depends strongly on temperature as seen in equation B.1. It has been shown that V_{OC} is inversely proportional to temperature [6, 39], as shown in figure B.8 [27].

B.3 MAXIMUM OUTPUT POWER

Between the two extremes of I_{SC} and V_{OC} and for a given value of temperature and solar radiation, there is a point on the I-V curve of a solar cell, where the product of the current and the voltage is a maximum. The locus of these points is shown in figure B.5.

Considering the effect of radiation, it is clear that the voltage along the locus line does not vary much, because it is a logarithmic function of the photon-generated current [5], as shown in equation B.7. Hence, when a suitable number of cells are inter-connected to form a module, they can charge a 12V battery. In doing so, they will be forced to work at the battery's nominal voltage, which would be close to the voltage along the maximum power curve [41]. This will eliminate the need for a maximum power point tracker (MPPT), whose benefit does not justify its price for small and intermediate size solar systems. On the other hand, the current varies linearly with insolation and this makes it possible for solar cells to be used as solarimeters.

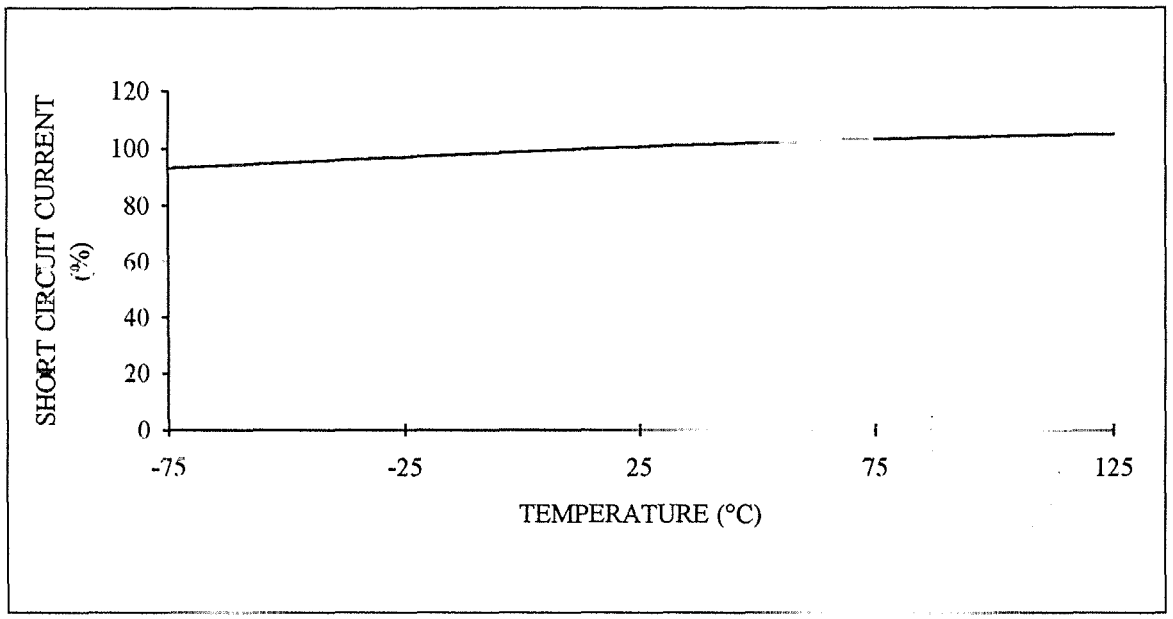

FIGURE B.7: Short-circuit current versus temperature for typical silicon cells [27].

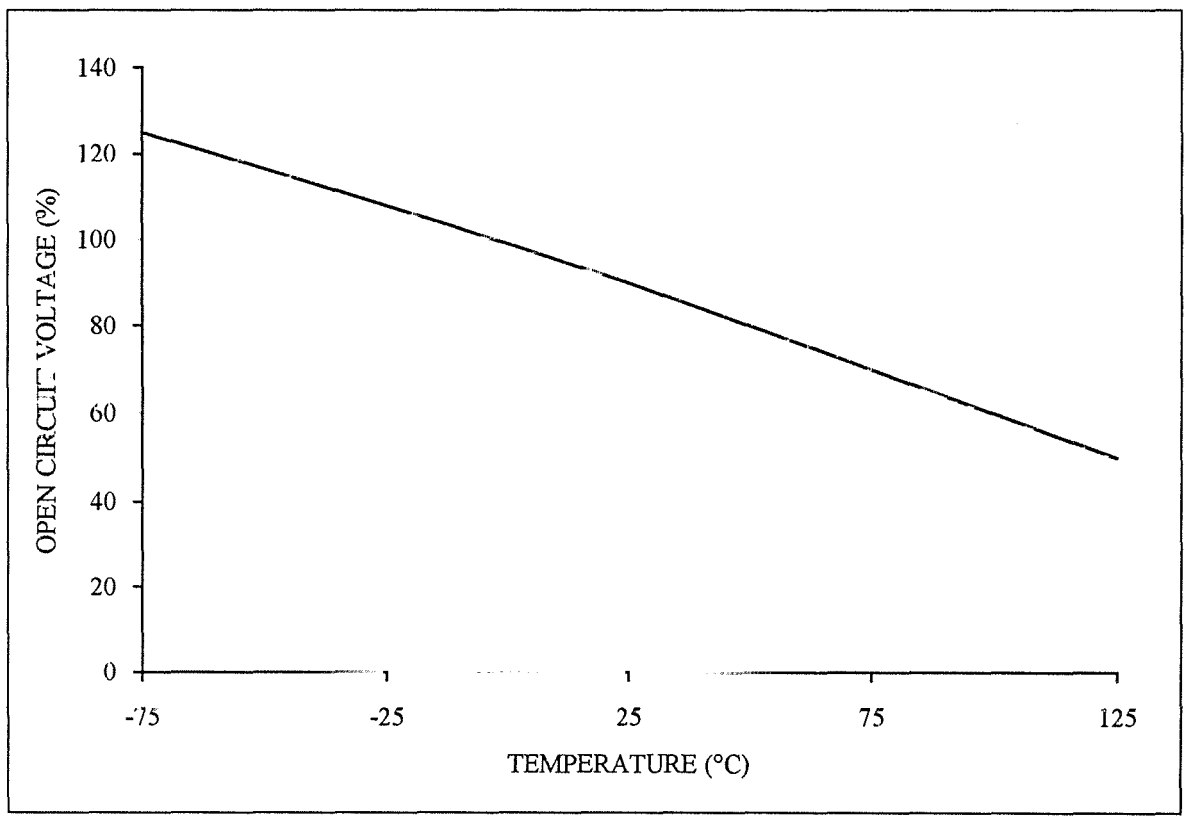

FIGURE B.8: Open-circuit voltage versus temperature for typical silicon cells [27].

The second factor that affects the power delivered from a cell is temperature. It has been mentioned before, that both the voltage and the current change with temperature, though the voltage is more sensitive to it. For silicon cells, the integral effect can be written as [4]:-

$$P_{(T)} = P_{(25°C)}[1 - 0.004(T - 25)] \quad \text{----------(B.8)}$$

where, $P_{(T)}$ = power at temperature T,

$P_{(25°C)}$ = power at the reference temperature of 25 °C.

B.4 LIMITATIONS TO CELL PERFORMANCE AND EFFICIENCY

There are many factors that influence the operation of PV cells Some of them can be deduced from figure B.6 [4]:

1. The photon-generated current must be a maximum by,

(a) careful manufacturing techniques, to reduce trapping areas in the cell;

(b) using anti-reflection coating and etching on the surface of the cell to enhance the absorption of solar radiation;

(c) minimising the top surface electric contact area, to allow maximum infiltration of solar radiation into the cell. The use of transparent contacts of indium tin oxide increases the effective area, but there are still difficulties in eliminating the degradation of the cell performance due to the chemical reduction of tin oxide to tin by silicon and the degradation at the tin-oxide-metal interface. Sealing of the solar modules in vacuum can solve this problem, but it entails higher costs [46];

(d) increasing the concentration of the dopants in the n-type layer at the surface, to enhance the absorption of the UV radiation, but taking care not to increase the rate of recombination;

(e) placing the junction deep enough to ensure good absorption of the generated electron-hole pairs.

2. The back surface series resistance of the cell must be minimised, by covering the whole back surface with conductor. However, it has the disadvantage of short-circuiting the whole module in case of a local p-n junction short circuit under a top-surface finger electrode [47]. It

can be prevented by using sets of finger electrodes on both sides of the cell, laterally offset from each other by a distance equal to l/2, where l is the distance between any two adjacent fingers on the same side of the cell. Local short circuits may occur in large area solar cells due to imperfect processing.

3. The shunt resistance should be a minimum, which can be achieved by careful manufacturing techniques of the cell.

The above conditions cannot be fully met during manufacture and a compromise has to be reached to satisfy all the conditions to an acceptable level. Here, the most important limitations are discussed.

First, the most energetic light photons in the ultra-violet region are absorbed in the first few micrometers of the cell. Being far from the junction, most of the electron-hole pairs that are generated there, do not make it to the junction because they recombine beforehand. The main reason for recombination is the presence of a highly doped layer which reduces the carrier life-time. This type of recombination is known as Auger recombination. A solution could be implemented by making the junction as close to the surface as possible, but this has a limit as well, because one must allow a space for the n-type layer at the top.

Second, the series resistance of the cell cannot be totally eliminated because the n-type layer has a considerable amount of resistance when compared to the p-type layer. The reason being that the top electrical contacts cannot cover the whole surface, otherwise they would hinder solar radiation from reaching the cell. A compromise usually sets the area covered by the contacts as 5% of the total area of the cell.

Third, doping the top n-type layer cannot be increased indefinitely because it increases the recombination at the surface, slows down the mobility of carriers and reduces the generated current [6]. Also it cannot be too dilute otherwise the open circuit voltage drops and the series resistance of the cell increases [8].

B.5 POWER LOSSES IN PV CELLS

Silicon cells do not make full use of the solar spectrum. Light photons that have energies higher than the band-gap of silicon can contribute an amount of energy equal to the band-gap, the remainder being lost as heat. Such photons are present in the ultra violet region of the solar spectrum. The percentage loss in absorption amounts to 31%.

Another major loss in absorption occurs for light photons whose energy content is less than the band-gap of silicon. These photons heat up the cell but do not produce current. They are found in the infra-red region and they amount to 24% of the solar spectrum.

Hence, the remaining useful percentage of the total solar radiation, that could be converted to an electric current is only 45%.

Now, other losses reduce this value even further. Some of these factors can be controlled but others are intrinsic properties of silicon that cannot be completely eliminated. They are summarised as follows:-

1. Open-circuit voltage loss (12%):

The open-circuit voltage (V_{OC}) of a cell cannot equal the band-gap E_g. The lost volts are due to the difference in potential between the Fermi level and the valence and conduction bands, as shown in figure B.3. Higher doping concentration decreases this effect but, at the same time, increases recombination.

2. Short-circuit current (I_{SC}) losses: There are four factors that contribute to the reduction of the value of I_{SC} [6]:

(a) Absorption losses (5%):

Silicon is an indirect band-gap semi-conductor that requires both energy and momentum to release an electron-hole pair. The energy comes from the absorbed light photons, while the momentum is supplied by phonons, that are produced by vibration in the crystal lattice. The energy is readily available, but the momentum takes some time before it is released, meanwhile the light photons would have travelled a considerable distance into the crystal. If the cell is not thick enough to utilise these photons before they emerge from the other side,

there would be no generation of current. A compromise between the cell's efficiency, thickness and cost, results in a minimum cell thickness of 250 μm that can absorb up to 95% of the useful solar radiation.

(b) Top surface contact grid losses (2%):

The top surface contacts occupy an area which reduces the surface available for the incident rays of the Sun.

(c) Surface reflection (1%):

Etching the surface of the cells and using anti-reflection coatings have made it possible to reduce reflection from the cell's surface considerably.

(d) Recombination losses (2%):

The main type of losses is known as Auger recombination, which characterises the early recombination of generated holes and electrons due to the presence of dopants.

3. Fill (Curve) factor losses (4%):

The fill factor is defined as the ratio of the maximum power that could be delivered by a cell to the product of V_{OC} and I_{SC}. This ratio gives an idea about the squareness of the I-V curve, i.e. how perfect the cell characteristics are. The greater the maximum power delivered, the squarer is the I-V curve and the higher is the fill factor. Its value is always less than 1 and it strongly depends on V_{OC}. Other factors that reduce the fill factor are the series and shunt resistances and the cell's temperature. In practice, the fill factor is used to compare different solar cells under identical conditions. [6, 58].

4. Series and shunt resistances losses (0.4%).

The series resistance is mainly caused by the top contacts while the shunt resistance is caused by defects in the cell. The latter is more pronounced in semi-crystalline cells.

Based on the above analysis, the efficiency of a single junction silicon cell cannot exceed 20%, unless an improvement in one or more of the above factors is achieved.

Other disadvantages of silicon cells include the mismatch between the maximum absorption wavelength of the cell and the maximum energy wavelength of solar radiation. The response of silicon cells peaks at a wavelength of 0.83 μm , while the maximum energy available in the solar spectrum is at a wavelength of 0.535 μm, for AM1.5. This explains why

silicon cells have higher efficiencies in cloudy weather conditions, when the solar spectrum shifts closer to the peak response of silicon cells, as shown in figure A.8.

B.6 SEMI-CRYSTALLINE SILICON CELLS

The methods implemented in the manufacturing of semi-crystalline silicon cells are cheaper than those used for mono crystalline cells, but the efficiency of the cells are lower as well. The common disadvantage is that both operations are batch processes, which means that the rate of production is low and this reflects adversely on the cost.

One difference in the end product is that semi crystalline silicon cells are produced as squares in shape, while mono-crystalline silicon cells are round. This allows the semi-crystalline cells to be stacked closer to each other to form a module that has an efficiency equal to that of a mono-crystalline module of the same size, thus offsetting the above mentioned effect of lower cell efficiency [16].

The cause for the decreased efficiency is attributed to the presence of more grain boundaries which are centres of recombination. This effect has been reduced by growing the crystals in such a way that they reach the edges of the wafer, so that only the lateral boundaries remain. Hence, the crystals are not really complete and so they are described as semi-crystalline [6]. Other names are used to mean this type of cell such as poly-crystalline and multi-crystalline cells [49]

The cost of such cells can be reduced by depositing a thin-film layer of polycrystalline silicon on a substrate. The method of deposition is simple and the quantity of silicon required is small. It has been shown that the efficiency does not drop with the decrease in the cell's thickness, provided that surface etching is applied to the top surface and a reflecting back surface is used to direct the unabsorbed light back into the cell [16]. Some challenges remain to be resolved such as good adhesion of the film to the substrate and efficiency. It has been demonstrated that such cells are chemically and mechanically stable [43] and the Mitsubishi Group has reported a 16.45% efficiency for a 2 cm square cell [65]. Recently, the Max Planck

Institute in Stuttgart, Germany, has produced a thin-film silicon cell of an area of 0.76 cm^2 and an efficiency of 17.3% [71], as indicated in figure C.1, of appendix C.

B.7 AMORPHOUS SILICON CELLS

Amorphous silicon cells are prepared by decomposing silane (SiH_4) on a substrate at a temperature between 200 °C and 300 °C. Dopants are added to the vapour to make the cell a p-type or an n-type layer. The low temperature allows the use of cheap substrates and reduces the energy requirements, while the process itself requires a small quantity of silicon.

The construction of an amorphous silicon cell differs somewhat from a crystalline one in that the n-type phosphorus doped silicon layer is separated from the p-type boron doped layer by an intrinsic layer of silicon. The electric field is created by the p-type and n-type layers, while the intrinsic layer serves as a low defect area, where most of the photovoltaic effect takes place [3].

These cells have some advantages over crystalline silicon cells in that, their optical absorption properties enable them to utilise a higher percentage of visible light. Hence, the need for a thick cell diminishes and thin film cells that are normally 1/1000 of that of mono-crystalline silicon cells suffice to absorb most of the useful solar radiation [50].

In spite of these benefits, amorphous silicon cells suffer from low efficiency and initial performance degradation of about 10%, when illuminated for the first time [42]. The cause of the low efficiency stems from the presence of many unsatisfied "dangling" bonds which are a result of the non-existence of periodicity in amorphous cells. These bonds act as very good trapping points for the generated electrons and holes. To reduce this effect, amorphous silicon can be doped with hydrogen to produce a cell with a band-gap of 1.4 eV or with hydrogen and fluorine to produce a cell with a band-gap, that could be tailored between 1.55 eV and 1.8 eV [4, 49]. For both cases, the new material has a band gap that is near to the maximum solar photon energy region. This factor makes it possible for a cell of 1μm thickness to absorb up to 90% of the visible light region [6, 42, 49].

The cause of the initial degradation in the cell's efficiency is not definitely known, although it has been perceived that the thinner the intrinsic i-layer is, the lower is the degradation. Heat treatment can bring the cell's efficiency to its former value [42].

Amorphous silicon cells have higher series resistance but this decreases when the cell is illuminated. These cells can be deposited on any surface and they can be made small so that no metal contact grids are needed.

Developments have been achieved to reduce the power loss in the top transparent conductive oxide film. This method is known as the "through hole contact" photo-etching. A 10 cm x 10 cm laboratory cell with an efficiency of 10.5% has been achieved [45]. Other improvements to solar cell efficiency can be made, as described in appendix B.

B.8 GALLIUM ARSENIDE CELLS

Besides silicon cells, gallium arsenide cells are crystalline semi-conductors which have a crystal structure similar to silicon except that two different elements are present simultaneously. These cells have the best conversion efficiency, because their band gap of 1.4 eV coincides very closely with the maximum energy wavelength in the solar spectrum.

The disadvantages of these cells is that the material is expensive and not as abundant as silicon. Also, arsenic is a toxic element and should be treated with caution. However, these cells are ideal to be used in systems that use concentrators because smaller cells are needed, which means that the cost could be reasonable and also because their efficiency is not much affected by temperature.

Unlike silicon, gallium arsenide is a direct band material, which produces at least one electron-hole pair for every light photon absorbed. The transition is direct and no phonons are needed. As a result, light photons are absorbed very quickly in the first few microns of the cell and a thin cell would suffice to absorb most of the incident useful radiation [49].

Recombination at the top layer of these cells is more serious than in silicon cells, but it can be reduced by making the top n-type layer much thinner than the lower p-type layer. In the manufacturing stage, the two layers are chemically built over one another, each one with its

own dopant. The method is somewhat different from that used for the manufacture of silicon cells, because there is no diffusion of dopants by heat. Such layers are known as epitaxial layers. Cells are processed in batches, and this causes a direct impact on the price and on the rate of production.

B.9 CADMIUM SULPHIDE/COPPER SULPHIDE (CdS/Cu_2S) CELLS

Poly-crystalline heterojunction thin film cells of cadmium sulphide/copper sulphide (CdS/Cu_2S) cells have been manufactured. The n-type layer is CdS that has a band gap of 2.4 eV, while the p-type layer is Cu_2S, with a band gap of 1.2 eV [6]. The effective band gap is about 1.1 eV [5, 40], which is similar to silicon, but the main advantage of this cell is the easy and cheap fabrication methods, though the cell's efficiency is still low. Moreover, this cell suffers from degradation when exposed to air and humidity and cadmium is rare and toxic. An improvement can be achieved by replacing the Cu_2S layer with a layer of copper indium diselenide (CIS).

B.10 CADMIUM SULPHIDE/COPPER INDIUM DISELENIDE (CdS/CIS) CELLS

These cells do not degrade in the presence of air or humidity. CIS is a direct band semi-conductor with a band-gap of 1.04 eV. It absorbs most of the solar spectrum and unlike Cu_2S, its lattice matches very well with that of CdS at their interface. This means that there are less allowed states in the forbidden gap and this reduces recombination [49]. Recently, great interest is shown towards the development of these cells. An efficiency of 16.9% has been achieved in the laboratory by EUROCIS Consortium in Europe, for an active cell area of 0.4 cm^2 [52], while the Royal Institute of Technology, Kista, Sweden, has manufactured a cell of equal area to the above with an efficiency of 17.6%, in April 1994 [71].

B.11 CADMIUM TELLURIDE (CdTe) CELLS

This cell has a band-gap of 1.5 eV, which is near to the optimum value. Cadmium telluride is a direct band-gap semi-conductor and this enables it to be manufactured as thin film cells. The efficiencies of these cells are above 10% [50] and their only disadvantage is the high toxicity of tellurium. Figure D.1, of appendix D, shows the evolution in efficiency of CdS/CIS, CdTe and thin film silicon cells [56].

B.12 IMPROVEMENTS TO CELL EFFICIENCY

One of the ways to improve the efficiency of solar cells is to stack different cells over one another to form tandem, cascade or multi-junction cells. The top layer would absorb the high energy short-wave radiation and allow the remainder to pass through to the lower layers. The layers must be carefully matched to produce equal currents at the different junctions, which are in series with each other. Some of the recent achievements in this field showed a 10.2% stabilised efficiency of a multi-junction, one square foot, amorphous silicon array [52], a 15.5% efficiency, 0.4 cm^2 copper indium diselenide with gallium cell (CIGS) [53] and a 29.5% efficiency, of a cell with total area of 0.2503 cm^2, GaInP/GaAs cell [55, 78].

Another method similar to the above one uses dichroic mirrors to split the radiation into different wavelengths and direct each band of rays to the appropriate cell. This method is known as "spectrum splitting". Dichroic mirrors can be replaced by reflection hologram beamsplitters that are less expensive, easily reproduced and can have their spectral selectivity varied according to the specific requirements [51].

PV cells that work under a concentrated beam of solar radiation have the potential of increasing the efficiency. Careful consideration of the cost and maintenance of the tracking system, the cleaning of lenses or mirrors and most importantly, the climate of the place, should be carried beforehand. A place that is characterised by frequent cloudy days is not suitable for such a system.

The efficiency of PV cells can also be improved by finding ways and means to reduce the losses that were mentioned in section B.5. Sunpower Corporation managed to produce a 21.6% efficient silicon cell module, by transferring the top contact grid to the bottom of the cell and using a highly reflective back surface together with special manufacturing of the contacts to increase the cell's voltage. These modules were used on the Honda Dream Solar-powered car, which took part and won the 1993 World Solar Challenge race in Australia [57]. Another striking result was announced by the University of New South Wales (Australia), of a 23% passivated emitter and rear local diffused (PERL) cell [68], that is surface etched in the shape of inverted pyramids. The upper and lower surfaces are passivated by an oxide and the contacts are buried in them, using a laser grooving technique. Boron is locally diffused near the contacts to reduce recombination.

In conclusion, the only way to reduce the cost of PV cells is to increase their efficiency [70] and decrease the complication and energy involved in their manufacture. This is possible and industry is already moving in this direction. For example, an innovative work has been achieved by Solec Incorporation, that produced a 20% efficient silicon cell, using a cheap process that has the potential of reducing the price to $2 per peak Watt [56].

B.13 CONSTRUCTION OF SOLAR MODULES

In preparing solar modules, one has to distinguish between the method used to build up modules of crystalline cells and modules of thin-film cells.

For crystalline cells, their surface is first etched to remove the effect of sawing and then treated with an anti-reflective coating. The conductive fingers and the bus-bar contacts are applied to the front surface of the cell, while the back surface is usually completely covered with a conductive material. Then the cells are tested and grouped together according to their output voltage and current.

Cells of equal or almost equal currents and voltages are then interconnected to produce a reasonable voltage and current. The common practice is to design modules that can charge

12 V batteries. In order to achieve the design requirements, PV cells are connected in series to increase the voltage and connected in parallel to other similar groups of series cells, to increase the output current of the module. The open-circuit voltage has to be 18 V - 20 V, because part of it will be lost in the by-pass and blocking diodes, in the mismatch between the modules and due to the rise in cell temperature during the day. The remaining voltage should be about 15 V

After that, the cells are encapsulated using one of the following methods [66]:

(a) substrate bonding: where the cells are bonded to a structural substrate such as aluminium or reinforced plastic;

(b) superstrate bonding: where the cells are bonded from the top to a transparent structural superstrate such as tempered or boro-silicate glass;

(c) laminated: where the cells are bonded on both sides, usually using the same transparent material.

The cells are stuck to the supporting surface by adhesives such as silicon elastomers, acrylics or fluorocarbons. These materials are also used as pottants, that totally encase the cells and their interconnects, to relieve the thermal stresses induced on them, due to the difference in the expansivity rate between the supporting surface and the cells. A layer of glass or reinforced plastic covers the pottant and an aluminium or stainless steel frame is attached to complete the module assembly.

Junction boxes and by-pass diodes are then added to the back surface and the module is tested. A certificate plate is attached to the back to give the module its individual characteristic open-circuit voltage, short-circuit current and maximum power at standard testing conditions (STC), which is defined as an irradiation of 1000 W/m^2, at an air mass ratio of 1.5 and cell temperature of 25 °C. Also, the output is given at the nominal operating cell temperature (NOCT), being defined as the temperature that the module would attain at steady ambient conditions of air temperature of 20 °C, solar irradiance of 800 W/m^2 and wind speed of 1 m/s.

As for thin-film cells, the transparent conductive oxide and interconnects are first deposited on the glass surface and patterned with laser, followed by the deposition of the

semi-conductor layers and the rear conductive oxide layer. Leads are attached and the whole structure is assembled in glass. A frame is usually fixed to facilitate the installation of the module. The junction box and the by-pass diode are added and the module is tested and given its characteristics.

Solar modules are designed to be rigid, weather resistant and easily transported and installed. The encapsulation of the cells should not degrade on exposure to ultra-violet radiation and should not create excessive thermal stresses, when exposed to varying ambient temperatures. Other requirements for a good module is impermiability to oxygen, humidity and rain, and resistance to dust and hail sputtering [66].

Clearly, all of the above processes require power that produces pollution, but when the modules are set in operation, they will pay the energy back within a fraction of a year up to 10 years, depending on the type of modules, the amount of energy produced which depends on the local solar radiation and on the efficiency of the manufacturing processes [6].

It has been mentioned that cells of equal or almost equal currents and voltages should be used for the construction of a module. Failure to do so will create a reverse-bias condition, when the output of one of the cells in the module is significantly lower than the others that are in series and this will cause the weak cell to overheat and eventually fail. Reverse-bias conditions can also occur if one or more cells are shadowed, cracked or degraded. The same also applies for a series of modules connected together.

In order to reduce the risk of self-destruction of a cell or module, two approaches are usually taken. First, multiple current paths are made in the wiring circuits of the cells and the modules. Second, by-pass diodes are used to limit the reverse current in the module and blocking diodes are used to protect a string of modules. [7, 67].

Even though every effort is made to match the cells' voltages and currents, there would still be some differences that will cause a drop in the efficiency of the modules. These losses are known as the mismatch losses.

B.14 THE ARRAY SUPPORTING STRUCTURE

Solar modules can be virtually mounted on any structure as long as it can withstand the static load and any resulting wind load. These structures could be ground-base supports, poles, roofs or walls.

One of the main concerns of designers and users is to reduce the costs of the balance of system (BOS) components. For a ground-based array, local material can be used to build-up the structure, while for roof or wall-mounted arrays, the use of large area modules would reduce workmanship and roof preparation. To reduce costs even further, sets of modules can be pre-assembled and wired together in the workshop, before they are mounted on the structure

[60, 70].

Some requirements have been identified as essential for any supporting structure [61]:

(a) to satisfy the design conditions regarding orientation and tilt angles of the array;

(b) where applicable, the structure should be portable and easily assembled;

(c) it should withstand adverse weather conditions and wind.

Also, one has to take care that the structure of one array does not cast a shadow on another array and that the modules are accessible for periodical cleaning.

B.15 THE BATTERY BANK

Batteries are extensively used in PV systems that require an energy storage. Ideally, the batteries should have the following characteristics [39]:

(a) high cycle life for deep discharges;

(b) low maintenance requirements;

(c) high charging efficiency;

(d) deep discharge capability;

(e) low rate of self discharge;

(f) reliability;

(g) minimal change in performance with changes in temperature.

Though lead acid batteries were mainly developed for use in vehicles and for traction purposes, they are now the major type of batteries used for energy storage in remote and stand-by PV systems, because of their cheap price. If they are developed further they could fare better in PV applications, especially regarding their life time. Also, they may find their way to the future market of electric vehicles. Other types of batteries are also available for PV applications, such as the nickel-cadmium cells but they are more expensive. Besides, cadmium is a very toxic material and this restricts their use to systems that require high reliability.

Recent developments aim at producing low-cost low-maintenance batteries that are more tolerant to over-charging and deep-discharging without reducing their life-time. Ovonic Battery Company Incorporation has produced a nickel-metal hydride (NiMH) battery, that has the potential to supply more power per unit mass than lead-acid batteries, at a lower life-cycle cost. The battery is 100% recyclable [62] and it can withstand overcharges and deep discharges without major degradation in its performance. It has a longer life-time and can be charged quite fast, though, like lead-acid batteries, it has a high self-discharge rate.

As for lead-acid batteries, one has to mention that there are also some advances in this field. GNB Batteries Company has developed a totally maintenance free lead-acid battery [63] to be used as a stand by power supply for telecommunications. This battery works on the 'oxygen cycle'. When the battery approaches full charge, oxygen gas is produced at the positive electrode. If it is allowed to flow to the negative electrode, the oxygen reacts to form lead sulphate and water. Further charging restores the lead sulphate back to lead. This battery performs well in both float charge and deep cycle applications. No stratification of the acid occurs, because the electrolyte is immobilised in a microporous absorbent matrix. Spilling and loss of acid through the vents does not occur.

Some general characteristics of lead-acid batteries should be understood before one can use and maintain them. Figure B.9 and B.10 show the effect of temperature on the capacity and rated life of lead acid batteries [64]. From the graphs, it can be inferred that the optimum range of operating temperatures is between 15 °C and 25 °C, where the battery capacity and rated life are close to 100%.

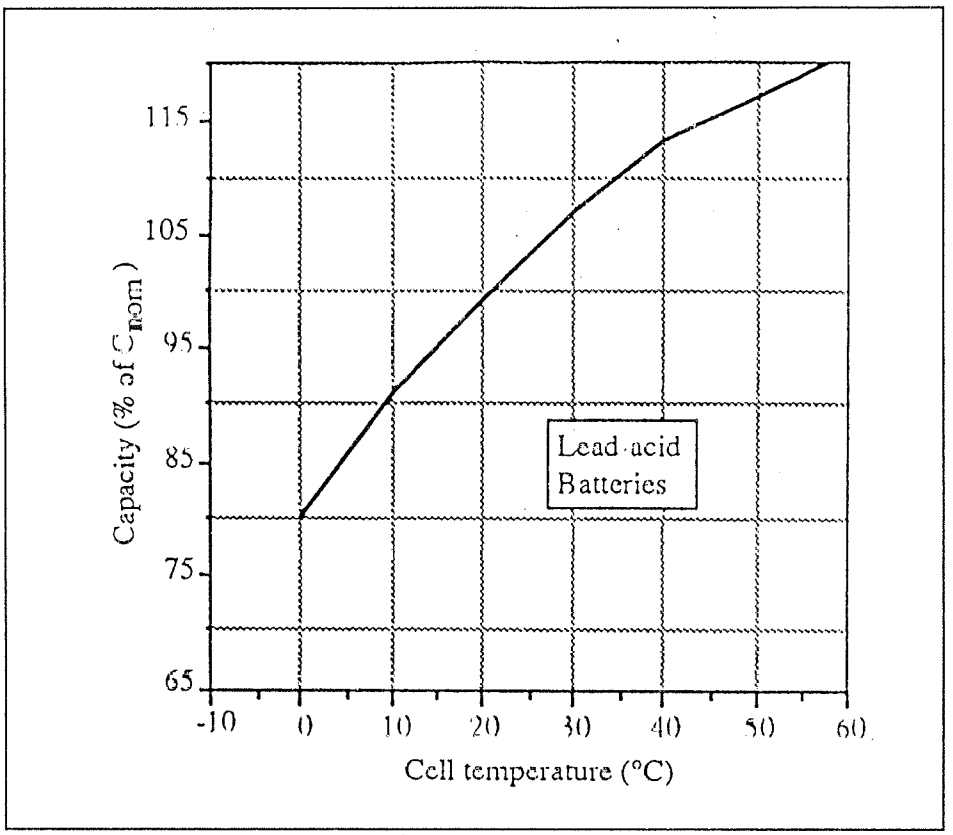

FIGURE B.9: Variation of capacity with temperature in a lead-acid battery [64].

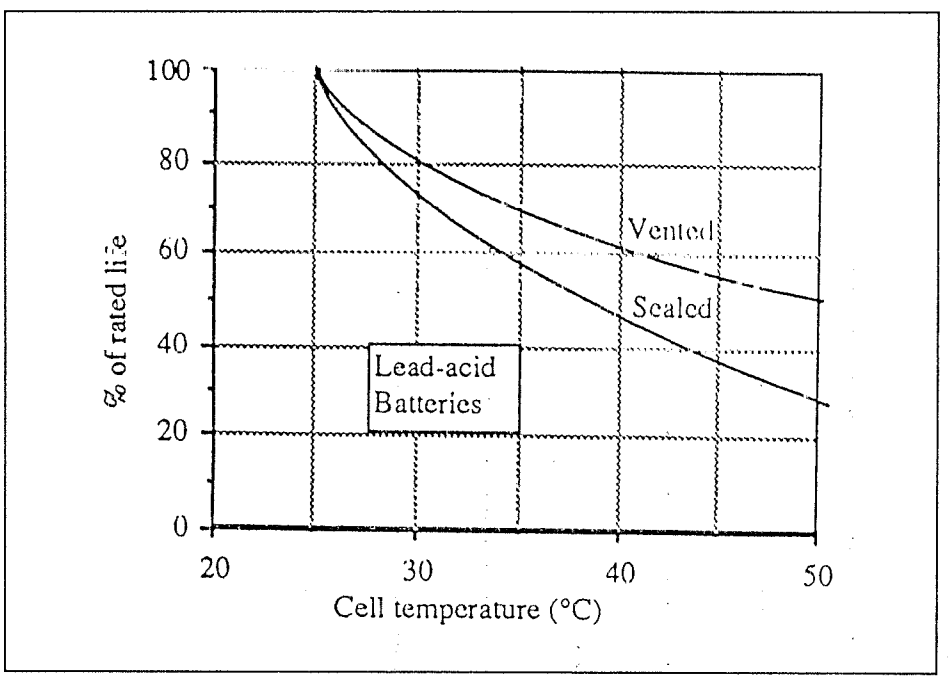

FIGURE B.10: Effect of temperature on the lifetime of lead-acid batteries [64].

Placing the battery where the temperature might drop to 0 °C should be avoided, as there will be the risk of freezing of the electrolyte, which would expand and crack the battery case.

The rate of energy consumption has an effect on the battery's capacity. As an example, a low discharge current over 100 hours (C_{100}) would deliver more total energy than a high discharge current over 5 hours (C_5), as shown in figure B 11 [64]

Figure B.12 shows the effect of the depth of discharge (DOD) on the life-time of lead-acid batteries. To make the battery live as long as possible, the DOD should not normally exceed 25% [64].

There are common requirements that should be fulfilled to ensure that the battery is in good condition:

1. Regular maintenance that includes:

(a) checking and topping-up of the electrolyte level.

(b) periodical cleaning of cell surface to reduce self-discharge.

(c) making sure that no over-charging or frequent deep discharging occur.

(d) applying an equalising charge whenever deviations are detected in the voltage of the different cells.

2. Monitoring of the batteries:

(a) measurement of the voltage of each cell.

(b) measurement of the specific gravity of the electrolyte in each cell.

(c) measurement of the temperature of the cells.

3. The batteries have to be kept in a cool, dry and well ventilated place. Placing them under the PV array, whenever possible, could be very useful as it will reduce the space requirements and the voltage losses. However, one has to take care that they are protected from rain, dew and vandalism.

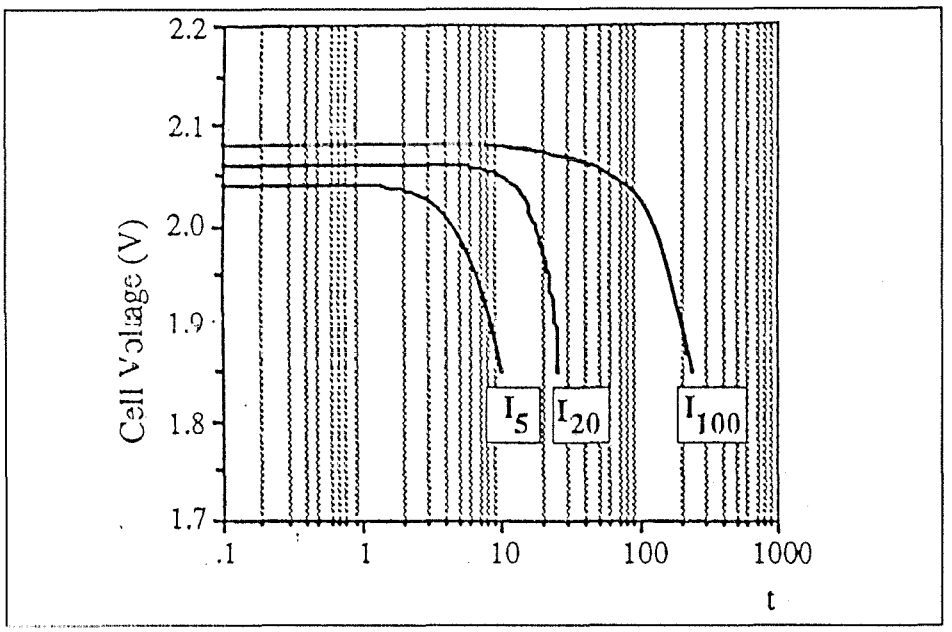

FIGURE B.11. Ampere hour capacity characteristic of a lead-acid battery [64].

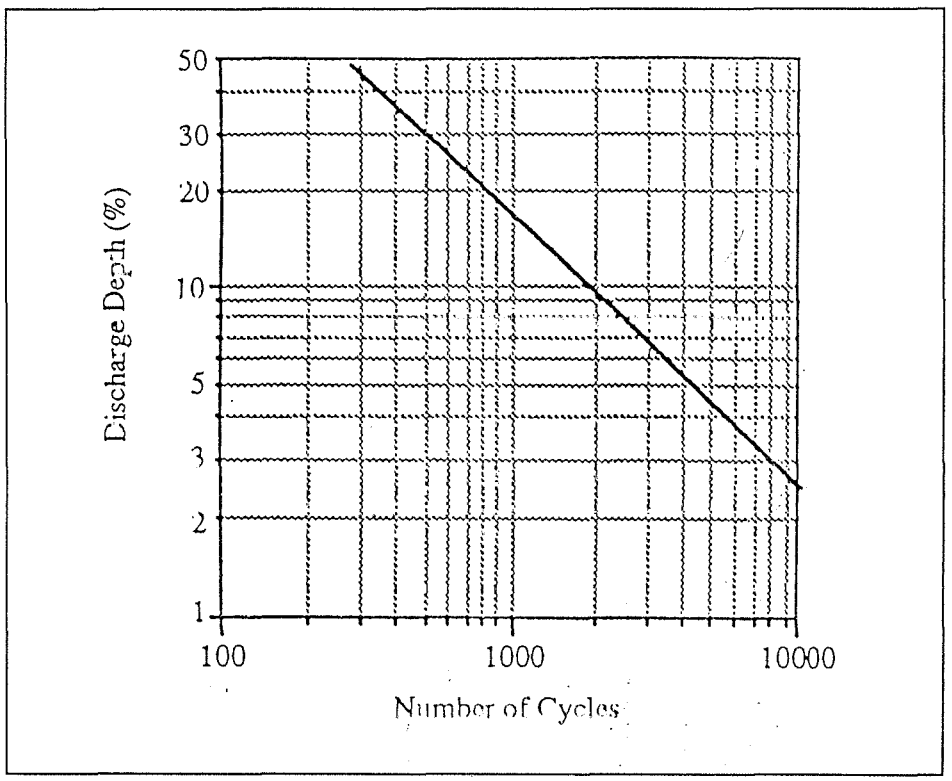

FIGURE B.12: Effect of discharge depth on the lifetime of a lead-acid battery designed for cycling [64].

B.16 THE BATTERY CONTROL UNIT (BCU)

Battery control units are very essential to safe-guard the proper charging and discharging of the batteries. There are two different designs available in the market. The first allows the charge to pass from the PV array to the batteries until a certain upper voltage is achieved, then the BCU cuts off the supply by shorting the array through a shunt transistor. When the battery voltage drops to a certain threshold value, the shunt switch opens and the current flows once more into the battery. As a result, the battery gets charged by a pulse charge, caused by switching the shunt transistor on and off.

The second type of BCU has the ability to charge the battery in two stages. The current flows to the batteries until they are nearly fully charged, then the mode of charging changes to a trickle charge. The choice between the two types mainly depends on the cost and the design requirements [39].

BCUs are the hearts of a PV system, so they are required to be very reliable and safe. One has to avoid subjecting the unit to high temperatures, humidity, rain and overloading.

B.17 POWER DISTRIBUTION AT LOW VOLTAGE

In distributing power to the various electric loads of a PV system, one has to make sure that the voltage drop along the cables does not exceed 0.5V, for a 12V system, otherwise these losses would reduce the overall system efficiency and might cause unsatisfactory operation of the load. The electric wires used must be of sufficient sizes and care must be taken that, when two wires are connected together, they would not incur an additional voltage drop [39].

For PV systems that operate d.c. appliances, the higher the voltage, the lower the losses in the wires. However, high d.c. voltages are lethal and proper precautions have to be taken to ensure the safety of the system and the users. A system voltage of 48V is considered as the maximum value that does not require special isolations, but there are very few d.c. appliances that work on 48V. In fact, it is found that most of the small systems operate at 12V or 24V.

In case the latter voltage is not satisfactory, one can probe the possibility of adding a d.c. to d.c. converter or an inverter to the system.

Finally, one has to mention the possibility of manufacturing AC MODULES that have all the necessary electronics attached to their back, to produce 220-240 V alternating current. There is a feasibility and development project in progress to assess their performance [69]. If such modules become economically feasible, they can solve the problem of fire risks and accidents that might occur in a high d.c. voltage system. Other advantages include reduced susceptibility for lightning, easier integration into the utility grid and lower costs for wiring.

APPENDIX C

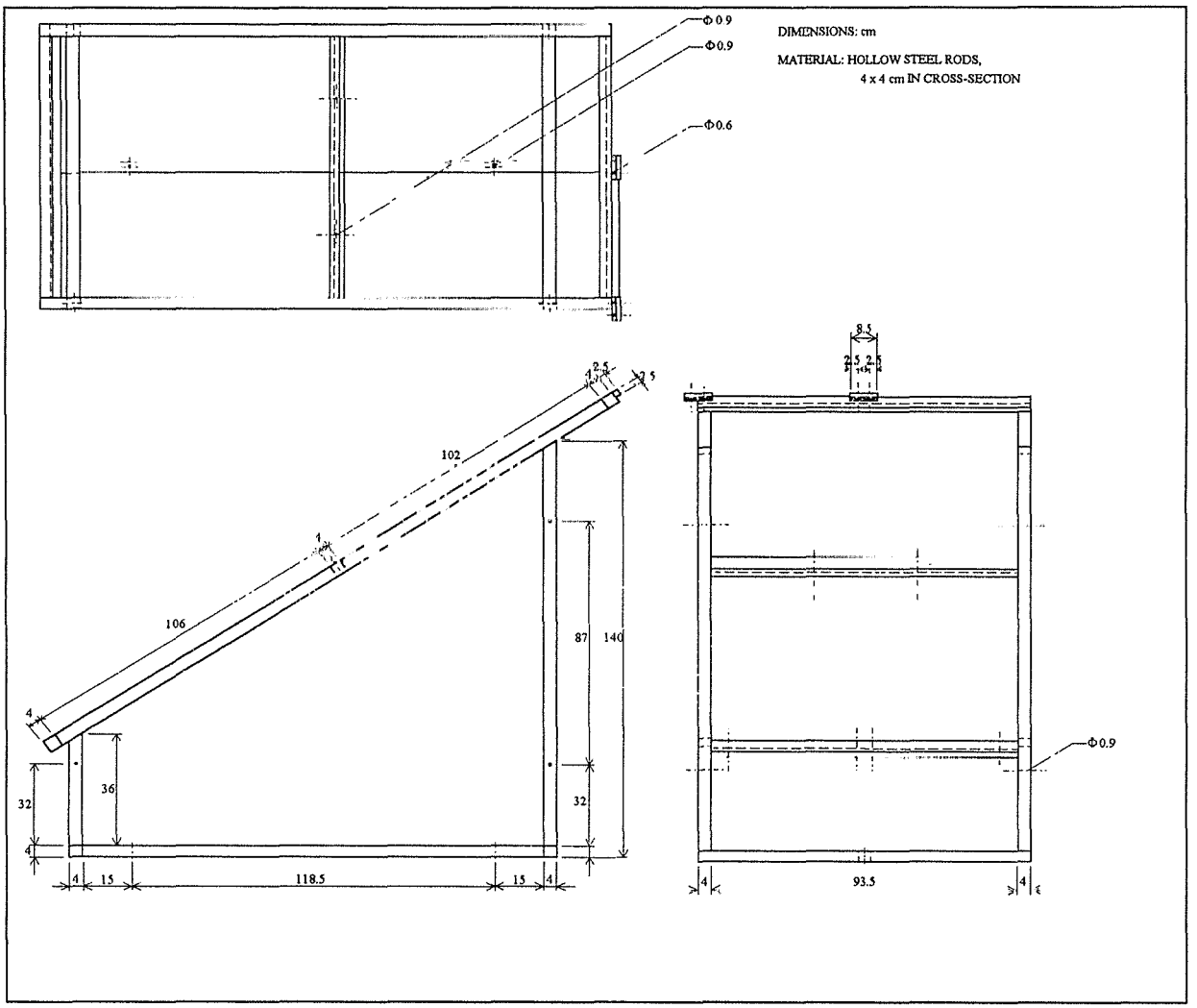

FIGURE C.1: Design drawing of the array structure

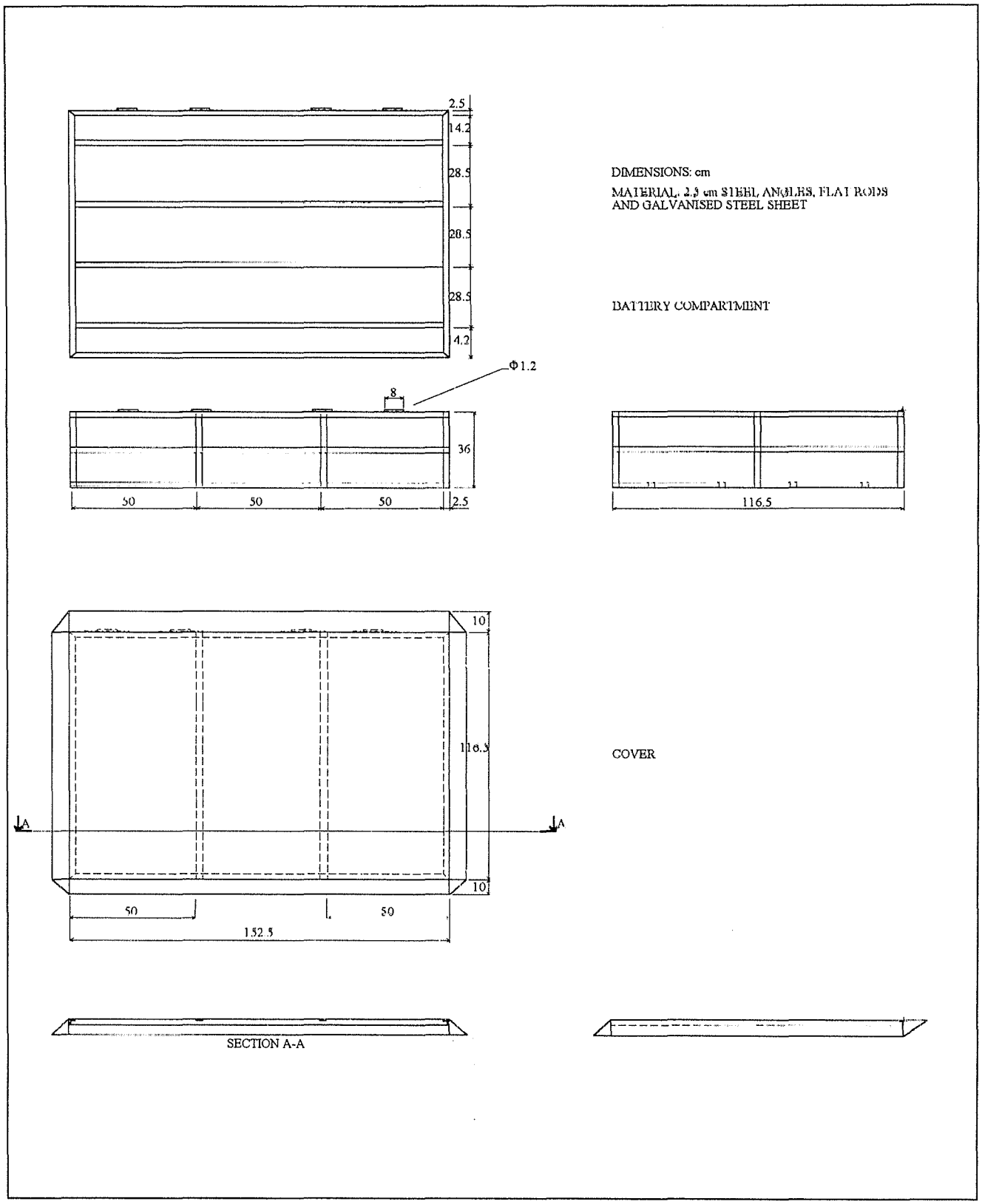

FIGURE C.2: The design drawing of the battery compartment and its cover.

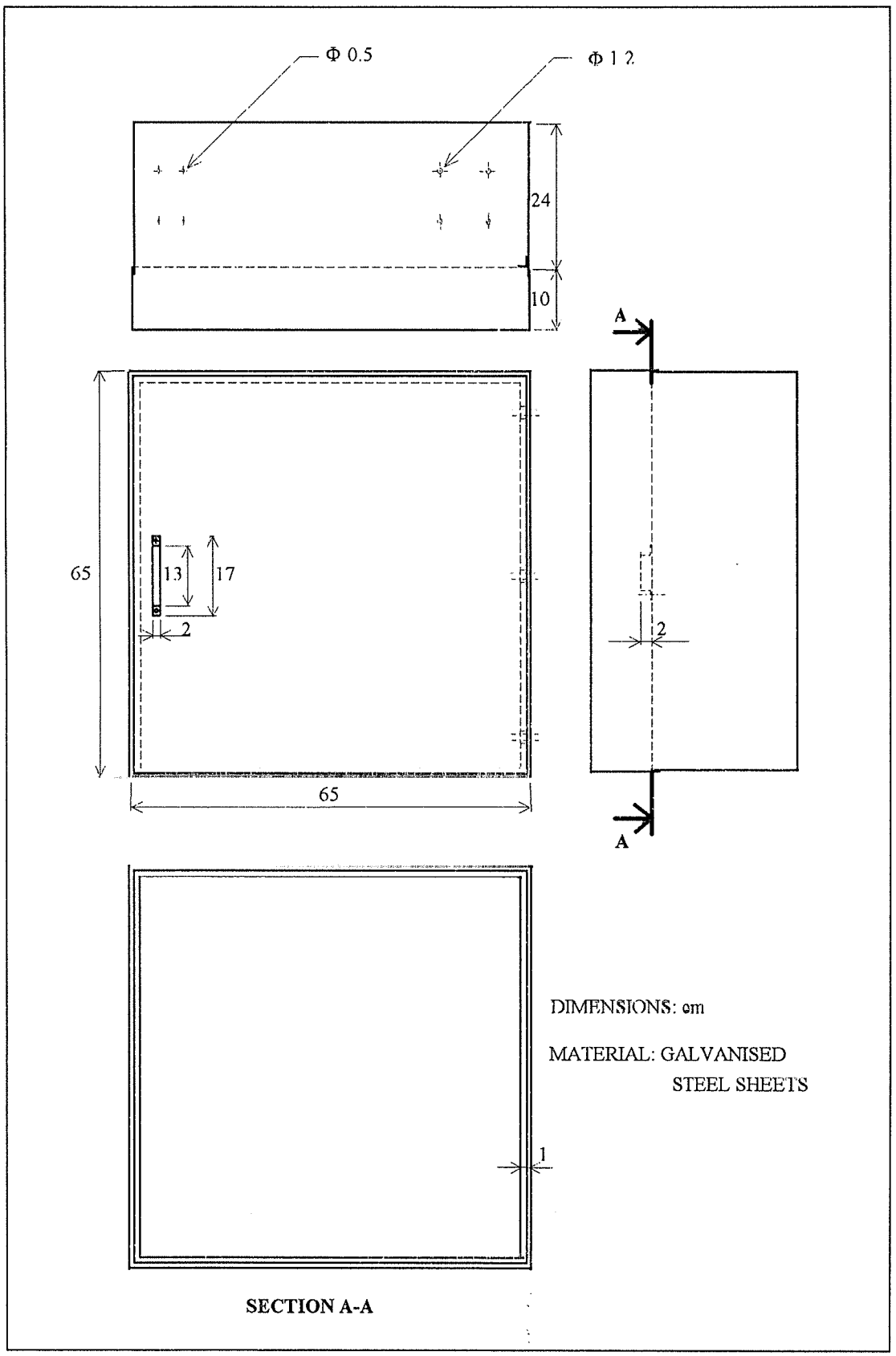

FIGURE C.3: Design drawing of the box for the integrators.

TABLE C.1: Executing programme of the micro-logger.

```
Flag Usage: None
Input Channel Usage:  1 [MP100 R.H.%, SINGLE-ENDED]
                      2 [MP100 AIR TEMP. SINGLE ENDED]
                      3 [LI200SZ, HORZ. IRRAD. (S.E.)]
                      4 [W200P, WIND DIRECTION, (S.E.)]
                      5 [Mk 1-G, INCLD. IRRAD., DIFF]
                      6 [SA1-T,BOTTOM MODULES TEMP.DIFF
                      7 [SA1-T,TOP SURFACE MODULE TEMP]
                      8 [CURRENT INTEGRATOR CH. 1 DIFF.
                      9 [CURRENT INTEGRATOR CH. 2 DIFF.
                     10 [POWER INTEGRATOR DIFFERENTIAL

Excitation Channel Usage: 1 [MP100]
                          2 [W200P]
Continuous Analog Output Usage: None
Control Port Usage: None
Pulse Input Channel Usage: 1 [A100R, WIND SPEED]
                           2 [ARG100, RAINFALL]
Output Array Definitions: 100 [15 Minute interval]
                          200 [Hourly interval]
                          300 [Daily interval]


*     1        Table 1 Programs
  01: 300      Sec. Execution Interval
 --- Readings every 5 minutes ---

01:  P4        Excite,Delay,Volt(SE)
  01: 1        Rep
  02: 5        5000 mV slow Range
  03: 1        IN Chan
  04: 1        Excite all reps w/EXchan 1
  05: 100      Delay (units .01sec)
  06: 5000     mV Excitation
  07: 1        Loc [:R.H. %    ] MP100
  08: 0.1      Mult
  09: 0.0000   Offset
 --- Relative Humidity from MP100 ---

02:  P4        Excite,Delay,Volt(SE)
  01: 1        Rep
  02: 5        5000 mV slow Range
  03: 2        IN Chan
  04: 1        Excite all reps w/EXchan 1
  05: 100      Delay (units .01sec)
  06: 5000     mV Excitation
  07: 2        Loc [:AIR TEMP.] MP100
  08: 0.1      Mult
  09: -40      Offset
 --- Air Temperature from MP100 ---
```

```
03:  P14        Thermocouple Temp (DIFF)
  01: 1         Rep
  02: 1         5 mV slow Range
  03: 4         IN Chan
  04: 1         Type T (Copper-Constantan)
  05: 2         Ref Temp Loc AIR TEMP.
  06: 3         Loc [:TOP TEMP ] SA1-T
  07: 1         Mult
  08: 0.0000    Offset
 ---Solar module temp. using thermocouple, SA1-T ---
 --- Top Surface Temp. ---

04:  P14        Thermocouple Temp (DIFF)
  01: 1         Rep
  02: 1         5 mV slow Range
  03: 5         IN Chan
  04: 1         Type T (Copper-Constantan)
  05: 2         Ref Temp Loc AIR TEMP.
  06: 4         Loc [:BOT. TEMP] SA1 T
  07: 1         Mult
  08: 0         Offset
 --- Solar Module Temp. Using Thermocouple, SA1-T ---
 --- Bottom Surface Temp. ---

05:  P10        Battery Voltage
  01: 13        Loc [:BAT. VOLT] BATTERY VOLTAGE
 --- Battery Voltage of logger ---

06:  P          End Table 1


*     2         Table 2 Programs
  01: 20        Sec. Execution Interval
 --- Readings every 20 seconds ---

01:  P1         Volt (SE)
  01: 1         Rep
  02: 3         50 mV slow Range
  03: 3         IN Chan
  04: 5         Loc [:HORZ. IRR] LI200SZ
  05: 0.0716    Mult  -- Enter Mult. for Sensor --
  06: 0.0000    Offset
 --- Horizontal Irradiation from LI200SZ, kW/m2 ---

02:  P89        If X<=>F
  01: 5         X Loc HORZ. IRR
  02: 4         <
  03: 0         F
  04: 30        Then Do

03:  P30        Z=F
  01: 0         F
  02: 5         Z Loc [:HORZ. IRR]

04:  P95        End
```

```
05:  P2          Volt (DIFF)
  01: 1          Rep
  02: 3          50 mV slow Range
  03: 3          IN Chan
  04: 6          Loc [:INCL. IRR] Mk 1-G
  05: 0.026      Mult -- Enter Mult. for Sensor --
  06: 0          Offset
---Inclined Irrad. at solar mod. from Mk 1-G, kW/m2---

06:  P89         If X<=>F
  01: 6          X Loc INCL. IRR
  02: 4          <
  03: 0          F
  04: 30         Then Do

07:  P30         Z=F
  01: 0          F
  02: 6          Z Loc [:INCL. IRR]

08:  P95         End

09:  P4          Excite,Delay,Volt(SE)
  01: 1          Rep
  02: 5          5000 mV slow Range
  03: 4          IN Chan
  04: 2          Excite all reps w/EXchan 2
  05: 1          Delay (units .01sec)
  06: 3600       mV Excitation
  07: 7          Loc [:WIND DIR.] W200P
  08: 0.1        Mult
  09: 0.0000     Offset
--- Wind Direction from W200P ---

10:  P3          Pulse
  01: 1          Rep
  02: 1          Pulse Input Chan
  03: 22         Switch closure; Output Hz.
  04: 8          Loc [:WIND SPD.] A100R
  05: 1.25       Mult
  06: 0.25       Offset
--- Wind Speed from A100R m/s ---

11:  P3          Pulse
  01: 1          Rep
  02: 2          Pulse Input Chan
  03: 2          Switch closure
  04: 9          Loc [:RAINFALL ] ARG100
  05: 0.198      Mult
  06: 0.0000     Offset
--- Rainfall from ARG100 mm ---
```

```
12:  P2         Volt (DIFF)
  01: 1         Rep
  02: 5         5000 mV slow Range
  03: 6         IN Chan
  04: 10        Loc [:BATT. IN ] INPUT CURRENT TO BATT.
  05: 0.0196    Mult
  06: 0.0000    Offset
-- Current Input to Batt.  Current Integrat. Ch.1 ---

13:  P89        If X<=>F
  01: 10        X Loc BATT. IN
  02: 4         <
  03: 0         F
  04: 30        Then Do

14:  P30        Z=F
  01: 0         F
  02: 10        Z Loc [:BATT. IN ] INPUT CURRENT TO BATTERY

15:  P95        End

16:  P2         Volt (DIFF)
  01: 1         Rep
  02: 5         5000 mV slow Range
  03: 7         IN Chan
  04: 11        Loc [:BATT. OUT] OUTPUT CURRENT FROM BATT.
  05: 0.0096    Mult
  06: 0.0000    Offset
-- Current Output from Batt.  Current Integrat. Ch.2 --

17:  P2         Volt (DIFF)
  01: 1         Rep
  02: 5         5000 mV slow Range
  03: 8         IN Chan
  04: 12        Loc [:POWER OUT] ARRAY OUTPUT ENERGY
  05: 0.2004    Mult
  06: 0.0000    Offset
--- Array Output Energy from Power Integrator ---

18:  P89        If X<=>F
  01: 12        X Loc POWER OUT
  02: 4         <
  03: 0         F
  04: 30        Then Do

19:  P30        Z=F
  01: 0         F
  02: 12        Z Loc [:POWER OUT]

20:  P95        End
-------------------------------------------------------
--- This block writes values to final storage area ---
-------------------------------------------------------
--- 15 minute averaging interval ---
```

```
21:  P92        If time is
  01: 0         minutes into a
  02: 15        minute interval
  03: 10        Set high Flag 0 (output)
--- set output flag high ---

22:  P80        Set Active Storage Area
  01: 1         Final Storage Area
  02: 100       Array ID or location
--- set output array ID ---

23:  P77        Real Time
  01: 110       Day,Hour-Minute
--- note day and time ---

24:  P71        Average
  01: 6         Reps
  02: 1         Loc R.H. %
--- Mean R.H.%, Air, Top & Bottom Mod. Temps. ---
--- Horiz. & Inclined Irradiation ---

25:  P69        Wind Vector
  01: 1         Rep
  02: 0         Samples per sub-interval
  03: 0         Polar Sensor/(S, D1, SD1)
  04: 8         Wind Speed/East Loc WIND SPD.
  05: 7         Wind Direction/North Loc WIND DIR.
--- Wind Vector from A100R & W200P ---

26:  P72        Totalize
  01: 1         Rep
  02: 9         Loc RAINFALL
--- Total Rainfall ---

27:  P71        Average
  01: 3         Reps
  02: 10        Loc BATT. IN
--- Mean Current Input to & Output from Battery ---
--- and Mean Array Output Power ---

--- Hourly averaging interval ---

28:  P92        If time is
  01: 0         minutes into a
  02: 60        minute interval
  03: 10        Set high Flag 0 (output)
--- set output flag high ---

29:  P80        Set Active Storage Area
  01: 1         Final Storage Area
  02: 200       Array ID or location
--- set output array ID ---

30:  P77        Real Time
  01: 110       Day,Hour-Minute
--- Note Day and Time ---
```

```
31:  P71        Average
  01: 6         Reps
  02: 1         Loc R.H. %
--- Mean R.H.%, Air, Top & Bottom Mod. Temp. ---
--- Horiz. & Incld. Irr. ---

32:  P69        Wind Vector
  01: 1         Rep
  02: 0         Samples per sub-interval
  03: 0         Polar Sensor/(S, D1, SD1)
  04: 8         Wind Speed/East Loc WIND SPD.
  05: 7         Wind Direction/North Loc WIND DIR.
    Wind Vector from A100R & W200

33:  P72        Totalize
  01: 1         Rep
  02: 9         Loc RAINFALL
--- Total Rainfall ---

34:  P71        Average
  01: 3         Reps
  02: 10        Loc BATT. IN
--- Mean Current Input to & Output from Battery ---
--- and Mean Array Power Output ---

--- Daily averaging interval ---

35:  P92        If time is
  01: 0         minutes into a
  02: 1440      minute interval
  03: 10        Set high Flag 0 (output)
--- set output flag high ---

36:  P80        Set Active Storage Area
  01: 1         Final Storage Area
  02: 300       Array ID or location
--- set output array ID ---

37:  P77        Real Time
  01: 100       Julian Day
--- note day ---

38:  P71        Average
  01: 6         Reps
  02: 1         Loc R.H. %
--- Mean R.H.%, Air, Top & Bottom Mod. Temp. ---
--- Horiz. and Incld. Irradiation ---

39:  P69        Wind Vector
  01: 1         Rep
  02: 0         Samples per sub-interval
  03: 0         Polar Sensor/(S, D1, SD1)
  04: 8         Wind Speed/East Loc WIND SPD.
  05: 7         Wind Direction/North Loc WIND DIR.
--- Wind Vector from A100R & W200P ---
```

```
40:  P72        Totalize
  01: 1         Rep
  02: 9         Loc RAINFALL
--- Total Rainfall ---

41:  P71        Average
  01: 3         Reps
  02: 10        Loc BATT. IN
--- Mean Current Input to & Output from Batt. ---
--- and Mean Array Power Output for the Day ---

42:  P74        Minimize
  01: 1         Rep
  02: 0         Value only
  03: 2         Loc AIR TEMP.
--- Minimum Air Temp. ---

43:  P73        Maximize
  01: 1         Rep
  02: 0         Value only
  03: 2         Loc AIR TEMP.
--- Maximum Air Temp. ---

44:  P70        Sample
  01: 1         Rep
  02: 13        Loc BAT. VOLT
--- Note Battery Voltage ---

45:  P          End Table 2


*     3         Table 3 Subroutines

01:  P          End Table 3


*     4         Mode 4 Output Options
  01: 00        Tape/Printer Option
  02: 00        Printer Baud Option


*     A         Mode 10 Memory Allocation
  01: 28        Input Locations
  02: 74        Intermediate Locations


*     C         Mode 12 Security (OSX-0)
  01: 00        Security Option
  02: 0000      Security Code
```

Input Location Assignments (with comments):

Key:
T=Table Number
E=Entry Number
L=Location Number

```
T:   E:   L:
1:   1:   1:   Loc [:R.H. %    ] MP100
1:   2:   2:   Loc [:AIR TEMP.] MP100
1:   3:   3:   Loc [:TOP TEMP ] SA1-T
1:   4:   4:   Loc [:BOT. TEMP] SA1-T
2:   1:   5:   Loc [:HORZ. IRR] LI200SZ
2:   3:   5:   Z Loc [:HORZ. IRR]
2:   5:   6:   Loc [:INCL. IRR] Mk 1-G
2:   7:   6:   Z Loc [:INCL. IRR]
2:   9:   7:   Loc [:WIND DIR.] W200P
2:  10:   8:   Loc [:WIND SPD.] A100R
2:  11:   9:   Loc [:RAINFALL ] ARG100
2:  12:  10:   Loc [:BATT. IN ] INPUT CURRENT TO BATT.
2:  14:  10:   Z Loc [:BATT. IN ] INPUT CURRENT TO BATTERY
2:  16:  11:   Loc [:BATT. OUT] OUTPUT CURRENT FROM BATT.
2:  17:  12:   Loc [:POWER OUT] ARRAY OUTPUT ENERGY
2:  19:  12:   Z Loc [:POWER OUT]
1:   5:  13:   Loc [:BAT. VOLT] BATTERY VOLTAGE
```

Input Location Labels:

```
1:R.H. %          5:HORZ. IRR      9:RAINFALL      13:BAT. VOLT
2:AIR TEMP.       6:INCL. IRR     10:BATT. IN      14:
3:TOP TEMP        7:WIND DIR.     11:BATT. OUT     15:
4:BOT. TEMP       8:WIND SPD.     12:POWER OUT     16:
```

TABLE C.2: Chart of hours of significant inplane irradiance (>80 W/m²) and PV array output (>5% of nominal array power).

NOMINAL POWER: 1.2 kWp TOTAL ARRAY AREA: 11.117 m^2

JULY 1993

DAY	IRRADIANCE		ARRAY OUTPUT	
	BEFORE NOON	AFTER NOON	BEFORE NOON	AFTER NOON
1	**********		**********	
2	**********		**********	
3	**********		**********	
4	**********		**********	
5	**********		**********	
6	**********		**********	
7	**********		**********	
8	**********		**********	
9	**********		**********	
10	**********		**********	
11	**********		**********	
12	**********		**********	
13	**********		**********	
14	**********		**********	
15	**********		**********	
	....	....	....	....

DAY	IRRADIANCE		ARRAY OUTPUT	
	BEFORE NOON	AFTER NOON	BEFORE NOON	AFTER NOON
16	**********		**********	
17	**********		**********	
18	**********		**********	
19	**********		**********	
20	**********		**********	
21	**********		**********	
22	**********		**********	
23	**********		****** *****	
24	**********		**********	
25	**********		**********	
26	**********		**********	
27	**********		**********	
28	**********		**********	
29	**********		**********	
30	**********		**********	
31	**********		**********	
	.....|	.....	.....|	.....

AUGUST 1993

DAY	IRRADIANCE		ARRAY OUTPUT	
	BEFORE NOON	AFTER NOON	BEFORE NOON	AFTER NOON
1	**********		**********	
2	**********		**********	
3	**********		**********	

DAY	IRRADIANCE		ARRAY OUTPUT	
	BEFORE NOON	AFTER NOON	BEFORE NOON	AFTER NOON
4	**********		**********	
5	**********		**********	
6	**********		**********	
7	**********		**********	
8	**********		**********	
9	**********		**********	
10	**********		**********	
11	**********		**********	
12	**********		**********	
13	**********		**********	
14	**********		**********	
15	**********		******* ****	
16	**********		**********	
17	**********		******* **	
18	**********		******* ***	
19	**********		**********	
20	**********		**********	
21	**********		******* ***	
22	**********		**********	
23	**********		**********	
24	**********		****** ***	
25	**********		**********	
26	**********		**********	
27	**********		**********	
28	**********		**********	

DAY	IRRADIANCE		ARRAY OUTPUT	
	BEFORE NOON	AFTER NOON	BEFORE NOON	AFTER NOON
29	**********		*********	
30	**********		*********	
31	**********		****** ***	
	.....	.....	.....	.....

SEPTEMBER 1993

DAY	IRRADIANCE		ARRAY OUTPUT	
	BEFORE NOON	AFTER NOON	BEFORE NOON	AFTER NOON
1	**********		****** ***	
2	*********		******* **	
3	*********		*********	
4	**********		******* ***	
5	*********		****** ***	
6	**********		******* ***	
7	*********		*********	
8	*********		*********	
9	*********		******* **	
10	*********		******* **	
11	*********		******* **	
12	*********		******* **	
13	**********		******* ***	
14	*********		****** ***	
15	*********		*********	
16	*********		******* ***	

DAY	IRRADIANCE		ARRAY OUTPUT	
	BEFORE NOON	AFTER NOON	BEFORE NOON	AFTER NOON
17	**********		****** ***	
18	**********		**********	
19	**********		**********	
20	**********		**********	
21	**********		**********	
22	**********		*** ******	
23	**********		**********	
24	**********		**********	
25	**********		**********	
26	**********		**********	
27	**********		**********	
28	*********		*********	
29	******		******	
30	**********		**********	
	.....	.....	.....	.....

OCTOBER 1993

DAY	IRRADIANCE		ARRAY OUTPUT	
	BEFORE NOON	AFTER NOON	BEFORE NOON	AFTER NOON
1	**********		**********	
2	**********		**********	
3	**********		**********	
4	**********		**********	
5	**********		**********	

DAY	IRRADIANCE		ARRAY OUTPUT	
	BEFORE NOON	AFTER NOON	BEFORE NOON	AFTER NOON
6	**********		**********	
7	**********		*********	
8	**********		**********	
9	*********		*********	
10	**********		**********	
11	**********		**********	
12	**********		*********	
13	**********		**********	
14	**********		**********	
15	**********		**********	
16	**********		*********	
17	**********		**********	
18	**********		**********	
19	**********		*********	
20	*********		*********	
21	*** **		*** **	
22	*******		*******	
23	*********		*********	
24	*********		*********	
25	******* *		******* *	
26	*********		*********	
27	***** **		**** **	
28	********		********	
29	*********		*********	
30	*********		*********	
31	* *****		* *****	

NOVEMBER 1993

DAY	IRRADIANCE		ARRAY OUTPUT	
	BEFORE NOON	AFTER NOON	BEFORE NOON	AFTER NOON
1	*******		*******	
2	********		********	
3	*********		*********	
4	*******		*******	
5	******		******	
6	********		********	
7	********		********	
8	*********		*********	
9	*********		*********	
10	*********		*********	
11	*********		*********	
12	*********		*********	
13	*********		********	
14	*********		*********	
15	*********		*********	
16	*****		*****	
17	*********		*********	
18	******		******	
19				
20	********		********	
21	******		******	
22	*********		*********	

DAY	IRRADIANCE		ARRAY OUTPUT	
	BEFORE NOON	AFTER NOON	BEFORE NOON	AFTER NOON
23	*********		*********	
24	****		****	
25	**********		**********	
26	*********		*********	
27	*********		*********	
28	*******		*******	
29	********		********	
30	********		********	
	. . . . .	. . . . .	. . . . .	. . . . .

DECEMBER 1993

DAY	IRRADIANCE		ARRAY OUTPUT	
	BEFORE NOON	AFTER NOON	BEFORE NOON	AFTER NOON
1	********		********	
2	*******		*******	
3	********		********	
4				
5	****		****	
6	*********		*********	
7	** ******		** ******	
8	********		********	
9	********		********	
10	*********		********	
11	*********		********	

DAY	IRRADIANCE		ARRAY OUTPUT	
	BEFORE NOON	AFTER NOON	BEFORE NOON	AFTER NOON
12	********		********	
13	**********		********	
14	********		********	
15	******		******	
16	********		********	
17	********		********	
18	********		********	
19	********		********	
20	********		********	
21	********		*******	
22	********		********	
23	********		********	
24	*******		*******	
25	********		********	
26	*******		*******	
27	********		********	
28	******		******	
29	*********		*********	
30	** *******		*******	
31	*********		*********	
	.....	.....	.....	.....

JANUARY 1994

DAY	IRRADIANCE		ARRAY OUTPUT	
	BEFORE NOON	AFTER NOON	BEFORE NOON	AFTER NOON
1	********		********	
2	**********		**********	
3	********		********	
4	**********		**********	
5	*******		********	
6	**********		**********	
7	**********		*** *****	
8	* **		****	
9	********		********	
10	**********		**********	
11	****		****	
12	** *****		** *****	
13	**********		**********	
14	**********		**********	
15	**********		**********	
16	********		********	
17	*******		*******	
18	********		********	
19	********		********	
20	********		********	
21	** *****		** *****	
22	********		********	
	. . . . .	. . . . .	. . . . .	. . . . .

DAY	IRRADIANCE		ARRAY OUTPUT	
	BEFORE NOON	AFTER NOON	BEFORE NOON	AFTER NOON
23	*** *		*** *	
24	********		********	
25	********		********	
26	**********		*********	
27	*********		********	
28	*********		********	
29	* *******		* *******	
30	**********		*********	
31	**********		**********	
	. . . . .	. . . . .	. . . . .	. . . . .

FEBRUARY 1994

DAY	IRRADIANCE		ARRAY OUTPUT	
	BEFORE NOON	AFTER NOON	BEFORE NOON	AFTER NOON
1	*********		********	
2	*********		*********	
3	**********		**********	
4	**********		*********	
5	*******		*******	
6	*******		*******	
7	********		********	
8	**********		*********	
9	** *****		* *****	
	. . . . .	. . . . .	. . . . .	. . . . .

DAY	IRRADIANCE		ARRAY OUTPUT	
	BEFORE NOON	AFTER NOON	BEFORE NOON	AFTER NOON
10	*********		*********	
11	*********		*********	
12	*******		******	
13	*********		********	
14	**********		**********	
15	**********		**********	
16	**********		*********	
17	********		********	
18	********		********	
19	**********		**********	
20	**********		**********	
21	*********		*********	
22	**********		**********	
23	**********		**********	
24	**********		**********	
25	**********		**********	
26	**********		**********	
27	**********		**********	
28	**********		**********	
	.....	.....	.....	.....

MARCH 1994

DAY	IRRADIANCE		ARRAY OUTPUT	
	BEFORE NOON	AFTER NOON	BEFORE NOON	AFTER NOON
1	*********		*********	

DAY	IRRADIANCE		ARRAY OUTPUT	
	BEFORE NOON	AFTER NOON	BEFORE NOON	AFTER NOON
2	**********		**********	
3	**********		**********	
4	**********		**********	
5	**********		**********	
6	**********		**********	
7	**********		**********	
8	**********		**********	
9	**********		**********	
10	**********		**********	
11	**********		**********	
12	**********		**********	
13	**********		**********	
14	**********		**********	
15	**********		**********	
16	*********		*********	
17			*	
18	**********		**********	
19	**********		**********	
20	**********		**********	
21	**********		**********	
22	**********		**********	
23	**********		**********	
24	**********		**********	
25	**********		**********	
26	**********		**********	

DAY	IRRADIANCE		ARRAY OUTPUT	
	BEFORE NOON	AFTER NOON	BEFORE NOON	AFTER NOON
27	* * * * * * * * * *		* * * * * * * *	
28	* * * * * * * * *		* * * * * * * * *	
29	* * * * * * * * * *		* * * * * * * * * *	
30	* * * * * * * * * *		* * * * * * * * * *	
31	* * * * * * * * * *		* * * * * * * * * *	
	. . . . .	. . . . .	. . . . .	. . . . .

APRIL 1994

DAY	IRRADIANCE		ARRAY OUTPUT	
	BEFORE NOON	AFTER NOON	BEFORE NOON	AFTER NOON
1	* * * * * * * * * *		* * * * * * * * * *	
2	* * * * * * * * * * *		* * * * * * * * * *	
3	* * * * * * * * *		* * * * * * * * *	
4	* * * * *		* * * * *	
5	* * * * * *		* * * * * *	
6	* * * * * * * * * *		* * * * * * * * * *	
7	* * * * * * * * * *		* * * * * * * * * *	
8	* * * * * * * * * *		* * * * * * * * * *	
9	* * * * * * * * * *		* * * * * * * * * *	
10	* * * * * * * * * * *		* * * * * * * * * * *	
11	* * * * * * * * * *		* * * * * * * * * *	
12	* * * * * * * * * *		* * * * * * * * * *	
13	* * * * * * * * * * *		* * * * * * * * * *	
14	* * * * * * * * * * *		* * * * * * * * * * *	
	. . . . .	. . . . .	. . . . .	. . . . .

DAY	IRRADIANCE		ARRAY OUTPUT	
	BEFORE NOON	AFTER NOON	BEFORE NOON	AFTER NOON
15	* ***** *		* ***** *	
16	**********		**********	
17	**********		**********	
18	**********		**********	
19	**********		**********	
20	**********		**********	
21	**********		**********	
22	**********		**********	
23	**********		**********	
24	**********		**********	
25	**********		**********	
26	********		*******	
27	**********		**********	
28	**********		**********	
29	**********		**********	
30	**********		*** *******	
	. . . . .	. . . . .	. . . . .	. . . . .

MAY 1994

DAY	IRRADIANCE		ARRAY OUTPUT	
	BEFORE NOON	AFTER NOON	BEFORE NOON	AFTER NOON
1	**********		**********	
2	**********		**********	
3	**********		**********	

DAY	IRRADIANCE		ARRAY OUTPUT	
	BEFORE NOON	AFTER NOON	BEFORE NOON	AFTER NOON
4	**********		**********	
5	**********		**********	
6	**********		**********	
7	**********		**********	
8	**********		**********	
9	**********		**********	
10	**********		**********	
11	**********		**********	
12	**********		**********	
13	**********		**********	
14	**********		**********	
15	**********		**********	
16	**********		**********	
17	**********		**********	
18	**********		**********	
19	**********		**********	
20	**********		**********	
21	**********		**********	
22	**********		**********	
23	**********		**********	
24	**********		**********	
25	**********		**********	
26	**********		**********	
27	**********		**********	
28	**********		**********	

DAY	IRRADIANCE		ARRAY OUTPUT	
	BEFORE NOON	AFTER NOON	BEFORE NOON	AFTER NOON
30	**********		**********	
29	**********		**********	
31	**********		**********	

JUNE 1994

DAY	IRRADIANCE		ARRAY OUTPUT	
	BEFORE NOON	AFTER NOON	BEFORE NOON	AFTER NOON
1	**********		**********	
2	**********		**********	
3	**********		**********	
4	**********		**********	
5	**********		**********	
6	**********		**********	
7	**********		**********	
8	**********		**********	
9	**********		**********	
10	**********		**********	
11	**********		**********	
12	**********		**********	
13	**********		**********	
14	**********		**********	
15	**********		**********	
16	**********		**********	
17	**********		**********	

DAY	IRRADIANCE		ARRAY OUTPUT	
	BEFORE NOON	AFTER NOON	BEFORE NOON	AFTER NOON
19	**********		**********	
18	**********		**********	
20	**********		**********	
21	**********		**********	
22	**********		**********	
23	**********		**********	
24	**********		**********	
25	**********		**********	
26	**********		**********	
27	**********		**********	
28	**********		**********	
29	**********		**********	
30	**********		**********	
	.....|	.....	.....|	.....

JULY 1994

DAY	IRRADIANCE		ARRAY OUTPUT	
	BEFORE NOON	AFTER NOON	BEFORE NOON	AFTER NOON
1	**********		**********	
2	**********		**********	
3	**********		**********	
4	**********		**********	
5	**********		**********	
6	**********		**********	

DAY	IRRADIANCE		ARRAY OUTPUT	
	BEFORE NOON	AFTER NOON	BEFORE NOON	AFTER NOON
7	**********		**********	
8	**********		**********	
9	**********		**********	
10	**********		**********	
11	**********		**********	
12	**********		**********	
13	**********		****	
14	**********		**********	
15	**********		**********	
16	**********		**********	
17	**********		**********	
18	**********		**********	
19	**********		**********	
20	**********		**********	
21	**********		**********	
22	**********		**********	
23	**********		**********	
24	**********		**********	
25	**********		**********	
26	**********		**********	
27	**********		**********	
28	**********		**********	
29	**********		**********	
30	**********		**********	
31	**********		**********	

AUGUST 1994

DAY	IRRADIANCE		ARRAY OUTPUT	
	BEFORE NOON	AFTER NOON	BEFORE NOON	AFTER NOON
1	**********		**********	
2	**********		**********	
3	**********		******** **	
4	**********		**********	
5	**********		**********	
6	**********		**********	
7	**********		**********	
8	**********		**********	
9	**********		**********	
10	**********		**********	
11	**********		**********	
12	**********		**********	
13	**********		**********	
14	**********		**********	
15	**********		**********	
16	**********		**********	
17	**********		**********	
18	**********		**********	
19	**********		**********	
20	**********		**********	
21	**********		**********	
22	**********		**********	
23	**********		**********	

DAY	IRRADIANCE		ARRAY OUTPUT	
	BEFORE NOON	AFTER NOON	BEFORE NOON	AFTER NOON
24	**********		**********	
25	**********		**********	
26	**********		**********	
27	**********		**********	
28	**********		**********	
29	**********		**********	
30	**********		**********	
31	**********		**********	

SEPTEMBER 1994

DAY	IRRADIANCE		ARRAY OUTPUT	
	BEFORE NOON	AFTER NOON	BEFORE NOON	AFTER NOON
1	**********		**********	
2	**********		**********	
3	**********		**********	
4	**********		**********	
5	**********		**********	
6	**********		**********	
7	**********		**********	
8	**********		**********	
9	**********		**********	
10	**********		**********	
11	**********		**********	

DAY	IRRADIANCE		ARRAY OUTPUT	
	BEFORE NOON	AFTER NOON	BEFORE NOON	AFTER NOON
12	**********		**********	
13	**********		**********	
14	**********		**********	
15	**********		**********	
16	**********		**********	
17	**********		**********	
18	********		********	
19	********		********	
20	**********		**********	
21	**********		**********	
22	**********		**********	
23	**********		**********	
24	**********		**********	
25	**********		**********	
26	**********		**********	
27	**********		**********	
28	**********		**********	
29	**********		**********	
30	**********		**********	

OCTOBER 1994

DAY	IRRADIANCE		ARRAY OUTPUT	
	BEFORE NOON	AFTER NOON	BEFORE NOON	AFTER NOON
1	**********		**********	

DAY	IRRADIANCE		ARRAY OUTPUT	
	BEFORE NOON	AFTER NOON	BEFORE NOON	AFTER NOON
2	**********		**********	
3	**********		**********	
4	********		********	
5	***	***	***	***
6	**********		**********	
7	*****	*	*****	*
8	**********		**********	
9	**********		**********	
10	*********		*********	
11	*********		*********	
12	**********		**********	
13	*********		*********	
14	**********		**********	
15	**********		**********	
16	******	**	******	**
17	**********		*********	
18	*	****	*	****
19	**********		**********	
20	*********		*********	
21	*********		*********	
22	********		********	
23	**********		**********	
24	**********		**********	
25	**********		**********	
26	**********		*********	

DAY	IRRADIANCE		ARRAY OUTPUT	
	BEFORE NOON	AFTER NOON	BEFORE NOON	AFTER NOON
27	**********		*********	
28	**********		*********	
29	**********		**********	
30	*********		*********	
31	*********		*********	
	. . . . .	. . . . .	. . . . .	. . . . .

APPENDIX D

TABLE D-1: Solar irradiance for different air mass values and constant turbidity factors of α = 1.30 and β = 0.02. (U.S. standard atmosphere of H_2O = 20 mm and O_3 = 3.4 mm) [5]

AIR MASS	TOTAL RAD. W/m²	PERCENTAGE OF THE TOTAL ENERGY IN THE		
		UV, $\lambda < 0.4$ μm	VI., 0.4 μm $< \lambda <$ 0.72 μm	IR, $\lambda > 0.72$μm
0	1353.0	8.7	40.1	51.1
1	956.2	4.8	46.9	48.3
4	595.2	1.23	44.2	54.4
7	413.6	0.35	39.4	60.3
10	302.5	0.102	34.7	65.2

α is the wavelength exponent and β is the Angström coefficient in the turbidity equation developed by A. Angström [5]. For a clear weather α = 1.30 and β = 0.02.

TABLE D 2: Transmission of solar radiation through different types of clouds [1].

Cloud Type	Cirrus	Cirrostratus	Cirrus & Cirrostratus	Altocumulus
Sun's Elevation	Transmission (%)			
5-15	62	46	----	10
15-25	68	53	58	13
25-35	76	61	63	15
35-45	80	63	65	25
45-55	84	73	72	----

TABLE D-3: Declination of the Sun and the Equation of Time for some days during the year [59]. Interpolation can be used for other days.

MONTH	JANUARY		FEBRUARY		MARCH		APRIL	
	γ	c_3	γ	c_3	γ	c_3	γ	c_3
	deg.	min.	deg.	min.	deg.	min.	deg.	min.
DAY								
1	-23.0	-3.6	-17.0	-13.7	-7.4	-12.5	+4.7	-4.0
6	-22.4	-5.9	-15.5	-14.2	-5.5	-11.4	+6.6	-2.5
11	21.7	8.0	13.9	14.4	3.5	10.2	+8.5	-1.1
16	-20.8	-9.8	-12.2	-14.2	-1.6	-8.8	+10.3	+0.1
21	-19.6	-11.4	-10.4	-13.8	+0.4	-7.4	+12.0	+1.2
26	-18.6	-12.6	-8.6	-13.1	+2.4	-5.8	+13.6	+2.2

MONTH	MAY		JUNE		JULY		AUGUST	
	γ	c_3	γ	c_3	γ	c_3	γ	c_3
	deg.	min.	deg	min	deg	min	deg	min
DAY								
1	+15.2	+2.9	+22.1	+2.4	+23.1	-3.6	+17.9	-6.2
6	+16.6	+3.5	+22.7	+1.6	+22.7	-4.5	+16.6	-5.8
11	+17.9	+3.7	+23.1	+0.6	+22.1	-5.3	+15.2	-5.1
16	+19.2	+3.8	+23.3	-0.4	+21.3	-5.9	+13.6	-4.4
21	+20.3	+3.6	+23.4	-1.5	+20.6	-6.2	+12.0	-3.1
26	+21.2	+3.2	+23.3	-2.6	+19.3	-6.4	+10.3	-1.8

MONTH	SEPTEMBER		OCTOBER		NOVEMBER		DECEMBER	
	γ	c_3	γ	c_3	γ	c_3	γ	c_3
	deg.	min.	deg.	min.	deg.	min.	deg.	min.
DAY								
1	+8.2	+0.0	-3.3	+10.2	-14.6	+16.3	-21.9	+11.6
6	+6.7	+1.6	-5.3	+11.8	-16.1	+16.3	-22.5	+9.0
11	+4.4	+3.3	-7.2	+13.1	-17.5	+15.9	-23.0	+6.8
16	+2.5	+5.0	-8.7	+14.3	-18.8	+15.2	-23.3	+4.4
21	+0.5	+6.8	-10.8	+15.3	-20.0	+14.1	-23.4	+2.0
26	-1.4	+8.6	-12.6	+15.9	-21.0	+12.7	-23.4	-0.5

γ = solar elevation

c_3 = equation of time

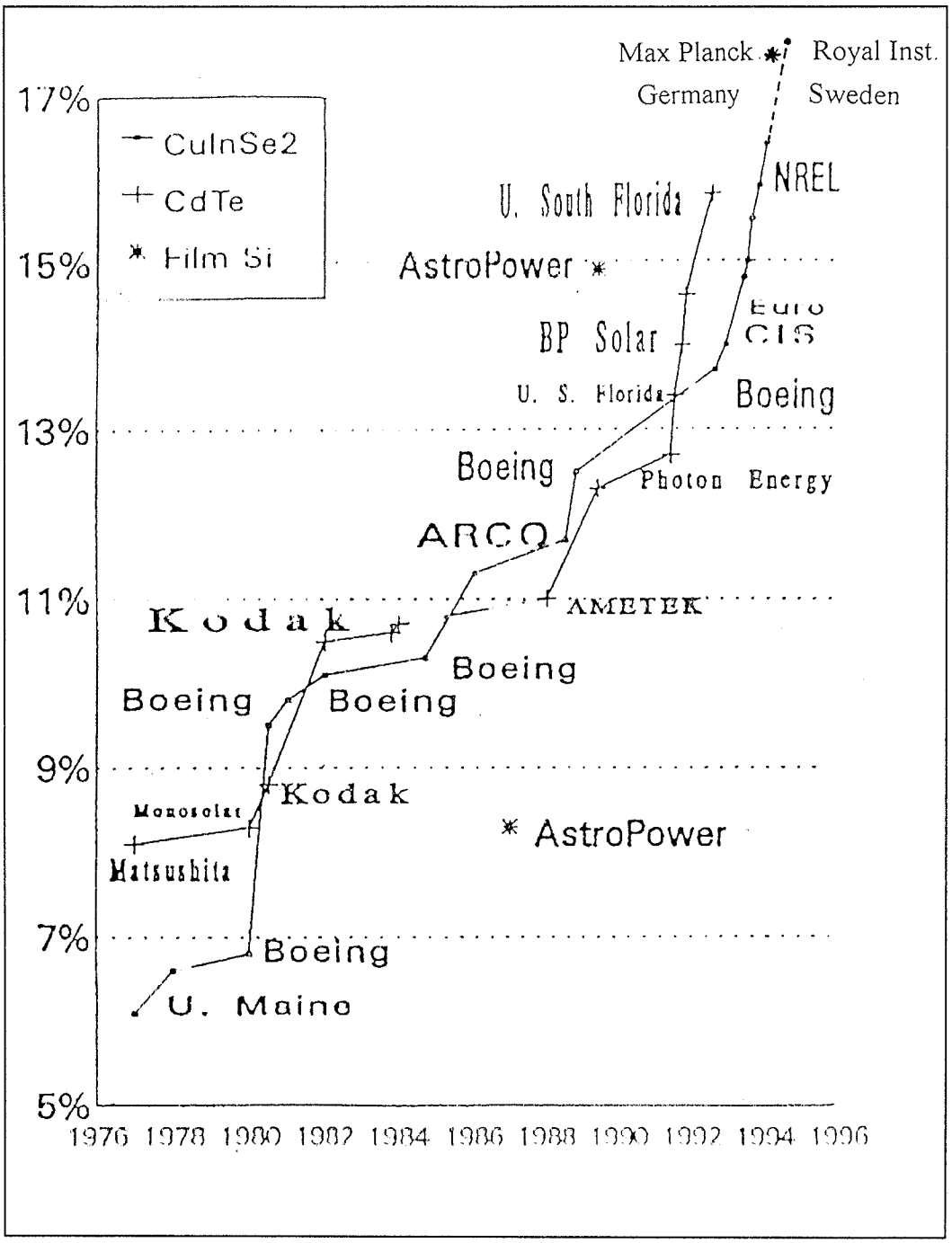

FIGURE D 1: Evolution in efficiency of copper-indium diselenide, cadmium-telluride and thin-film silicon PV cells [56].

TABLE D.4: Mean monthly and mean maximum air temperatures in Malta for the period from 1st September 1947 to 31st December 1990. (Data kindly supplied by the Meteo rological Office of Malta, on 7th January 1993).

MONTH	MEAN MONTHLY	MEAN MAXIMUM
JANUARY	12.2	15.2
FEBRUARY	12.4	15.5
MARCH	13.4	16.7
APRIL	15.5	19.1
MAY	19.1	23.3
JUNE	23.0	27.5
JULY	25.9	30.7
AUGUST	26.3	30.7
SEPTEMBER	24.1	28.0
OCTOBER	20.7	24.2
NOVEMBER	17.0	20.1
DECEMBER	13.8	16.7

TABLE D.5: Specifications of the Solarex MSX60 polycrystalline modules.

V_{OC}	20.8-21.0 V	NOCT	49 °C
I_{SC}	3.66-3.90 A	Voltage at peak power	17.1 V
P_{NOCT}	53.7-55.2 W	Current at peak power	3.5 A
I_{NOCT}	3.50-3.68 A		
V_{NOCT}	15.0-15.5 V	Temp. effect on voltage	-73 mV/°C
P_{NOM}	59.0-60.8 W	Temp. effect on current	+3 mA/°C
P_{MIN}	59.0 W	Temp. effect on power	-0.38%/°C

STC = standard testing conditions, defined as a solar irradiance of 1000 W/m^2, an air mass ratio of 1.5 and a PV cell temperature of 25 °C.

NOCT – nominal operating cell temperature, defined as the temperature that the PV cell will attain at an irradiance of 800 W/m^2, an ambient temperature of 20 °C and a wind speed of 1 m/s

TABLE D.6: Detailed characteristics of each of the 20 PV modules, as supplied by the manufacturer.

Type of Modules: SOLAREX (U S A), MSX60, Poly-crystalline Silicon Cells;

Model no.: MMVBAB000;

Maximum Operating Voltage: 600 V; Minimum Output Power at STC: 58 W

1	2	3	4	5	6	7	8	9	10
20	19	18	17	16	15	14	13	12	11

The PV array comprising of 20 modules being conventionally numbered at the back. The modules are divided into 4 parallel strings, each made up of 5 modules, connected in parallel.

STRING NO. 1

ARRAY NO.	1	2	3	4	5
SERIAL NO.	FW91I23 257543	FW91I23 257664	FW191I2 3257548	FW191I2 3257561	FW191I1 9257005
V_{OC} (V)	21.0	20.8	21.0	20.9	21.0
I_{SC} (A)	3.66	3.81	3.73	3.80	3.87
P_{NOCT} (W)	53.8	53.7	54.3	53.9	55.0
I_{NOCT} (A)	3.50	3.54	3.55	3.59	3.61
V_{NOCT} (V)	15.4	15.2	15.3	15.0	15.2
P_{NOM} (W) at STC	59.0	59.0	59.6	59.4	60.4
I_{SC} at 49 °C	3.72	3.86	3.79	3.86	3.93

STRING NO. 2

PANEL NO.	6	7	8	9	10
SERIAL NO.	FW191I1 9256994	FW191I2 3257671	FW191I1 9256997	FW191I1 9257008	FW191I2 3257591
V_{OC} (V)	21.0	20.9	21.1	21.0	20.9
I_{SC} (A)	3.90	3.74	3.84	3.87	3.82
P_{NOCT} (W)	54.4	54.0	54.9	54.9	54.7
I_{NOCT} (A)	3.63	3.53	3.56	3.61	3.59
V_{NOCT} (V)	15.0	15.3	15.4	15.2	15.3
P_{NOM} (W) at STC	59.9	59.3	60.2	60.3	60.1
I_{SC} (A) AT 49°C	3.96	3.80	3.89	3.92	3.88

STRING NO. 3

PANEL NO.	11	12	13	14	15
SERIAL NO.	FW91I23 257571	FW91I19 257001	FW91I19 257003	FW91I19 257000	FW91I23 257693
V_{OC} (V)	21.0	21.0	21.0	21.0	20.9
I_{SC} (A)	3.74	3.87	3.86	3.86	3.73
P_{NOCT} (W)	53.7	54.9	54.5	54.2	54.0
I_{NOCT} (A)	3.51	3.66	3.62	3.60	3.51
V_{NOCT} (V)	15.3	15.0	15.1	15.0	15.4
P_{NOM} (W) at STC	59.0	60.5	60.1	59.6	59.3
I_{SC} (A) AT 49°C	3.80	3.93	3.92	3.92	3.78

STRING NO: 4

PANEL NO.	16	17	18	19	20
SERIAL NO.	FW91I23 2578588	FW91I23 257550	FW91I23 257669	FW91I19 256958	FW91I23 257687
V_{OC} (V)	21.1	21.1	20.9	21.0	21.0
I_{SC} (A)	3.78	3.88	3.82	3.71	3.75
P_{NOCT} (W)	54.6	55.2	53.9	54.2	54.3
I_{NOCT} (A)	3.51	3.68	3.55	3.54	3.59
V_{NOCT} (V)	15.5	15.0	15.2	15.3	15.1
P_{NOM} (W) at STC	59.9	60.8	59.2	59.5	59.7
I_{SC} (A) AT 49°C	3.83	3.94	3.88	3.77	3.80

TABLE D.7: Manufacturing sequence, encapsulation and testing of Solarex PV modules.

(a) MANUFACTURING PROCEDURE:

- Patented Solarex casting process;
- Internal diameter (ID) or wire sawing;
- Silver thick film paste cell process;
- Patented Solarex Aluminum-Babbitt back spray process;
- Titanium dioxide anti-reflection coating.

(b) ASSEMBLY:

- Cells tabbed with solder plated copper tabs;
- Each tab is soldered in four places on the front using hot iron in automated machine;
- Cells assembled into matrix using robot;
- Each tab soldered to back of cell in two places using hot iron in automated machine.

(c) LAMINATION.

- Low iron tempered glass superstrate;

  One layer of ethylene vinyl acetate (EVA) between glass and cells,
- One layer of EVA between cells and back sheet;
- Three back sheets of blue polyethylene, mylar and white tedlar.

(d) TESTING:

- Flash testing (I-V) curve using pulsed Xenon simulator per IEC-904-1, 2 and 3.
- Use IEC-891 to transform data to other conditions.

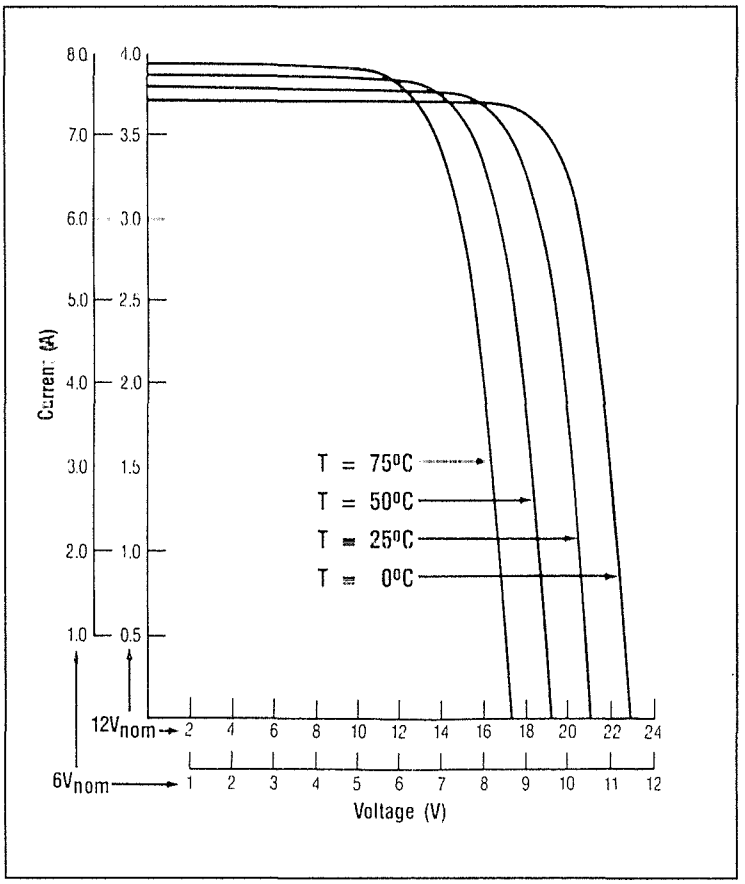

FIGURE D.2: I-V characteristic curves for the Solarex MSX60 modules, as supplied by the manufacturer.

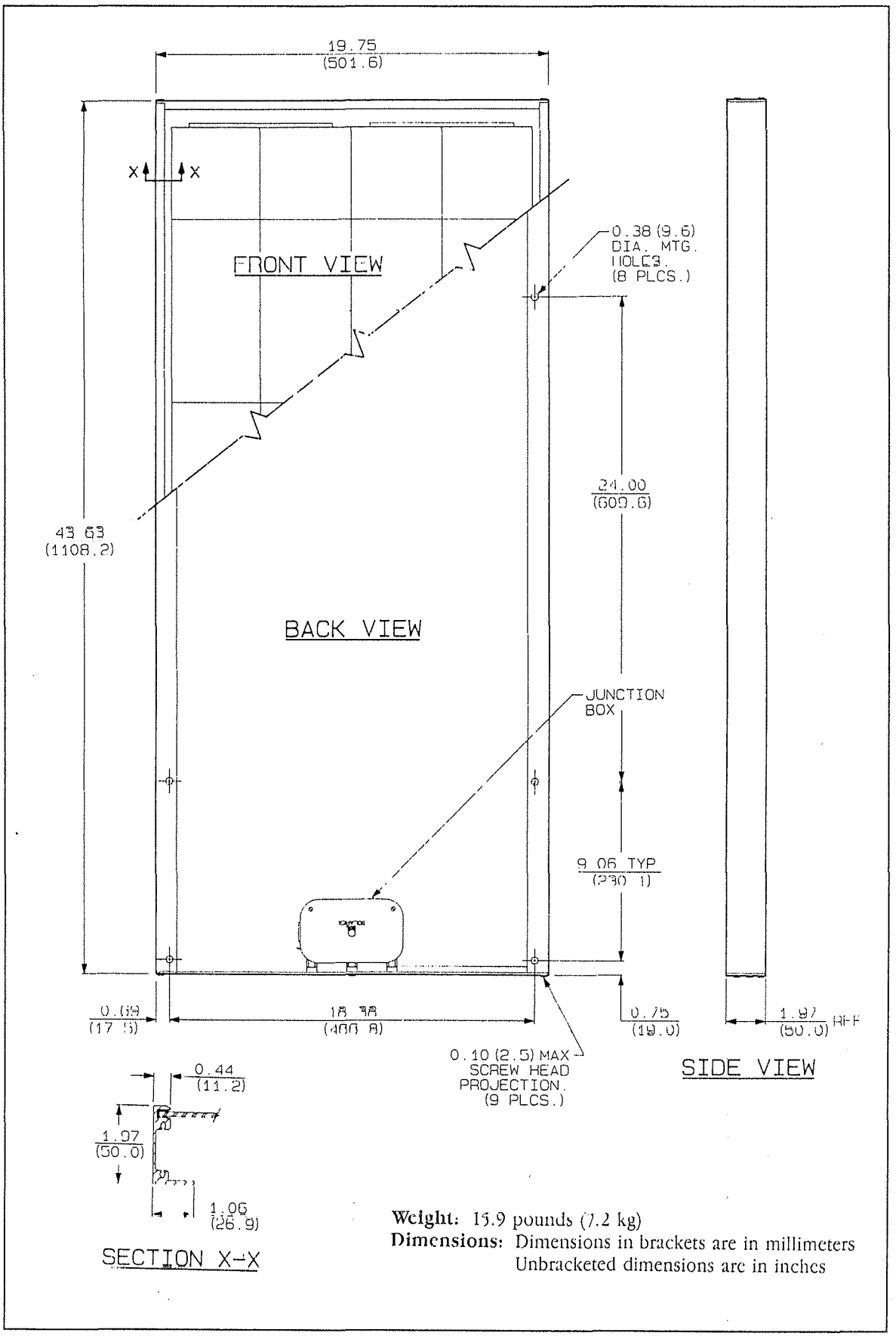

FIGURE D.3: The mechanical characteristics of the Solarex MSX60 PV module.

TABLE D.8: The electrical and mechanical characteristics of the battery control unit.

Type: Photowatt (France) PWR5421AS.

Electrical characteristics: The master circuit is powered from the Batteries of the system and it principally ensures:

- the battery connection to the busbar;
- the control of the solar array and the load connecting relays;
- the connection of other busbars;
- the installation of the voltmetric detection circuit and the alarm circuit.

The voltmetric detection circuit is powered by the battery and gets a voltage which is not disrupted by the input and output currents. It analyses the voltage and according to the following conditions it controls the relays of the input and output power circuits:

- Solar PV array disconnection at 2.4 x U/2 V;
- Reconnection at 2.15 x U/2 V;
- Load cut-off at 1.9 x U/2 V;
- Reconnection at 2.1 x U/2 V, where U is the nominal battery voltage.
- Consumption of voltmetric detection circuit is 5.5 mA.
- Consumption of solar array connection and disconnection circuit is 2.5 W, in action.
- Consumption of the load cut-off circuit is 4 W (for 35 A relay).

ALARM CIRCUIT:

The alarm circuit is independently supplied from the battery so that it is not disrupted by the input and output currents

- High voltage indication at 2.6 x U/2 ± 1% V;
- Low voltage indication at 1.95 x U/2 ± 1% V;
- Consumption: normal 6 mA;
- high alarm 20 mA;
- low alarm 5.5 mA.

LIGHTNING PROTECTION

The lightning protection circuit eliminates any overvoltage caused by lightning on the solar input circuits and discharges this energy to the Earth.

MECHANICAL CHARACTERISTICS

The BCU cover box is made from polyester, with a screw-on lid and stainless steel screws.

- Dimensions: 445 x 389 x 170 mm.

All the electrical connections are screwed down on a busbar itself being fixed on a rail. This presents the advantage of rapidly and easily replacing the faulty part.

TABLE D.9: Technical data of the FINDER light sensitive relay.

- Maximum output current. 10 A,
- Input voltage: 220 V a.c., modified to 12 V d.c.;
- Operating temperature range. 30 °C 170 °C,
- Original calibration: 33 Lux = ON, 8 Lux = OFF;
- Delayed operation: 4 seconds before switching on, 15 seconds before switching off;
- Size: 85 x 56 x 33 mm.

TABLE D.10: Technical characteristics of the SERAI timer

- Supply: 12 - 24 V ± 10% V;
- Consumption: 0.6 W, at 12 V and 1.9 W, at 24 V;
- Operating temperature range: -10 °C - +60 °C;

- Functions: 6 different functions, 8 time scales and multi output features;
- Maximum response time: 100 mseconds;
- Mechanical duration of relay: 10 million switchings;
- Output relays 2, each 5 A;
- Dimensions: 99.5 x 69 x 49.5 mm
- Weight 150 g.

TABLE D.11: Specifications for the 21X micro-logger

Valid for an ambient temperature range of -25°C to +50°C unless otherwise specified.

ANALOGUE INPUTS

NUMBER OF CHANNELS: 8 differential or up to 16 single-ended. One differential channel can be used as two single-ended channels.

VOLTAGE MEASUREMENT TYPES: Single-ended or differential

ACCURACY OF VOLTAGE MEASUREMENTS AND ANALOGUE OUTPUT VOLTAGES:
Differential and positive single-ended: 0.1% of FSR, 0.05% of FSR (0 to 40°C)
Negative single-ended: 0.15% FSR (0.06%, 0 to 40°C)

RANGE AND RESOLUTION. Ranges are software selectable for any channel. Resolution for single ended measurements is twice the value shown.

Full Scale Range	Resolution
±5V	333.0µV
±0.5V	33.3µV
±50mV	3.33µV
±15mV	1µV
±5mV	0.33µV

INPUT NOISE VOLTAGE:
Fast differential: 0.83µV RMS
Slow differential: 0.1µV RMS

COMMON MODE RANGE: ±5V

INPUT RESISTANCE: 200 gigohms

ANALOGUE OUTPUTS

NUMBER OF ANALOGUE OUTPUTS: 4 switched, 2 continuous

DESCRIPTION: A switched output is active only during a measurement and is switched off (high impedance) immediately following the measurement. Only one switched output can be active at any one time. The 2 continuous outputs hold a preset voltage until updated by an analogue output command.

RANGE: ±5V

RESOLUTION: 0.67mV

ACCURACY: Same as voltage input

OUTPUT CURRENT:
Switched: 20mA at ±5V, 50mA at ±2.5V
Continuous: same at +V, 5mA at V

RESISTANCE AND CONDUCTIVITY

ACCURACY: 0.035% (0.02% 0 to 40°C) of full scale bridge output, provided the matching bridge resistors are not the limiting factor.

MEASUREMENT TYPES: 6-wire full bridge, 4 wire full bridge, 4 wire, 3 wire and 2-wire half bridge. High accuracy, low impedance bridge measurements are ratiometric with dual polarity measurements of excitation and output to eliminate thermal EMFs. AC resistance and conductivity measurements use a 750µs excitation pulse with the signal

integration occurring over the last 250µs. An equal duration pulse of opposite polarity is applied for ionic de-polarisation.

PULSE COUNTERS

NUMBER OF PULSE COUNTER CHANNELS: 4 slow or 2 fast, software selectable

MAXIMUM COUNT RATE: 2550Hz, slow counters: 250kHz, fast counters. Pulse counter channels scanned at a maximum rate of 10Hz.

MODES: Switch closure, high frequency pulse and low level AC

DIGITAL CONTROL OUTPUTS

Six digital control outputs, set or reset on command

OUTPUT VOLTAGES (no load):
High: 5±0.1V
Low: <0.1V

OUTPUT RESISTANCE: 400 ohms

TRANSIENT PROTECTION

All input and output connections protected with spark gaps. 12V power input and charger inputs protected with transzorbs.

ELECTRONICS

PROCESSOR: Hitachi 6303 CMOS 8-bit microprocessor

MEMORY: 24K ROM, 40K RAM. 21X stores 19,200 low resolution data points and has a capacity of 978 bytes available for programming.

CLOCK ACCURACY: ±1 minute per month

POWER REQUIREMENTS

VOLTAGE: 9.6 to 15V DC

TYPICAL CURRENT DRAIN: 1.0mA quiescent, 25mA during processing and 60mA during analogue measurement.

INTERNAL BATTERIES: 8 alkaline D cells with 7.5Ah capacity. The 21XL includes sealed lead acid batteries (2.5Ah capacity per charge) intended for trickle charge applications.

EXTERNAL BATTERIES: Any 12V external battery can be connected as a primary power source with the internal batteries providing backup while changing external batteries.

PHYSICAL SPECIFICATIONS

SIZE: 210 x 146 x 85mm. Input terminal strips extend 12mm above the panel surface.

WEIGHT: 2.8kg

GUARANTEE

Three years

TABLE D.12: Technical description of the 'ROTRONIC' temperature and humidity sensor

HUMIDITY MEASUREMENT:

Sensing element:	Rotronic hygromer C-80;
Measuring range:	0-100% relative humidity, linear;
Accuracy at 25 °C:	< ± 1% in reference to calibration;

Precision:	< 0.5%, long term stable;
Hysteresis for a 4 hour cycle	
10-95-10% relative humidity:	< 1%;
Time constant at 25 °C:	10 seconds, for 63% change;
Temperature error:	± 0.5% for a change of 70 °C;
Linear output:	0-1 V d.c. (equal to 0-100%, relative humidity)
Minimum load impedance:	1 kΩ;
Long term stability:	1% over 12 months.

TEMPERATURE MEASUREMENT:

Sensing element:	Platinum resistance thermometer (100 Ω);
Measuring range:	-40 °C to +60 °C;
Accuracy:	> 0.2% from -30 to + 150 °C;
Precision:	0.1 °C, long-term stable;
Time constant (90%) in air:	10 seconds;
Temperature error limits:	± 0.35 °C for a change of 70 °C;
Linear output.	0 1 V d.c.equals -40 °C to + 60 °C,
Calibration points:	0 °, 100 °C;
Minimum load impedance:	1 kΩ.

GENERAL DATA:

Power supply:	On power-up: 5 V at approximately 150 mA for the first 15 ms;
	5 V at 7 mA, for continuous operation;
Operating temperature:	- 40 °C to +60 °C;
Dimensions:	195 mm x 25 mm diameter;
Weight:	150 g.

TABLE D.13. Specifications of the LICOR LI200SZ silicon cell pyranometer

Light sensitivity:	400-1100 nm;
Typical output:	90 W/m² per mV;
Absolute accuracy:	± 5% (typically < ± 3%);
Stability:	< ± 2% over 1 year;
Cosine corrected head error:	< ± 5% up to 80 °;
Response time:	10 μs;
Cell type:	blue-enhanced silicon cell;
Protection:	weather-proof anodised aluminium case with acrylic diffuser;
Operating temperatures:	-20 ° to +65 °C.

TABLE D.14: Specification of the MATRIX silicon cell pyranometer

Type:	MATRIX Mk1-G;
Spectral response:	0.35 - 1.15 microns;
Accuracy:	± 5%;
Stability:	5 years;
Cosine and air mass effects:	corrected during calibration;
Response:	< 1 ms for 100% response;
Operating temperature.	40 - 140 °F,
Output:	38.45 mv per 1000 W/m²;
Protection:	glass dome and anodised aluminium base.

TABLE D.15: Specifications of the A100R switching anemometer

Stalling speed:	0.25 m/s;
Maximum speed:	> 75 m/s;

Accuracy:	1% ± 0.1 m/s;
Distance constant:	5 m;
Calibration:	0.8 revolutions per metre (1 pulse per 1.25 m);
Temperature range:	- 30 °C to +55 °C;
Size:	height 200 mm, case diameter 55 mm;
Rotor:	standard 150 mm diameter 3-cup rotor;
Weight:	350 g;
Material:	Cups: weather-resisting plastics,
	Hub arms: anodized aluminium alloys;
Switching voltage:	100 V d.c. max.
Switching current:	0.5 A max.
Switching rating:	28 W max.
Contact resistance:	0.05 Ω;
Actuating time:	1.5 ms;
Switch life:	25 x 10^6 operations min.

TABLE D.16: Specification of the W200P potentiometer windvane

Height:	270 mm;
Fin clearance:	180 mm;
Body diameter:	56 mm;
Weight:	350 g;
Material:	anodised aluminium, stainless steel and ABS plastics;
Threshold speed:	0.6 ,m/s;
Maximum speed:	75 m/s;
Range:	360 °;
Accuracy:	± 1°;
Resolution:	0.3 °;
Temperature range:	-50 °C to +70 °C;

Life:	10^8 revolutions;
Potentiometer resistance:	1 kΩ + 10%
Dissipation:	.5 W (-50°C to 20°C); derate linearly to 0.25 W at 70 °C;
Insulation resistance.	50 MΩ minimum,
Wiper current:	20 mA max.;
Voltage supply.	16 V max.
Linearity:	0.5%.

TABLE D.17: Specifications of the back-up integrators·

All the three integrators carry the same specifications:

Display.	mechanical counter;
Power supply:	12 V d.c.
Power consumption:	2 W approximately;
Fuse:	1 A;
Temperature range:	0 °C to 40 °C,
Case.	wall mounting;
Dimensions:	263 x 214 x 147 mm;
Weight:	1 kg approximately.

TABLE D.18: Description of the SC932 9-pin to RS232-DCE interface

This is a modem which produces true RS232 signal levels.

Power supply:	5 V;
Setting options:	one way or interactive communication.
Consumption:	5 mA;
Size:	25 x 57 x102 mm;
Temperature range:	-25 ° C to +50 °C;

Humidity limits: up to 95% non-condensing.

TABLE D.19: Specification of the RAD SRM asynchronous short haul modem

Data rate:	up to 9600 baud,
Transmission line:	4-wire unconditioned cable;
Transmission mode:	asynchronous, full duplex;
Transmission level:	-6 dBm;
Transmission range:	up to 10.5 km;
Line interface:	4 wires and ground;
Power requirements:	< 2 mA when inactive, 11 mA when active;
Operating temperatures:	0 °C to 50 °C;
Humidity limit:	up to 95% non-condensing;
Size:	110 x 52 x 22 mm;
Weight:	75 g.

TABLE D.20. Temperature corrections for specific gravity and voltage measurements of lead-acid batteries [39].

	Specific gravity at various temperatures											
	0 °C 32 °F	5 °C 41 °F	10 °C 50 °F	15 °C 59 °F	20 °C 68 °F	25 °C 77 °F	30 °C 86 °F	35 °C 95 °F	40 °C 104 °F	45 °C 113 °F	50 °C 122 °F	55 °C 131 °F
	1325	1320	1315	1310	1305	1300	1295	1290	1285	1280	1275	1270
	1315	1310	1305	1300	1295	1290	1285	1280	1275	1270	1265	1260
	1305	1300	1295	1290	1285	1280	1275	1270	1265	1260	1255	1250
	1290	1290	1285	1280	1275	1270	1265	1260	1255	1250	1245	1245
	1280	1275	1270	1270	1265	1260	1255	1250	1250	1245	1240	1235
	1270	1265	1260	1260	1255	1250	1245	1240	1240	1235	1230	1225
	1260	1255	1250	1250	1245	1240	1235	1230	1230	1225	1220	1215
	1250	1245	1240	1240	1235	1230	1225	1220	1220	1215	1210	1205
	1240	1235	1230	1230	1225	1220	1215	1210	1210	1205	1200	1195
	1225	1225	1220	1215	1215	1210	1205	1205	1200	1195	1190	1190
	1215	1215	1210	1205	1205	1200	1195	1195	1190	1185	1180	1180
	1205	1205	1200	1195	1195	1190	1185	1185	1180	1175	1170	1170
	1195	1195	1190	1185	1185	1180	1176	1175	1170	1165	1160	1160
	1185	1185	1180	1175	1175	1170	1165	1165	1160	1155	1150	1150
	1175	1175	1170	1165	1165	1160	1155	1155	1150	1150	1145	1140
	1165	1165	1160	1155	1155	1150	1145	1145	1140	1135	1135	1130
	1155	1155	1150	1145	1145	1140	1135	1135	1130	1125	1120	1120
	1145	1140	1140	1135	1130	1130	1125	1125	1120	1115	1115	1110
	1135	1130	1130	1125	1125	1120	1115	1115	1110	1110	1105	1100
Voltage correction to 25 °C (77 °F) for four nominal battery voltages												
2 V	−0.12	−0.10	−0.07	−0.05	−0.02	0	+0.02	+0.05	+0.07	+0.10	+0.12	+0.15
6 V	−0.37	−0.30	−0.22	−0.15	−0.07	0	+0.07	+0.15	+.0.22	+0.30	+0.37	+0.45
12 V	−0.75	−0.60	−0.45	−0.30	−0.15	0	+0.15	+0.30	+0.45	+0.60	+0.75	+0.90
24 V	−1.5	−1.2	−0.9	−0.6	−0.3	0	+0.3	+0.6	+0.9	+1.2	+1.5	+1.8

TABLE D.21: Description of the constituents of NO CRODE anti-corrosion jelly, as supplied by the manufacturer.

CONSTITUENTS	PERCENTAGE
Polymerised Isobutylene	2%
Dye	1%
Petroleum Jelly	55%
Mineral oil	43%
Substituted Imidazoline	2%
Paraffin Wax	6%

REFERENCES

[1] W.M.O. No. 557, Technical Note No. 172 (1981), *Meteorological Aspects of the Utilisation of Solar Radiation as an Energy Source,* Secretariat of the World Meteorological Organization, Geneva.

[2] Böer, K. W. (editor) (1992), *Advances in Solar Energy - An Annual Review of Research and Development, Vol. 7,* American Solar Energy Society (ASES).

[3] Spiers, D. J. (April 1989), *Solar Electricity and Solar Fuels,* NEMO Report No. 7, NESTE Advanced Power Systems, NAPS, Helsinki University of Technology, UK.

[4] Twidell, J. W. and Weir, A. D. (1985), *Renewable Energy Resources,* The University Press, Cambridge.

[5] Sayigh, A.A.M. (1977), *Solar Energy Engineering,* Academic Press Inc. (London).

[6] Green, M. A. (1982), *Solar Cells: Operating Principles, Technology and System Applications,* The University of New South Wales, Australia.

[7] Parker, B. F. (editor), (1991), *Energy in World Agriculture - Solar Energy in Agriculture - Vol. 4,* Elsevier Scientific Publishing Co., New York.

[8] Taylor, R. H. (1983), *Alternative Energy Sources, for the Centralized Generation of Electricity,* Adam Hilger Ltd., Bristol.

[9] Imamura. M. S. et al (1992), *Photovoltaic System Technology,* Commission of the European Communities, A European Handbook, H. S. Stephens and Associates, England.

[10] Thekaekara, M. P. and Drummond, A. J., Standard values for the Solar Constant and its Spectral Components, *Nat. Phys. Sci.*, Vol. 229, No. 6, 1971.

[11] Terrestrial Photovoltaic Measuremant Procedures (1977), *Report ERDA/NASA* 1022 - 77/16.

[12] Neville, R. C. (1978), *Solar Energy Conversion: The Solar Cell,* Studies in Electrical and Electronic Engineering 1, Elsevier Scientific Publishing Company, New York.

[13] Michalsky, J. J. et al, A Microprocessor-based Rotating Shadowband Radiometer, *Solar Energy,* Vol. 36, No. 5, pp. 465-470, 1986.

[14] Cannon, T. W. and Hulstrom, R. L., A Multichannel Radiometer for Measurement of the Optical Properties of the Atmosphere, *SPIE,* Vol. 1109, pp. 152-159, 1989.

[15] Diabate, L. et al (1988), An Operational Tool for the Fine-Scale Mapping of the Incident Solar Radiation Using Satellite Images: The Heliostat Station, *Solar '88,* p. 11, Proceedings of the 1988 Annual Meeting of the American Solar Energy Society, Cambridge, Massachusetts, U.S.A.

[16] Burnham, J. (editor) (1993), *Renewable Energy: Sources for Fuels and Electricity,* Earthscan Publications Ltd., London.

[17] Riordan, C. and Hulstrom, R. (1990), *Outdoor Spectral Solar Radiation Variations and Their Relationship to Photovoltaic Device Performance in Current Topics in Photovoltaics,* Vol. 4, pp.1-23, T. J. Coutts and J. D. Meakin, editors, Academic Press, New York.

[18] Böer, K. W., The Solar Spectrum at Typical Weather Days, *Solar Energy,* Vol. 19, pp. 525-538, 1977.

[19] Scerri, E. (1965), *Solar Radiation on Inclined Surfaces,* M. Sc. Thesis, Woolwich Polytechnic, U.K.

[20] Scerri, E., Performance Analysis Between Thermopile and Silicon Solarimeters, *Renewable Energy,* Vol. 2, No. 4/5, pp. 513-520, 1992.

[21] Dalmin, M. N. and Chakrabarty, P. K., Gathering of Daily Instantaneous Global Solar Radiation Using A Microcomputer-based Data Acquisition System, *Solar and Wind Technology,* Vol. 5, No. 2, pp. 181-183, 1988.

[22] Michalsky, J. J. et al, Spectral and Temperature Correction of Silicon Photovoltaic Solar Radiation Detectors, *Solar Energy,* Vol. 47, No. 4, pp. 299-305, 1991.

[23] Nast, P. M., Measurements of the Accuracy of Pyranometers, *Solar Energy,* Vol. 31, No.3, pp. 279-282, 1983.

[24] Mohr, A. J. et al, Experiences With Tests And Calibrations of Pyranometers for a Mesoscale Solar-irradiance Network, *Solar Energy,* Vol. 22, pp. 197-203, 1979.

[25] Suehrcke, H. et al, The Dynamic Response of Instruments Measuring Instantaneous Solar Radiation, *Solar Energy,* Vol. 44, No. 3, pp. 145-148, 1990.

[26] Michalsky, J. J. et al, Empirical Radiometric Correction of a Silicon Photodiode Rotating Shadowband Pyranometer, *Solar Energy,* Vol. 39, No. 2, pp. 87-96, 1987.

[27] Evans, W. and Menetrey, W. R. (1960), *Energy Conversion Systems Reference Handbook, Direct Solar Conversion, Vol. 5,* Wadd Technical Report 60-699, Wright-Patterson Air Force Base, Ohio, U.S.A.

[28] Kipp and Zonen Brochure, Sep. 1993, SOLRAD, Solar Radiation Measurement System.

[29] Suehrcke, H. (1988), *The Performance Prediction of Solar Thermal Systems,* Ph. D. Thesis, University of Western Australia, Nedlands, Australia.

[30] Jamal, M. A. and Muaddi, J. A., The Efficiency of a Silicon Solar Cell for Different Light Sources, *Renewable Energy,* Vol. 1, No. 2, pp. 207-210, 1991.

[31] Yellott, J. L. and Selcuk, K., Measurement of Direct, Diffuse and Total Solar Radiation With Silicon Photovoltaic Cells, *Solar Energy,* Vol. 6, No. 4, 1962.

[32] Radiation Sensors Instruction Manual, LI COR Inc., Publication 8609 60, Lincoln, Nebraska, U.S.A.

[33] Riches, M. R. et al (editors) (1982), International Energy Agency Conference on Pyranometer Measurements, Publication no. SERI/TR-642-1156, Solar Energy Research Institute.

[34] Ossenbrink, H., The ESTI Sensor - A New Reference Cell for Monitoring of PV Plant Performance, *11th EC PV Solar Energy Conference,* Switzerland, pp. 333-336, 1992.

[35] Brine, D. T. and Iqbal, M., Diffuse and Global Solar Spectral Irradiance Under Cloudless Skies, *Solar Energy,* Vol. 30, No. 5, pp. 447-453, 1983.

[36] Skartveit, A. and Olseth, J. A., Some Simple Formulas for Multiple Rayleigh Scattered Irradiance, *Solar Energy,* 41, 1, pp. 19-20, 1988.

[37] *Guidelines for The Assessment of Photovoltaic Plants, Document A, Photovoltaic System Monitoring,* Issue 4, (June 1991) - Commission of The European Communities, Joint Research Centre, Ispra Establishment, Italy.

[38] Brinkworth, B. J. (1972), *Solar Energy for Man,* Compton Press Ltd., UK.

[39] Roberts, S (1991), *Solar Electricity, A Practical Guide to Designing and Installing Small Photovoltaic Systems,* Prentice-Hall, Hertfordshire, U.K.

[40] Seraphin, B. O. (editor) (1979), *Topics in Applied Physics, Vol. 31, Solar Energy Conversion,* Springer Verlag.

[41] Salameh, Z. and Taylor, D., Step-up Maximum Power Point Tracker for Photovoltaic Arrays, *Solar '88,* Proceedings of the 1988 Annual Meeting of ASES, edited by M. J. Coleman, Cambridge, Massachusetts.

[42] Böer, K. W. (editor) (1989), *Advances in Solar Energy - An Annual Review of Research and Development - Vol. 5,* American Solar Energy Society (ASES).

[43] Zhengrong Shi, et al, Investigation of Polycrystalline Silicon Deposition on Glass Substrates, *Solar Energy Materials and Solar Cells,* Vol. 31, No. 1, pp. 51 - 60, October 1993, C. M. Lampbert (editor).

[44] Campbell, P. et al, Light Trapping and Reflection Control in Solar Cells Using Tilted Crystallographic Surface Textures, *Solar Energy Materials and Solar Cells,* Vol 31, pp 133-153, 1993.

[45] Nishiwaki, H. et al, Through-Hole Contact (THC) Integrated Type a-Si Solar Cell Submodule By A New Laser Photo-etching Method, *Solar Energy Materials and Solar Cells,* Vol. 31, pp. 97-108, 1993.

[46] Advani, G. N. and Jordan, A. G., Stability of SnO_2 Thin Films Used for PV Devices, *Solar Energy,* Vol. 30, No. 1, pp. 71-73, 1983.

[47] Lehovec, K. and Fedotowsky A., Degradation of Solar Cell Efficiency by Sheet Resistance, *Solar Energy,* Vol. 21, pp. 81-86, 1978.

[48] Palz, W. (editor) (1984), *European Solar Radiation Atlas, Vol. 1, Horizontal Surfaces,* Commission of the European Communities.

[49] Bolton, J. R., Solar Cells - A Technology Assessment, *Solar Energy,* Vol. 31, No. 5, pp. 483-502, 1983.

[50] Böer, K. W., State-of-the-Art in Photovoltaic Research and Application, *Solar and Wind Technology,* Vol. 4, No. 1, pp. 21-35, 1987.

[51] Herz, K. et al, Holographic Optical Elements for The Construction of Tandem Cells, *10th European PV Solar Energy Conference, Portugal,* pp. 15-18, April 1991.

[52] Curry, R., *PV Insider's Report Newsletter,* 7, 6, June 1993.

[53] Curry, R., *PV Insider's Report Newsletter,* 8, 2, Feb. 1994.

[54] Curry, R., *PV Insider's Report Newsletter,* 7, 9, Sep. 1993.

[55] Curry, R., *PV Insider's Report Newsletter,* 7, 7, July 1993.

[56] Curry, R., *PV Insider's Report Newsletter,* 8, 3, March 1994.

[57] Curry, R., *PV Insider's Report Newsletter,* Vol. 8, No. 4, April 1994.

[58] Nguyen, T. T. (May 1982), *Photovoltaic Properties of Semi-crystalline Silicon,* (M.Sc. Thesis), California State University, Long Beach, U.S.A.

[59] Garg, H P and Datta G, Fundamentals and Characteristics of Solar Radiation, *Renewable Energy,* Vol. 3, No. 4/5, pp. 305-319, 1993.

[60] Russell, M C and Kern, E C (1986), *Stand-off Building Block Systems for Roof-Mounted Photovoltaic Arrays,* Massachusetts Institute of Technology, Sandia Laboratories Publication no. 85-7020, U.S.A.

[61] Scerri, E. and Iskander, C. Hands-on Experience of the Setting-up of a Stand-alone Photovoltaic Demonstration Project in Malta, *Renewable Energy,* Vol. 4, No. 3, pp. 359-363, 1994.

[62] Neill, D. R. and Zhiqiang, G., EV, EB and Remote Power - NiMH is The Battery of Choice, *Renewable Energy,* Vol. 3, No. 2/3, pp. 239-243, 1993.

[63] Szymborski, J. and Eggers M. L., Development of a Totally Maintenance Free Lead-acid Battery for Telecommunications Standby Power, *Solar & Wind Technology,* Vol. 2, No. 2, pp. 133-137, 1985.

[64] Hill, M. and Mc Carthy S., (April 1992), *PV Battery Handbook,* Hyperion Energy Systems Ltd., Ireland.

[65] Takami, A. et al., High Efficiency (16.45%) Thin Film Silicon Solar Cells Pepared by Zone-melting Recrystallisation, *Proceedings of the 12th European PV Solar Energy Conference, Amsterdam*, pp. 59-62, April 1994.

[66] Cuddihy, E. F., Baum, B. and Willis, P., Low-cost Encapsulation Materials for Terrestrial Solar Cell Modules, *Solar Energy,* Vol. 22, pp. 389-396, 1979.

[67] Lopez Pineda, C. F., Experimental Evaluation of Reverse Bias Stress Induced on Photovoltaic Modules for Different Configurations, *Solar & Wind Technology,* Vol. 3, No. 2, pp. 85-88, 1986.

[68] Green, M. A., Recent Advances in Silicon Solar Cell Performance, *Proceedings of the 10th European Photovoltaic Solar Energy Conference,* 1991, p. 250.

[69] Dunselman, C.P.M. et al, Feasibility and Development of PV Modules with Integrated Inverter: AC-Modules, *Proceedings of the 12th European PV Solar Energy Conference, Amsterdam*, pp. 313-315, April 1994.

[70] Cace, J., Bisschop, F., 250 kWp Grid Connected PV Power Plant on 66 Newly Built Houses in Amsterdam, *Proceedings of the 12th European PV Solar Energy Conference, Amsterdam*, pp. 1091-1094, April 1994.

[71] Curry, R., *PV Insider's Report Newsletter,* 8, 6, June 1994.

[72] De Bakker, P. H. A. and Schulte, K. M., (1991), *Fact Sheets of Selected Photovoltaic Applications,* Deutsche Gesellschaft Fur Technische Zusammenarbeit (GTZ) GmbH, (German Industry for Technical Cooperation), Eschborn.

[73] Som, A. K. and Al-Alawi, S. M. Evaluation of Efficiency and Degradation of Mono- and Polycrystalline PV Modules Under Outdoor Conditions. *Renewable Energy,* Vol. 2, No. 1, pp. 85-91, 1992.

[74] *Photovoltaic Systems Design Manual,* Marbek Resource Consultants, Darentek Corporation and the Canadian Photovoltaics Industries Association, Canada, March 1991.

[75] Pern,, F. J. and Czanderna, A. W., Characterization of Ethylene Vinyl Acetate (EVA) Encapsulant: Effects of Thermal Processing and Weathering Degradation on its Discoloration, *Solar Energy Materials and Solar Cells,* Vol. 25, pp. 3 23, 1992.

[76] Berman, D. et al, Efficiency Loss Associated With EVA Laminate Browning Observed in the Negev Desert. *Proceedings of the 12th European PV Solar Energy Conference, Amsterdam*, pp. 1202-1205, April 1994.

[77] Bannister, A. et al (1992), *Surveying*, 6th edition, Longman Scientific (U.K.).

[78] Green, M. A. and Emery, K. Solar Cell Efficiency Tables (Version 3), *Progress in Photovoltaics:Research and Applications,* Vol. 2, pp. 27-34, January 1994.

[79] *Guidelines for The Assessment of Photovoltaic Plants, Document B, Analysis and Presentation of Monitoring Data,* Issue 2, (June 1990) - Commission of The European Communities, Joint Research Centre, Ispra Establishment, Italy.

[80] Munro, D. K. and Blaesser G., The Performance of PV Systems and Components in the Thermie Programme, Proceedings of the World Renewable Energy Congress, Reading, U.K. *Renewable Energy,* Vol. 5, Part 1, pp. 172-178, 1994.

[81] Derrick, A. et al (1991), *Solar Photovoltaic Products: A Guide for Development Workers,* Intermidiate Technology Publications, U.K.

[82] Katsoulis D. and Papachristopoulos E., Analysis of Solar Radiation Measurements at Athens Observatory and Estimates of Solar Radiation in Greece, *Solar Energy,* Vol. 21, pp. 217-226, 1978.

[83] Hammond, R. L. and Backus C. E., Photovoltaic System Testing, *Renewable Energy,* Vol. 5, No. 1, pp. 268-274, 1994.

[84] Larson, R. W. et al (Dec. 1992), *Economics of Solar Energy Technologies,* American Solar Energy Society (ASES).

[85] Brealey, R. A. and Myers, S. C., *Principles of Corporate Finance,* McGraw Hill, 1988.

[86] Central Bank of Malta - Quarterly Review Vol. 27, No. 3, September 1994.

[87] U.S. Department of Commerce, *Stand-alone Photovoltaic Systems: A Handbook of Recommended Design Practices,* Sandia National Laboratories, April 1988, Albuquerque, U.S.A.

[88] *Opportunities and Potential for Using Photovoltaic Solar Energy in Malta,* A Report by IT Power Ltd., Solarex Corporation and The University of Malta, November 1991, IT Power Ltd. Publication no. 91404, U.K.